Synthesis, Reactivity, and Catalytic Applications of Ruthenium and Palladium Complexes Supported by New Pincer Ligands

by

Morgan C. MacInnis

Submitted in partial fulfilment of the requirements
for the degree of Doctor of Philosophy

at

Dalhousie University
Halifax, Nova Scotia
August 2011

DALHOUSIE UNIVERSITY

DEPARTMENT OF CHEMISTRY

The undersigned hereby certify that they have read and recommend to the Faculty of Graduate Studies for acceptance a thesis entitled "Synthesis, Reactivity, and Catalytic Applications of Ruthenium and Palladium Complexes Supported by New Pincer Ligands" by Morgan C. MacInnis in partial fulfilment of the requirements for the degree of Doctor of Philosophy.

Dated: August 8, 2011

Supervisor: _____

Readers: _____

_____

_____

_____

Departmental Representative: _____

DALHOUSIE UNIVERSITY

DATE: August 8, 2011

AUTHOR: Morgan C. MacInnis

TITLE: Synthesis, Reactivity, and Catalytic Applications of Ruthenium and Palladium Complexes Supported by New Pincer Ligands

DEPARTMENT OR SCHOOL: Department of Chemistry

DEGREE: PhD CONVOCATION: October YEAR: 2011

_____

Signature of Author

Table of Contents

List of Tables

List of Figures

List of Schemes

Abstract

Cyclometalated phosphine-based PNP and PCP 'pincer' complexes of the platinum group metals have been the subject of intense research in recent years, owing to the remarkable stoichiometric and catalytic reactivity exhibited by such complexes. With the goal of discovering new metal-mediated reactivity patterns and extending the versatility of metal pincer chemistry, significant effort has been devoted to the synthesis of structurally and/or electronically related systems where strategic alterations have been introduced to the pincer ligand architecture, including variation of the central and peripheral donor fragments, as well as the ancillary ligand backbone. In this context, the synthesis and study of Ru and Pd complexes supported by pincer-like tridentate ancillary ligands that feature a central anionic phosphorus ([NPN]) or silicon ([PSiP]) donor in the pincer ligand backbone are described herein. The decreased propensity for forming π-bonds to P was anticipated to lead to a higher degree of electronic unsaturation in complexes supported by tridentate phosphido ligation relative to structurally related metal amido ($M\text{-}NR_2$) species. In the case of [PSiP] ligation, the reduced electronegativity of Si relative to C should promote the formation of electron-rich late metal species that can readily undergo oxidative addition reactions. The *trans*-labilizing silyl donor was also expected to stabilize coordinatively and electronically unsaturated late metal complexes.

The synthesis and reactivity of Ru complexes featuring bis(phosphino)silyl ligation of the type $[\kappa^3\text{-}(2\text{-}R_2PC_6H_4)2SiMe]^-$ ([R-PSiP]; R = Ph, Cy) are described. The 5-coordinate complex [Ph-PSiP]RuCl(PPh_3) was shown to be catalytically active for the transfer hydrogenation of ketones in basic isopropanol. These transfer hydrogenation studies are among the first catalytic studies of silyl-pincer complexes and establish [R-PSiP]M species as viable candidates for catalysis. The synthesis and reactivity of 4- and 5-coordinate Ru^{II} complexes featuring the [Cy-PSiP] ligand were explored. Reaction of [Cy-PSiP]H with $[(p\text{-cymene})RuCl_2]_2$ in the presence of NEt_3 and PCy_3 resulted in the formation of $([Cy\text{-}PSiP]RuCl)_2$, which serves as a precursor to a series of unprecedented 4-coordinate, formally 14-electron [Cy-PSiP]RuX (X = NHAr, $N(SiMe_3)_2$, O^tBu) complexes that feature an unusual trigonal pyramidal geometry at Ru. The reactivity of these novel diamagnetic complexes is described, including the reaction of [Cy-PSiP]RuO^tBu with amine-boranes resulting in the formation of rare bis(σ-BH) complexes. Computational studies confirmed the key role of the strongly σ-donating silyl group of the Cy-PSiP ligand in facilitating the synthesis of such low-coordinate Ru species and enforcing the unusual trigonal pyramidal geometry. The mechanism of ammonia-borane activation was also examined computationally.

Lastly, the synthesis and structural characterization of Pd^{II} complexes supported by the pincer-like bis(amino)phosphido ligand $[\kappa^3\text{-}(2\text{-}Me_2NC_6H_4)_2P]^-$ ([NPN]) is described. Examples of κ^1-, κ^2-, and κ^3-NPN coordination to Pd are described, as is the catalytic activity of $([NPN]PdX)_2$ (X = Cl, OAc, OTf) complexes in the Heck olefin arylation reaction. In an effort to discourage the formation of phosphido-bridged dinuclear complexes, pre-coordination of the Lewis acid BPh_3 to [NPN] was pursued. Upon reaction of $[N(P{\cdot}BPh_3)N]K$ with $[PdCl(C_3H_5)]_2$, the η^1-allyl complex $[\kappa^3\text{-}N(P{\cdot}BPh_3)N]Pd(\eta^1\text{-}C_3H_5)$ was isolated, which establishes the coordination of a Lewis acid to the phosphido donor of the [NPN] ligand as a viable strategy for encouraging the formation of mononuclear κ^3-*NPN* complexes.

List of Abbreviations and Symbols Used

η = hapticity (contiguous donor atoms)
κ = hapticity (non-contiguous donor atoms)
Anal. Calcd. = Analysis Calculated
Å = angstrom
COSY = Homonuclear Shift *CO*rrelation *S*pectroscop*Y*
Cp* = pentamethylcylcopentadienyl
Cy = cyclohexyl
[Cy-PSiP] =

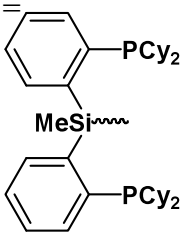

d = doublet
δ = chemical shift
DEPT = *D*istortionless *E*nhancement by *P*olarization *T*ransfer
DMAP = 4-(N,N-dimethyl)aminopyridine
E = main group element
eq = equation
equiv = equivalents
Et = ethyl
h = hour
HMBC = *H*eteronuclear *M*ultiple *B*ond *C*orrelation
HSQC = *H*eteronuclear *S*ingle *Q*uantum *C*orrelation
Hz = hertz
IR = infrared
^{i}Pr = isopropyl
$^{n}J_{XX'}$ = n bond coupling constant between atom X and atom X`
L = two-electron donor ligand
m = multiplet
m = meta
M = generic transition metal *or* mol/L
Me = methyl
Mes = 2,4,6-trimethylphenyl
min = minutes
NMP = N-methyl-2-pyrrolidone
NMR = Nuclear Magnetic Resonance
[NSiN] =

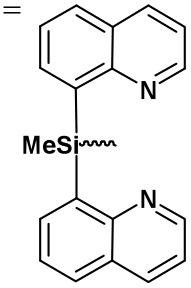

o = ortho
ORTEP = Oak Ridge Thermal Ellipsoid Plot
OAc = acetate
OTf = trifluoromethylsulfonate
p = para
ppm = parts per million
Ph = phenyl
[Ph-PSiP] = 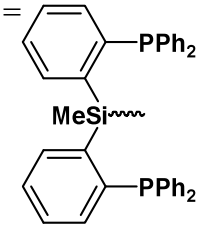

[POCOP] = 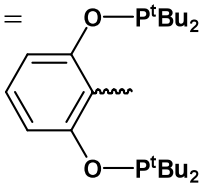

q = quartet
R = alkyl or aryl group
s = singlet
T_1 = spin-lattice relaxation time
t = triplet
^{t}Bu = *tert*-butyl
TBE = *tert*-butyl ethylene
THF = tetrahydrofuran
TOF = turn over frequency
TON = turn over number
X = anion *or* anionic ligand

Acknowledgements

I was able to complete this work because of the support of many people. First and foremost, I would like to express my gratitude to my supervisor, Laura Turculet. She has been nothing less than an excellent mentor to me and I have thoroughly enjoyed working in her lab. She has always been willing to help me to the fullest extent and I am continually impressed by her intellect and chemical insight.

I would like to thank Prof. Sven Tobisch (University of St. Andrews) for performing a thorough computational investigation, the results of which are discussed in Chapter 3. I would also like to thank Mike Lumsden and Kathy Robertson for all of their assistance regarding various NMR experiments. Bob MacDonald and Mike Ferguson (University of Alberta) are thanked for their expertise and assistance in X-ray crystallography related studies.

I would also like to thank my supervisory committee of Neil Burford, Norm Schepp, and Kevin Grundy for their support and advice during my time at Dalhousie. Furthermore, Mark Stradiotto and his group are acknowledged for providing valuable insight into my chemistry. In particular, I would like to acknowledge Rylan Lundgren who was always willing to talk about chemistry and most of the time my chemistry.

I have met some great people in the Turculet group that have made coming to work a pleasant experience. In particular, I would like to acknowledge Darren MacLean. Although we were the only two graduate students in the lab during our first two years I never tired of hanging around with him at the lab and afterward.

I would like to thank my parents who have provided me with unending support. Finally, I would like to acknowledge Ashley who has always been there for me, and who never fails to make me laugh.

Chapter 1: Introduction

1.1 Overview

Catalysis is ubiquitous in chemistry. Numerous biochemical processes, industrial scale reactions, and laboratory syntheses involve catalytic protocols. In particular, modern synthetic chemistry has benefited tremendously from the development of rapid, efficient, and selective transition metal-mediated methods.[1] In typical applications, such catalysts are used to facilitate the conversion of relatively abundant and inexpensive feedstocks (such as simple alkanes and alkenes, CO, H_2, H_2O) into molecules of greater commercial value, including complex organic molecules. Over the past fifty years, great advances have been made in the area of homogeneous transition metal catalysis, and the tremendous impact was recognized in the awarding of the 2001, 2005, and 2010 Nobel Prizes in Chemistry for developments in asymmetric catalysis, olefin metathesis, and transition metal catalyzed coupling reactions.[2] This work culminated in the development of catalysts for the enantioselective synthesis of pharmaceuticals and fine chemicals, as well as powerful polymerization catalysts, all of which have applications in the synthesis of new materials on both laboratory and benchtop scales.

Although asymmetric catalysis, olefin metathesis, and C-C coupling reactions have emerged as techniques of tremendous scope in synthesis and have wide-ranging application, significant breakthroughs of this type are ultimately rooted in the fundamental study of transition metal chemistry. The design and synthesis of new transition metal complexes that display novel and/or improved reactivity is one of the most important means by which advances in catalytic methods are achieved. In this context, this thesis focuses on the synthesis, reactivity, and catalytic application of new

platinum-group transition metal complexes featuring entirely new classes of 'pincer'-type ligands that incorporate anionic silicon or phosphorus donors. To place this work in an appropriate context, an overview of more traditional classes of pincer complexes (Figure 1-1) is provided in the following sections, with particular emphasis on recent breakthroughs in the area of transition metal pincer chemistry. Some of the most notable breakthroughs that will be highlighted involve the application of transition metal pincer complexes in the functionalization of relatively inert molecules, such as alkanes. The catalytic functionalization of such unreactive substrates represents a long-standing challenge in synthetic chemistry. Specific examples that will be described include the [PCP]Ir-catalyzed dehydrogenation of alkanes,[3] as well as the [PNN]Ru-catalyzed direct synthesis of amides from alcohols and amines.[4]

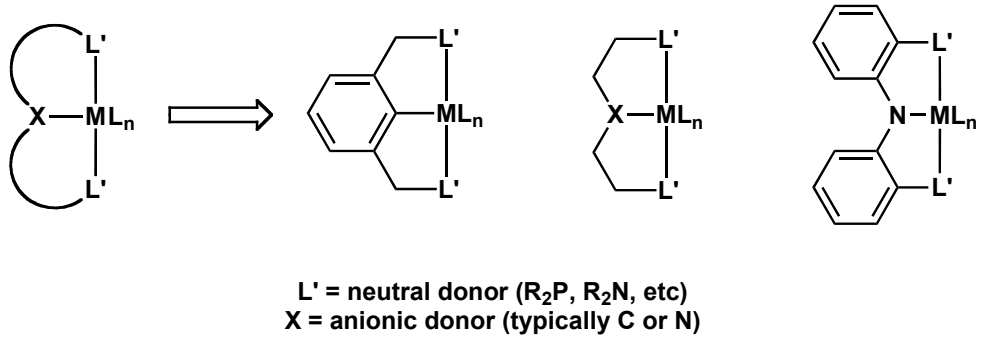

Figure 1-1. Traditional pincer ligand complexes.

1.2 The Utility of Pincer Ligand Design in Tuning Metal Reactivity

The platinum group metals (Ru, Os, Rh, Ir, Pd, Pt) are well established as particularly capable catalysts for the mediation of many types of organic transformations,

including hydrogenation, hydrosilylation, transfer hydrogenation, dehydrogenation, coupling reactions, etc. Variation of the metal can result in dramatic changes in the reactivity of a complex, due to the inherently different properties (e.g. preferred oxidation states and geometries, d-electron configuration, etc.) of different transition metals. However, the reactivity of a transition metal complex depends not only on the metal, but also on the ligand system used to support the reactive metal center, which can influence the steric and electronic features of the coordination environment. It is desirable to use a supporting ligand system that can influence the reactivity of the metal center without taking part in bond making or bond breaking processes. Ligands of this type are referred to as ancillary ligands. Typically the ancillary ligand(s) of a metal complex should be designed such that small scale adjustments can easily be made in order to fine tune the reactivity exhibited by the complex in a strategic manner. The use of appropriate ancillary ligands is key to achieving a stable yet reactive metal center, making ligand design an essential aspect of fundamental organometallic chemistry.

In this context, metal complexes supported by 'pincer'-type ancillary ligands have been the subject of intense research in recent years, owing to their remarkable stoichiometric and catalytic reactivity with relatively inert substrates.[5] Pincer ligands are tridentate chelating ligands made up of an [LXL] (L = neutral donor, X = anionic donor) framework in which the donor atoms are linked by an organic backbone (Figure 1-1). The donor atoms and ligand backbone can be easily modified and therefore fine-tuning the steric and electronic features of the pincer framework – and in turn the reactivity of the metal center – is a systematic exercise. For example, the rigidity of the ligand backbone can be tailored by changing from an aliphatic to an aromatic backbone, or by

changing the chelate ring size. In addition to affecting the rigidity of a transition metal complex, aliphatic and aromatic backbones have substantially different electronic influences on the metal center. With respect to chelate ring size, a two-atom linker between donor atoms results in the formation of five-membered metalacycles, while a three-atom linker leads to the formation of six-membered metalacycles (Figure 1-2). Five- and six-membered chelate rings are the most commonly utilized architectures in multidentate ligand design, as these minimize the strain that would be associated with smaller ring sizes, thereby promoting chelation. Chelate ring sizes larger than this are typically non-rigid and their ability to stabilize the metal center and form monomeric complexes is often diminished as a result. Protasiewicz and co-workers have reported examples of Pd pincer complexes that feature two seven-membered metallacycles.[6] Several examples of pincer-like complexes featuring four-membered metalacycles have been reported by Caulton and co-workers (Ru) and by Jones and Cavell (Zr and Hf).[7]

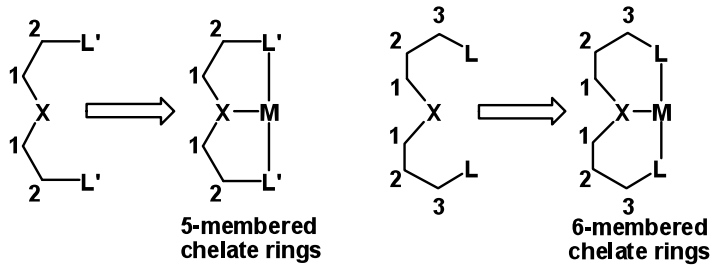

Figure 1-2. Examples of different metalacycle sizes in transition metal pincer complexes.

The electronic properties and steric features of pincer ligands are also readily tuned by varying the three donor groups and their substituents. While the neutral L donor atoms are usually either P[5b] or N,[8] examples involving C,[9] S,[10] O,[11] or Se[12] at this position

are also known. Much like the ligand backbone, the steric bulk and electron withdrawing or electron donating character of the substituents on the L donor atoms largely influence the sterics and electronics of the metal center. The central anionic donor atoms (X) incorporated into pincer ligands have been restricted almost exclusively to C[5] and N.[13]

The first examples of pincer ligation in transition metal chemistry appeared in the literature in the 1970's in reports by Shaw and co-workers, who reported a number of cyclometalated [PCP] complexes of Rh, Ir, Pd, and Pt.[14] This work stemmed from an interest in the oxidative addition of C-H bonds to a low valent metal center. Only a few reports of such C-H bond activation chemistry were known at the time, and Shaw's research provided the first examples of rapid chelate-assisted C-H oxidative addition at or below room temperature. Notably, facile formation of dimeric complexes was often observed in the course of this chemistry.[14d,e] The propensity for dimer formation could be attributed to the non-rigid nature of the aliphatic ligand backbone, highlighting the importance of ligand rigidity for the formation of mononuclear, coordinatively unsaturated complexes. Since Shaw's initial reports, transition metal pincer chemistry has evolved into a prominent sub-discipline of organometallic chemistry research.[5] Due to the pioneering contributions of Shaw, a review of the evolution of pincer chemistry most appropriately begins with a discussion of [PCP]-supported complexes.

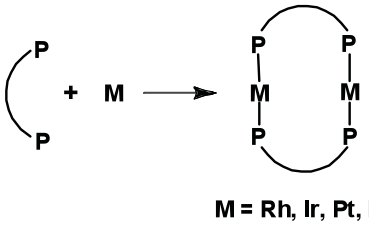

Figure 1-3. Dimers formed during attempts to synthesize late metal pincer complexes by Shaw.

1.3 The Development of Complexes Employing [LCL] Based Ligands

The first pincer complexes to be developed incorporated C as the central anionic donor,[14] and the vast array of reactions mediated by such [LCL]-supported complexes has sustained their prevalence in pincer research. Highlights of reactivity that is mediated by [LCL]ML_n complexes include numerous organic transformations (e.g. C-C coupling reactions, alkane dehydrogenation, hydroamination, etc), and challenging bond activation reactions (e.g. C-O, C-H, C-C).[5b] Although numerous research groups have contributed to this area over the past twenty years, the groups of Milstein, van Koten, Goldman, and Jensen have made seminal contributions to both the synthesis of [LCL]-supported complexes, and to the study of their stoichiometric and catalytic reaction chemistry. Some of these contributions will be highlighted herein.

The synthesis of [LCL] pincer complexes requires an efficient synthetic route for preparation of the pincer pro-ligand. A typical synthesis involves the reaction of the appropriate dibrominated xylene (e.g. **1-1** in Scheme 1-1, Route A) with two equivalents of a secondary phosphine to give the bis(phosphonium) dibromide salt (Scheme 1-1, Route A).[14a] Reaction of this salt with two equivalents of a base such as NaOAc yields the desired bis(phosphino) aryl product. Alternatively, the reaction of two equivalents of

a secondary chlorophosphine with the appropriate dilithiated ligand backbone, will also yield a bis(phosphino) pincer-type pro-ligand (Scheme 1-1, Route B).[14c]

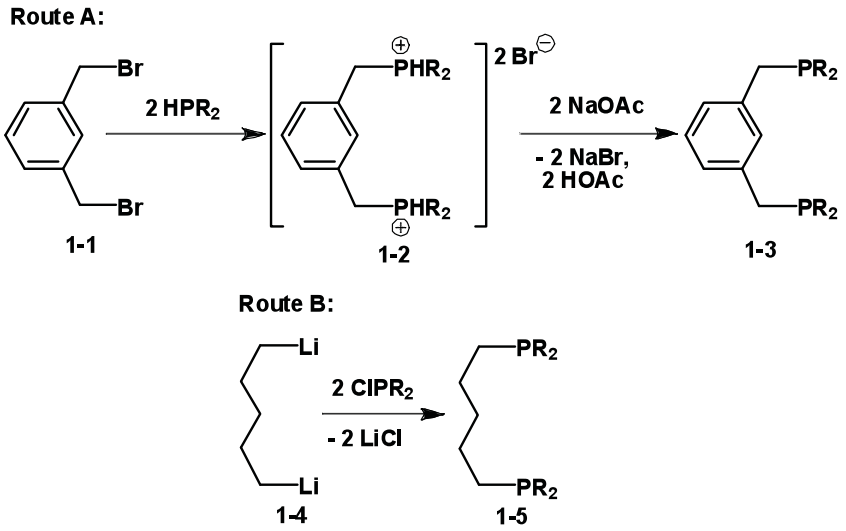

Scheme 1-1. Two examples of common synthetic routes to [PCP]-type pincer pro-ligands.

The construction of a new M-C σ-bond is not trivial and thus facile delivery of a ligand precursor to a transition metal center is desirable. Several strategies for the formation of [LCL] pincer complexes – known as metalation – have been developed, including transmetalation, cyclometalation (oxidative addition), and transcyclometalation (Scheme 1-2).[5a] Transmetalation and cyclometalation are most commonly seen in the literature.

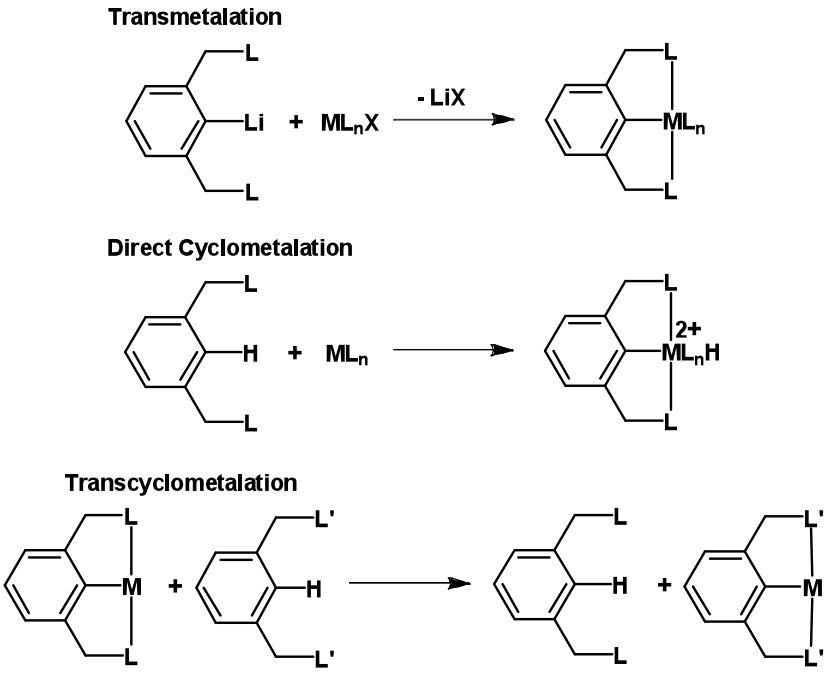

Scheme 1-2. Different methods of delivering a pincer ligand to a metal center.

Transmetalation is the exchange of one [LCL]-ligated metal (usually Li) for the desired transition metal, and it has been established successfully in the formation of Ir,[15] Ni,[16] Pd,[17] Pt,[17] and Ru[18] [NCN] pincer complexes. Transmetalation is the only method that has proven successful for the formation of [NCN]Ru complexes. However, the prefunctionalization of the ligand with the sacrificial metal creates an extra synthetic step, and can sometimes lead to complications. For example, pro-ligands of the type (1,3-$(CH_2PR_2)_2C_6H_3$) (**1-6**, Scheme 1-3) are often lithiated at the benzylic position on the ligand arm rather than the desired aryl C-H *ortho*- to both ligand arms. Synthesis and subsequent lithiation of the analogous aryl-halide precursor[8] leads to the aryllithium species. However, this compound is not stable and readily isomerizes to the undesired benzyllithium form. Only in cases where R = Me is the aryllithium compound stable enough to be utilized for the synthesis of [PCP] pincer complexes.

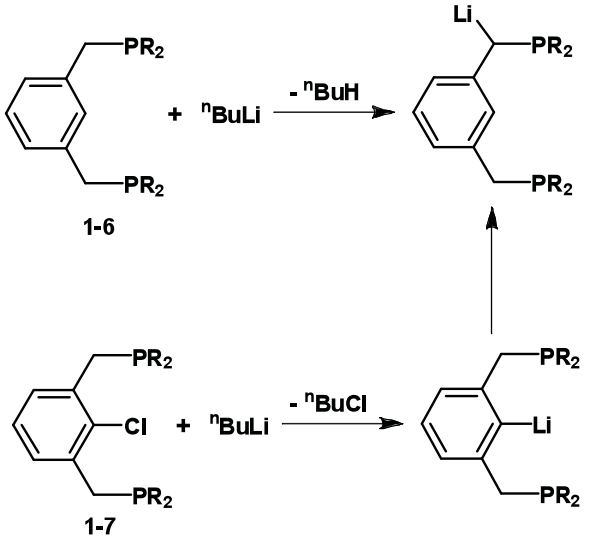

Scheme 1-3. Lithiation of **1-6** and **1-7**.

Complementing transmetalation is direct cyclometalation (Scheme 1-2), which is a more common method for the formation of [PCP] pincer complexes.[14] In most cases, direct cyclometalation involves the activation (most commonly via oxidative addition) of a C-R bond (R = H, C, or Si; R = H is most common).[14,19] Direct cyclometalation is established as a viable route for the synthesis of pincer complexes of all of the platinum group metals (the formation of Pd and Pt complexes by this route has been studied most extensively);[14] it is a more attractive route than transmetalation since prefunctionalization of the ligand is not required. However, the oxidative addition of C-H, C-Si, or C-C bonds is not a facile process, and as such, elevated temperatures and long reaction times are often necessary to promote this reaction. The oxidative addition reaction is facilitated by coordination of the neutral pincer donors to the metal center, and thus cyclometalation occurs most readily for phosphine substituted ligands that can readily form M-P bonds to a platinum group metal center. Electron donating substituents (e.g. alkyl) on the

phosphine donors further promote cyclometalation, as electron rich late metal centers can undergo oxidative addition more easily. Complexes supported by NCN pincers are more readily prepared via oxidative addition of a C-X bond (X = Cl, Br, I); complexes of Ni, Pd, and Pt have been formed by this route.[20]

Transcyclometalation (Scheme 1-2) was introduced by van Koten and co-workers in 2000 as an alternative strategy for the formation of pincer complexes.[21] Transcyclometalation is the substitution of one cyclometalated pincer for another pincer ligand. Initial experiments from the van Koten group involved the synthesis of an [SCS]Pd pincer complex. The yield of the reaction was dramatically improved (> 90%) when transcyclometalation of a [CN]Pd complex was performed rather than direct cyclometalation of $[Pd(OAc)_2]_3$ (< 10% yield). Bis-cyclometalated starting materials such as [NCN]PtCl and [NCN]RuCl(PPh_3) have been used as precursors for the formation of the analogous [PCP] complexes via transcyclometalation. It has been proposed that preferential formation of M-PR_3 linkages is the main driving force in this process.[22]

1.3.1 [PCP]Ir pincer complexes in the dehydrogenation of alkanes.

The functionalization of unactivated C-H bonds in simple molecules such as alkanes could lead to more effective use of hydrocarbon resources for the synthesis of complex molecules such as fine chemicals and pharmaceuticals. However, such C-H bonds are inherently unreactive, rendering the activation and subsequent functionalization of hydrocarbons a challenging process.[23] Nonetheless, studies have shown that appropriately designed transition metal complexes can effectively cleave C-H bonds

under mild conditions. For example, Bergman has shown that $[(\eta^5\text{-}C_5Me_5)(PMe_3)IrMe]^+$ complexes can readily activate alkane C-H bonds, including those of methane.[24] In 1979, Jensen and co-workers discovered that the dehydrochlorination of [PCP]RhHCl ([PCP] = 2,6-($^tBu_2PCH_2)_2C_6H_3$) using $NaN(SiMe_3)_2$ led to the formation of Rh-dihydride complexes in the presence of pentane, octane, or cyclohexane.[3] Presumably these dihydride species are formed via alkane C-H oxidative addition to the coordinatively and electronically unsaturated Rh center followed by β-hydride elimination to liberate the corresponding alkene. Therefore, if the Rh center could somehow lose H_2, a catalytic cyclic could be envisioned for the dehydrogenation of alkanes. However, the coordinatively and electronically unsaturated '[PCP]Rh' intermediate proved too unstable to isolate, and attempts at *in situ* generation of this species from [PCP]RhHCl for use in the catalytic dehydrogenation of alkanes were unsuccessful. Shifting focus to the development of [PCP]Ir complexes seemed logical since some "P_2IrH_2" species had previously been known to catalytically dehydrogenate alkanes.[25]

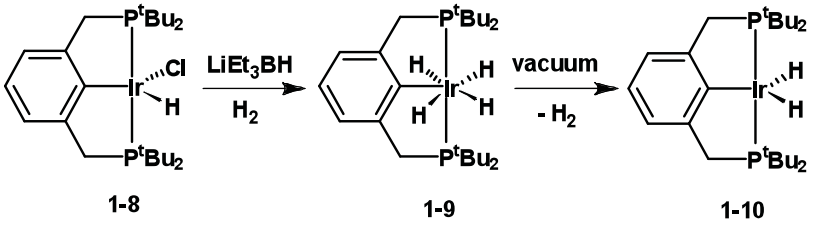

1-8 **1-9** **1-10**

Scheme 1-4. Transformation of the [PCP]IrHCl precursor **1-8** into **1-10**.

Anticipating that the related Ir complexes might prove to be more readily handled and isolated, Jensen and co-workers prepared [PCP]IrH_2 (**1-10**) by reduction of the [PCP]IrHCl precursor **1-8** with $LiEt_3BH$ to give the tetrahydride complex [PCP]IrH_4 **1-9**,

which when heated under vacuum lost H_2 to give the desired dihydride complex **1-10** (Scheme 1-4). Using *tert*-butyl ethylene as a hydrogen acceptor, **1-10** catalyzes the dehydrogenation of cyclooctane at a rate (TOF) of 82 min^{-1} at 150 °C. Considerable activity (20.5 min^{-1}) was also observed at 100 °C. Importantly, and in contrast to the Rh system, no decomposition of the Ir catalyst occurred in the time necessary to hydrogenate all of the hydrogen acceptor when employing excess cyclooctane.

The selective dehydrogenation of alkanes to terminal alkenes is a particularly attractive transformation since α-olefins are important precursors for a number of industrially produced compounds. However, α-olefins are the least thermodynamically stable olefin isomer, requiring researchers to develop a kinetically controlled catalytic cycle that would preferentially form α-olefins over the more thermodynamically favorable internal olefin products. Goldman and co-workers discovered that the hydrogen acceptor used in the [PCP]Ir mediated dehydrogenation of alkanes affected the secondary isomerization of the α-olefinic product.[26] Isomerization was known to occur via insertion of the terminal olefin into the Ir-H bond of [PCP]IrH_2 **1-10;** this step is the same as the first step in the hydrogenation of the hydrogen acceptor. Less sterically hindered hydrogen acceptors reacted more quickly with **1-10**, thereby decreasing the amount of terminal olefin that was isomerized. Using dec-1-ene as the hydrogen acceptor, **1-10** as the catalyst, and *n*-octane as the substrate resulted in 68% selectivity for the formation of 1-octene after 143 turnovers (Scheme 1-5). Notably, this was among the first catalytic systems to effectively perform this transformation, and was the best result obtained for the selective dehydrogenation of alkanes to terminal alkenes.

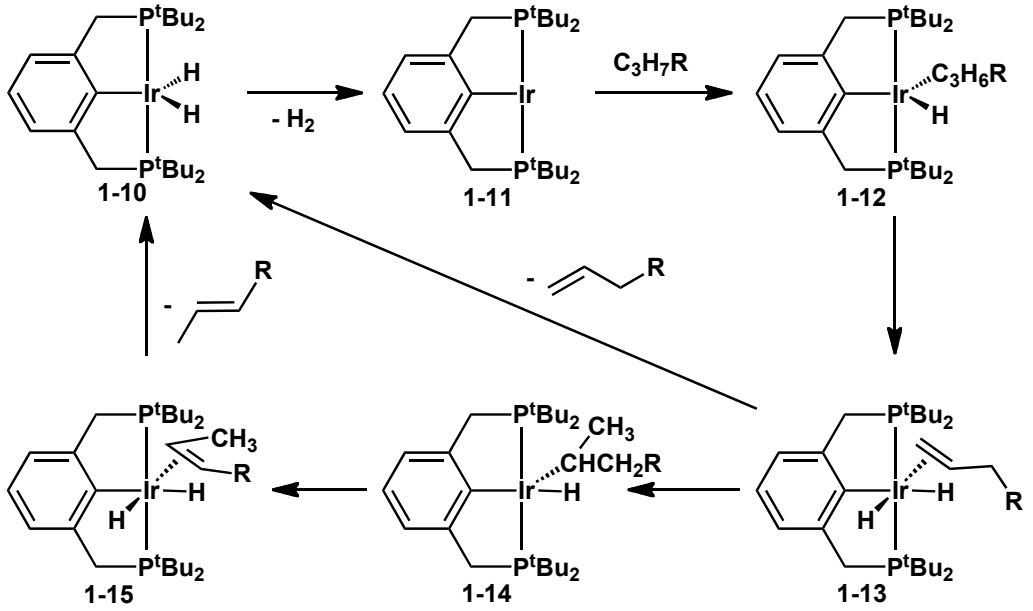

Scheme 1-5. The [PCP]Ir-mediated dehydrogenation of linear alkanes to give α-olefins.

A major advancement in the catalytic system involved circumventing the use of a hydrogen acceptor. Liu and Goldman[27] reported turnover numbers of close to 1000 for the acceptorless dehydrogenation of cyclodecane using [PCP]IrH_2 as the catalyst. The reaction required that a flow of inert gas be used to purge hydrogen through an open reflux setup as it was generated.

Despite the advances that [PCP]Ir species afforded in catalytic alkane dehydrogenation chemistry, existing catalysts remain severely limited. The known catalysts are deactivated by N_2 gas (typically the reaction atmosphere of choice) and by the presence of alkenes. Degassing the solution before heating and performing the reaction under an Ar atmosphere prevents formation of the catalytically inactive dimer, [PCP]Ir(μ-N_2)Ir[PCP], which forms upon the initial loss of H_2 from [PCP]IrH_2.[3] The exclusion of sacrificial alkenes from the reaction medium is much more difficult,

however. For reactions run in the presence of an alkene hydrogen acceptor, incremental addition of the hydrogen acceptor was shown to prevent catalyst inhibition.[3] Such a technique is not practical however for the large scale conversion of alkanes to alkenes.

Although there are limitations to the widespread application of [PCP]IrH_2 complexes as efficient catalysts for C-H bond functionalization, the basic understanding of aliphatic C-H bond activation has been advanced significantly by these discoveries. It is possible that further modification of the reaction conditions, as well as modification of the [PCP] ligand and its complexes may lead to significant improvements in the rate, selectivity, and substrate scope of this reaction. As well, more substantial changes to the pincer ligand architecture may also lead to the discovery of more active and/or more selective catalysts for C-H bond activation and functionalization. To this end, Brookhart and co-workers have shown that [POCOP]$Ir(H)_2$ ([POCOP] = 2,6-(^{t}Bu$_2$PO)$_2$C$_6$H$_4$)) achieve unprecedented rates in the dehydrogenation of alkanes.[28] It is thought that the [POCOP] ligand generates a more electron deficient metal center, thus leading to enhanced rates of reaction.

1.3.2 Catalytic transfer hydrogenation using [LCL]Ru pincer complexes.

Hydrogenation involves the addition of H_2 across an unsaturated bond in the presence of a metal catalyst. However, the use of gaseous H_2 sometimes at relatively high pressures is both expensive and inconvenient and thus alternative sources of H_2 are desired for such transformations. Transition metal catalyzed transfer hydrogenation (eq 1-1), makes use of a donor substrate such as isopropanol (usually under basic conditions)

in order to provide H_2 to an unsaturated species.[29] It is an effective reaction for the reduction of ketones and imines to alcohols and amines, respectively.

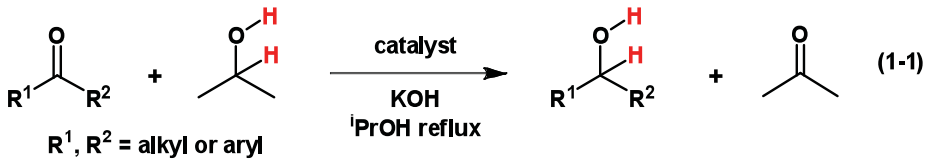

Historically, the most active catalysts for the transfer hydrogenation of ketones have been known to act via a concerted bifunctional metal-ligand process involving a Ru(H)-NH_2R intermediate, whereby the Ru center delivers H^- to the substrate and simultaneously the ligand delivers H^+ to the substrate via an N-H functionality in the ligand (Figure 1-4).[29a,b] These types of systems have led to what is known as an 'N-H effect' that is operative in transition metal catalyzed transfer hydrogenation. The requirement of an N-H group in the ligand limits the design possibilities of ligands for transfer hydrogenation catalysts. Studies on the catalytic activity of metal complexes supported by non-N-H bearing ligands could potentially lead to advances in transition metal catalyzed transfer hydrogenation chemistry.

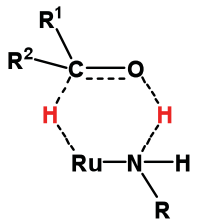

Figure 1-4. Proposed transition state in ketone transfer hydrogenation depicting metal-ligand bifunctional catalysis involving an 'N-H effect'.

The van Koten group has contributed significantly to the design and implementation of [LCL]Ru-based pincer catalysts for the transfer hydrogenation of ketones.[30] Unlike previously reported catalysts, such pincer complexes lack the ligand N-H functionality, and are therefore postulated to operate by a different mechanism. In their initial report, van Koten and co-workers showed that [PCP]- and [NCN]Ru complexes of the type [2,6-$(ECH_2)_2C_6H_3$] (E = NMe_2, **1-16**; PPh_2, **1-17**) were effective catalyst precursors for the transfer hydrogenation of ketones (Figure 1-5).[30c]

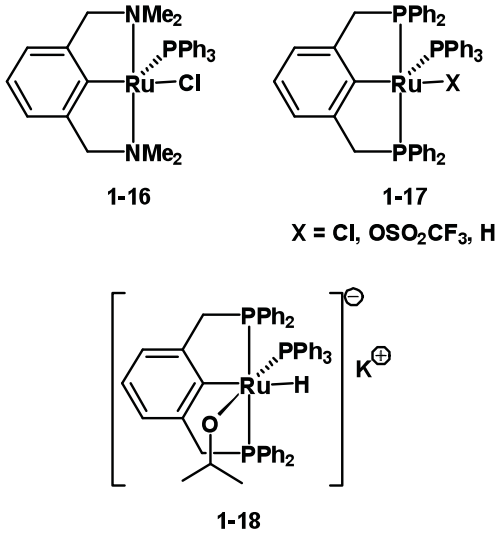

Figure 1-5. Precatalysts (**1-16** and **1-17**) and proposed 'resting state' (**1-18**) of active catalyst for transfer hydrogenation.

The experiments by van Koten utilized ^{i}PrOH as the hydrogen source in the presence of KOH, which acts as a base to assist in the generation of a Ru-O^{i}Pr species (such as **1-18**) *in situ*. Reactions were carried out at 82 °C and the best turnover frequencies for each catalyst were observed in the case of cyclohexanone as the substrate. Turnover frequencies of 1100 h^{-1} (0.1mol% catalyst), 10000 h^{-1} (0.01mol%), and 27000 h^{-1} (0.01mol%) were obtained for [NCN]RuCl(PPh_3), [PCP]RuCl(PPh_3), and

[PCP]Ru(OTf)(PPh_3) (OTf = trifluoromethylsulfonate), respectively. These results exceed the activity of the monodentate phosphine complexes $RuCl_2(PPh_3)_3$ and $RuCl(H)(PPh_3)_3$, which have been long known as reasonably effective transfer hydrogenation catalysts. It is important to note that the [NCN]Ru species were the least active catalysts under these reaction conditions.

The reactions were monitored *in situ* by ^{31}P NMR spectroscopy, and neither free PPh_3 nor 1,3-$(Ph_2PCH_2)_2C_6H_4$ were detected under catalytic conditions. It was therefore determined that the [PCP]Ru(PPh_3) unit remained intact during the course of the reaction, indicating the importance of the pincer ligand in stabilizing the catalytically active species. It has been proposed that neutral Ru^{II} hydrido complexes are the actual catalytic species in reductions involving low-valent Ru complexes.[29e] However, an anionic Ru-hydrido complex (**1-18**) was observed by ^1H and ^{31}P NMR spectroscopy in the absence of ketone substrate, the first time that such a species had been observed in transfer hydrogenation in ^{i}PrOH. Van Koten and co-workers proposed that this complex represents a resting state or 'stabilizing reservoir' for the active catalyst, which is likely the neutral [PCP]Ru(PPh_3) complex. Mechanistically (Scheme 1-6), it is proposed that the pre-catalyst **1-19** reacts with isopropoxide to give **1-20**, which in turn can undergo β-hydride elimination to give **1-21**, and subsequently the active species **1-22** upon loss of acetone. The hydride **1-22** coordinates the ketone (giving **1-23**) and this undergoes a 1,2-insertion into the Ru-H bond to give a Ru-alkoxide **1-24**, which is subsequently protonated by isopropanol and decoordinated from the metal center. The resulting Ru-isopropoxide complex **1-20** then undergoes β-hydride elimination to regenerate the catalytically active Ru-hydride.

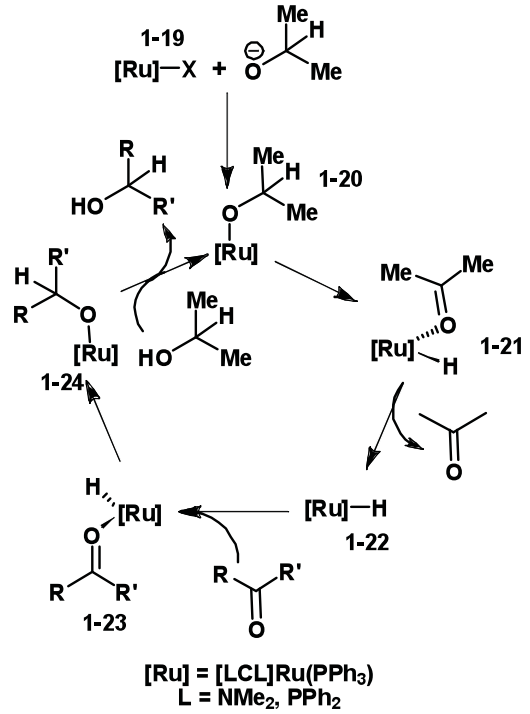

Scheme 1-6. Proposed mechanism in the [LCL]Ru-mediated transfer hydrogenation of ketones.

Electronic effects on the transfer hydrogenation activity of [PCP]Ru complexes have been studied.[30b] By changing the pincer ligand phosphine substituents it was found that ^{i}Pr and C_6F_5 substituents gave the lowest TOFs, while the *p*-MeO(C_6H_4) and the *p*-CF_3(C_6H_4) substituents gave TOFs of 8000 and 35700 h^{-1} (TOF for Ph version = 33600 h^{-1}). The steric bulk of the C_6F_5 and ^{i}Pr substituents is thought to contribute to the lower activity observed for those variants. Significantly, the *p*-CF_3(C_6H_4) substituents did not require any pretreatment time (refluxing in ^{i}PrOH with base), whereas the other complexes required a pretreatment time of 1 h to obtain good activity. As such, the higher initial activity of the *p*-CF_3(C_6H_4) substituents was likely due to faster formation of the active catalyst. Asymmetric variants of the PCP ligands were synthesized and

tested in the hydrogen transfer reaction, and although high yields were obtained, the enantiomeric excess was poor (14% ee).[30a]

In summary, ruthenium pincer complexes have been shown by the van Koten group to be effective catalysts for the transfer hydrogenation of ketones, providing both high yields of the corresponding secondary alcohols and fast rates. Facile modification of the pincer ligand has allowed for the study and comparison of ligand substituent effects, however, further studies are necessary in order to elucidate a mechanism and determine which factors most affect the reactivity. In recent years, innovations in ligand design have led to the development of even more highly active Ru catalysts for the transfer hydrogenation of ketones.[31] In this context, the effects of changing from a C-based pincer ligand to a Si-centered one were investigated. The [Ph-PSiP]RuCl(PPh_3) complex was shown to be effective in mediating the reduction of ketones using basic ^{i}PrOH as the hydrogen transfer agent and will be discussed in Chapter 2 of this document.

1.3.3 Heck olefin arylation using [PCP]Pd.

The formation of C-C bonds is a powerful transformation for organic synthesis. Transition metal complexes, most notably Pd complexes, have demonstrated a remarkable aptitude for catalyzing C-C bond forming reactions.[32] The Heck reaction (eq 1-2), which involves the coupling of an aryl halide fragment with an olefinic fragment to form a C-C bond in the presence of base, is a well established reaction that relies on complexes of Pd as catalysts.[32] Metalated monophosphine complexes have been shown to be excellent catalysts for the Heck reaction,[32c] prompting the exploration of pincer-ligated complexes as catalysts for the transformation.

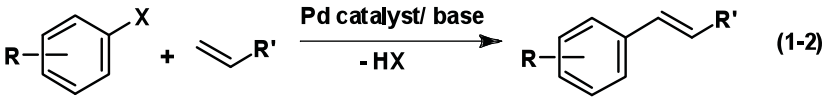

(1-2)

Pincer-ligated [PCP]Pd^{II} complexes have been shown to be very efficient catalysts for the Heck reaction, primarily due to their high thermal stability.[33] They are typically also oxygen stable, allowing for reactivity under aerobic conditions. Aryl-phosphino [PCP] variants have been studied in the context of Heck chemistry by Milstein and co-workers (e.g. **1-25** and **1-26**),[33a] while [PCP]-phosphinito complexes have been studied in this context by Jensen and co-workers (e.g. **1-27**, Figure 1-6).[33b] Milstein's catalysts were the first pincer-based catalysts reported for the Heck reaction and were able to reach TONs of over 500,000 and provide yields for unactivated aryl bromides. No catalyst degradation was observed at temperatures of 140 °C for 300 h, attesting to the thermal stability of the pincer supported complexes. Jensen's phosphinito-based pincer Pd complex displayed excellent catalytic activity with aryl chlorides, which are typically unreactive substrates for Heck chemistry relative to the corresponding aryl bromides. Jensen's catalyst also displayed excellent regioselectivity in the coupling of disubstituted alkenes with aryl bromides and iodides.

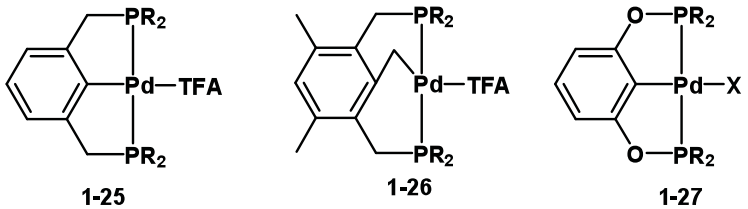

Figure 1-6. [PCP]Pd Heck reaction catalysts.

A subtle balance between steric and electronic factors clearly affects the activity of [PCP]Pd derived Heck catalysts. For example, in Milstein's studies, the benzyl-based [PCP]Pd complex **1-26** was shown to be a more reactive catalyst than the corresponding aryl-Pd species **1-25**. The more electron donating benzyl substituent leads to a more electron rich Pd center that can more readily undergo Ar-X oxidative addition. By comparison, the ^{t}Bu-phosphino substituted variant of **1-25** was shown to be less active than the corresponding ^{i}Pr-phosphino derivative, which can be attributed to increased steric crowding at the metal center due to the bulky ^{t}Bu groups.

There is considerable debate about the mechanism of the [PCP]Pd-catalyzed Heck reaction. It has long been known that Pd^{II} complexes are reduced to Pd^{0} as they enter the catalytic cycle of the Heck reaction, and Heck catalysts are classically known to follow a cycle of Pd^{0}/Pd^{II} species (Scheme 1-7).[32a] In this mechanism, the L_2Pd^{0} species (**1-28**) oxidatively adds RX to give **1-29**. Alkene coordination gives **1-30**, which in turn can insert into the Pd-R bond to give **1-31**. Subsequent β-hydride elimination gives the product and **1-32**, which reforms the active catalyst upon reductive elimination of HX. However, evidence suggests that PCP-Pd catalysts may not operate via this classical mechanism. Experiments have shown that a PCP-Pd^{0} complex may not be accessible, and instead pincer based Heck catalysts are suggested to operate via a Pd^{II}/Pd^{IV} cycle (Scheme 1-8).[33b] In this reaction, a catalyst such as **1-33** oxidatively adds a vinyl C-H bond to give a Pd^{IV} intermediate **1-34**. Reductive elimination gives **1-35**, and subsequent oxidative addition of R-X (e.g. Ar-Cl in Scheme 1-8) affords **1-36**. Reductive elimination of a C-C linkage gives the product and regenerates **1-33**. Although some

Pd^{IV} complexes are known, they are rare and isolation of a Pd^{IV} intermediate has not yet been achieved for the Heck reaction.

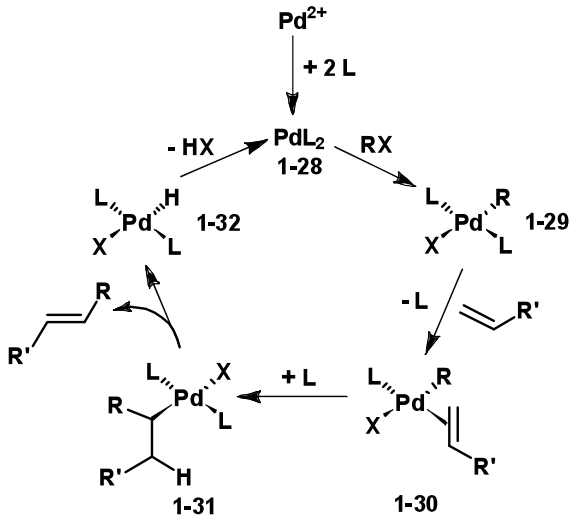

Scheme 1-7. Accepted mechanism for the Heck reaction involving a Pd^0/Pd^{II} cycle.

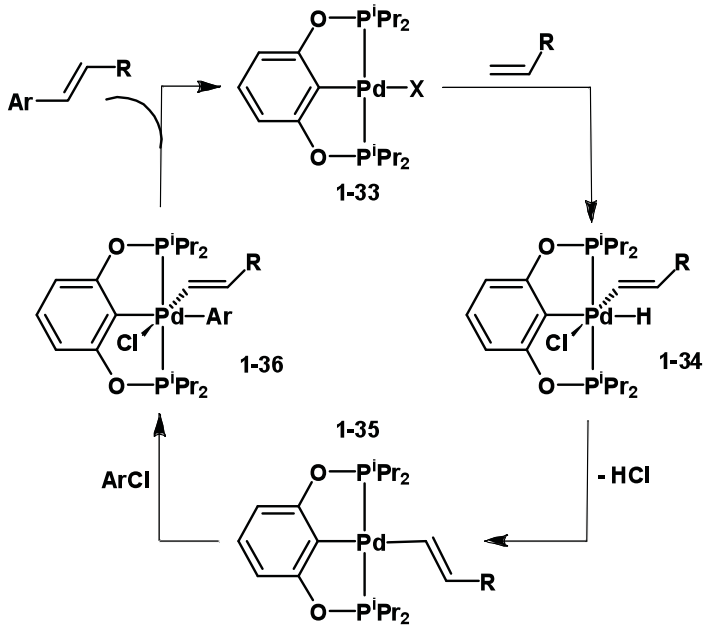

Scheme 1-8. Possible Pd^{II}/Pd^{IV} mechanism for the Heck reaction.

There are several experimental results that support a Pd^{IV} based mechanism. Bergbreiter and Sulikowski reported that the catalytic activity of a [PCP]Pd^{II} catalyst was shut down by substrates that contained a 1,4-diene moiety.[34] When a well-known Pd^0 Heck catalyst was used under the same conditions, the catalytic activity was unaffected. Coordination of the diene to Pd^{II} was believed to occur for each type of catalyst; however, in the case of [PCP]Pd^{II}, coordinative saturation – whereby all of the coordination sites at the metal center are occupied, thus preventing any further ligand association – would lead to deactivation. Also, Milstein has shown that two likely intermediates in a Pd^0/Pd^{II} pathway – [PCP]Pd-H and [PCP]Pd-Ph – do not go on to form Heck-type products upon reaction with *p*-iodoanisole and methyl acrylate, respectively, thereby supporting the hypothesis that a Pd^0/Pd^{II} pathway is unlikely.[33a] Although there has been much debate about the mechanism of [PCP]Pd-mediated Heck chemistry, recent literature has shown that pincer-Pd complexes in actuality serve as precatalysts in the Heck reaction by releasing colloidal Pd^0 nanoparticles that are the active catalysts for the transformation.[5d]

Clearly, more work needs to be done to elucidate the mechanism of [PCP]Pd^{II} complexes as Heck catalysts. Although the observations reported to date suggest a mechanism involving a Pd^{IV} intermediate the evidence for such a mechanism is not yet conclusive. The development of new pincer-based catalysts may aid in this endeavor, as new ligand architectures may, for example, facilitate the isolation of a kinetically competent Pd^{IV} intermediate.

1.3.4 [PCP]Ir-mediated activation of NH_3.

The use of ammonia in organometallic chemistry has historically been limited to the formation of simple Lewis acid-base adducts in which the lone pair on N forms a dative bond to the metal center. Activation of an N-H bond of ammonia has the potential to lead to useful new catalytic reactions. For example, many existing catalytic processes (such as hydrogenation, hydrosilylation, etc.) begin with the oxidative addition of an E-H bond (e.g. H-H, Si-H, B-H) to a metal center; transition metal catalyzed hydroamination of unsaturated substrates such as alkenes and alkynes is a known reaction, however no examples of metal catalyzed hydroamination using ammonia are known. Such a reaction would be a powerful synthetic tool for the synthesis of new amines, and Haggin[35] has recently pointed out that reactions of ammonia have been identified as two of the top ten catalytic challenges facing chemists, emphasizing the importance of ammonia activation under mild conditions as a precursor to the development of catalytic systems requiring N-H oxidative addition as the initial step.

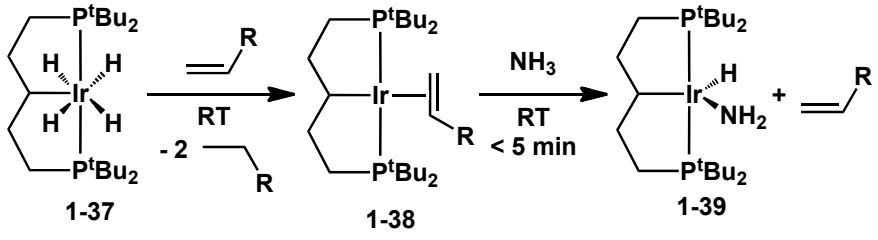

Scheme 1-9. Activation of ammonia by [PCP]Ir.

In this context, Ir-pincer complexes have shown the ability to activate the N-H bond of ammonia. Hartwig and co-workers made a breakthrough contribution in 2005

when they reported that a [PCP]Ir-olefin complex ([PCP] = [2,6-(^{t}Bu$_2$P(CH$_2$)$_2$)$_2$CH]) oxidatively adds ammonia at room temperature to give [PCP]Ir(H)(NH$_2$) with concomitant olefin displacement (Scheme 1-9).[36] The group had previously reported that the amido hydride complex [2,6-(^{t}Bu$_2$PCH$_2$)$_2$C$_6$H$_3$]Ir(H)(NH$_2$) (**1-41**), which is produced at low temperature by the reaction of [2,6-(^{t}Bu$_2$PCH$_2$)$_2$C$_6$H$_3$]Ir(H)(Cl)(NH$_3$) (**1-40**) with KN(SiMe$_3$)$_2$, reverted to the ammonia Lewis base adduct **1-42** upon warming to room temperature (Scheme 1-10).[37] It was hypothesized that a more electron rich metal center would favor the formation of the N-H oxidative addition product. This was achieved by altering the ligand framework such that it possessed an aliphatic rather than an aromatic backbone. Thus, the synthesis of [PCP]IrL ([PCP] = [(^{t}Bu$_2$P(CH$_2$)$_2$)$_2$CH]; L = olefin) provided a complex capable of cleaving the N-H bond of ammonia. When ammonia was reacted with the [PCP]Ir-olefin complex **1-38** (prepared from **1-37**, Scheme 1-9), release of the olefin and activation of NH$_3$ was observed in under five minutes at room temperature.

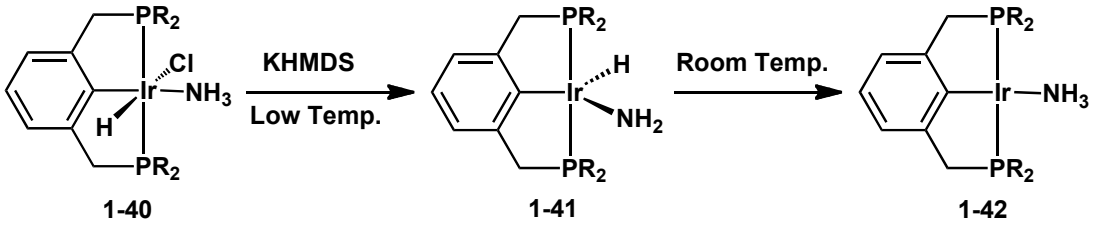

1-40 1-41 1-42

Scheme 1-10. Formation of **1-41** from **1-40** at low temperature, followed by formation of **1-42** upon warming to room temperature.

While the subsequent reactivity of [PCP]Ir(H)(NH$_2$) species remains to be explored, the Hartwig group has recently extended N-H activation chemistry to the N-H

oxidative addition of hydrazine derivatives using both aliphatic and aromatic [PCP]Ir complexes. Depending on the hydrazine substrate used, single or double N-H activation is possible, leading to the formation of hydrido hydrazido complexes or aminonitrene complexes with the loss of H_2, respectively.[38]

The development of alternative late metal pincer complexes that are able to mediate N-H bond activation chemistry remains a challenge. The increased σ-donating ability of Si relative to C should provide a more electron rich metal center that is better situated electronically to favor oxidative addition of ammonia. To this end, our group has recently shown that the [Cy-PSiP]IrH(Cl) **1-43**, which features a highly *trans*-labilizing and electron-donating central silyl donor in the pincer ligand backbone, is a precursor to N-H bond cleavage of anilines and amines including ammonia (Scheme 1-11).[39] Reaction of **1-43** with RLi (R = CH_2SiMe_3 or CH_2CMe_3) generates the alkyl hydride complex [Cy-PSiP]IrH(R) (**1-44**), which rapidly reductively eliminates RH to generate the Ir^I intermediate "[Cy-PSiP]Ir" (**1-45**). When exposed to an atmosphere of ammonia this 14-electron intermediate is able to cleave an N-H bond at room temperature resulting in the formation of the isolable amido hydride complex [Cy-PSiP]Ir(H)(NH_2) (**1-46**). This result confirms the hypothesis that pincer ligands featuring increased electron donation from a central silyl donor can promote oxidative addition of inert E-H (E = main group element) bonds.

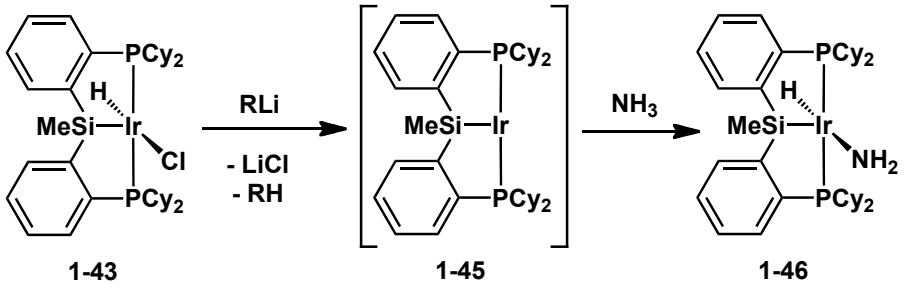

1-43 1-45 1-46

Scheme 1-11. Oxidative addition of an N-H bond of ammonia by [Cy-PSiP]Ir[I].

1.4 The Development of Complexes Employing [LNL] Based Ligands

In an effort to extend the chemistry of transition metal pincer complexes, and due to the success of the [LCL] framework, [LNL] pincer ligands that feature a central amido donor have been developed.[5c,13,40] The chemistry of complexes supported by these new amido pincer-type ligands was anticipated to be quite different from that of the related [LCL] complexes. One of the main differences between [LNL] and [LCL] ligation is the presence of a lone pair of electrons on the amido nitrogen that is available for donation to the metal center. Amido ligands of this type were initially developed in the context of early transition metal chemistry, as such highly Lewis acidic and electron deficient metal centers can readily undergo π-bonding to the amido donor.[41] However, in recent years the ability of such ligands to stabilize reactive late metal complexes has also been demonstrated.

Contrary to the popular methods of [LCL] complex formation, transmetalation is the most common method of delivery of an [LNL] ligand to a transition metal. Most commonly the [LNL]Li salt is used to deliver the ligand to a metal center.[12] However,

examples of N-H and N-C oxidative addition from [LNL]H and [LNL]Me, respectively, have been reported by Ozerov and coworkers.[40]

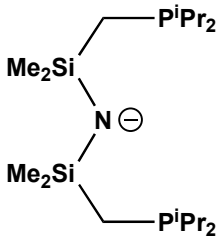

1-47

Figure 1-7. Fryzuk's [PNP] amido ligand [(^{i}Pr$_2$PCH$_2$SiMe$_2$)$_2$N]$^-$ **1-47**.

Fryzuk was the earliest major contributor to the field of [LNL] transition metal chemistry with his design of the [PNP] amido ligand [(Ph$_2$PCH$_2$SiMe$_2$)$_2$N] (Figure 1-7, **1-47**).[41] In the early 1980s, Fryzuk observed that the combination of a 'hard' amido donor and 'soft' phosphine donors was ideally suited for stabilizing a variety of both early and late transition metal amido complexes. Most notably, reactive Zr, Rh, Ir, Ni, Pd, and Pt [PNP] complexes were reported.[41] Remarkably, Fryzuk and coworkers were able to demonstrate that [PNP]ZrCl$_3$ can be reduced with sodium amalgam under a nitrogen atmosphere to give the dimeric species ([PNP]ZrCl)$_2$(μ-N$_2$) (eq 1-3, **1-48**), in which the bridging N$_2$ fragment has been reduced by four electrons.[42] Furthermore, the N$_2$ fragment is coordinated in an unusual 'side-on' fashion to the Zr centers. This reaction represents an important first step in the reduction and functionalization of dinitrogen.

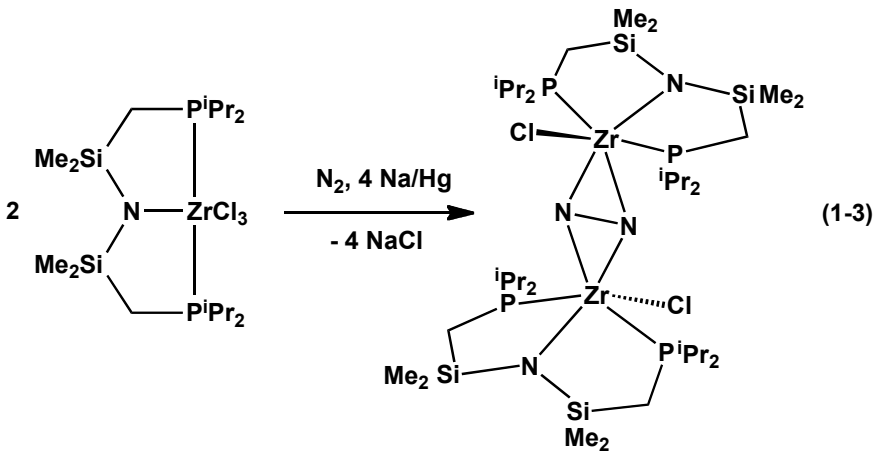

1-48

Since Fryzuk's early contributions to [LNL] pincer chemistry, many other research groups have shown that [LNL] complexes exhibit a rich reaction chemistry. Using Fryzuk's ligand with Ru, Caulton was able to synthesize an isolable, electronically unsaturated 14-electron Ru^{II} complex.[43] The recent evolution of Fryzuk's ligand to a more rigid [PNP] framework featuring an *o*-arylene backbone has attracted significant attention with the research groups of Liang,[44] Ozerov,[40] and Mindiola[45] among those that have most extensively studied this ligand. Derivatives whereby the phosphine donor groups are replaced with amines ([NNN])[46] or N-heterocyclic carbenes ([CNC])[47] have also recently been developed. Pyridyl derivatives that can be readily dearomatized in the presence of base to give anionic [PNN] ligands have been developed by Milstein, and [PNN] complexes of this type are efficient catalysts for the transformation of alcohols and amines directly into organic amides.[4] These contributions are highlighted in detail below.

1.4.1 The synthesis of 14-electron, square planar [PNP]Ru^{II} complexes.

The isolation of coordinatively and electronically unsaturated transition metal complexes is difficult because of the inherent reactivity of such species. However, the systematic study of stabilized low-coordinate complexes is worthwhile because it can provide insight into reaction mechanisms, as most catalytic reactions are proposed to access unsaturated, reactive intermediates at some point during their catalytic cycle. Examples of isolable, low-coordinate complexes typically feature ligands that impart stabilizing features such as π-donation, steric bulk, or agostic interactions on the metal center. Two examples from the recent literature that best exemplify the incorporation of these ligand design features are the square planar [R-PNP]RuCl complexes from the groups of Caulton ([$SiMe_2$-PNP] = ($^tBu_2PCH_2SiMe_2)_2N$, **1-49**)[43] and Schneider ([CH_2-PNP] = ($^tBu_2P(CH_2)_2)_2N$, **1-50**).[48] Isolable, 14-electron Ru^{II} complexes are very rare and it was long thought that some degree of agostic interaction was necessary for the stabilization of such unsaturated species.[49] However, Caulton and Schneider have shown that such highly unsaturated complexes can instead be stabilized by π-donation from an amido-centered [PNP] ligand. Additionally, the comparison of **1-49** and **1-50** provides an excellent example of fine tuning the electronic properties at a metal center through subtle changes in the ligand design.

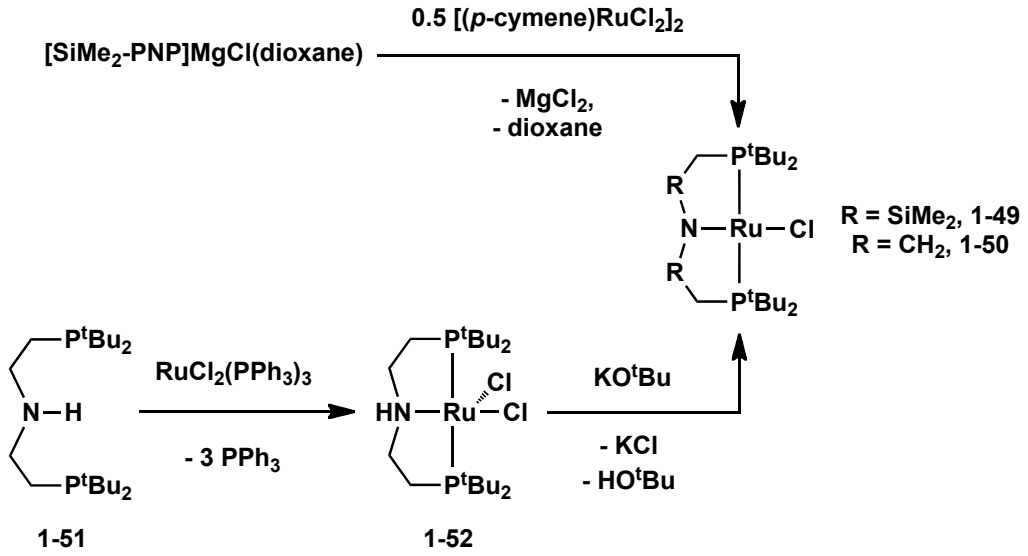

Scheme 1-12. Synthesis of the four-coordinate square planar [PNP]RuCl complexes **1-49** and **1-50**.

Complexes **1-49** and **1-50** were obtained via substantially different synthetic routes as outlined in Scheme 1-12. The synthesis of complex **1-49** requires reaction of [$SiMe_2$-PNP]MgCl(dioxane) with [(cymene)$RuCl_2$] to give the four-coordinate complex. Reaction of the amine **1-51** with $RuCl_2(PPh_3)_3$ results in the formation of the amino-dichloride complex [CH_2-PNP-H]$RuCl_2$ (**1-52**), which forms **1-50** upon reaction with KO^{t}Bu. Unlike previous examples of four-coordinate Ru^{II} complexes that have a *cis*-divacant octahedral structure and feature agostic interactions to stabilize the low-coordinate structures,[50] **1-49** and **1-50** are rare examples of square planar, formally 14-electron Ru^{II} complexes, with no indication of agostic interactions with the ^{t}Bu substituents on phosphorus. Despite the structural similarities, the two complexes are electronically quite different as **1-49** is shown to be paramagnetic, which is very unusual for a complex of Ru^{II} (the presence of two unpaired electrons is confirmed by magnetic measurements), while **1-50** is a diamagnetic complex.

To help explain the difference in the spin states of **1-49** and **1-50**, Figure 1-8 depicts three simplified d-orbital splitting diagrams for [PNP]RuCl. Splitting pattern A represents a complex that has no N-Ru π-interaction. Splitting pattern B represents a complex with a moderate N-Ru π-interaction, which raises the energy of the d_{yz} orbital above that of the d_{z2}. However, the ΔE for d_{yz} and d_{z2} is less than the pairing energy resulting in half population of each orbital (triplet state). Splitting pattern C represents a complex with a strong N-Ru π-interaction, which further raises the energy of the d_{yz} orbital. In this case the ΔE is greater than the pairing energy and the electrons therefore both occupy the d_{z2} orbital (singlet state). Clearly, splitting pattern B is consistent with **1-49**, which features a disilylamido donor and is characterized as a paramagnetic complex. Splitting pattern C is consistent with **1-50**, which features the more strongly π-donating (in comparison to **1-49**) dialkylamido ligand and is characterized as a diamagnetic complex. It should also be pointed out that the orbital best suited for an agostic interaction (d_{x2-y2}) is too high in energy and sterically inaccessible for the ^{t}Bu groups to access.

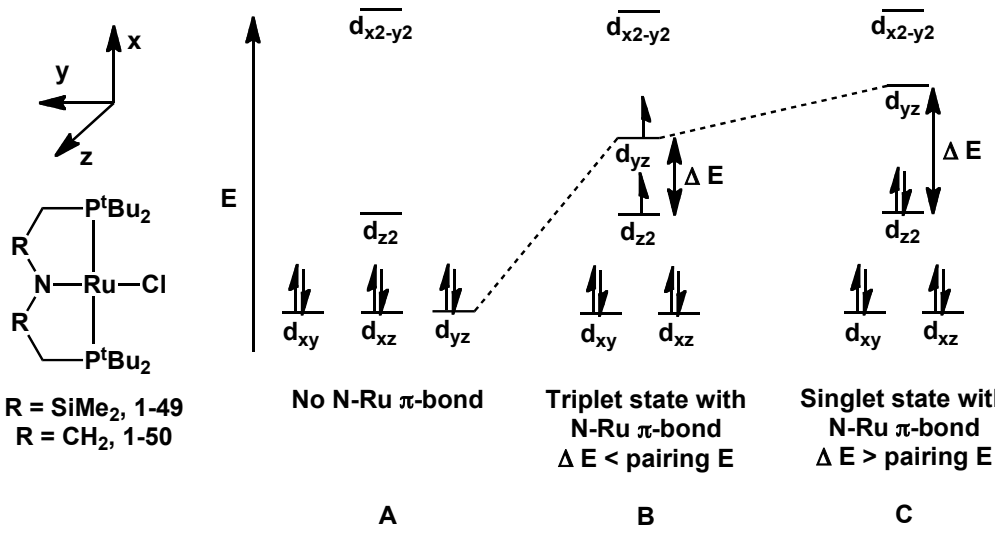

Figure 1-8. A simplified d-orbital splitting diagram for [PNP]RuCl showing three separate bonding possibilities. The molecule exists in the triplet state with a N-Ru π-bond.

1.4.2 A novel pincer ligand rearrangement featuring a Co_2N_2 diamond core.

In order to achieve the goal of synthesizing and isolating a reactive low-coordinate transition metal species it is essential to somehow stabilize the target molecule. Some general approaches involve using bulky, electron donating ligands to prevent dimerization, for example. Agostic interactions and π-donation from appropriate donors are also good stabilization strategies, although these types of metal-ligand interactions can be somewhat more difficult to purposely incorporate into a complex. A key principle in designing ancillary ligands that can support reactive, low-coordinate metal centers is that the stabilizing features that are incorporated into the ligand (i.e. π-donors, bulky substituents, etc.) must be sufficient for allowing the synthesis and/or isolation of the desired complex, but not so stabilizing that the resulting complex is rendered inert. Thus, an ideal strategy is to engineer an ancillary ligand that can

somehow undergo a rearrangement process that effectively, and reversibly, 'masks' a highly reactive low-coordinate transition metal species. Although in most transition metal complexes ancillary ligand rearrangement is typically undesired, such a rearrangement can be beneficial if it is reversible in a controlled manner.

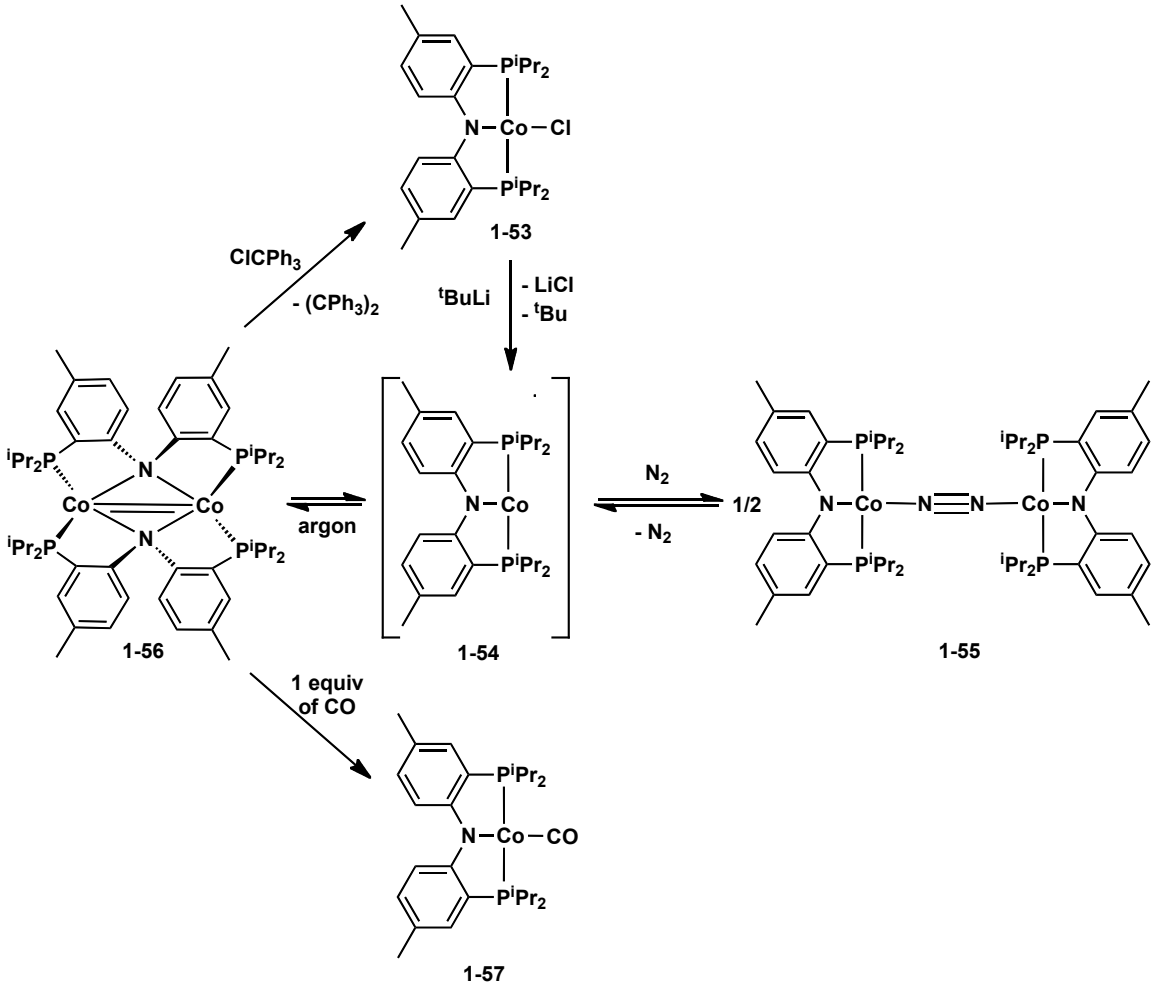

Scheme 1-13. Monomer-dimer equilibrium in [PNP]Co chemistry.

An example of a reversible [PNP] pincer ligand rearrangement resulting in the formation of a masked low-coordinate Co^{I} fragment (Scheme 1-13, **1-56**) has been reported by Mindiola and co-workers.[45] The researchers were able to synthesize the precursor [PNP]CoCl (**1-53**) by reaction of Li[PNP] and $CoCl_2$. The one electron

reduction of [PNP]CoCl with ^{t}BuLi under an N_2 atmosphere yields the unobserved intermediate [PNP]Co^I (**1-54**), which forms the N_2 adduct ([PNP]Co)$_2$(μ^2-N_2) (**1-55**). However, when the reaction is carried out under an argon atmosphere, the formation of a ([PNP]Co)$_2$ dimer (**1-56**) is observed, which appears to be a resting state for the low-coordinate complex [PNP]Co^I. The solid state structure of dimeric ([PNP]Co)$_2$ features a Co_2N_2 diamond core in which the [PNP] ligand amido N atom is bridging between the Co^I centers. This rearrangement of the pincer ligand is unusual in the context of transition metal pincer chemistry, as the more commonly utilized [PCP] pincer frameworks do not typically support such a bridging structure. However, given that an amido N donor features an additional lone pair of electrons, such a bridging structure is not uncommon for metal amido complexes. The ([PNP]Co)$_2$ dimer **1-56** behaves as a masked source of the highly reactive, three coordinate species [PNP]Co^I **1-54**. For example, exposure of **1-56** to an N_2 atmosphere leads to formation of **1-55**. Similarly, the reaction of **1-56** with one equivalent of CO leads to the formation of the four-coordinate Co^I CO adduct [PNP]Co(CO) **1-57**, while the reaction with $ClCPh_3$ leads to regeneration of the Co^{II} species [PNP]CoCl (**1-53**, Scheme 1-13).

Mindiola's report of a novel arrangement of a [PNP] pincer ligand in order to stabilize a reactive metal center clearly demonstrates that appropriately designed pincer ligands are able to attain unusual bonding structures in order to stabilize reactive metal centers. In particular, the incorporation of a heteroatom (in place of C) bearing an additional lone pair of electrons leads to the possibility of forming dinuclear structures that may serve to mask highly reactive monomeric intermediates. The rigid and strained nature of the ligand framework, as well as steric crowding from the P substituents, likely

contribute to the reversible nature of this ligand rearrangement. It is possible that reorganizations of this type may play a role in the mechanisms of catalytic reactions mediated by such pincer complexes.

1.4.3 [PNL]Ru-catalyzed synthesis of esters, amides, and imines.

The contributions the Milstein group has made to the chemistry of late metal [PNL] (L = NR_2 or PR_2) complexes cannot be overstated. In the last decade alone the group has used [PNL] complexes for the synthesis of a rare example of a Pt^{IV}-oxo complex,[51] the evolution of H_2 and O_2 from water,[52] and the N-H activation of amines and ammonia.[53] Some of the most noteworthy contributions from the group have been toward the catalytic synthesis of small organic molecules, such as ketones,[54] esters,[55] amides,[4] amines,[56,57] imines,[57] and acetals[58] mediated by [PNL]Ru complexes. Due to the large amount of work on [PNL]Ru-mediated transformations from the group, this section will focus on the catalytic synthesis of amides, imines, and esters in order to best highlight the ligand design features that lead to the results obtained.

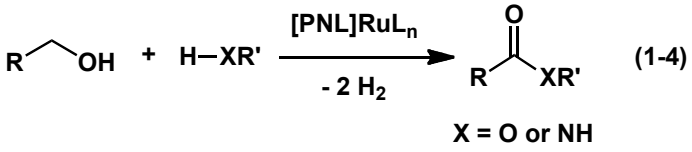

(1-4)

The development of economical and environmentally safe synthetic routes to commonly utilized reagents is an area of considerable interest in the chemical industry. Traditional syntheses of esters and amides require reaction of activated carboxylic acid derivatives (e.g. acyl chlorides, acid anhydrides) with an alcohol or amine, respectively.

These reactions often require large amounts of expensive and often highly toxic condensing reagents and activators such as dicyclohexylcarbodiimide (DCC), phenyl dichlorophosphate, and diethyl azodicarboxylate. Ideally, a catalyst would be able to dehydrogenatively couple two alcohols to form an ester or an alcohol and an amine to give an amide (eq 1-4). Examples of transition metal complexes that dehydrogenate alcohols to ketones are known,[54] but these reactions almost always require a hydrogen acceptor. The requirement of a sacrificial molecule reduces the atom efficiency of a reaction. The Milstein group has been able to avoid the need for a sacrificial hydrogen acceptor by designing a substituted pyridyl ligand that is able to undergo dearomatization at the *o*-benzyl position (eq 1-5), which promotes the acceptorless loss of H_2 thus allowing for catalytic turnover. In addition to this metal-ligand cooperativity, [PNL]Ru systems in which L = NR_2 have the added feature of hemilability, whereby the weak amine donor can dissociate from the Ru center to provide a vacant coordination site for substrate binding.

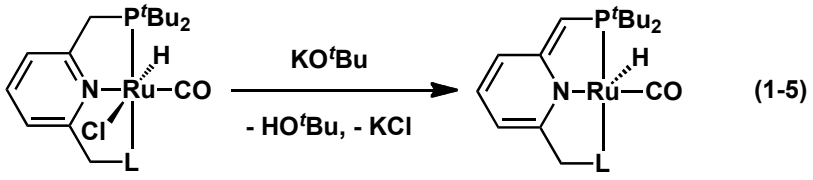

1-58a, L = NEt_2
1-58b, L = P^{t}Bu$_2$

1-59a, L = NEt_2
1-59b, L = P^{t}Bu$_2$

(1-5)

The syntheses of the precatalyst complexes **1-58** (**1-58a**, L = NEt_2; **1-58b**, L = P^{t}Bu$_2$) are achieved by reaction of 2-(^{t}Bu$_2$PCH$_2$)-6-(Et_2NCH_2)py or 2,6-(^{t}Bu$_2$PCH$_2$)$_2$py (py = pyridine) with $RuHCl(CO)(PPh_3)_3$.[4,57] Complexes **1-58** react with one equivalent

of KO^{t}Bu to yield the dearomatized compounds **1-59** (eq 1-5), which result from deprotonation at a benzylic position (in the case of **1-58a**, deprotonation only occurs at the benzylic phosphine arm). When the resulting hydrido carbonyl complexes **1-59** are reacted with H_2, the benzylic arm is reprotonated and the [PNL]Ru$(H)_2$(CO) (**1-60**) complexes are formed (i.e. the dihydrido analogs of **1-58**). Significantly, the dihydride complexes lose H_2 at room temperature to revert back to **1-59**. The acceptorless loss of H_2 under mild conditions is the unifying feature of Milstein [PNL]Ru complexes making them ideal catalysts for dehydrogenative coupling reactions involving alcohols.

The isolated [PNN]Ru(H)(CO) complex **1-59a** functions as an efficient precatalyst for the acceptorless dehydrogenative esterification of alcohols (Scheme 1-12).[55] Ester yields of over 90 % (TON > 900, Table 1-1) were obtained from primary alcohols in relatively short reaction times utilizing 0.1 mol% of catalyst under reflux conditions. The mechanism of the reaction is proposed to proceed by initial dehydrogenation of the alcohol by **1-59** to give the corresponding aldehyde and [PNN]Ru$(H)_2$CO **1-60** (Scheme 1-14). Hemiacetal formation from the aldehyde and a second equivalent of alcohol is then followed by dehydrogenation (involving **1-62**) to give the desired ester.

Table 1-1. Dehydrogenation of primary alcohols to esters and H_2[a].

KOH (equiv)	Alcohol	Temp (°C)	Time (h)	Conversion (%)	Ester Yield (%)
0	1-butanol	117	5	91	90
0	1-hexanol	157	2.5	91.5	91.4
0	1-hexanol	115[b]	6	99	99
0	benzyl alcohol	115[b]	4	93.2	92.1

[a] 0.01 mmol KOH, 0.01 mmol catalyst, and 10 mmol alcohol were heated neat under Ar flow. [b] 2 mL of toluene was added, and the solution was refluxed.

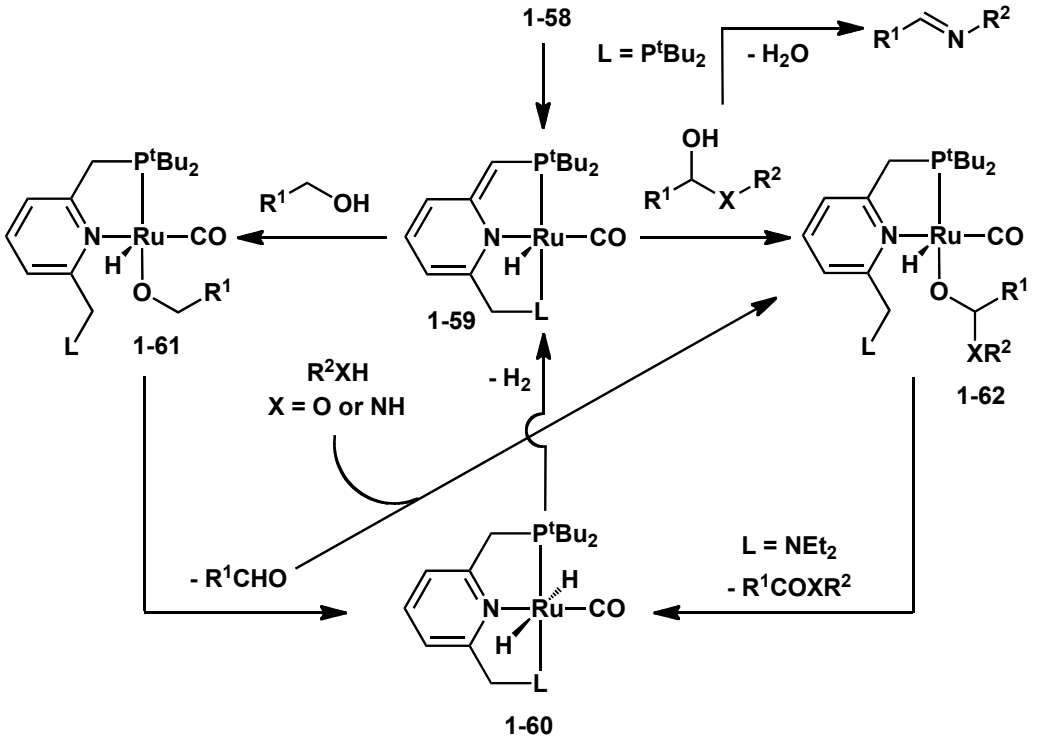

Scheme 1-14. [PNN]Ru-catalyzed dehydrogenative coupling of alcohols to form esters.

The catalyst **1-59** was also shown to similarly catalyze the direct synthesis of amides from the corresponding alcohols and amines (X = NH, Scheme 1-14).[4] In the proposed mechanism the primary alcohol is first dehydrogenated to give the corresponding aldehyde, which, upon reaction with the amine, yields a hemiaminal. This hemiaminal is then dehydrogenated to yield the desired amide by a mechanism similar to that proposed for the [PNN]Ru-mediated ester synthesis. In the case of [PNP]Ru, the formation of intermediate **1-62** is disfavored, and the reactive hemiaminal goes on to lose water resulting in the formation of an imine rather than an amide. This result provides evidence that dissociation of the hemilabile amine arm in [PNN]Ru species plays a significant role in amide synthesis.[57]

Milstein's system is an excellent example of how simple ligand modification (i.e. substituting a phosphine donor for an amine) can drastically change the reactivity of a pincer complex. The ability to shuttle H_2 via reversible dearomatization of the pyridyl ligand backbone is a key component of [PNN]Ru complexes allowing them to act as effective catalysts in dehydrogenative coupling reactions.[53-58] Furthermore, the stability of the dearomatized form of the [PNL] complex **1-59** is significant because this allows for the release of H_2 to regenerate the catalytically active species. This chemistry provides yet another example of how pincer ligand modification can result in the isolation of unusual and highly reactive complexes that are able to mediate new catalytic transformations.

1.5 Towards the Synthesis and Reactivity of Ru and Pd Pincer Complexes Featuring Formally Anionic Heavier Main Group Element Donors

The use of strategically engineered ancillary ligands to influence and fine tune transition metal reactivity is a useful method for the development of novel and/or improved reactivity. The examples highlighted thus far clearly indicate that pincer ligands have the ability to support a wide variety of transition metal complexes. Significantly, these complexes have thus far shown both interesting structural and bonding features, as well as the ability to mediate new and useful reactions, both stoichiometrically and catalytically. Despite the reactivity advances that have been described in the previous sections, numerous opportunities for improvement and innovation still exist in transition metal pincer chemistry.

There are many features of the pincer ligand architecture that can be rationally modified in order to bring about changes in the reaction chemistry of the corresponding metal complexes. A number of advantageous design features for pincer ligands have been highlighted, including ligand rigidity and the incorporation of electron-rich donors. The incorporation of such elements into the design of a pincer ligand can be exploited in the targeted synthesis of low-coordinate, electronically unsaturated metal complexes that are able to participate in aggressive bond activation reactions, such as the oxidative addition of E-H bonds (E = main group element).

In this context, research in the Turculet group targets the synthesis of transition metal complexes supported by new pincer ligands that feature previously under-explored, formally anionic heavier main group element donors (e.g. Si, P). While significant effort has been devoted to the synthesis of new types of pincer complexes, alterations to the

pincer ligand architecture have been limited to variation of the L donor atoms and the pincer ligand backbone; by comparison, the central anionic donor (X) has largely been restricted to the elements C and N. It is anticipated that novel ligand architectures that incorporate silyl ($M\text{-}SiR_3$) and phosphido ($M\text{-}PR_2$) groups as the central X donors in a pincer ligand framework will impart unique reactivity properties to the ensuing complexes, leading to new applications in synthesis and catalysis. For example, the increased electron-donating character of Si relative to C is anticipated to lead to a more electron-rich late metal center, thereby promoting the oxidative addition of typically unreactive substrates such as hydrocarbons. In addition, the strong *trans*-labilizing ability of Si can better promote the generation of reactive, coordinatively unsaturated complexes. In the case of P, while the reduced electronegativity relative to N should also promote the formation of electron-rich late metal phosphido species, the decreased propensity for forming π-bonds to P may lead to a higher degree of electronic unsaturation relative to structurally related metal amido ($M\text{-}NR_2$) complexes.

The following chapters will detail the syntheses of [R-PSiP] (R = Cy, Ph) bis(phosphino)silyl and [NPN] bis(amino)phosphido pincer ligand precursors, as well as progress made in developing the coordination chemistry of [R-PSiP] and [NPN] derivatives. This includes the synthesis and characterization of a variety of coordinatively and electronically unsaturated [R-PSiP]Ru complexes, a selection of which were studied computationally in order to examine the role that the [R-PSiP] ligand plays in determining the geometry and stability of the complexes. We have shown that [R-PSiP]Ru species are active catalysts for the transfer hydrogenation of ketones to secondary alcohols, which indicate that [R-PSiP]Ru derivatives have significant potential

in catalysis. The synthesis and characterization of a number of dimeric [NPN]Pd complexes will also be discussed. The catalytic activity of such species in the Heck coupling of aryl halides with ethyl acrylate was studied, and these studies have shown that such dimeric complexes are effective pre-catalysts for C-C coupling reactions. Future studies in the areas of both [R-PSiP] and [NPN] Ru chemistry will also be described.

Chapter 2: Synthesis, Characterization, and Reactivity of Ru^{II} Complexes Supported by a Bis(diphenylphosphino)silyl Ligand ([Ph-PSiP])

2.1 Introduction

Cyclometalated phosphine-based [PCP] and [PNP] pincer complexes of the platinum group metals have been the subject of intense research in recent years, owing to the remarkable stoichiometric and catalytic reactivity exhibited by such complexes.[3,5,36] With the goal of discovering new metal-mediated reactivity patterns and extending the versatility of metal pincer chemistry, significant effort has been devoted to the synthesis of structurally and/or electronically related systems where strategic alterations have been introduced to the pincer ligand architecture, including variation of the central and peripheral donor fragments, as well as the ancillary ligand backbone.[4,5,13,40,41] In this context, research in the Turculet group targets the synthesis and study of pincer-like metal complexes supported by new tridentate ancillary ligands featuring formally anionic heavier main group element donors, in anticipation that such novel ligand architectures will impart unique physical and reactivity properties to the ensuing complexes.

In this chapter, the synthesis of the bis(phosphino)silyl pincer ligand precursor $[(2\text{-}Ph_2PC_6H_4)_2SiMe]H$ ([Ph-PSiP]H) and the preparation of [Ph-PSiP]Ru complexes are described. Although metal-silicon chemistry is well-precedented across the transition series,[59] relatively little attention has been given to the incorporation of silyl donor fragments into the framework of a preformed tridentate ancillary ligand.[60] A notable exception is the work of Stobart and co-workers,[61] who have reported late transition metal complexes featuring bi-, tri-, and tetradentate phosphinosilyl ligands (Figure 2-1).

In addition, Tilley and co-workers[62] have recently reported late metal complexes featuring a rigid, tridentate [NSiN] ligand framework (Figure 2-1). While it has been proposed that the incorporation of strongly electron donating and *trans*-labilizing silyl groups into multidentate ligand architectures may promote the formation of coordinatively unsaturated complexes that exhibit enhanced reactivity properties, the catalytic utility of metal complexes supported by such ancillary ligands has not been widely demonstrated.[62c,63]

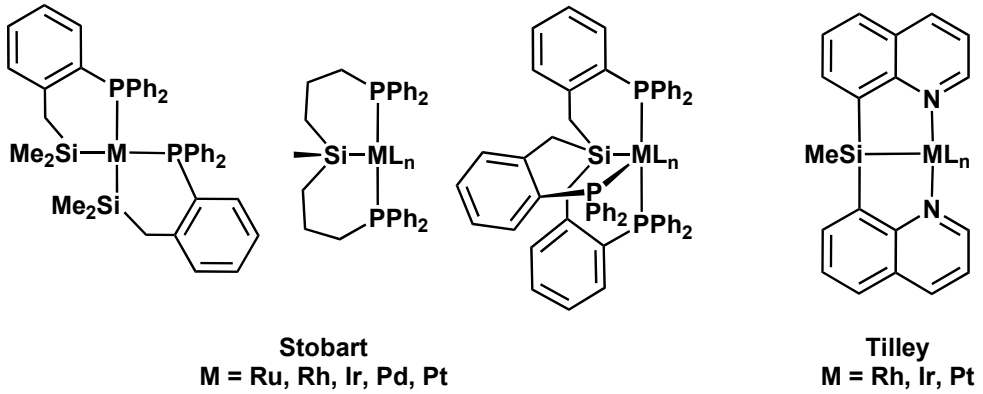

Figure 2-1. Previously reported bi-, tri-, and tetradentate phosphinosilyl complexes.

In contrast to the phosphinosilyl complexes previously reported by Stobart and co-workers that feature an aliphatic or benzylic ligand backbone,[61] it was anticipated that the reduced conformational flexibility associated with the rigid *o*-phenylene backbone of [Ph-PSiP] could provide enhanced stability and selectivity in metal-mediated substrate transformations. The lack of β-hydrogens within the *o*-phenylene backbone also eliminates the possibility of ligand decomposition via a β-hydride elimination pathway. Furthermore, although the bis(quinolyl)silyl ligand reported by Tilley and co-workers[62]

possesses a very rigid pincer framework, this design offers little opportunity for studying substituent effects at the quinolyl-N donor atoms. Additionally, phosphino substituents are anticipated to be more compatible with the electron rich Ru^{II} center.

The studies described herein have established that [Ph-PSiP]Ru complexes show a propensity for E-H bond activation (E = C, Si, N, B, etc) and are promising catalysts for the transfer hydrogenation of ketones to the corresponding secondary alcohols. This work represents one of the first applications of silyl pincer-type complexes in catalysis.

2.2 Results and Discussion

2.2.1 Ligand synthesis.

Tertiary bis(phosphino)silanes are effective ligand precursors for the installation of bis(phosphino)silyl ligands, as the Si-H bond can oxidatively add to an electron-rich transition metal center with relative ease in order to produce the desired cyclometalated complexes. The general synthetic route developed in the Turculet group for the synthesis of bis(phosphino)silane ligand precursors is outlined in Scheme 2-1. The phosphino donor is first installed by way of a Pd-catalyzed P-C bond forming reaction employing commercially available 2-bromoiodobenzene and a secondary phosphine to give the corresponding 2-bromo(phosphino)benzene derivative. The synthesis of 2-bromo(diphenylphosphino)benzene (96% yield) was accomplished in this manner, utilizing $Pd(PPh_3)_4$ (0.5 mol %) as catalyst and Et_3N (1.2 equiv) as base.[64] The phenyl-substituted bis(phosphino)silane $[(2\text{-}Ph_2PC_6H_4)_2SiMe]H$ ([Ph-PSiP]H, **2-1**) was obtained by lithiation of 2-bromo(diphenylphosphino)benzene with ^{n}BuLi, followed by in situ treatment with 0.5 equiv of $MeSiHCl_2$ (Scheme 2-1). Isolated **2-1** was obtained as a

peach-colored solid in 90% yield. The ^{1}H NMR spectrum of **2-1** (benzene-d_6) features a multiplet at 6.03 ppm corresponding to the Si-*H*, as well as a doublet at 0.81 ppm ($^{3}J_{HH}$ = 3 Hz) corresponding to the silyl methyl substituent. The ^{31}P NMR resonance of **2-1** is found at -10.9 ppm, while the ^{29}Si NMR resonance appears at -23.2 ppm (benzene-d_6).

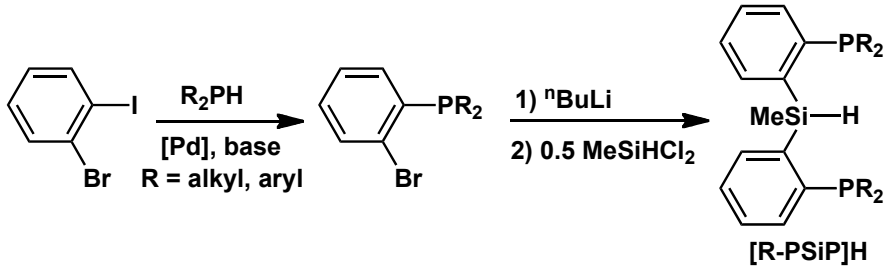

Scheme 2-1. General synthetic scheme for bis(phosphino)silane ligand precursors.

2.2.2 Synthesis and characterization of [Ph-PSiP]RuCl(PPh$_3$) (2-2).

Treatment of **2-1** with $RuCl_2(PPh_3)_3$ in the presence of Et_3N resulted in quantitative (by ^{31}P NMR) formation of the cyclometalated 16-electron Ru complex **2-2**, which was isolated in 89% yield (eq 2-1). The X-ray crystal structure of **2-2**·$(OEt_2)_{1.5}$ (Figure 2-2) confirms the formation of a five-coordinate *fac*-[Ph-PSiP] complex with distorted square-pyramidal geometry at Ru, in which a phosphine arm of the [Ph-PSiP] ligand occupies the apical coordination site, while the remaining phosphine arm and the silyl group occupy basal sites. The Si donor in **2-2** is positioned *trans*- to Cl, with a Ru-Si distance of 2.3361(6) Å. These structural features differ somewhat from those of the related complex (biPSi)RuCl(CO) (biPSi = κ^3-Me*Si*($CH_2CH_2CH_2$-*P*Ph_2)$_2$), which features the biPSi ligand in a *mer*-type configuration with Si positioned *trans* to the vacant coordination site (Ru-Si, 2.339(5) Å).[65] While the acute P2-Ru-Si angle of 79.23(2)° in

2-2 may arise due to the geometric constraints of the rigid [Ph-PSiP] ligand (P1-Ru-Si, 81.53(2)°), it is also feasible that the structure of **2-2** might be influenced by electronic effects involving the distortion of five-coordinate d^6 complexes. Such distortion results in a "Y-shaped" molecular geometry in which a ligand with poor σ-donor but good π-donor properties (such as Cl^-) is positioned opposite the acute angle of the "Y".[66] However, in the case of **2-2** the chloride ligand is positioned significantly closer to P2 than to Si (Cl-Ru-P2, 119.66(2)°; Cl-Ru-Si, 160.41(2)°), such that the complex is better represented as square pyramidal.

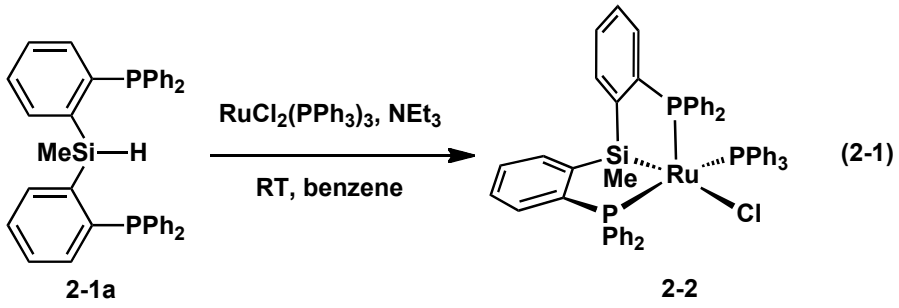

2-1a 2-2 (2-1)

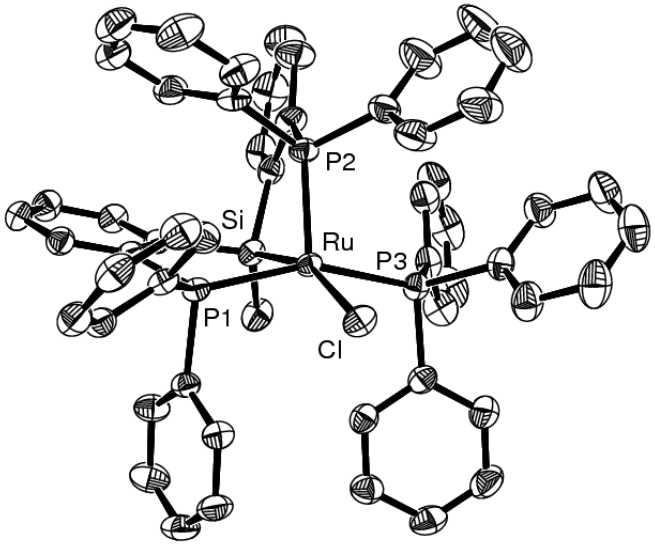

Figure 2-2. ORTEP diagram for **2-2**·$(OEt_2)_{1.5}$ shown with 50% displacement ellipsoids; selected hydrogen atoms and the ether solvate have been removed for clarity. Selected bond lengths (Å) and angles (deg): Ru-Cl 2.4492(6); Ru-P1 2.3040(6); Ru-P2 2.2093(6); Ru-P3 2.3891(6); Ru-Si 2.3361(6); Si-C1 1.882(3); Si-Ru-Cl 160.41(2); P1-Ru-P2 100.67(2); P1-Ru-P3 156.79(2); P2-Ru-P3 100.92(2); C1-Si-Ru 122.59(9).

In methylene chloride-d_2 solution, both the ^{1}H and ^{31}P NMR spectra of **2-2** exhibit significant line broadening at 300K. The $^{31}P\{^1H\}$ NMR spectrum of **2-2** (300K) features three resonances in a 1:1:1 ratio, consisting of a broad singlet at 96.8 ppm, a broad doublet at 67.1 ppm (J = 289 Hz), and a doublet at 29.1 ppm (J = 258 Hz). Upon cooling of the solution to 223K, the ^{31}P NMR resonances sharpen significantly, revealing further PP coupling (98.5 ppm, apparent t, $^2J_{PPcis}$ = 25 Hz; 69.9 ppm, dd, $^2J_{PPcis}$ = 27 Hz, $^2J_{PPtrans}$ = 281 Hz; 32.4 ppm, dd, $^2J_{PPcis}$ = 24 Hz, $^2J_{PPtrans}$ = 282 Hz). No further decoalescence phenomena are observed at temperatures below 223K. The resonances observed at low temperature in the ^{31}P NMR spectrum of **2-2** are consistent with the structure observed in

the solid state, where the three inequivalent phosphine donors are arranged in a T-type configuration. These temperature-dependent NMR line shape changes may arise due to intramolecular rearrangement processes (e.g., pseudorotation) and/or Ru-P dissociation.

2.2.3 Synthesis of [Ph-PSiP]Ru alkyl complexes.

In an attempt to generate a coordinatively unsaturated [Ph-PSiP]Ru^{II} alkyl complex, **2-2** was treated with one equiv of an alkyllithium reagent in benzene at room temperature (Scheme 2-2). Treatment of **2-2** with Me_3SiCH_2Li did not lead to formation of the desired Ru alkyl complex, rather ^{1}H NMR spectroscopy of the *in situ* reaction mixture indicated the formation of Me_4Si along with a new [Ph-PSiP]Ru complex **2-3**. The $^{31}P\{^1H\}$ NMR spectrum of **2-3** features three broad resonances at 72.1 (br d), 64.7 (br s), and -34.2 (d, J_{PP} = 213 Hz) ppm (1:1:1 ratio). Treatment of **2-2** with MeLi (1.6 M in Et_2O) resulted in the formation of **2-3** along with a new [Ph-PSiP]Ru species **2-4** that exhibited three ^{31}P NMR resonances at room temperature at 76.6 (dd, $^2J_{PP}$ = 24 Hz, $^2J_{PP}$ = 266 Hz), 52.4 (apparent t, J = 26 Hz), and -25.6 (dd, $^2J_{PP}$ = 30 Hz, $^2J_{PP}$ = 268 Hz) ppm (1:1:1 ratio). The ^{1}H NMR spectrum of the mixture (benzene-d_6) featured a peak at -0.04 ppm that was assigned as the Ru-*Me* resonance. After one night at room temperature in benzene-d_6 solution, **2-4** was completely converted to **2-3**, as observed by ^{31}P NMR spectroscopy, with concomitant liberation of MeH and disappearance of the ^{1}H NMR signal at -0.04 ppm. Compound **2-3** was isolated as a red solid in 71% yield from a scale-up of the reaction between **2-2** and Me_3SiCH_2Li. The X-ray crystal structure of **2-3**·(OEt_2) (Figure 2-3) indicates a five coordinate Ru complex featuring *fac*-type [Ph-PSiP] coordination and a cyclometalated PPh_3 ligand. The Ru center in **2-3** features

distorted square pyramidal geometry with Si occupying the apical position and a Ru-Si bond distance of 2.285(1) Å. The four-membered RuPCC metalacycle resulting from *ortho*-metalation of a phenyl substituent on the PPh_3 ligand exhibits a Ru-P3-C71 bond angle of 84.8(1)° and a P3-Ru-C72 bond angle of 67.8(1)°.

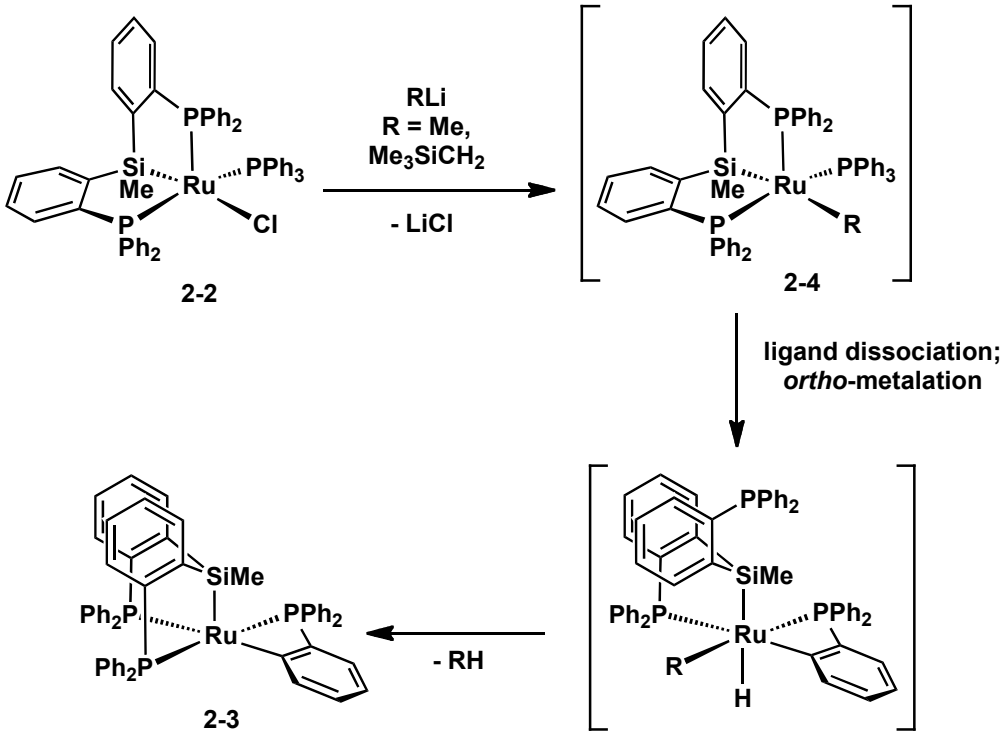

Scheme 2-2. Reaction of **2-2** with RLi to give the *ortho*-metalated product **2-3** via alkyl intermediate **2-4**.

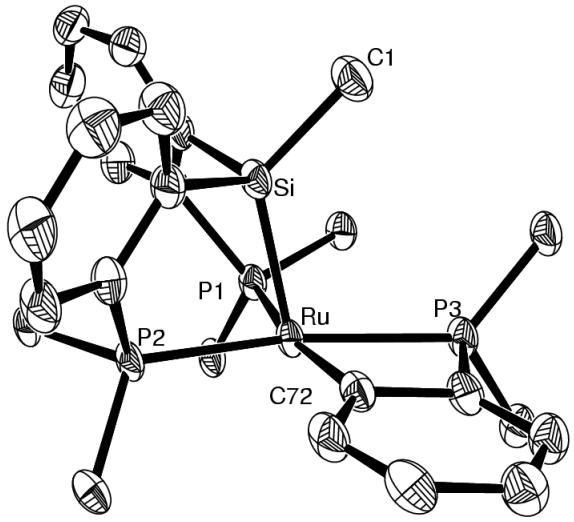

Figure 2-3. ORTEP diagram for **2-3**·(OEt_2) shown with 50% displacement ellipsoids; selected hydrogen and carbon atoms have been removed for clarity. Selected bond lengths (Å) and angles (deg): Ru-P1 2.3037(11); Ru-P2 2.3035(10); Ru-P3 2.3665(10); Ru-C72 2.121(4); Ru-Si 2.2850(11); Si-C1 1.877(4); C72-Ru-P3 67.84(10); Ru-P3-C71 84.80(12); P3-C71-C72 101.9(3); C71-C72-Ru 105.1(2); Si-Ru-C72 97.08(10); C1-Si-Ru 125.45(14).

Although the ^{31}P NMR spectrum of complex **2-3** exhibits significant line broadening at 300K (benzene-d_6, *vide supra*), upon cooling to 233K (toluene-d_8) the $^{31}P\{^1H\}$ NMR resonances sharpen somewhat to reveal a doublet at 76.8 ppm ($^2J_{PP}$ = 236 Hz), a broad singlet at 68.2 ppm, and a doublet of doublets at -28.7 ppm ($^2J_{PPtrans}$ = 236 Hz, $^2J_{PPcis}$ = 22 Hz). No further decoalescence phenomena were observed at temperatures below 233K. The resonances observed at low temperature in the ^{31}P NMR spectrum of **2-3** are consistent with the C_1-symmetric structure observed in the solid state. Interestingly, upon heating a toluene-d_8 solution of **2-3** above room temperature, coalescence of the two most downfield shifted ^{31}P resonances is observed, such that at 353K the $^{31}P\{^1H\}$ NMR spectrum of **2-3** features two resonances in a 2:1 ratio, consisting of a broad singlet at 73.1 ppm and a triplet at -27.9 ppm (J = 102 Hz). The ^{31}P NMR spectrum observed at 353K is consistent with a C_s-symmetric structure in which the [Ph-

PSiP] ligand phosphine environments are rendered equivalent by a mirror plane as would occur in a complex that featured *mer*-[Ph-PSiP] coordination. As in the case of **2-2**, these temperature-dependent NMR line shape changes likely arise due to intramolecular rearrangement processes and/or Ru-P dissociation.

The formation of **2-3** likely proceeds via a highly reactive [Ph-PSiP]RuR(PPh_3) alkyl intermediate, which upon dissociation of a [Ph-PSiP] phosphine arm can oxidatively add the *ortho*-CH bond of a PPh_3 phenyl substituent in an intramolecular fashion (Scheme 2-2). Subsequent RH reductive elimination and re-coordination of the [Ph-PSiP] phosphine arm leads to the formation of **2-3**. An intermediate (**2-4**) was indeed observed in the reaction of **2-3** with MeLi, and this intermediate is thus tentatively assigned as the product of direct alkylation at Ru, [Ph-PSiP]RuMe(PPh_3). No such alkyl intermediate was observed when the alkylation of **2-2** with Me_3SiCH_2Li was attempted, and it is likely that the increased steric bulk of the Me_3SiCH_2 group accelerates the reductive elimination step to liberate Me_4Si.

When **2-3** was placed under an atmosphere of CO, quantitative (by ^{31}P NMR) formation of the CO adduct **2-5** was observed (eq 2-2). The $^{31}P\{^1H\}$ NMR spectrum of isolated **2-5** features two resonances in a 2:1 ratio at 61.7 (d, $^2J_{PP}$ = 17 Hz) and -40.5 ppm (t, $^2J_{PP}$ = 19 Hz), respectively, consistent with a C_s-symmetric structure. The ^1H NMR spectrum of **2-5** in benzene-d_6 solution features a resonance for the SiMe group at 0.62 ppm (d, J_{HP} = 3 Hz). This resonance appears as a singlet in the $^1H\{^{31}P\}$ NMR spectrum of **2-5** (benzene-d_6), which confirms the presence of HP coupling. Such HP coupling is most likely due to the positioning of the cyclometalated phosphine *trans* to the silyl donor in **2-5**.

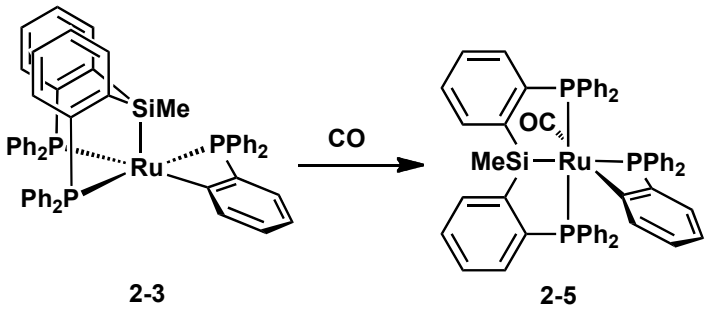

2-3 2-5 (2-2)

The X-ray crystal structure of **2-5** (Figure 2-4) confirms the formation of the expected 6-coordinate CO adduct featuring *trans* orientation of the silyl group and the metalated phosphine. Interestingly, the solid state structure of **2-5** features *mer*-coordination of the [Ph-PSiP] ligand to the Ru center, such that the [Ph-PSiP] phosphino donors are oriented *trans* to each other. This represents the first example of crystallographically confirmed *mer*-[Ph-PSiP] coordination to a metal center. Although at first glance such a coordination mode seems unlikely given the presence of an sp^3-hybridized Si central donor, examination of the bond angles at Si in the structure of **2-5** indicates only minor distortion from ideal tetrahedral bond angles (Figure 2-4). Thus, it appears that bis(phosphino)silyl pincers that feature a phenylene ligand backbone exhibit sufficient conformational flexibility to accommodate both *fac*- (*cis*-P-Ru-P) and *mer*-type (*trans*-P-Ru-P) coordination. In the case of **2-5**, it is possible that rearrangement from *fac*- (in the starting compound **2-3**) to *mer*-[Ph-PSiP] coordination is dictated by the electronic requirements of the strongly *trans*-directing silyl and CO ligands.

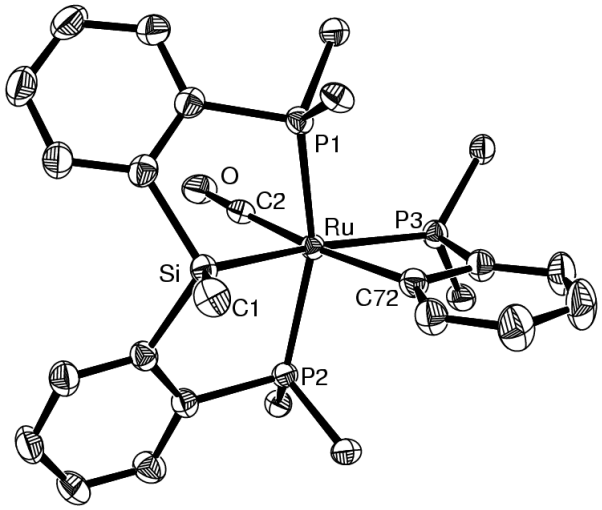

Figure 2-4. ORTEP diagram for **2-5** shown with 50% displacement ellipsoids; selected hydrogen and carbon atoms have been removed for clarity. Selected bond lengths (Å) and angles (deg): Ru-P1 2.3469(5); Ru-P2 2.3451(5); Ru-P3 2.4375(5); Ru-C72 2.1553(19); Ru-Si 2.4041(6); Si-C1 1.888(2); Ru-C2 1.885(2); C2-O 1.154(2); C72-Ru-P3 66.31(5); Ru-P3-C71 84.48(7); P3-C71-C72 102.55(14); C71-C72-Ru 106.35(13); C2-Ru-C72 171.87(8); C1-Si-Ru 125.39(7); C12-Si-Ru 104.03(7); C22-Si-Ru 107.67(6).

Because the attempt to form a Ru-alkyl species of the type [Ph-PSiP]RuR(PPh_3) led to cyclometalation of a phenyl substituent on the PPh_3 ligand, the PEt_3 derivative [Ph-PSiP]RuR(PEt_3) was targeted, with the expectation that the C(sp^3)-H bonds of PEt_3 would be less likely to undergo metalation. Treatment of **2-2** with one equiv of PEt_3 in benzene solution resulted in the quantitative (by ^{31}P NMR) formation of [Ph-PSiP]RuCl(PEt_3) (**2-6**) along with displacement of 1 equiv of PPh_3 (eq 2-3). The X-ray crystal structure of **2-6** (Figure 2-5) confirms the formation of a five-coordinate *fac*-[Ph-PSiP] complex with distorted square pyramidal geometry at the 16-electron Ru center. The silyl donor occupies the apical site of the square pyramid while the [Ph-PSiP] phosphine arms each occupy basal sites. Similar to **2-2**, it is possible that electronic effects involving the distortion of five-coordinate d^6 complexes may play a factor in the structure of **2-6**, however the chloride ligand is positioned much closer to Si than to P2 in

this case (Cl-Ru-Si, 124.83(5)˚; C1-Ru-P2, 154.95(5)˚) and the complex is thus better represented as square-pyramidal.

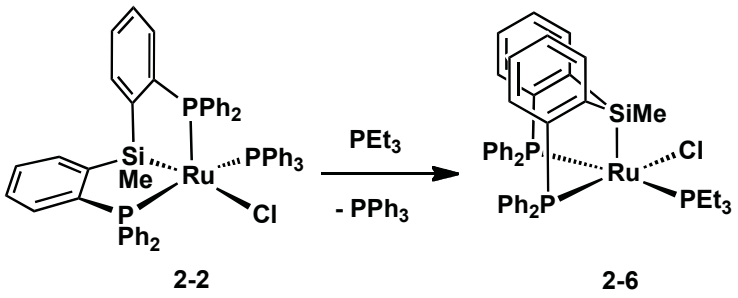

2-2 2-6 (2-3)

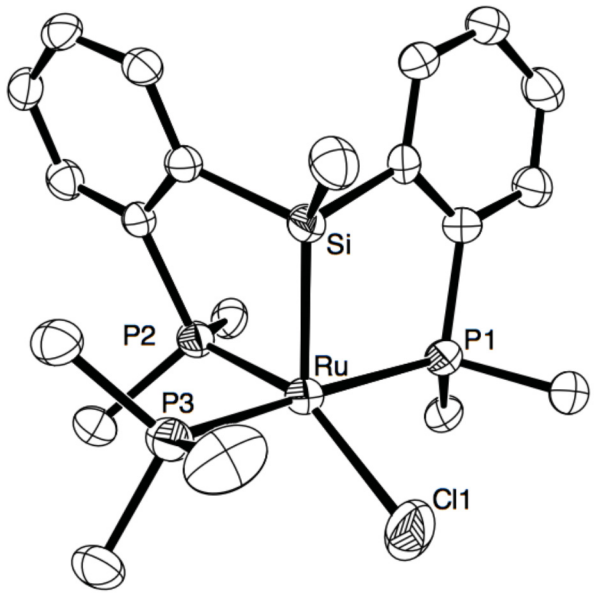

Figure 2-5. ORTEP diagram for **2-6**·$(CH_2Cl_2)_{1.17}$·(OEt_2) shown with 50% displacement ellipsoids; selected hydrogen and carbon atoms have been removed for clarity. Selected bond lengths (Å) and angles (deg): Ru-Cl 2.3942(12); Ru-P1 2.3238(11); Ru-P2 2.2449(11); Ru-P3 2.4012(11); Ru-Si 2.2944(11); Cl-Ru-P1 86.66(4); Cl-Ru-P2 154.95(5); Cl-Ru-P3 85.62(4); Cl-Ru-Si 124.83(5); P1-Ru-P3 168.68(4); P1-Ru-Si 84.27(4); P2-Ru-Si 80.22(4); P3-Ru-Si 93.37(4).

In benzene-d_6 solution both the ^1H and ^{31}P NMR spectra of **2-6** exhibit significant line broadening at room temperature. The $^{31}P\{^1H\}$ NMR spectrum of **2-6** (300K)

features three resonances in a 1:1:1 ratio, consisting of a broad singlet at 94.7 ppm, a broad doublet at 64.5 ppm (J = 283 Hz), and a doublet at 17.4 ppm (J = 255 Hz). Upon cooling of a toluene-d_8 solution of **2-6** to 213K the ^{31}P NMR resonances sharpen significantly, revealing further PP coupling (92.2 ppm, apparent t, $^2J_{PPcis}$ = 24 Hz; 65.1 ppm, dd, $^2J_{PPcis}$ = 24 Hz, $^2J_{PPtrans}$ = 283 Hz; 17.8 ppm, dd, $^2J_{PPcis}$ = 26 Hz, $^2J_{PPtrans}$ = 283 Hz). No further decoalescence phenomena are observed at temperatures below 213K. The resonances observed at low temperature in the ^{31}P NMR spectrum of **2-6** are consistent with the solid state structure, where the three inequivalent phosphine donors are positioned in a T configuration. Much like **2-2**, these temperature-dependent NMR line shape changes may arise due to intramolecular rearrangement processes (e.g., pseudorotation) and/or Ru-P dissociation.

Treatment of **2-6** with one equiv of MeMgBr (2.0 M in THF) resulted in the quantitative formation (by ^{31}P NMR) of a new product tentatively assigned as [Ph-PSiP]RuMe(PEt_3) (**2-7**). The $^{31}P\{^1H\}$ NMR spectrum of **2-7** features three resonances at 55.8 (t, J = 20 Hz), -1.3 (t, J = 19 Hz), and -8.2 (t, J = 19 Hz) ppm (1:1:1 ratio), while signals at 1.49 ppm in the ^{1}H NMR spectrum and 1.6 in the ^{13}C NMR spectrum correspond to the RuMe ligand. The resonance for the SiMe protons appears as a doublet at 1.0 ppm in the ^{1}H NMR spectrum. This coupling is not present in the $^1H\{^{31}P\}$ NMR spectrum indicating that the silyl donor and PEt_3 phosphine ligand are oriented *trans* to each other. There is no evidence to suggest that metalation of an C(sp^3)-H bond of the PEt_3 ligand occurs.

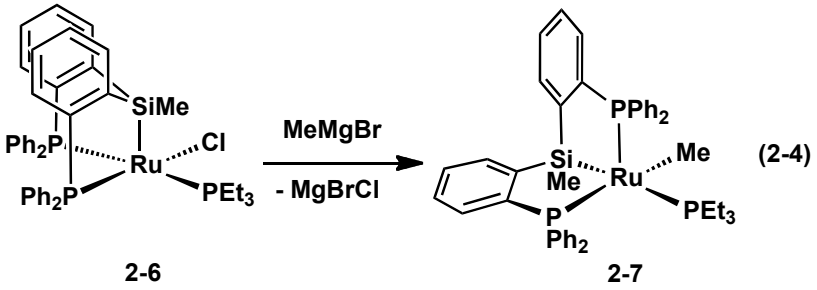

2-6 2-7

2.2.4 Synthesis of [Ph-PSiP]Ru hydride complexes.

In an attempt to generate a coordinatively unsaturated [Ph-PSiP]Ru^{II} hydride complex, **2-2** was treated with 1 equiv of $LiEt_3BH$ (1.0 M in THF). *In situ* ^{31}P and ^{1}H NMR analysis of the reaction mixture indicated the formation of three Ru hydride species (**2-8a**-**c**) that each exhibit C_s symmetry in solution (Scheme 2-3). In benzene-d_6 solution, the major hydride product (**2-8a**) features a Ru-H ^{1}H NMR resonance at -13.66 ppm (td, $^{2}J_{HP}$ = 10 Hz, $^{2}J_{HP}$ = 27 Hz) and two ^{31}P NMR resonances in a 2:1 ratio at 64.6 (d, $^{2}J_{PP}$ = 19 Hz) and 34.8 (t, $^{2}J_{PP}$ = 19 Hz) ppm, corresponding to the [Ph-PSiP] and PPh_3 ligands, respectively. By comparison, **2-8b** features a Ru-H ^{1}H NMR resonance at -7.18 ppm (br s), and two ^{31}P NMR resonances at 71.0 ppm (d, 2 P, [Ph-PSiP], $^{2}J_{PP}$ = 14 Hz) and 47.7 ppm (t, 1 P, PPh_3, $^{2}J_{PP}$ = 14 Hz) and **2-8c** features a Ru-H ^{1}H NMR resonance at -11.04 ppm (br d, $J \sim 140$ Hz), and two ^{31}P NMR resonances at 71.3 ppm (br, 2 P, [Ph-PSiP]) and 54.7 ppm (t, 1 P, PPh_3, $^{2}J_{PP}$ = 16 Hz). The ratio of **2-8a**:**b**:**c** observed *in situ* was approximately 2:1:1, and heating of the mixture (20 h, 70 °C, benzene-d_6) did not change the observed ratio of these three Ru-H species. In a preparative scale reaction of **2-2** with $LiEt_3BH$, **2-8a** was readily isolated in 64% yield by washing of the crude product (which also contained **2-8b** and **2-8c**) with diethyl ether. The increased isolated yield of **2-8a**

relative to the yield observed in situ is attributed to the conversion of **2-8b** and/or **2-8c** to **2-8a** upon workup. The IR spectrum of isolated **2-8a** features a Ru-H stretch at 1910 cm^{-1} as well as a RuN_2 stretch at 2131 cm^{-1}. On the basis of these data, complex **2-8a** is assigned as a dinitrogen adduct of the type [Ph-PSiP]RuH(N_2)(PPh_3). Facile formation of dinitrogen adducts has been reported in related [PCP]Ru and [PNP]Ru pincer chemistry.[67]

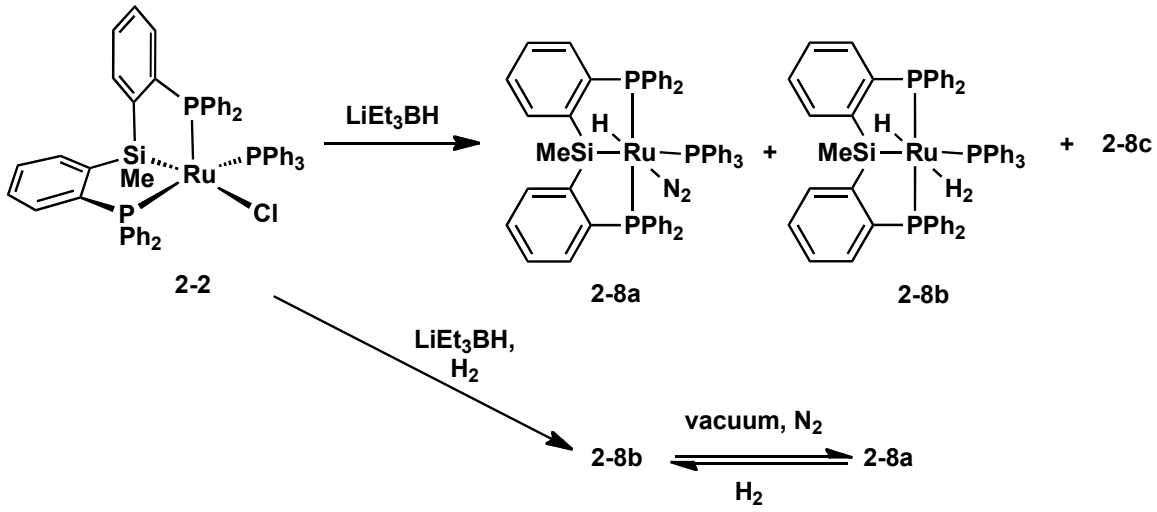

Scheme 2-3. Formation of [Ph-PSiP]Ru-hydride products **2-8a-c** upon reaction of $LiEt_3BH$ and exclusive formation of **2-8b** under an H_2 atmosphere.

The exposure of either isolated **2-8a** or an *in situ* generated (from the reaction of **2-2** with $LiEt_3BH$) mixture of **2-8a-c** to an atmosphere of H_2 led to the quantitative (by ^1H and ^{31}P NMR spectroscopy) formation of **2-8b** (Scheme 2-3). Although the room temperature ^1H NMR spectrum of **2-8b** features a single broad Ru-H resonance at -7.18 ppm (benzene-d_6), two Ru-H resonances in a 2:1 ratio are observed at low temperature at -5.90 and -10.22 ppm (toluene-d_8 solution). Exposure of a solution of **2-8b** to vacuum followed by exposure to an atmosphere of N_2 leads to the quantitative formation of **2-8a**. On the basis of these data, **2-8b** is formulated as a fluxional non-classical hydrido-

dihydrogen complex of the type [Ph-PSiP]Ru(H)(H_2)PPh_3.[68] This formulation was further supported by measurement of the $T_{1(min)}$ relaxation time for the resonance observed at -7.18 in the ^{1}H NMR spectrum. It is generally accepted in the literature that a qualitative relationship exists between the $T_{1(min)}$ value and the H-H distance of a metal bound H_2 ligand,[69] and that $T_{1(min)}$ values less than 80 ms indicate the presence of a dihydrogen ligand.[70] The $T_{1(min)}$ value for the resonance at -7.18 ppm in the ^{1}H NMR of **2-8b** was measured to be 14 ms and is consistent with the formulation of **2-8b** as a hydrido-dihydrogen complex.[70] The formation of related [PCP]Ru(H)(H_2)PPh_3 species from the reaction of [PCP]Ru(H)(N_2)PPh_3 has previously been reported.[67] The mechanism for the formation of **2-8b** from the reaction of **2-2** with $LiEt_3BH$ has not been identified, although it can potentially be attributed to the presence of protic contaminants that could react with $LiEt_3BH$ to generate H_2. The identity of **2-8c** remains unknown at this time.

2.2.5 Synthesis of [Ph-PSiP]RuX (X = NR_2, OR) complexes.

By comparison to the understanding of late transition metal complexes featuring metal-carbon covalent bonds, the understanding of late metal complexes that feature anionic heteroatomic ligands (e.g. amido) is lagging.[71] These complexes can be difficult to synthesize due to the unfavorable electron-electron repulsion between the lone pair electrons on the heteroatom and the d-electrons of the late metal center. In this context we attempted the synthesis of [Ph-PSiP]Ru amido and alkoxo complexes with the goal of accessing reactive, low coordinate [Ph-PSiP]Ru species.

Reaction of **2-2** with 1 equiv of $NaN(SiMe_3)_2$ in benzene solution at room temperature resulted in the quantitative (by ^{31}P NMR) formation of [Ph-PSiP]$RuN(SiMe_3)_2$ (**2-9**, eq 2-4), which was isolated as a red solid. The *in situ* $^{31}P\{^1H\}$ NMR spectrum of **2-9** features a singlet at 93.2 ppm corresponding to the formation of a C_s symmetric product and a singlet at -4.0 ppm corresponding to free PPh_3, which is displaced by the bulky $N(SiMe_3)_2$ ligand. The room temperature ^1H NMR spectrum of **2-9** features two broad, overlapping singlets at 0.51 ppm and 0.46 ppm that correspond to the Si*Me* protons of the $N(SiMe_3)_2$ ligand. It is possible that the unique signals for the $SiMe_3$ groups are a result of restricted rotation about the Ru-N bond due to a π-type interaction of the N lone pair with an empty d-orbital on Ru. However, it cannot be ruled out that the steric requirements of the [Ph-PSiP] and $N(SiMe_3)_2$ ligands prevent rotation about the Ru-N bond. Complex **2-9** can be isolated as a red solid in 75% yield, and no conversion to **2-3** is observed upon workup. X-ray quality crystals of **2-9** have thus far remained elusive, and as such the formulation of **2-9** as a monomeric species is tentatively based on the structure of the analogous complex [Cy-PSiP]$RuN(SiMe_3)_2$ (see Chapter 3). However, a dinuclear structure cannot be strictly eliminated based on the data currently available for **2-9**.

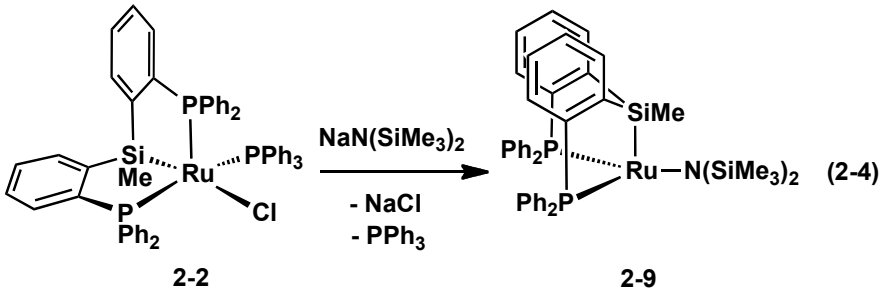

2-2 **2-9**

Reaction of **2-2** with 1 equiv. of KO^{t}Bu in THF solution at room temperature resulted in the quantitative (by ^{31}P NMR) formation of a new product proposed to be [Ph-PSiP]RuO^{t}Bu, **2-10** (*cf.* [Cy-PSiP]RuO^{t}Bu in Chapter 3). The *in situ* ^{31}P{^{1}H} NMR spectrum of **2-10** shows a singlet at 99.2 ppm corresponding to the product along with a peak for free PPh_3 at -4.0 ppm. The ^{1}H NMR spectrum features a singlet at 1.14 ppm corresponding to the O^{t}Bu protons. Although complex **2-10** is stable at room temperature in THF solution for 2-3 days, attempted isolation of the product led to the formation of complex **2-3** with concomitant loss of HO^{t}Bu (Scheme 2-4). It is possible that in the presence of PPh_3, association of phosphine to an empty coordination site of **2-10** leads to metalation of PPh_3 and loss of HO^{t}Bu resulting in the formation of **2-3**. Such a process is likely accelerated upon workup as the solution containing **2-10** and PPh_3 is concentrated. In the case of **2-9**, the formation of **2-3** is impeded by the steric bulk of the $N(SiMe_3)_2$ ligand, which prevents coordination of PPh_3 to the Ru center.

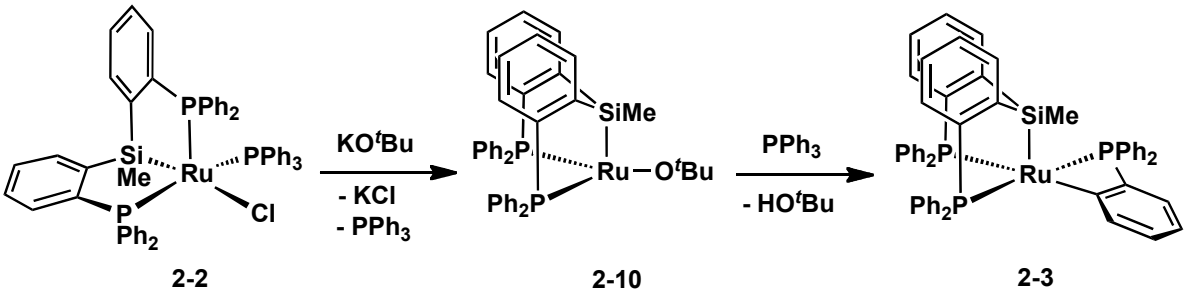

2-2 **2-10** **2-3**

Scheme 2-4. *In situ* synthesis of **2-10**.

2.2.6 E-H (E = main group element) bond activation mediated by 2-3.

The coordinatively unsaturated 16-electron complex **2-3** is potentially a promising candidate for studying E-H bond activation reactions. One can imagine that upon

oxidative addition of an E-H bond to the Ru center in **2-3**, subsequent reductive elimination of an aryl C-H bond to 'release' the *ortho*-metalated PPh_3 phenyl substituent would be a very favorable process, as it would relieve ring strain associated with the four-membered metalacycle. Alternatively, a σ-bond metathesis mechanism for E-H bond activation resulting in the same net transformation could also be envisioned.

In this regard, preliminary reactivity studies to investigate the reactivity of **2-3** with hydrogen, hydrosilanes, and amine-boranes have been performed. Compound **2-3** reacted with an atmosphere of H_2 in benzene solution to quantitatively (by ^{31}P NMR) generate **2-8b** (Scheme 2-5). One equiv of either diphenyl- or dimesitylsilane reacted with **2-3** to generate **2-8a** quantitatively (^{31}P and ^{1}H NMR, Scheme 2-4). This reaction formally generates "R_2Si", however, the fate of silicon in the course of the reaction remains unknown. Compound **2-3** also reacted in a dehydrogenative manner with amine-borane reagents (Scheme 2-5). Ten equiv of $H_3N{\cdot}BH_3$ were consumed upon reaction with **2-3** in THF solution at room temperature to form **2-8b** quantitatively. Hydrogen evolution was observed and a white insoluble precipitate was formed. The ^{11}B NMR of the reaction mixture indicated that all of the $H_3N{\cdot}BH_3$ was consumed, however, no new ^{11}B NMR signal was observed, which is consistent with the formation of insoluble boron-containing product(s). This observation is also consistent with results recently published by Goldberg and co-workers, who observed the formation of boron-containing insolubles in the dehydrogenation of $H_3N{\cdot}BH_3$ by an iridium PCP pincer complex.[72] On the basis of solid-state ^{11}B NMR spectroscopy, IR, and X-ray powder diffraction data, Goldberg and co-workers assigned the dehydrogenated boron-containing product as the cyclic pentamer $[H_2NBH_2]_5$.

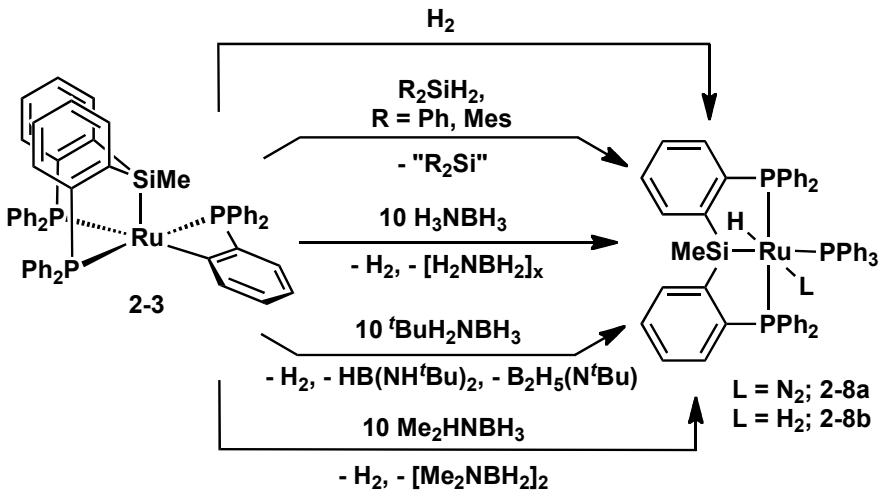

Scheme 2-5. Reactivity of **2-3** with E-H bonds (E = H, Si, B).

Substituted amine-boranes such as $^{t}BuH_2N{\cdot}BH_3$ and $Me_2HN{\cdot}BH_3$ were also found to react with **2-3** in a dehydrogenative manner (Scheme 2-5). One equiv of $^{t}BuH_2N{\cdot}BH_3$ reacted upon mixing in benzene to generate a mixture of products by ^{31}P NMR spectroscopy. Compounds **2-8a** and **2-8b** were identified from this mixture as the major products. Upon addition of 10 equiv of $^{t}BuH_2N{\cdot}BH_3$ to a benzene solution of **2-3**, immediate gas evolution was observed and only **2-8b** was observed in the ^{31}P NMR spectrum. After standing for 14 h at room temperature, the ^{11}B NMR spectrum of the reaction mixture indicated that ca. 80% of the starting $^{t}BuH_2N{\cdot}BH_3$ had been consumed, and subsequent heating at 45 °C for 45 min resulted in complete consumption of the $^{t}BuH_2N{\cdot}BH_3$. The ^{11}B NMR spectrum of the reaction mixture indicated the formation of four new B-containing products, observed at 35.5 (t, $^{1}J_{BH}$ = 131 Hz), 31.0 (br, minor), 25.9 (d, $^{1}J_{BH}$ = 125 Hz), and -25.9 (t, $^{1}J_{BH}$ = 126 Hz) ppm. The mixture of boron-containing products is similar to that observed by Baker and co-workers in their report on dehydrogenation of amine-boranes, which they assigned as $^{t}BuHNBH_2$, $(^{t}BuNBH)_3$,

$HB(NH^tBu)_2$, and $B_2H_5(NH^tBu)$, respectively.[73] The complete consumption of 10 equiv of $^tBuH_2N{\cdot}BH_3$ by **2-3** indicates that the dehydrogenation occurs in a catalytic fashion. Ten equiv of $Me_2HN{\cdot}BH_3$ were also consumed upon reaction with **2-3** (72 h, room temperature, benzene solution). The B-containing product formed in this reaction was identified as the dimer $(Me_2NBH_2)_2$ based on its ^{11}B NMR shift of 5.4 (t, $^1J_{BH}$ = 111 Hz) ppm.[74] The metal-catalyzed dehydrogenation of $H_3N{\cdot}BH_3$ and related amine-boranes has attracted significant attention, as such compounds are promising candidates for hydrogen storage materials.[72-74]

2.2.7 [Ph-PSiP]Ru complexes as catalysts for the transfer hydrogenation of ketones.

The hydrogenation of unsaturated substrates by use of gaseous H_2 at relatively high pressures is both expensive and inconvenient. Milder sources of H_2 can be utilized for hydrogenation reactions by way of transition metal catalyzed transfer hydrogenation (eq 2-5), which makes use of a donor substrate such as isopropanol (usually in the presence of base) in order to deliver H_2 to an unsaturated substrate.[29] Previous work has established that Ru^{II} PCP-, NCN-, CNC-, and CNN-pincer complexes are effective catalysts for the transfer hydrogenation of ketones, and it has been proposed that the Ru-C σ-bond plays an important role in the formation of long-lived, catalytically active species.

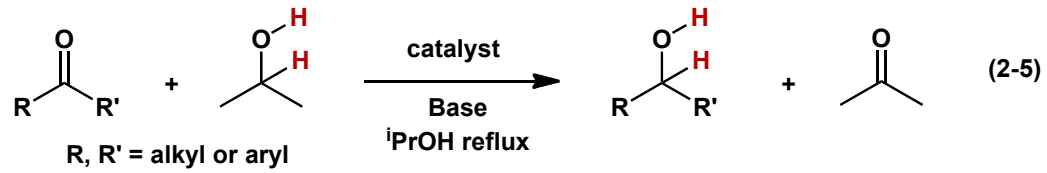

In this context, we became interested in surveying the catalytic activity of [Ph-PSiP]RuCl(PPh_3) (**2-2**) and [Ph-PSiP]RuH(N_2)(PPh_3) (**2-8a**) in the transfer hydrogenation of ketones, employing basic ^{i}PrOH as the hydrogen source. The results obtained in this preliminary survey are summarized in Table 2-1. The activity of **2-2** as a precatalyst in this reaction is comparable to that of related Ru pincer catalysts that lack an NH functionality.[31c] When employing 0.2 mol % of **2-2** with 2 mol % of KO^{t}Bu at 82 °C, high conversion to the corresponding secondary alcohols was observed for several ketone substrates, including diaryl, dialkyl, and alkyl/aryl ketones. As is the case for most metal-catalyzed transfer hydrogenation processes conducted in ^{i}PrOH, less than 5% conversion was observed in the absence of KO^{t}Bu as base. The preformed Ru hydride complex **2-8a** was similarly inactive for transfer hydrogenation of cyclohexanone in the absence of added KO^{t}Bu, although 94% conversion was obtained when using 2 mol % KO^{t}Bu along with 0.2 mol % **2-8a** (entry 6, Table 2-1). Although the [Ph-PSiP]Ru species investigated are not among the most highly active catalysts known for the transfer hydrogenation of ketones, the results of this study establish the potential utility of such [Ph-PSiP]Ru complexes in catalysis.

Table 2-1. [Ph-PSiP]Ru as a catalyst for the transfer hydrogenation of ketones[a].

Entry	Catalyst	Substrate	Time (h)	Conversion (%)[b]
1	**2-2**	acetophenone	6	96
2	**2-2**	benzophenone	6	92
3	**2-2**	2-heptanone	4.5	99
4	**2-2**	cyclopentanone	3	>99
5	**2-2**	cyclohexanone	3	>99
6	**2-8a**	cyclohexanone	3	94

[a]Reactions were performed on a 1 mL scale (0.1 M ketone, 0.2 mol % Ru, 2 mol % KO^{t}Bu) in ^{i}PrOH at 82 °C under N_2. [b]Determined by GC-FID.

2.3 Conclusions

In summary, the facile synthesis of Ru^{II} complexes supported by the versatile new pincer-like bis(phosphino)silyl ligand [κ^3-(2-$Ph_2PC_6H_4)_2SiMe]^-$ ([Ph-PSiP]) has been described. Coordination chemistry studies have indicated that [Ph-PSiP] can bind to Ru in either a *fac*- or *mer*-type κ^3-configuration. The formally 16-electron complex [Ph-PSiP]RuCl(PPh_3) **2-2** provides a convenient entry for the study of further reactivity in this system. Substitution of the PPh_3 ligand in **2-2** with PEt_3 afforded the alkylphosphino analog [Ph-PSiP]RuCl(PEt_3) **2-6**. Attempts to alkylate **2-2** with alkyl lithium reagents resulted in the formation of a coordinatively unsaturated Ru complex that features an *ortho*-metalated PPh_3 phenyl group (**2-3**). This strained metalated complex has thus far exhibited a propensity to dehydrogenate substrates such as secondary silanes and amine-boranes. Attempted alkylation of **2-6** does not result in cyclometalation of the PEt_3 ligand, and the 16-electron alkyl complex [Ph-PSiP]RuMe(PEt_3) proved isolable.

Hydride complexes of the type [Ph-PSiP]Ru(H)(PPh_3)L (**2-8a**, L = N_2; **2-8b**, L = H_2) have also been prepared and characterized. Amido and alkoxo complexes of the type [Ph-PSiP]RuX (X = $N(SiMe_3)_2$, O^{t}Bu) are readily prepared, however the RuO^{t}Bu complex reacts in the presence of PPh_3 to form the metalated species **2-3** with loss of HO^{t}Bu. The steric bulk of the X ligand plays an important role in preventing the formation of **2-3**, as the Ru($N(SiMe_3)_2$) complex does not appear to undergo such reactivity.

In one of the first applications of silyl pincer-type complexes in catalysis, both chloro- and hydrido-[Ph-PSiP]Ru species (**2-2** and **2-8a**) were shown to be effective in mediating the transfer hydrogenation of ketones to secondary alcohols, employing basic ^{i}PrOH as the hydrogen source. These preliminary studies establish [Ph-PSiP]-ligated platinum group metal complexes as promising candidates for further catalytic studies.

2.4 Experimental Section

2.4.1 General considerations.

All experiments were conducted under nitrogen in an MBraun glovebox or using standard Schlenk techniques. Dry, oxygen-free solvents were used unless otherwise indicated. All non-deuterated solvents were deoxygenated and dried by sparging with nitrogen and subsequent passage through a double-column solvent purification system provided by MBraun Inc. Tetrahydrofuran and diethyl ether were purified over two activated alumina columns, while benzene and pentane were purified over one activated alumina column and one column packed with activated Q-5. All purified solvents were stored over 4 Å molecular sieves. Purification of ^{i}PrOH (Aldrich, anhydrous 99.5%) was

achieved by sparging with nitrogen over a period of 0.25 h followed by storage over 4 Å molecular sieves (approximately 10 grams/100 mL ^{i}PrOH) for a minimum of 24 h. Benzene-d_6, toluene-d_8, and methylene chloride-d_2 were degassed via three freeze-pump-thaw cycles and stored over 4 Å molecular sieves. The compound $RuCl_2(PPh_3)_3$ was purchased from Strem and used as received. Triethylamine was deoxygenated and dried by sparging with nitrogen and subsequent distillation from CaH_2. All ketone substrates were obtained from commercial sources in high purity; solid ketones were dried *in vacuo* for 12 h before use, while liquid ketones were degassed by use of three repeated freeze-pump-thaw cycles. The compound 2-$Ph_2PC_6H_4Br$ was prepared according to literature procedures.[64] All other reagents were purchased from Aldrich and used without further purification. Unless otherwise stated, ^{1}H, ^{13}C, ^{31}P, ^{11}B, and ^{29}Si NMR characterization data were collected at 300K on a Bruker AV-500 spectrometer operating at 500.1, 125.8, 202.5, 160.5, and 99.4 MHz (respectively) with chemical shifts reported in parts per million downfield of $SiMe_4$ (for ^{1}H, ^{13}C, and ^{29}Si), $BF_3{\cdot}OEt_2$ (for ^{11}B), or 85% H_3PO_4 in D_2O (for ^{31}P). Variable-temperature NMR data were collected on a Bruker AC-250 spectrometer. ^{1}H and ^{13}C NMR chemical shift assignments are based on data obtained from ^{13}C-DEPT, ^{1}H-^{1}H COSY, ^{1}H-^{13}C HSQC, and ^{1}H-^{13}C HMBC NMR experiments. ^{29}Si NMR assignments are based on ^{1}H-^{29}Si HMQC and ^{1}H-^{29}Si HMBC experiments. In some cases, fewer than expected unique ^{13}C NMR resonances were observed, despite prolonged acquisition times. Infrared spectra were recorded as Nujol mulls between NaCl plates using a Bruker VECTOR 22 FT-IR spectrometer at a resolution of 4 cm^{-1}. Elemental analyses were performed by Desert Analytics, Inc. of Tucson, Arizona and Canadian Microanalytical Service Ltd. of Delta, British Columbia. X-ray data collection,

solution, and refinement were carried out by Drs. Robert MacDonald and Michael J. Ferguson at the University of Alberta X-ray Crystallography Laboratory, Edmonton, Alberta.

2.4.2 Synthetic details and characaterization data.

[(2-$Ph_2PC_6H_4)_2$SiMe]H ([Ph-PSiP]H, 2-1). A stirring solution of 2-$Ph_2PC_6H_4Br$ (2.0 g, 5.9 mmol) in ca. 10 mL of diethyl ether was cooled to -78 °C. ^{n}BuLi (3.7 mL, 1.6 M in hexanes, 5.9 mmol) was added dropwise to this solution, resulting in a white precipitate. The resulting slurry was allowed to warm to room temperature over the course of 1 h. The mixture was once again cooled to -78 °C, and Cl_2SiHMe (0.3 mL, 2.9 mmol) was added via syringe. The resulting pale peach colored reaction mixture was allowed to warm to room temperature and continue stirring for an additional 14 h at room temperature. The volatile components were then removed in vacuo and the remaining residue was extracted into 20 mL of benzene. The benzene extracts were filtered through Celite to give a peach colored solution. The benzene was removed *in vacuo* to afford an orange oil that was triturated with pentane (2 × 5 mL) to give **2-1** (1.5 g, 90%) as a pale peach colored solid. ^{1}H NMR (500 MHz, benzene-d_6): δ 7.78 (m, 2 H, H_{arom}), 7.29 – 7.23 (10 H, H_{arom}), 7.06 – 6.98 (16 H, H_{arom}), 6.03 (m, 1 H, Si*H*), 0.81 (d, 3 H, Si*Me*, $^3J_{HH}$ = 3 Hz). ^{13}C{^{1}H} NMR (125.8 MHz, benzene-d_6): δ 145.4 (d, C_{arom}, J_{CP} = 47 Hz), 144.8 (d, C_{arom}, J_{CP} = 11 Hz), 138.8 (d, C_{arom}, J_{CP} = 13 Hz), 137.7 (d, CH_{arom}, J_{CP} = 17 Hz), 135.0 (CH_{arom}), 134.4 (d, CH_{arom}, J_{CP} = 19 Hz), 134.2 (d, CH_{arom}, J_{CP} = 17 Hz), 130.3 (CH_{arom}), 129.0 – 128.7 (CH_{arom}), -1.9 (t, Si*Me*, $^4J_{CP}$ = 8 Hz). ^{31}P{^{1}H} NMR (202.5 MHz,

benzene-d_6): δ -10.9. $^{29}Si\{^1H\}$ NMR (99.4 MHz, benzene-d_6): δ -23.2. Anal. Calcd for $C_{37}H_{32}P_2Si$: C, 78.42; H, 5.69. Found: C, 78.19; H, 5.79.

[Ph-PSiP]RuCl(PPh_3) (2-2). A solution of **2-1** (0.22 g, 0.39 mmol) in 5 mL of benzene was added to a slurry of $RuCl_2(PPh_3)_3$ (0.37 g, 0.39 mmol) in 5 mL of benzene at room temperature. Et_3N (54 μL, 0.39 mmol) was added to the reaction mixture via syringe. The resulting wine colored solution was allowed to stir at room temperature for 1 h, over the course of which a fine precipitate was observed. The reaction mixture was filtered through Celite, and the volatile components were removed in vacuo. The remaining residue was washed with pentane (6 × 10 mL) to remove all traces of PPh_3. The residue was dried in vacuo to give **2-2** (0.33 g, 89%) as a red solid. The NMR spectra of **2-2** at 300K exhibit significant line broadening. Where possible, low temperature characterization data are provided. ^1H NMR (300K, 500 MHz, methylene chloride-d_2): δ 8.0 - 5.5 (broad overlapping resonances, H_{arom}), 0.55 (s, Si*Me*). ^1H NMR (183K, 250 MHz, methylene chloride-d_2): δ 7.83 – 6.99 (broad overlapping resonances, H_{arom}), 6.79 (br m, 2 H, H_{arom}), 6.63 (br m, 2 H, H_{arom}), 6.35 (br m, 2 H, H_{arom}), 6.17 (br m, 2 H, H_{arom}), 5.70 (br m, 2 H, H_{arom}), 0.38 (br s, 3 H, Si*Me*). $^{13}C\{^1H\}$ NMR (125.8 MHz, benzene-d_6): δ 143.9 – 143.5 (br, C_{arom}), 135.7 (CH_{arom}), 135.0 (br m, CH_{arom}), 134.2 (d, J_{CP} = 19 Hz), 130.9 (br m, CH_{arom}), 130.0 – 129.1 (broad overlapping resonances, CH_{arom}), 128.2 – 127.6 (broad overlapping resonances, CH_{arom}), 1.7 (Si*Me*). $^{31}P\{^1H\}$ NMR (300K, 202.5 MHz, methylene chloride-d_2): δ 96.8 (br s, 1 P, [Ph-PSiP]), 67.1 (br d, 1 P, [Ph-PSiP], $^2J_{PP}$ = 289 Hz), 29.1 (d, 1 P, PPh_3, $^2J_{PP}$ = 258 Hz). $^{31}P\{^1H\}$ NMR (223K, 101.3 MHz, methylene chloride-d_2): δ 98.5 (apparent t, 1 P, [Ph-PSiP], $^2J_{PPcis}$ = 25 Hz), 69.9 (dd, 1 P, [Ph-PSiP], $^2J_{PPcis}$ = 27 Hz, $^2J_{PPtrans}$ = 281 Hz), 32.4 (dd, 1 P,

$P\text{Ph}_3$, $^2J_{\text{PPcis}}$ = 24 Hz, $^2J_{\text{PPtrans}}$ = 282 Hz). $^{29}\text{Si}\{^1\text{H}\}$ NMR (99.4 MHz, methylene chloride-d_2): δ 61.8. Anal. Calcd for $C_{55}H_{46}ClP_3RuSi$: C, 68.49; H, 4.81. Found: C, 68.67; H, 5.04. A single crystal of **2-2**·$(OEt_2)_{1.5}$ suitable for X-ray diffraction analysis was grown from diethyl ether at -30 °C.

[Ph-PSiP]Ru(κ^2-$C_6H_4P\text{Ph}_2$) (2-3). A solution of $(CH_3)_3SiCH_2Li$ (0.006 g, 0.064 mmol) in ca. 2 mL of benzene was added to a room temperature solution of **2-2** (0.062 g, 0.064 mmol) in ca. 3 mL of benzene. The reaction mixture was filtered through Celite and the volatile components were removed in vacuo. The remaining residue was washed with pentane (3 × 2 mL) and dried *in vacuo* to give spectroscopically pure **2-3** as a red solid (0.042 g, 71%). ^{1}H NMR (300K, 500 MHz, benzene-d_6): δ 7.85 – 7.60 (broad overlapping resonances, H_{arom}), 7.14 (br s, H_{arom}), 7.08 – 6.53 (broad overlapping resonances, H_{arom}), 0.41 (s, 3 H, Si*Me*). $^{13}\text{C}\{^1\text{H}\}$ NMR (343K, 125.8 MHz, benzene-d_6): δ 179.8 (apparent t, C_{arom}, J = 26 Hz), 159.4 (d, C_{arom}, J = 52 Hz), 147.4 (d, C_{arom}, J = 48 Hz), 140.7 (d, C_{arom}, J = 29 Hz), 138.3 (d, $C\text{H}_{\text{arom}}$, J = 20 Hz), 135.5 – 134.5 (broad overlapping resonances, $C\text{H}_{\text{arom}}$), 134.3 (d, $C\text{H}_{\text{arom}}$, J = 11 Hz), 133.1 ($C\text{H}_{\text{arom}}$), 132.1 (d, $C\text{H}_{\text{arom}}$, J = 22 Hz), 130.0 ($C\text{H}_{\text{arom}}$), 129.6 ($C\text{H}_{\text{arom}}$), 129.0 ($C\text{H}_{\text{arom}}$), 128.8 ($C\text{H}_{\text{arom}}$), 128.0 ($C\text{H}_{\text{arom}}$), 127.8 – 127.4 (overlapping resonances, $C\text{H}_{\text{arom}}$), 124.5 ($C\text{H}_{\text{arom}}$), 1.7 (Si*Me*). $^{31}\text{P}\{^1\text{H}\}$ NMR (300K, 202.5 MHz, benzene-d_6): δ 72.1 (br d, 1 P, [Ph-PSiP]), 64.7 (br s, 1 P, [Ph-PSiP]), -34.2 (d, 1 P, $C_6H_4P\text{Ph}_2$, J_{PP} = 213 Hz). $^{31}\text{P}\{^1\text{H}\}$ NMR (233K, 101.3 MHz, toluene-d_8): δ 76.8 (d, 1 P, [Ph-PSiP], $^2J_{\text{PPtrans}}$ = 236 Hz), 68.2 (br s, 1 P, [Ph-PSiP]), -28.7 (dd, 1 P, $C_6H_4P\text{Ph}_2$, $^2J_{\text{PPtrans}}$ = 236 Hz, $^2J_{\text{PPcis}}$ = 22 Hz). $^{31}\text{P}\{^1\text{H}\}$ NMR (353K, 101.3 MHz, toluene-d_8): δ 73.1 (br s, 2 P, [Ph-PSiP]), -27.9 (apparent t, 1 P, $C_6H_4P\text{Ph}_2$, J = 102 Hz). $^{29}\text{Si}\{^1\text{H}\}$ NMR (99.4 MHz, benzene-d_6): δ 56.8. A single

crystal of **2-3**·(OEt_2) suitable for X-ray diffraction analysis was grown from diethyl ether at -30 °C.

[Ph-PSiP]Ru(CO)(κ^2-$C_6H_4PPh_2$) (2-5). A solution of **2-3** (0.12 g, 0.13 mmol) in ca. 3 mL benzene was degassed via three freeze-pump-thaw cycles. An atmosphere of CO was added to the solution to afford an immediate color change from red to yellow. The solution was left stirring overnight at room temperature after which time the solvent was removed in vacuo and the remaining white solid was washed with pentane (3 × 1 mL) to afford **2-5** (0.10 g, 83 %). IR (Film from THF, cm^{-1}): ν(CO) 1921 (strong). ^1H NMR (500 MHz, benzene-d_6): δ 8.42 (d, 2 H, H_{arom}, J = 7 Hz), 7.52 (m, 4 H, H_{arom}), 7.49 (m, 4 H, H_{arom}), 7.33 (m, 1 H, H_{arom}), 7.25 (m, 2 H, H_{arom}), 6.95 – 6.85 (overlapping resonances, 8 H, H_{arom}), 6.82 – 6.68 (overlapping resonances, 11 H, H_{arom}), 6.66 (m, 4 H, H_{arom}), 6.61 (m, 4 H, H_{arom}), 6.45 (t, 1 H, H_{arom}, J = 7 Hz), 6.16 (m, 1 H, H_{arom}), 0.63 (d, 3 H, Si*Me*, J_{HP} = 7 Hz). $^{13}C\{^1H\}$ NMR (125.8 MHz, benzene-d_6): δ 204.8 (br, *C*O), 174.9 (br, *C*O), 158.0 (t, C_{arom}, J = 25 Hz), 149.8 (t, C_{arom}, J = 28 Hz), 149.6 (t, C_{arom}, J = 28 Hz), 148.9 (C_{arom}), 148.6 (C_{arom}), 140.1 (CH_{arom}), 139.9 (CH_{arom}), 138.0 (br t, C_{arom}, J = 17 Hz), 137.9 (br t, C_{arom}, J = 17 Hz), 137.0 (C_{arom}), 136.9 (C_{arom}), 134.9 (t, C_{arom}, J = 21 Hz), 134.6 (m, CH_{arom}), 134.3 (CH_{arom}), 133.3 (br m, CH_{arom}), 133.2 (br m, CH_{arom}), 132.9 (br m, CH_{arom}), 132.8 (CH_{arom}), 132.1 (CH_{arom}), 132.0 (CH_{arom}), 131.3 (CH_{arom}), 129.7 (CH_{arom}), 129.2 (CH_{arom}), 128.5 (CH_{arom}), 128.4 (CH_{arom}), 127.7 (CH_{arom}), 127.5 (m, CH_{arom}), 121.9 (CH_{arom}), 121.8 (CH_{arom}), 7.2 (d, Si*Me*, J_{CP} = 8 Hz). $^{31}P\{^1H\}$ NMR (202.5 MHz, benzene-d_6): δ 61.0 (d, 2 P, [Ph-*P*Si*P*], J = 18 Hz), 64.5 (t , 1 P, $C_6H_4PPh_2$, J = 18 Hz). ^{29}Si NMR (99.4 MHz, benzene-d_6): δ 62.5 (d, J_{SiP} = 100 Hz). A single crystal of **2-**

5 suitable for X-ray diffraction analysis was grown from a concentrated diethyl ether solution at -30 °C.

[Ph-PSiP]RuCl(PEt_3) (2-6). A solution of **2-2** (0.16 g, 0.16 mmol) in ca. 5 mL of benzene was treated with PEt_3 (0.02 mL, 0.16 mmol). A slight color change from red to orange was observed. The volatile components of the reaction mixture were removed in vacuo and the remaining residue was washed with pentane (5 × 2 mL) to yield **2-6** as an orange solid (0.12 g, 87%). The NMR spectra of **2-6** at 300K exhibit significant line broadening. Where possible, variable temperature characterization data are provided. ^{1}H NMR (500 MHz, benzene-d_6): δ 8.4 – 7.5 (broad overlapping resonances, 12 H, H_{arom}), 7.03 (br m, 4 H, H_{arom}), 6.93 (br m, 4 H, H_{arom}), 6.86 (br m, 4 H, H_{arom}), 6.7 – 6.2 (broad overlapping resonances, 4 H, H_{arom}), 1.35 (3 H, Si*Me*), 1.26 (br m, 6 H, P(CH_2CH$_3$)$_3$), 0.70 (dt, 9 H, P(CH$_2$CH_3)$_3$, J = 13 Hz, J = 8 Hz). ^{13}C{^{1}H} NMR (125.8 MHz, benzene-d_6): δ 131.5 (*C*H$_{arom}$), 129.6 (*C*H$_{arom}$), 128.7 (*C*H$_{arom}$), 127.6 (*C*H$_{arom}$), 18.1 (d, P(*C*H$_2$CH$_3$)$_3$, J_{CP} = 21 Hz), 9.8 (s, P(CH$_2$*C*H$_3$)$_3$), 3.5 (Si*Me*). ^{31}P{^{1}H} NMR (300K, 202.5 MHz, benzene-d_6): δ 94.8 (br s, 1 P, [Ph-PSiP]), 64.5 (br d, 1 P, [Ph-PSiP], J = 283 Hz), 17.5 (d, 1 P, *P*Et$_3$, J = 255 Hz). ^{31}P{^{1}H} NMR (273K, 202.5 MHz, toluene-d_8): δ 93.8 (s, 1 P, [Ph-PSiP]), 64.6 (dd, 1 P, [Ph-PSiP], J_{PP}*trans* = 283 Hz, J_{PP}*cis* = 21 Hz), 17.3 (m, 1 P, *P*Et$_3$). ^{31}P{^{1}H} NMR (353K, 202.5 MHz, toluene-d_8): δ 80.0 (br d, 2 P, [Ph-PSiP]), 17.6 (m, 1 P, *P*Et$_3$). ^{29}Si NMR (99.4 MHz, benzene-d_6): δ 62.5. A single crystal suitable for X-ray diffraction analysis was grown from a concentrated solution of **2-6**·$(CH_2Cl_2)_{1.17}$·Et_2O in diethyl ether/dichloromethane at -30 °C.

[Ph-PSiP]RuMe(PEt_3) (2-7). A benzene solution of **2-6** (0.056 g, 0.069 mmol) was treated with MeMgBr (3.0 M in ether, 0.023 mL). A slight color change from red to

orange was observed. The volatile components of the reaction mixture were removed in vacuo and the remaining orange solid was dissolved in benzene and filtered through Celite. The volatile components of the reaction mixture were removed *in vacuo* and the resulting orange residue was washed with pentane (3 × 1 mL) and dried *in vacuo* to give **2-7** (0.044 g, 81%) as an orange solid. ^{1}H NMR (500 MHz, benzene-d_6): δ 8.27 (d, 1 H, H_{arom}, J = 7 Hz), 7.94 (d, 1 H, H_{arom}, J = 7 Hz), 7.78 (t, 2 H, H_{arom}, J = 8 Hz), 7.23 (m, 2 H, H_{arom}), 7.11 (m, 2 H, H_{arom}), 6.98 – 6.72 (overlapping resonances, 15 H, H_{arom}), 6.72 (m, 1 H, H_{arom}), 1.51 (m, 3 H, PCH_2CH$_3$), 1.48 – 1.35 (overlapping resonances, 6 H, PCH_2CH$_3$ + Ru*Me*; signals at 1.42 and 1.41 were assigned to the PCH_2CH$_3$ and Ru*Me* protons, respectively, on the basis of a ^{1}H-^{13}C HMQC experiment), 1.01 (d, 3 H, Si*Me*, J = 1 Hz), 0.57 (dt, 9 H, PCH$_2$*CH$_3$*, J_{HP} = 13 Hz, J_{HH} = 8 Hz). ^{13}C{^{1}H} NMR (125.8 MHz, benzene-d_6): δ 166.8 (m, C_{arom}), 158.0 (d, C_{arom}, J = 59 Hz), 154.1 (m, C_{arom}), 151.6 (d, C_{arom}, J = 48 Hz), 149.8 (dd, C_{arom}, J = 46 Hz, J = 8 Hz), 147.1 (m, C_{arom}), 142.6 (d, C_{arom}, J = 29 Hz), 141.0 (d, C_{arom}, J = 20 Hz), 134.8 (*C*H$_{arom}$), 134.7 (*C*H$_{arom}$), 134.3 (*C*H$_{arom}$), 134.1 (*C*H$_{arom}$), 133.8 (*C*H$_{arom}$), 133.7 (*C*H$_{arom}$), 133.3 (*C*H$_{arom}$), 133.1 (*C*H$_{arom}$), 132.8 (*C*H$_{arom}$), 129.6 (m, *C*H$_{arom}$), 19.3 (d, P*C*H$_2$CH$_3$, J = 15 Hz), 7.8 (SiMe), 6.8 (PCH$_2$*CH$_3$*), -1.6 (Ru*Me*). ^{31}P{^{1}H} NMR (202.5 MHz, benzene-d_6): δ 55.8 (t, 1 P, [Cy-PSiP], J = 20 Hz), -1.3 (t, 1 P, [Cy-PSiP], J = 19 Hz), -8.2 (t, 1 P, CH$_2$CH$_2$*P*Et$_2$, J = 19 Hz). ^{29}Si{^{1}H} NMR (99.4 MHz, benzene-d_6): δ 59.4 (d, J_{SiP} = 138 Hz).

[Ph-PSiP]RuH(N$_2$)(PPh$_3$) (2-8a). LiEt$_3$BH (0.10 mL, 1.0 M in THF, 0.10 mmol) was added to a room temperature solution of **2-2** (0.10 g, 0.10 mmol) in 5 mL of benzene. The resulting red solution was allowed to stir at room temperature for 16 h. The volatile components were removed *in vacuo*, and the remaining residue was extracted into ca. 5

mL of benzene. The benzene extract was filtered through Celite, and the benzene was then removed *in vacuo*. The remaining red-pink residue was washed with 3 × 3 mL of diethyl ether to afford **2-8a** (0.061 g, 64%) as a pale pink solid. IR (Nujol, cm^{-1}): $\nu(N_2)$ 2131 (m), ν(RuH) 1910 (w). ^{1}H NMR (500 MHz, tetrahydrofuran-d_8): δ 8.26 (d, 2 H, H_{arom}, J_{HH} = 7 Hz), 7.31 – 7.12 (16 H, H_{arom}), 7.03 (apparent t, 2 H, H_{arom}, J_{HH} = 7 Hz), 7.00 – 6.86 (15 H, H_{arom}), 6.74 (apparent t, 6 H, H_{arom}, J_{HH} = 7 Hz), 6.68 (br s, 2 H, H_{arom}), 0.36 (s, 3 H, Si*Me*), -14.05 (td, 1 H, Ru*H*, $^2J_{HP}$ = 10 Hz, $^2J_{HP}$ = 27 Hz). ^{13}C{^{1}H} NMR (125.8 MHz, tetrahydrofuran-d_8): δ 157.2 (m, C_{arom}), 152.4 (br m, C_{arom}), 140.3 (apparent t, C_{arom}, J_{CP} = 23 Hz), 139.2 (m, C_{arom}), 135.7 (m, CH_{arom}), 134.6 (CH_{arom}), 133.2 (CH_{arom}), 132.6 (apparent t, CH_{arom}, J_{CP} = 11 Hz), 132.1 (CH_{arom}), 129.7 (CH_{arom}), 129.2 (CH_{arom}), 129.0 (CH_{arom}), 128.7 (CH_{arom}), 128.3 (CH_{arom}), 128.2 (CH_{arom}), 128.0 (CH_{arom}), 127.9 (CH_{arom}), 5.4 (Si*Me*). ^{31}P{^{1}H} NMR (202.5 MHz, tetrahydrofuran-d_8): δ 64.3 (d, 2 P, [Ph-PSiP], $^2J_{PP}$ = 19 Hz), 34.2 (t, 1 P, PPh_3, $^2J_{PP}$ = 19 Hz). ^{29}Si{^{1}H} NMR (99.4 MHz, tetrahydrofuran-d_8): δ 67.4. Anal. Calcd for $C_{55}H_{47}N_2P_3RuSi$: C, 68.95; H, 4.94; N, 2.92. Found: C, 68.68; H, 5.22; N, 2.79.

[Ph-PSiP]RuH(H_2)(PPh_3) (2-8b). A solution of **2-8a** in *ca.* 0.7 mL of d_6-benzene was degassed via three freeze-pump-thaw cycles and an atmosphere of H_2 was introduced to the sample. Upon mixing a color change from pink to pale yellow was observed. ^{1}H NMR (250 MHz, benzene-d_6): δ 8.36 (d, 2 H, H_{arom}, J = 7 Hz), 7.86 – 7.24 (br overlapping resonances, 12 H, H_{arom}), 6.98 (m, 10 H, H_{arom}), 6.85 (m, 10 H, H_{arom}), 6.67 (m, 4 H, H_{arom}), 0.97 (3 H, Si*Me*), -7.13 (br s, 3 H, Ru(*H*)(*H*$_2$)). ^{31}P{^{1}H} NMR (101.2 MHz, benzene-d_6): δ 70.0 (d, 2 P, [Ph-*P*Si*P*], J = 15 Hz), 46.9 (t, 1 P, PPh_3, J = 15 Hz).

[Ph-PSiP]RuN(SiMe$_3$)$_2$ (2-9). A solution of NaN(SiMe$_3$)$_2$ (0.05 g, 0.27 mmol) in ca. 2 mL of THF was added to a solution of **2-2** (0.26 g, 0.27 mmol) in ca. 3 mL of THF. The solution was allowed to stand for 1 h at room temperature. The volatile components of the reaction mixture were removed *in vacuo* and the remaining residue was dissolved in benzene. The solution was filtered through Celite and the benzene solvent was removed *in vacuo*. The isolated solid was washed with pentane (10 × 1 mL) to afford **2-9** as a red powder (0.17 g, 75%). ^{1}H NMR (500 MHz, benzene-d_6): δ 8.07 (m, 4 H, H_{arom}), 7.77 (d, 2 H, H_{arom}, J = 7 Hz), 7.08 (apparent t, 4 H, H_{arom}, J = 8 Hz), 7.03 (apparent t, 4 H, H_{arom}, J = 7 Hz), 7.00 (apparent t, 2 H, H_{arom}, J = 7 Hz), 6.88 (apparent t, 2 H, H_{arom}, J = 7 Hz), 6.76 (apparent t, 2 H, H_{arom}, J = 7 Hz), 6.65 – 6.57 (overlapping resonances, 8 H, H_{arom}), 1.26 (s, 3 H, Si*Me*), 0.51 – 046 (br overlapping resonances, 18 H, N(Si*Me*$_3$)$_2$). ^{13}C{^{1}H} NMR (125.8 MHz, benzene-d_6): δ 159.4 (m, C_{arom}), 146.0 (d, C_{arom}, J = 57 Hz), 138.9 (d, C_{arom}, J = 44 Hz), 136.4 (m, C_{arom}), 134.6 (m, CH$_{arom}$), 133.2 (m, CH$_{arom}$), 131.7 (apparent t, CH$_{arom}$, J = 11 Hz), 130.0 (CH$_{arom}$), 129.7 (CH$_{arom}$), 129.6 (CH$_{arom}$), 128.7 (CH$_{arom}$), 127.4 (CH$_{arom}$), 6.1 (N(Si*Me*$_3$)$_2$), 3.8 (N(Si*Me*$_3$)$_2$), 2.1 (Si*Me*). ^{31}P{^{1}H} NMR (202.5 MHz, benzene-d_6): δ 93.2. ^{29}Si NMR (99.4 MHz, benzene-d_6): δ 58.1 (*Si*Me), 56.4 (N(*Si*Me$_3$)$_2$).

[Ph-PSiP]RuO^{t}Bu (2-10). A solution of **2-2** (0.02 g, 0.02 mmol) in *ca.* 0.7 mL of d_8-THF was treated with KO^{t}Bu (0.002 g, 0.02 mmol) and the reaction mixture was allowed to stand at room temperature for 1 h. ^{1}H NMR (500 MHz, tetrahydrofuran-d_8): δ 7.91 (d, 1 H, H_{arom}, J = 7 Hz), 7.87 (m, 2 H, H_{arom}), 7.36 (m, 2 H, H_{arom}), 7.26 – 7.15 (broad overlapping resonances, 15 H, H_{arom}), 7.04 (apparent t, 4 H, H_{arom}), 6.75 (apparent

t, 2 H, H_{arom}), 6.63 (m, 2 H, H_{arom}), 1.20 (s, 3 H, Si*Me*), 1.14 (s, 9 H, O^t*Bu*). $^{31}P\{^1H\}$ NMR (202.5 MHz, THF-d_8): δ 99.2.

2.4.3 Crystallographic solution, refinement, and structural details for 2-2·$(OEt_2)_{1.5}$, 2-3·(OEt_2), 2-5, and 2-6·$(CH_2Cl_2)_{1.17}$·(OEt_2).

Crystallographic data for **2-2**·$(OEt_2)_{1.5}$, **2-3**·(OEt_2), and **2-5** were obtained at 193(±2)K on a Bruker PLATFORM/SMART 1000 CCD diffractometer using a graphite-monochromated Mo Kα (λ = 0.71073 Å) radiation, employing a sample that was mounted in inert oil and transferred to a cold gas stream on the diffractometer. Crystallographic data for **2-6**·$(CH_2Cl_2)_{1.17}$·(OEt_2) were obtained at 173(±2)K on a Bruker D8/APEX II CCD diffractometer using a graphite-monochromated Mo Kα (λ = 0.71073 Å) radiation, employing a sample that was mounted in inert oil and transferred to a cold gas stream on the diffractometer. Programs for diffractometer operation, data collection, and data reduction (including SAINT) were supplied by Bruker. Gaussian integration (face-indexed) was employed as the absorption correction method for **2-2**·$(OEt_2)_{1.5}$, **2-3**·(OEt_2), and **2-6**·$(CH_2Cl_2)_{1.17}$·(OEt_2). *SADABS* (Bruker) was employed as the absorption correction method for **2-5**. The structures for **2-2**·$(OEt_2)_{1.5}$ and **2-5** were solved by use of the Patterson search/structure expansion while the structure for **2-3**·(OEt_2) and **2-6**·$(CH_2Cl_2)_{1.17}$·(OEt_2) were solved using direct methods. The structures were refined by use of full-matrix least-squares procedures (on F^2) with R_1 based on $F_o^2 \geq 2\sigma(F_o^2)$ and wR_2 based on $F_o^2 \geq -3\sigma(F_o^2)$. During the structure solution process for **2-2**·$(OEt_2)_{1.5}$, 1.5 molecules of diethyl ether were located in the asymmetric unit and refined in a satisfactory manner. During the structure solution process for **2-3**·(OEt_2), 1 molecule of

diethyl ether was located in the asymmetric unit and refined in a satisfactory manner. During the structure solution process for **2-6**·$(CH_2Cl_2)_{1.17}$·(OEt_2), 1 molecule of diethyl ether was located in the asymmetric unit and refined in a satisfactory manner. Attempts to refine peaks of residual electron density near the unit cell origin as disordered or partial-occupancy solvent dichloromethane chlorine or carbon atoms were unsuccessful. The data were corrected for disordered electron density through use of the SQUEEZE procedure. A total solvent-accessible void volume of 436.9 $Å^3$ with a total electron count of 107 (consistent with 3 molecules of solvent dichloromethane, or 1/6 molecule of CH_2Cl_2 per formula unit of the ruthenium complex molecule) was found in the unit cell. Furthermore, one ethyl group of the triethylphosphine ligand was found to be disordered and required the following distances to be restrained to be equal (within 0.03 Å) during refinement: d(P3–C6A) = d(P3–C6B); d(C6A–C7A) = d(C6B–C7B). Atoms C6A and C7A were refined anisotropically with an occupancy factor of 0.6, while atoms C6B and C7B were refined anisotropically with an occupancy factor of 0.4. Anisotropic displacement parameters were employed throughout for the non-hydrogen atoms, and all hydrogen-atoms were added at calculated positions and refined by use of a riding model employing isotropic displacement parameters based on the isotropic displacement parameter of the attached atom. All relevant crystal data for **2-2**·$(OEt_2)_{1.5}$**, 2-3**·(OEt_2)**, 2-5**, and **2-6**·$(CH_2Cl_2)_{1.17}$·(OEt_2) are provided in Appendix A.

2.4.4 Typical procedure for the catalytic transfer hydrogenation of ketones.

All catalytic runs were conducted under a nitrogen atmosphere in resealable glass reaction cells fitted with a PTFE stopcock. The Ru pre-catalyst **2-2** (2.2 mg; 0.0023

mmol) was dissolved in THF (2.000 mL) and from this freshly prepared stock solution a 175 μL (0.20 μmol) aliquot was delivered by use of an Eppendorf pipette to a cell containing a magnetic stir bar. The solvent within the cell was then removed *in vacuo*, and subsequently 1.000 mL of a freshly prepared solution of ketone and KO^{t}Bu in ^{i}PrOH was added (8.000 mL ^{i}PrOH, 1.8 mg KO^{t}Bu, 70.8 μL cyclopentanone; [ketone] = 0.1M; Ru:KO^{t}Bu:ketone = 1:10:500). Stirring was initiated and the solution was then heated in an 82(±2) °C oil bath. Conversions were determined by use of GC-FID (average of at least two runs) and the identities of the hydrogenation products were confirmed by comparison to authentic samples.

Chapter 3: Synthesis and Reactivity of Four-Coordinate, Formally 14-electron Ru^{II} Complexes Featuring a Bis(cyclohexylphosphino)silyl Ligand

3.1 Introduction

Coordinatively and electronically unsaturated late transition metal complexes that feature less than 16 valence electrons are invoked as key intermediates in numerous stoichiometric and catalytic metal-mediated processes.[1] Although there is significant interest in the preparation and study of such complexes in order to better understand their role in organometallic reactivity, their isolation is typically thwarted by their highly reactive nature. As such, the identification of strategies for the preparation of isolable transition metal complexes that formally feature less than 16 valence electrons continues to attract significant interest. In the case of Ru^{II}, the vast majority of isolated complexes are either five- or six-coordinate species that feature 16- or 18-electron configurations, respectively.[75] In contrast, crystallographically characterized four-coordinate, formally 14-electron Ru^{II} complexes are exceedingly rare,[43,48-50,76-78] and with few exceptions,[76,77] feature the presence of stabilizing C-H agostic interactions[49,50,78] that facilitate their isolation. Notably, Caulton and co-workers have reported the unusual square planar, 14-electron Ru^{II} complex $(({}^{t}Bu_2PCH_2SiMe_2)_2N)RuCl$ that does not feature agostic stabilization as a consequence of adopting a triplet spin state.[43] More recently, Schneider and co-workers reported the synthesis of the closely related square planar complex $(({}^{t}Bu_2PCH_2CH_2)_2N)RuCl$ that adopts a singlet ground state as a result of increased π-donation from the chelating dialkyl amido ligand relative to Caulton's disilyl amido.[48]

Given the rarity of formally 14-electron Ru^{II} complexes devoid of agostic stabilization and the insights that might be obtained through the systematic study of such species, the development of alternative new strategies for the synthesis of unsaturated Ru complexes is an important challenge. Moreover, the identification of new structural motifs in such low coordinate species represents a significant advance, as examples that do not require agostic stabilization are currently limited to square planar species. The discovery of new classes of four-coordinate Ru^{II} complexes that adopt novel structures is anticipated to broaden our understanding of the electronic and steric factors underlying the preferred geometries of four-coordinate Ru^{II} complexes as well as provide access to new types of reactivity for such unsaturated species.

In this context, the Turculet group has recently reported on the synthesis and reactivity of a variety of coordinatively unsaturated late transition metal complexes supported by tridentate bis(phosphino)silyl ligands of the type $[\kappa^3\text{-}(2\text{-}Cy_2PC_6H_4)_2SiMe]^-$ ([Cy-PSiP]),[39,79] including examples of pincer-like Ir species that can undergo facile intermolecular C-H and N-H bond activation chemistry,[39,79b] as well as a series of square planar Group 10 complexes that undergo unusual Si-C bond cleavage reactions.[79d] In building on these studies, tridentate bis(phosphino)silyl ligation can be envisioned to provide an attractive entry point for the synthesis of low-coordinate Ru^{II} complexes, whereby both the steric demands of the phosphino substituents and the strongly *trans*-directing silyl group would enforce the formation of such coordinatively unsaturated species. In this regard the isolation and solution/solid state characterization of diamagnetic, four-coordinate, formally 14-electron [Cy-PSiP]RuX (X = amido, alkoxo) complexes that do not require agostic stabilization and that adopt a highly unusual

trigonal pyramidal coordination geometry are reported herein. Computational studies carried out in collaboration with Dr. Sven Tobisch (University of St. Andrews) confirm the key role of the strongly σ-donating silyl group of the Cy-PSiP ligand in enforcing this unusual geometry. While silyl ligation affords stability to the four-cordinate [Cy-PSiP]RuX complexes featured herein, these low-coordinate species are still capable of reacting with substrate E-H bonds, as demonstrated by their ability to undergo N-H/B-H bond activation upon treatment with amine borane reagents.

3.2 Results and Discussion

3.2.1 Synthesis and structural characterization of four-coordinate [Cy-PSiP]RuX complexes.

The reaction of the tertiary silane [(2-$Cy_2PC_6H_4)_2$SiMe]H (**3-1**, [Cy-PSiP]H) with 0.5 [(*p*-cymene)$RuCl_2]_2$ in the presence of Et_3N and PCy_3 afforded orange, diamagnetic ([Cy-PSiP]$RuCl)_2$ (**3-2**) in 74% yield (Scheme 3-1). The solid state structure of **3-2**·$(C_6H_6)_{3.5}$ was determined by single crystal X-ray diffraction analysis (Figure 3-1), and is consistent with the formulation of **3-2** as a dinuclear complex that features bridging chloride ligands.

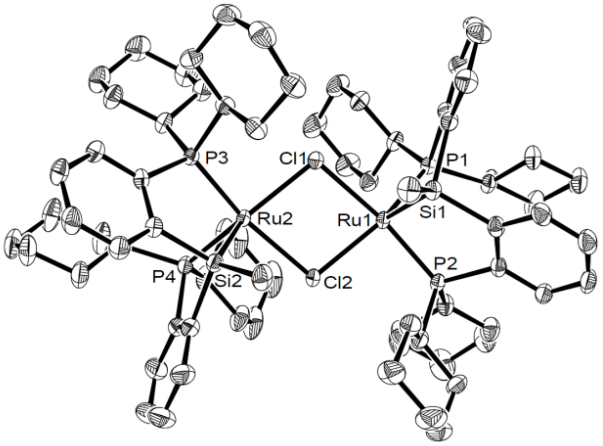

Figure 3-1. The crystallographically determined structure of **3-2**·$(C_6H_6)_{3.5}$ shown with 50% ellipsoids; H atoms and the C_6H_6 solvate have been omitted for clarity. Selected interatomic distances (Å) and angles (deg): Ru1-Cl1 2.4597(7), Ru1-Cl2 2.4591(7), Ru1-Si1 2.2770(8), Ru2-Cl1 2.4815(7), Ru2-Cl2 2.4748(7), Ru2-Si2 2.2733(8), P1-Ru1-P2 97.05(3), P3-Ru2-P4 96.52(3).

Complex **3-2** serves as a useful precursor for the synthesis of novel 14-electron [Cy-PSiP]RuX (X = amido, alkoxo) complexes (Scheme 3-1). Thus, treatment of **3-2** with KO^{t}Bu in benzene solution at room temperature led to the formation of red, diamagnetic [Cy-PSiP]RuO^{t}Bu (**3-3**), which exhibits a single ^{31}P NMR resonance at 110.5 ppm. Complex **3-3** was readily isolated in 97% yield and is formulated as a monomeric, formally 14-electron species on the basis of solution NMR and X-ray diffraction data (Figure 3-2). Surprisingly, despite the prevalence of square planar and tetrahedral geometries for four-coordinate transition metal complexes, the solid state structure of **3-3** exhibits slightly distorted trigonal pyramidal coordination geometry at Ru, with Si in the apical site. The sum of P1-Ru-P2 (99.25(2)°), P1-Ru-O (127.21(5)°) and P2-Ru-O (129.16(5)°) angles is 355.62°, which is very close to idealized trigonal planar geometry at Ru in the equatorial plane. Notably, no agostic interactions are apparent in the solid state structure of **3-3** (all Ru···C > 3 Å). The geometry at the O^{t}Bu

ligand oxygen is bent (Ru-O-C2 = 152.0(2)°), and the Ru-O distance of 1.909(1) Å is statistically shorter than the analogous linkage found in Ru alkoxide complexes where Ru-O π-bonding has been invoked (e.g. 1.99(1) Å for $Cp^*Ru(PCy_3)(OCH_2CF_3)$).[80]

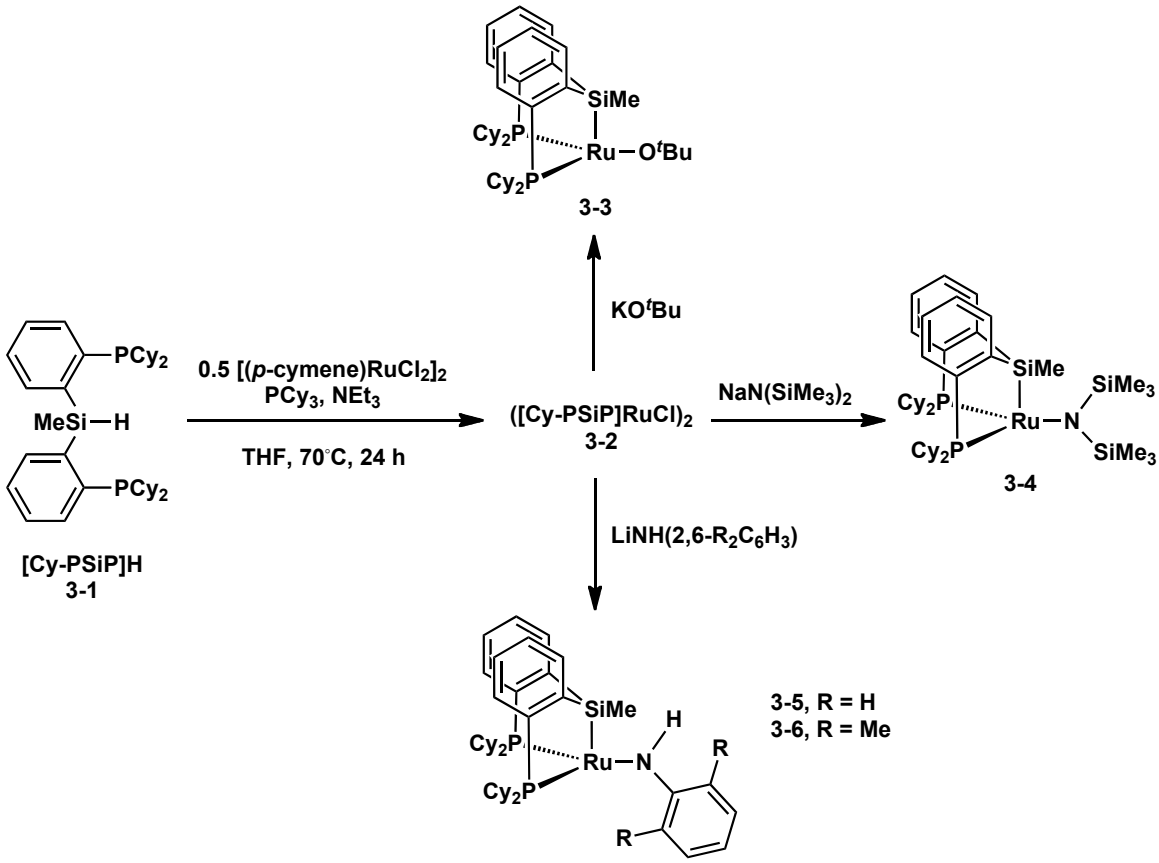

Scheme 3-1. Synthesis of [Cy-PSiP]Ru complexes.

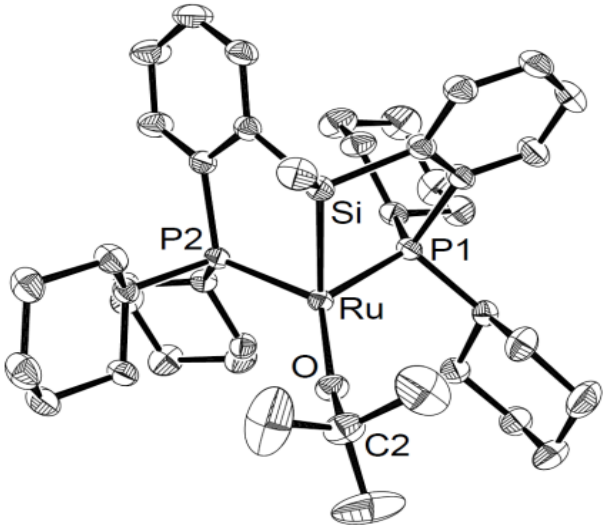

Figure 3-2. The crystallographically determined structure of **3-3**·C_6H_6·$(C_5H_{12})_{0.5}$ shown with 50% ellipsoids; H atoms and the C_6H_6 and C_5H_{12} solvates have been omitted for clarity. Selected interatomic distances (Å) and angles (deg): Ru-Si 2.2859(6), Ru-O 1.9090(14), P1-Ru-P2 99.25(2), P1-Ru-O 127.21(5), P2-Ru-O 129.16(5).

The alkoxide complex **3-3** represents a rare example of a four-coordinate, formally 14-electron Ru^{II} complex. A rare example of a comparable species for which crystallographic data have been presented is $(Cy_3P)(^tBuO)_2Ru{=}CHPh$ (Ru-O = 1.9412(15), 1.9558(15) Å), in which the phosphine ligand occupies the apical position of the distorted trigonal pyramidal structure.[81,82] Conversely, the spin triplet 14-electron complex *trans*-$Ru(^tBu_2PCH_2SiMe_2O)_2$ reported by Caulton and co-workers features square planar geometry.[76] Interestingly, although mononuclear **3-3** can be viewed as being isoelectronic with Cp*RuOR, Cp*RuO^tBu has been reported to be unstable[83a] and complexes such as Cp*Ru(OCH_2CF_3) and Cp*Ru(OMe) are dimers in the solid state.[80,83b]

In an effort to further explore the synthesis of such four-coordinate [Cy-PSiP]RuX species, the synthesis of related amido complexes was also pursued. Thus, treatment of **3-2** with $NaN(SiMe_3)_2$ in benzene solution at room temperature led to the formation of dark red, diamagnetic [Cy-PSiP]Ru$N(SiMe_3)_2$ (**3-4**, 70% yield), which

exhibits a single ^{31}P NMR resonance at 98.9 ppm. The solid state structure of **3-4** (Figure 3-3) indicates a monomeric complex that, as in the case of complex **3-3**, exhibits a highly unusual distorted trigonal pyramidal coordination geometry at Ru with Si in the apical site ($\Sigma_{PRuP,PRuN}$ = 357.70°). As in the case of **3-3**, no agostic interactions are apparent in the solid state structure of **3-4** (all Ru···C > 3 Å). The planar amido ligand ($\Sigma_{SiNSi,SiNRu}$ = 359.65°) is oriented perpendicular to the trigonal plane of the complex, with a Ru-N bond distance of 2.047(1) Å that is comparable to that observed for Caulton's square planar ((^{t}Bu$_2$PCH$_2$SiMe$_2$)$_2$N)RuCl (Ru-N = 2.050(1) Å),[43] suggesting the possibility of π-donation from N to Ru. Notably, the Ru-N distance reported by Schneider and co-workers for the related square planar complex (^{t}Bu$_2$PCH$_2$CH$_2$)$_2$N)RuCl, where significant Ru-N π-bonding is invoked, is much shorter at 1.890(2) Å.[48]

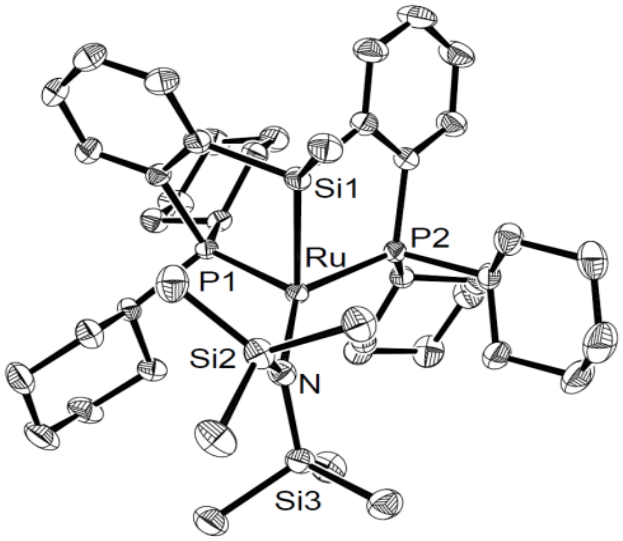

Figure 3-3. The crystallographically determined structure of **3-4** shown with 50% ellipsoids; H atoms have been omitted for clarity. Selected interatomic distances (Å) and angles (deg): Ru-Si1 2.3087(4), Ru-N 2.0465(12), P1-Ru-P2 97.341(14), P1-Ru-N 125.61(4), P2-Ru-N 134.75(4).

The synthesis of related anilido complexes was also pursued by treating **3-2** with LiNH(2,6-$R_2C_6H_3$) (R = H, Me) reagents. The corresponding anilido complexes [Cy-PSiP]RuNH(2,6-$R_2C_6H_3$) (**3-5**, R = H; **3-6**, R = Me) were each isolated as dark red solids in >90% yield. Complexes **3-5** and **3-6** each exhibit a single ^{31}P NMR resonance at 96.5 and 94.2 ppm, respectively. In addition, the ^{1}H NMR spectra of **3-5** and **3-6** (benzene-d_6) each feature a broad resonance corresponding to the N*H* proton of the anilido ligand at 6.35 and 7.57 ppm, respectively. Although X-ray quality crystals of **3-5** proved elusive, the solid state structure of **3-6** (Figure 3-4) indicates a monomeric complex that, as in the case of complexes **3-3** and **3-4**, exhibits slightly distorted trigonal pyramidal coordination geometry at Ru with Si in the apical site ($\Sigma_{PRuP,PRuN}$ = 359.34°). The Ru-N distance of 1.995(2) Å is somewhat shorter than the Ru-N distance in **3-4** and is considerably shorter than the Ru-N distances in the dimeric species [Cp*Ru(μ-NHPh)]$_2$ (2.101(8) and 2.117(7) Å).[84] The anilido phenyl ring in **3-6** is oriented nearly perpendicular to the P_2RuN plane, as indicated by the Ru-N-C-C torsional angle of 175.9(2)°. This orientation positions a methyl substituent (C9) on the anilido ligand proximal to the empty coordination site *trans* to Si. The resulting short Ru···C9 distance of 2.749(3) Å is consistent with a C-H agostic interaction, the existence of which is authenticated by computational data (*vide infra*). The absence of stabilizing agostic interactions in complexes **3-3** and **3-4** suggests that such an interaction in **3-6** may result from the fortuitous positioning of an anilido methyl substituent arising from the sterically and/or electronically preferred orientation of the anilido ligand. The predisposition for such *ortho*-Me substituents to engage in agostic interactions due to their inherent proximity to a coordinatively unsaturated metal center has been previously documented for *ortho*-Me-

substituted aryl phosphine ligands.[49]

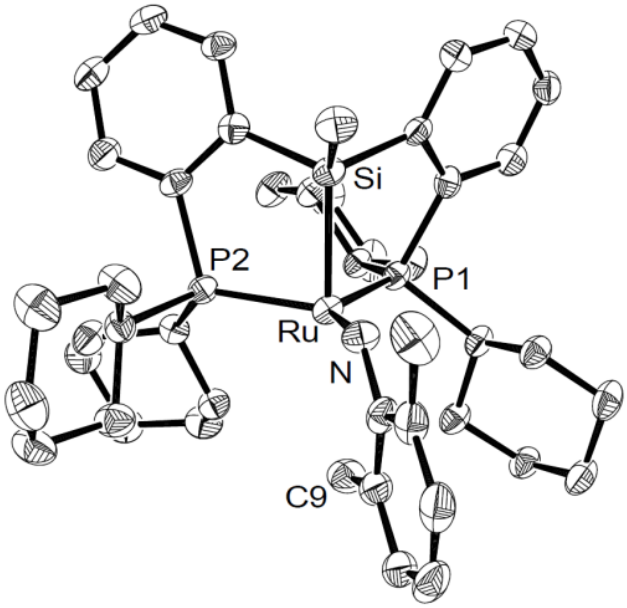

Figure 3-4. The crystallographically determined structure of **3-6** shown with 50% ellipsoids; selected H atoms have been omitted for clarity. Selected interatomic distances (Å) and angles (deg): Ru-Si 2.2813(11), Ru-N 1.995(2), Ru···C9 2.749(3), P1-Ru-P2 100.26(4), P1-Ru-N 133.62(8), P2-Ru-N 125.46(8).

3.2.2 Reactivity studies.

It was anticipated that the polarized Ru-X bonds in the four-coordinate [Cy-PSiP]Ru complexes would be reactive toward substrates featuring polar unsaturated bonds. Complex **3-6** was found to react quantitatively (^{31}P NMR) with one equiv of 2,6-xylylisocyanide to form the new iminocarbamoyl complex [Cy-PSiP]RuC(NHAr)=NAr (Ar = 2,6-$Me_2C_6H_3$, **3-7**, eq 3-1), the product of 1,1-insertion of the isocyanide into the Ru-N bond. Attempts to obtain a single crystal of **3-7** suitable for X-ray diffraction studies were unsuccessful, making unambiguous formulation of the product difficult. The ^{31}P NMR spectrum of **3-7** features a singlet at 48 ppm, indicative of equivalent [Cy-

PSiP] ligand phosphine groups. The aryl methyl protons are observed in the ^{1}H NMR spectrum (benzene-d_6) at 2.71 (s, 3 H), 2.49 (br s, 6 H), and 1.35 (s, 3 H) ppm. These data suggest that one of the aryl groups in **3-7** is able to freely rotate about the C_{ipso}-N bond leading to equivalent methyl groups (2.49 ppm), while the rotation of the second aryl group is hindered, leading to inequivalent methyl signals at 2.71 and 1.35 ppm. The NH proton is observed at 0.72 ppm, and this assignment was confirmed by a ^{1}H-^{15}N HMQC experiment. Additionally, the resonance at 2.71 ppm in the ^{1}H NMR spectrum of **3-7** correlates to Si in a ^{1}H-^{29}Si HMBC NMR experiment, indicating that an interaction exists between Ru and this methyl group. No such correlation was observed for the methyl resonance at 1.35 ppm. It is possible that an interaction between the Ru center and the methyl group is enough to effectively hinder the C_{ipso}-N bond rotation that would lead to equivalent methyl groups.

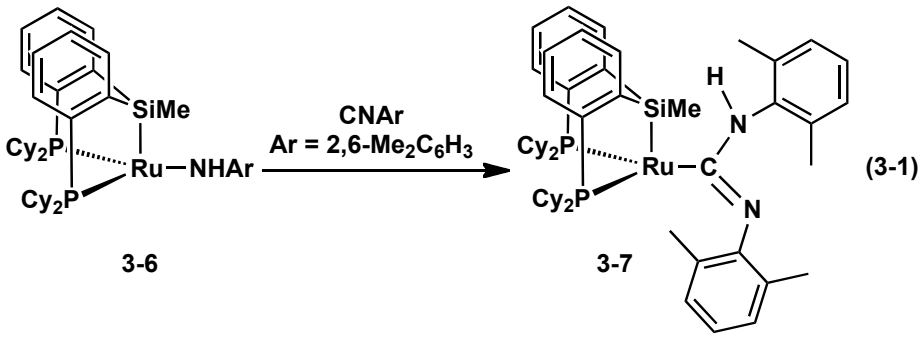

In an effort to determine if complexes such as **3-3** and **3-4** could serve as precursors to new low-coordinate Ru species via protonolysis reactions, the reactivity of these complexes with reagents that feature relatively acidic O-H groups was probed. The reactivity of **3-3** and **3-4** with H_2O and PhOH was probed, as the corresponding hydroxo

and phenoxo Ru complexes were not accessible via reactions of **3-2** with the corresponding alkali metal salts (MOH or MOPh, where M = alkali metal). Both **3-3** and **3-4** were found to react quantitatively (^{31}P NMR) with one equiv of degassed H_2O to form the new dimeric hydroxo complex **3-8** (Scheme 3-2). The solid state structure of **3-8** (Figure 3-5) is similar to that previously observed for **3-2** and confirms the formation of a dinuclear Ru complex with bridging hydroxo ligands. Each Ru center features distorted square based pyramidal coordination geometry, with Si occupying the apical site. The Ru-O distances in **3-8** (2.070(3) – 2.124(3) Å) are all significantly longer than the Ru-O distance of 1.909(1) Å observed for **3-3**. The dimeric nature of **3-8** relative to monomeric **3-3** confirms that steric bulk plays an important role in attaining a monomeric structure for complexes of the type [Cy-PSiP]RuX. In room temperature benzene solution, **3-8** exhibits inequivalent phosphorus environments on the NMR timescale, as evidenced by two $^{31}P\{^1H\}$ NMR resonances observed at 91.2 (d, 2 P, $^2J_{PP}$ = 25 Hz) and 86.5 (d, 2 P, $^2J_{PP}$ = 25 Hz) ppm. Coalescence of these resonances is observed upon warming, such that a single ^{31}P NMR resonance (94.8 ppm) is observed for the complex at 363K.

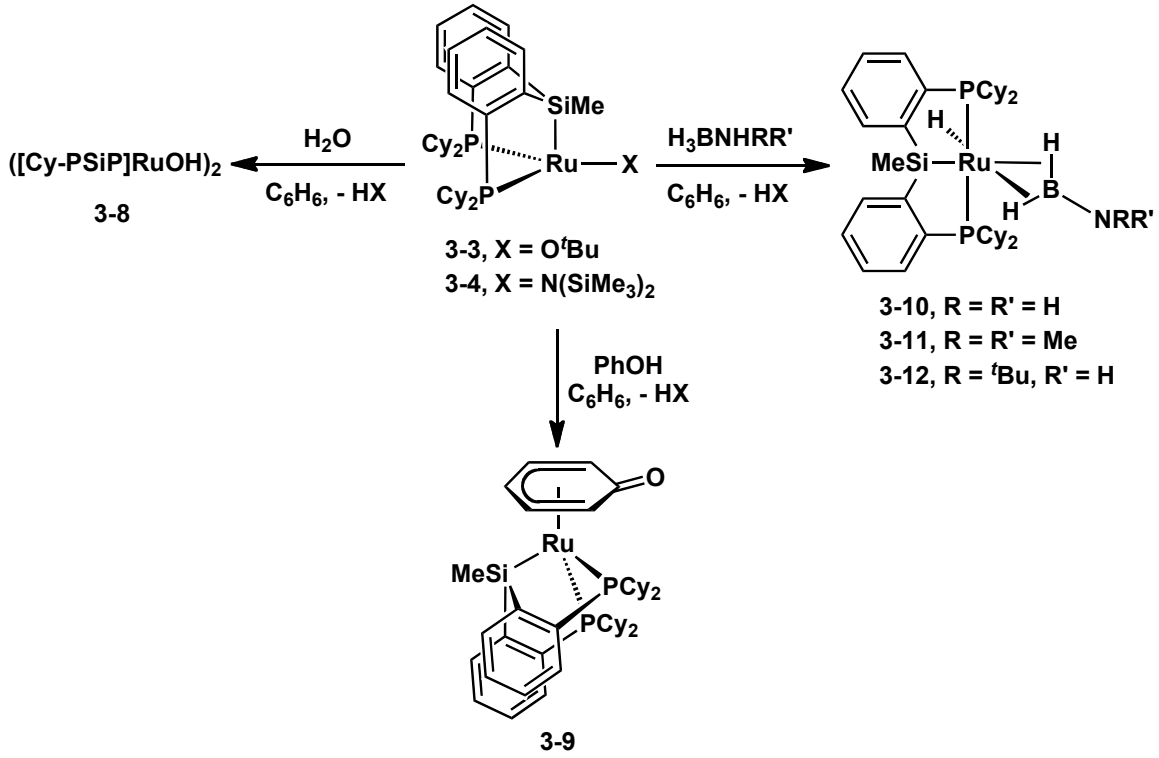

Scheme 3-2. Reactivity of four-coordinate [Cy-PSiP]RuX (X = O^{t}Bu, N(SiMe$_3$)$_2$) complexes.

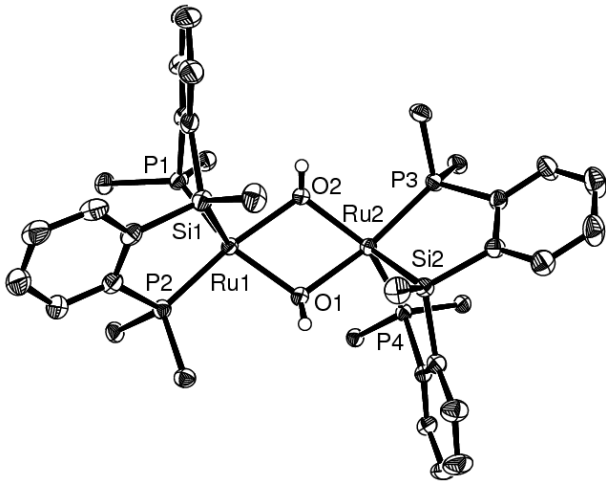

Figure 3-5. The crystallographically determined structure of **3-8**·C_7H_8 shown with 50% ellipsoids; selected H and cyclohexylphosphino C atoms, as well as the C_7H_8 solvate have been omitted for clarity. Selected interatomic distances (Å) and angles (deg): Ru1-Si1 2.2647(12), Ru2-Si2 2.2692(12), Ru1-O1 2.079(3), Ru2-O1 2.124(3), Ru1-O2 2.115(3), Ru2-O2 2.070(3), P1-Ru1-P2 99.98(4), P3-Ru2-P4 101.11(4), O1-Ru1-O2 70.74(11), O1-Ru2-O2 70.74(11), Ru1-O1-Ru2 107.81(13), Ru1-O2-Ru2 108.43(13).

Although complexes **3-2** and **3-8** are dimers in the solid-state, it is of interest to probe the nuclearity of these complexes in solution, since monomeric species of the type [Cy-PSiP]RuX are clearly viable. ^{1}H DOSY NMR techniques were employed to measure the diffusion coefficients of **3-2** and **3-8** in order to determine the nature of these complexes in solution.[85] Waldeck and co-workers have shown that the diffusion coefficients of two molecules in the same solvent are related to the cube root of the inverse ratio of their molecular weights as shown in eq 3-2.[86] This relationship assumes that the Stokes-Einstein theory of diffusion is true for the molecules in question and that the molecules can be approximated as uniform spheres. We chose to measure the diffusion coefficient of monomeric **3-3** to compare with that of **3-2** and **3-8**. The diffusion coefficients of **3-2**, **3-3**, and **3-8** were measured to be 5.13×10^{-10}, 6.16×10^{-10},

and 5.37×10^{-10} m^2 s^{-1}, respectively. Using the relationship given in eq 3-2 the molecular weights of **3-2** and **3-8** are determined to be 1323 (*cf.* 1452 g mol^{-1} calculated for **3-2**) and 1153 g mol^{-1} (*cf.* 1416 g mol^{-1} calculated for **3-8**), respectively, which suggests that these complexes are dimers in solution.

$$\frac{D_1}{D_2} = \sqrt[3]{\frac{MW_1}{MW_2}} \quad \textbf{(3-2)}$$

Complexes **3-3** and **3-4** were also observed to react quantitatively (^{31}P NMR) with one equiv of PhOH to form the new 18-electron η^5-oxocyclohexadienyl complex **3-9** (Scheme 3-2). The solid state structure of **3-9** (Figure 3-6) confirms the pentadienyl nature of the η^5-C_6H_5O ligand, as indicated by the shortened C-C bond distances within the pentadienyl ring (1.392(3) - 1.408(3) Å) relative to the C-C bonds to C2 (C2-C3 1.453(4) Å, C2-C7 1.438(3) Å). The O-C2 distance of 1.249(3) Å is consistent with double bond character and is comparable to analogous distances previously reported for η^5-oxocyclohexadienyl complexes (e.g. 1.256(4) Å for Cp*Ru(η^5-2,6-^{t}Bu$_2$$C_6H_3O$)[83b] and 1.277 Å for Ru(H)(PPh_3)$_2$(η^5-C_6H_5O)·MeOH[87]). The phenyl ring is slightly folded such that the *ipso* carbon C2 is bent further away from the Ru center, as indicated by examination of the least squares planes. The *ipso* carbon and O atoms lie 0.191(3) and 0.419(4) Å, respectively, out of the plane defined by the pentadienyl carbon atoms. The angle between the pentadienyl plane and that defined by C2, C3, C7 and O is 11.84(9)°, which confirms the puckering of the C_6H_5O ligand. In solution, the protons of the η^5-C_6H_5O ring are observed at 5.62 (br m, 2 H, Ru-η^5-$C_6\mathit{H}_5O$), 5.14 (br d, 2 H, Ru-η^5-$C_6\mathit{H}_5O$, J = 5 Hz), and 3.98 (apparent t, 1 H, Ru-η^5-$C_6\mathit{H}_5O$, J = 5 Hz) ppm. The upfield

shift of these protons is comparable to that previously reported for related η^5-oxocyclohexadienyl complexes.[83b,87] The formation of this 18-electron π-type phenol complex parallels the chemistry observed for the Cp*Ru fragment, where π-complexation of phenol and most phenol derivatives, including perfluorinated phenols, is thermodynamically preferred and is observed almost exclusively.[83,88]

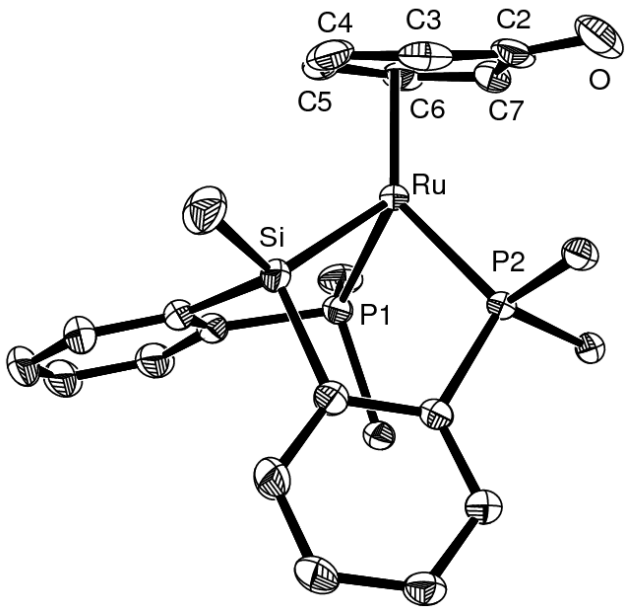

Figure 3-6. The crystallographically determined structure of **3-9**·C_6H_6 shown with 50% ellipsoids; H atoms and cyclohexylphosphino C atoms, as well as the C_6H_6 solvate have been omitted for clarity. Selected interatomic distances (Å) and angles (deg): Ru-Si 2.3276(6), O-C2 1.249(3), C2-C3 1.453(4), C2-C7 1.438(3), C3-C4 1.405(4), C4-C5 1.405(3), C5-C6 1.408(3), C6-C7 1.392(3), Ru-C2 2.582(2), Ru-C3 2.279(2), Ru-C4 2.217(2), Ru-C5 2.257(2), Ru-C6 2.320(2), Ru-C7 2.418(2), P1-Ru-P2 94.214(18), P1-Ru-Si 79.30(2), P2-Ru-Si 82.985(19).

In an initial survey of E-H (E = main group element) bond activation chemistry, complexes **3-3** and **3-4** were found to readily undergo multiple E-H bond activation steps upon treatment with one equiv of $H_3B{\cdot}NH_3$ to quantitatively form the bis(σ-B-H)

complex [Cy-PSiP]RuH(η^2:η^2-H_2BNH_2) (**3-10**), with concomitant formation of either HO^{t}Bu or HN($SiMe_3$)$_2$, respectively (Scheme 3-2). Complex **3-10**, which represents a rare example of a bis(σ-B-H) aminoborane complex,[89] was readily isolated in 81% yield and has been characterized both in solution and in the solid state (Figure 3-7). Only one previous example of a crystallographically characterized bis(σ-B-H) complex of H_2BNH_2 has been recently reported by Alcaraz, Sabo-Etienne, and co-workers.[89a] The substituted amine-boranes $H_3B{\cdot}NHMe_2$ and $H_3B{\cdot}NH_2{}^t$Bu reacted in a similar manner (Scheme 3-2) to form the related bis(σ-B-H) complexes [Cy-PSiP]RuH(η^2:η^2-H_2BNMe_2) (**3-11**, Figure 3-7) and [Cy-PSiP]RuH(η^2:η^2-H_2BNH^tBu) (**3-12**). Each of complexes **3-10** - **3-12** feature two distinctive upfield shifted ^{1}H NMR resonances corresponding to the Ru-*H*-B protons that are observed as broad singlets at - 3.36 and - 7.50 ppm for **3-10**, -3.29 and -7.49 ppm for **3-11**, and -3.34 and -7.56 ppm for **3-12** (benzene-d_6). In addition, the ^{1}H NMR spectrum of each complex features a resonance corresponding to the terminal Ru-H ligand (-12.62 ppm for **3-10**, -13.07 ppm for **3-11**, and -12.66 ppm for **3-12**). The ^{11}B{^{1}H} NMR spectra of **3-10** - **3-12** feature a broad signal at ca. 40 ppm, which is characteristic of a three-coordinate boron atom and is comparable to the ^{11}B NMR shift of 46 ppm reported for RuH_2(η^2:η^2-H_2BNH_2)(PCy_3)$_2$.[89a] The X-ray crystal structures of **3-10** and **3-11** indicate that in each case the Ru center adopts a pseudo-octahedral coordination environment featuring *trans*-disposed phosphino groups. The Ru···B distances of 2.031(6) and 2.021(2) Å are shorter than the sum of the covalent radii for Ru and B (2.09 Å),[89a,b] but are somewhat longer than the Ru···B distance of 1.956(2) Å reported for RuH_2(η^2:η^2-H_2BNH_2)(PCy_3)$_2$.[89a] The coordinated aminoborane ligand in both **3-10** and **3-11** features a short B-N distance (1.359(8) Å for **3-10** and 1.386(3) Å for

3-11; *cf.* 1.58(2) Å for $H_3B{\cdot}NH_3$[90]) that is consistent with appreciable π-bonding character. Notably such bis(σ-B-H) complexes represent possible intermediates in the metal-mediated dehydrogenation of amineboranes, including ammonia-borane, which has attracted significant attention as a hydrogen storage material.[74b,89b,91,92] In this context, the formation of **3-10** – **3-12** from either **3-3** or **3-4** confirms that such four-coordinate, formally 14-electron [R-PSiP]RuX complexes are capable of promoting multiple bond activation steps in a manner that may be synthetically useful in the transformation of main group substrates.

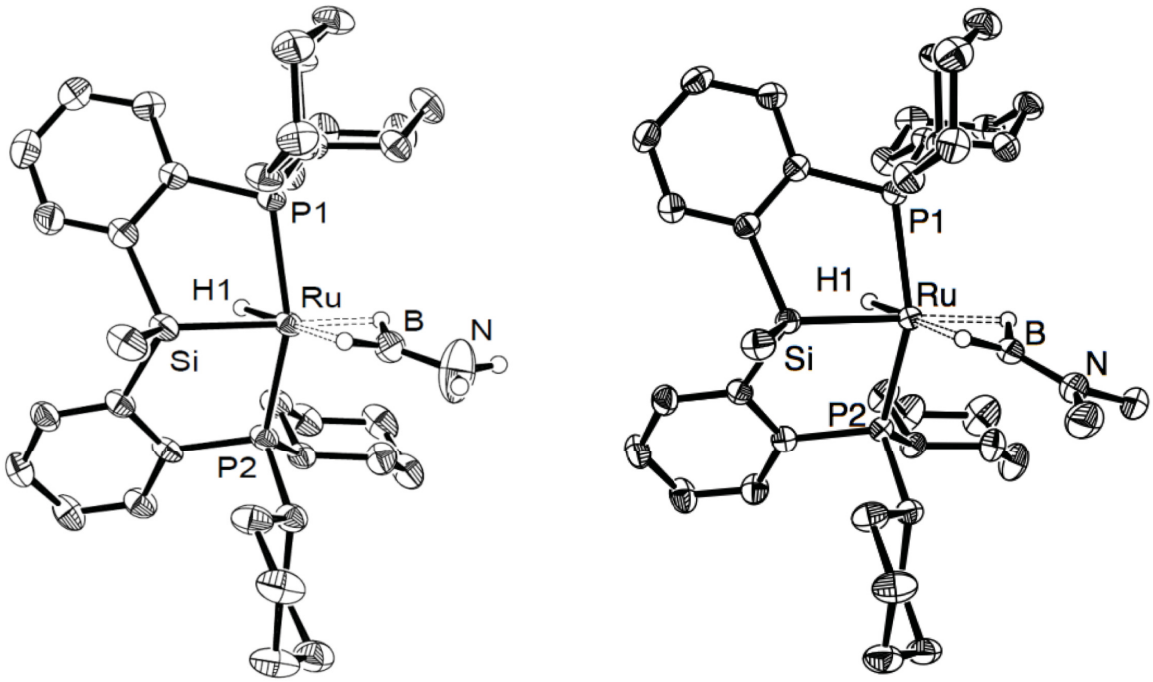

3-10 3-11

Figure 3-7. The crystallographically determined structures of **3-10** and **3-11** shown with 50% ellipsoids; selected H atoms have been omitted for clarity. Selected interatomic distances (Å) and angles (deg) for **3-10**: Ru-Si 2.3276(14), Ru···B 2.031(6), B-N 1.359(8), P1-Ru-P2 155.22(5), Ru-B-N 173.3(5). Selected interatomic distances (Å) and angles (deg) for **3-11**: Ru-Si 2.3317(5), Ru···B 2.021(2), B-N 1.386(3), P1-Ru-P2 154.32(2), Ru-B-N 168.52(14).

3.2.3 Computational studies.

The experimental work was complemented by DFT (TPSS/SDD+TZVP) studies of the structural and electronic features of the four-coordinate complexes **3-3**, **3-4**, and **3-6**. All computational studies were carried out by Dr. Sven Tobisch of the University of St. Andrews. The DFT optimized structures in the singlet state were in excellent agreement with X-ray diffraction data. DFT confirmed the slightly distorted trigonal pyramidal geometry of the four-coordinate complexes **3-3**, **3-4**, and **3-6** featuring *fac*-κ^3-

[Cy-PSiP]Ru^{II} ligation, whereby the alternative *mer*-κ^3-pincer–Ru^{II} coordination mode that is preferably adopted in a non-planar *cis*-divacant octahedral geometry at Ru is higher in energy by 28.8 (**3-3**), 34.2 (**3-4**) and 32.0 (**3-6**) kcal mol^{-1}, respectively. The ability to establish Ru^{II}–X π interactions efficiently is a crucial factor that favours the *fac*-κ^3 over the *mer*-κ^3 ligation mode. Taking complex **3-3** as an example, optimized Ru–O distances of 1.91 and 1.98 Å for *fac*-κ^3 and *mer*-κ^3 forms, respectively, are indeed suggestive of stronger Ru^{II}-O π interactions in the former. The stability of the diamagnetic, four-coordinate, formally 14-electron [Cy-PSiP]RuX complexes outlined in this chapter cannot be attributed to a triplet spin state,[43] but rather appears to be a consequence of the highly electron releasing Cy-PSiP ligand set that supports spin pairing. Given the strong donor ability of the silyl group, it comes as no surprise that for **3-3**, **3-4**, and **3-6** a triplet spin state, which also favours a *fac*-κ^3-[PSiP]Ru^{II} ligation, is higher in energy by more than 24 kcal mol^{-1}. The strong metal d_{x2-y2} character of the HOMO, together with a smaller metal d_{xz} component that is involved in some Ru–X π bonding, is not particularly well suited to accommodate an agostic interaction at the vacant axial coordination site, while the LUMO exhibits Ru-X π* character featuring a strong metal d_{xy} component. Hence, agostic C–H interactions are not essential for stabilizing the singlet ground state. The rather weak C–H agostic interaction in **3-6**, which is estimated for [Cy-PSiP]RuNH(2-MeC_6H_4) (**3-6***) to amount to 2.3 kcal mol^{-1}, confirms this aspect.

In an attempt to put these findings in a broader perspective, analogues of **3-3**, **3-4**, and **3-6** that have the silyl group replaced by either C(sp^3)–Me (**3-3c** – **3-6c**), phosphido (**3-3p** – **3-6p**) and amido (**3-3n** – **3-6n**) donor groups were also studied computationally.

According to the above rationale, key features of the modified compounds are expected to correlate with the donor ability of the pincer's central donor. In agreement with chemical reasoning, the assessed NBO charge distribution reveals the following order of descending donating ability: PSiP > PPP > PCP > PNP. With regard to the strength of the C–H agostic interaction in **3-6***, DFT shows that it directly correlates with the degree of electron deficiency at Ru and hence increases in the following order (given in kcal mol^{-1}): **3-6*** (2.3) < **3-6*p** (3.8) < **3-6*c** (4.4) < **3-6*n** (7.3). The nature of the central donor group also has a profound influence on the gap in stability between *fac*-κ^3- and *mer*-κ^3-[Cy-PXP]Ru^{II} forms, which follows a regular trend as exemplified for complex **3-6** (given in kcal mol^{-1}): **3-6** (32.0) > **3-6p** (25.3) > **3-6c** (17.5) > **3-6n** (10.8). Of particular importance is the marked dependency revealed by DFT between the charge density at Ru and the size of the gap between the singlet and triplet spin states. The ΔE(S–T) gap decreases regularly for the silylamido complex from 24.2 (**3-4**) to 23.6 (**3-4p**), 22.7 (**3-4c**) and to 20.5 kcal mol^{-1} (**3-4n**), thereby reinforcing the pivotal role of a strongly donating central donor group for the stabilization of the singlet state of the four-coordinate 14-electron Ru^{II} complexes described in this chapter.

In order to acquire a more detailed view of the E–H bond activation steps involved in the formation of [Cy-PSiP]-supported bis(σ-B-H) aminoborane Ru complexes, two plausible routes have been explored computationally for the reaction of κ^3-[Me-PSiP]RuN($SiMe_3$)$_2$ (**3-4'**), in which the PCy_2 donor groups have been replaced by PMe_2, with $H_3B{\cdot}NH_3$ (Scheme 3-3). One route (route A) entails an initial N–H bond activation of ammonia-borane (AB) in **3-4'**·AB to cleave the Ru–X bond protonolytically, thereby giving rise to adduct **3-13'**·XH. This intermediate is likely to readily release XH

to furnish **3-13'**, which subsequently undergoes oxidative addition of the borane at the Ru^{II} center to generate the bis(σ-B–H) aminoborane complex **3-10'**. Oxidative addition of a B–H bond commencing from **3-4'·**AB, followed by Ru–X bond protonolysis via ammonia N–H bond activation describes an alternate route B (Scheme 3-3).

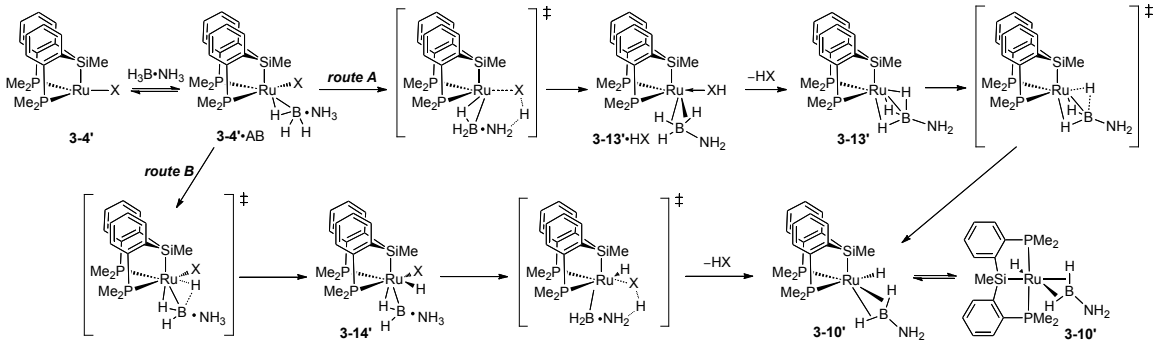

Scheme 3-3. Plausible paths for E–H (E = B, N) bond activation of ammonia-borane (AB) by a four-coordinate, formally 14-electron (R-PSiP)RuX complex (X = $N(SiMe_3)_2$).

The details of the computational study into the activation of ammonia borane by **3-4** can be found in Appendix B. The conclusion of this study was that ammonia-borane activation by [R-PSiP]RuX complexes likely proceeds in a stepwise fashion via ammonia N–H activation and subsequent borane B–H bond oxidative addition steps (route A in Scheme 3-3). The assessed moderate activation barriers together with the strong driving force for the overall transformation are in agreement with the observed multiple, facile E–H bond activation steps. The alternate route that initiates through borane oxidative addition to the Ru^{II} center in **3-4'·**AB has a prohibitively high barrier of 33.1 kcal mol^{-1} to overcome and is thus at odds with the observed smooth activation of ammonia borane by **3-4**. Notably, a TS structure for simultaneous N–H and B–H activation was not located, suggesting that this pathway is not viable in this system.

3.3 Conclusions

In summary, unprecedented diamagnetic, four-coordinate, formally 14-electron [Cy-PSiP]RuX (X = amido, alkoxo) complexes that do not require agostic stabilization and that adopt a highly unusual trigonal pyramidal coordination geometry have been prepared and characterized by use of NMR spectroscopic, X-ray crystallographic and DFT methods. Computational studies confirm the key role of the strongly σ-donating silyl group of the Cy-PSiP ligand in enforcing the unusual trigonal pyramidal coordination geometry. Unlike previously reported square planar examples of four-coordinate Ru^{II} complexes, the stability of the diamagnetic, four-coordinate, [Cy-PSiP]RuX complexes outlined in this chapter cannot be attributed to a triplet spin state, but rather appears to be a consequence of the highly electron releasing Cy-PSiP ligand set. These results substantiate a new strategy for the synthesis of low-coordinate Ru species, whereby the use of a strongly σ-donating silyl ligand set helps to enforce coordinative unsaturation at the metal center.

Whereas silyl ligation serves to afford stability to the unusual trigonal pyramidal [Cy-PSiP]RuX complexes featured herein, these low-coordinate species are still capable of undergoing insertion reactions and reacting with substrate E-H bonds. In exploring the reactivity of **3-3** and **3-4** as representative examples of trigonal pyramidal [Cy-PSiP]RuX species, it was found that these serve as precursors for the synthesis of a Ru hydroxo complex as well as an η^5-oxocyclohexadienyl complex. Complexes **3-3** and **3-4** also undergo N-H/B-H bond activation reactions upon treatment with amine-borane reagents, including ammonia borane, to form unusual bis(σ-B-H) complexes of the type [Cy-PSiP]RuH(η^2:η^2-H_2BNRR') (R, R' = H, alkyl). The mechanism of the activation of

ammonia-borane by such low-coordinate [R-PSiP]RuX species was studied computationally and was determined to most likely proceed in a stepwise fashion via intramolecular deprotonation of ammonia and subsequent borane B–H bond oxidative addition. These studies confirm that such four-coordinate, formally 14-electron [R-PSiP]RuX complexes are capable of promoting multiple bond activation steps in a manner that may be synthetically useful in the transformation of main group substrates.

3.4 Experimental Section

3.4.1 General considerations.

All experiments were conducted under argon in an MBraun glovebox or using standard Schlenk techniques. Dry, oxygen-free solvents were used unless otherwise indicated. All non-deuterated solvents were deoxygenated and dried by sparging with nitrogen and subsequent passage through a double-column solvent purification system purchased from MBraun Inc. Tetrahydrofuran and diethyl ether were purified over two activated alumina columns, while benzene, toluene, and pentane were purified over one activated alumina column and one column packed with activated Q-5. All purified solvents were sparged with argon prior to use and stored over 4 Å molecular sieves. Benzene-d_6 and toluene-d_8 were degassed via three freeze-pump-thaw cycles and stored over 4 Å molecular sieves. The compound [(*p*-cymene)$RuCl_2$]$_2$ was purchased from Strem and used as received. The compound (2-$Cy_2PC_6H_4)_2SiMeH$ was prepared according to literature procedures.[79b] Triethylamine was distilled from CaH_2. Water was degassed by sparging with argon. All other reagents were purchased from Aldrich and used without further purification. Unless otherwise stated, ^{1}H, ^{13}C, ^{31}P, ^{15}N and ^{29}Si NMR

characterization data were collected at 300K on a Bruker AV-500 spectrometer operating at 500.1, 125.8, 202.5, 50.7 and 99.4 MHz (respectively) with chemical shifts reported in parts per million downfield of $SiMe_4$ (for ^{1}H, ^{13}C, and ^{29}Si), $MeNO_2$ (for ^{15}N), and 85% H_3PO_4 in D_2O (for ^{31}P). ^{1}H and ^{13}C NMR chemical shift assignments are based on data obtained from ^{13}C-DEPTQ, ^{1}H-^{1}H COSY, ^{1}H-^{13}C HSQC, and ^{1}H-^{13}C HMBC NMR experiments. ^{29}Si NMR assignments are based on ^{1}H-^{29}Si HMBC experiments. ^{15}N NMR assignments are based on ^{1}H-^{15}N HMQC experiments. In some cases, fewer than expected unique ^{13}C NMR resonances were observed, despite prolonged acquisition times. Elemental analyses were performed by Canadian Microanalytical Service Ltd. of Delta, British Columbia, Canada and Columbia Analytical Services of Tucson, Arizona. X-ray data collection, solution, and refinement were carried out by Drs. Robert MacDonald and Michael J. Ferguson at the University of Alberta X-ray Crystallography Laboratory, Edmonton, Alberta. Infrared spectra were recorded using a Bruker VECTOR 22 FT-IR spectrometer at a resolution of 4 cm^{-1}.

3.4.2 Computational details.

Calculations were performed by Dr. Sven Tobisch of the University of St. Andrews. All calculations based on Kohn-Sham density functional theory (DFT)[93] were performed by means of the program package TURBOMOLE[94] using the almost nonempirical meta-GGA Tao–Perdue–Staroverov–Scuseria (TPSS) functional[95] within the RI-J integral approximation[96] in conjunction with flexible basis sets of triple-ζ quality. The Stuttgart–Dresden scalar-relativistic effective core potential (SDD, 28 core electrons)[97] was used for Ru in combination with the (7s7p5d1f)/[6s4p3d1f] (def2-TZVP)

valence basis set.[98] All remaining elements were represented by Ahlrich's valence triple-ζ TZVP basis set[99] with polarization functions on all atoms. The good to excellent performance of the TPSS functional for a wide range of applications, with transition-metal complexes in particular, has been demonstrated previously.[100] In order to probe the influence of the DFT Hamiltonian on the singlet-triplet energy gap the hybrid meta-GGA TPSSh functional (i.e. TPSS with 10% exchange),[95,100a,101] which was reported to adequately describe spin-state energetics for transition metal complexes,[102] was also employed. The two DFT methods were shown of being equally capable of adequately describing spin-state energetics for the herein studied four-coordinate, 14-electron Ru^{II} complexes. Analytical frequency calculations were performed to confirm that the reported transition states possess exactly one negative Hessian eigenvalue, while all other stationary points exhibit exclusively positive eigenvalues. The reaction and activation enthalpies and free energies (ΔH, $\Delta H^{\ddagger}$ and ΔG, $\Delta G^{\ddagger}$ at 298 K and 1 atm) were evaluated according to standard textbook procedures[103] using computed harmonic frequencies. Enthalpies were reported as ΔE + zero point energy corrections at 0 K + thermal motion corrections at 298 K and Gibbs free-energies were obtained as $\Delta G = \Delta H - T\Delta S$ at 298 K. The analysis of the bonding situation was performed with the aid of Wiberg bond orders (WBO)[104] that are known to provide a good measure of the covalent bond order between two interacting atoms. Natural population analyses (NPA)[105] were performed with the NBO[106] in conjunction with the MAG-ReSpect[107] module. Optimized structures were visualized by employing the StrukEd program,[108] which was also used for the preparation of 3D molecule drawings.

3.4.3 Synthetic details and characterization data

(2-$Cy_2PC_6H_4)_2SiHMe$ ([CyPSiP]H, 3-1). A stirring solution of 2-$Cy_2PC_6H_4Br$ (3.0 g, 8.5 mmol) in ca. 60 mL of pentane was cooled to -78 °C. ^{n}BuLi (5.3 mL, 1.6 M in hexanes, 8.5 mmol) was added dropwise to this solution, resulting in a red-orange colored solution. The resulting solution was allowed to warm to room temperature over the course of 3 h, over the course of which a white precipitate was observed and the solution became yellow-orange in color. The mixture was once again cooled to -78 °C and Cl_2SiHMe (0.44 mL, 4.3 mmol) was added via syringe. The resulting pale yellow-orange coloured reaction mixture was allowed to warm to room temperature and continue stirring for an additional 14 h at room temperature. The volatile components were then removed *in vacuo* and the remaining residue was extracted into ca. 20 mL of benzene. The benzene extracts were filtered through Celite and the benzene was removed *in vacuo* to afford a yellow solid that was triturated with pentane (2 × 5 mL) to give **3-1** (1.73 g, 69%) as a pale yellow colored solid. ^{1}H NMR (500 MHz, benzene-d_6): δ 7.77 (m, 2 H, H_{arom}), 7.45 (m, 2 H, H_{arom}), 7.21 – 7.14 (4 H, H_{arom}), 6.28 (m, 1 H, Si*H*), 1.98 – 1.84 (8 H, P*Cy*), 1.72 (apparent br t, 4 H, P*Cy*), 1.60 – 1.52 (12 H, P*Cy*), 1.39 – 1.03 (20 H, P*Cy*), 0.96 (d, 3 H, Si*Me*, $^{3}J_{HH}$ = 4 Hz). $^{13}C\{^{1}H\}$ NMR (125.8 MHz, benzene-d_6): δ 147.6 (d, C_{arom}, J_{CP} = 46 Hz), 144.2 (d, C_{arom}, J_{CP} = 17 Hz), 138.0 (d, CH_{arom}, J_{CP} = 15 Hz), 132.7 (CH_{arom}), 129.1 (CH_{arom}), 36.1 (d, CH_{Cy}, J_{CP} = 36 Hz), 36.0 (d, CH_{Cy}, J_{CP} = 36 Hz), 31.4 (apparent t, CH_{2Cy}, J = 16 Hz), 30.8 (d, CH_{2Cy}, J_{CP} = 11 Hz), 30.5 (d, CH_{2Cy}, J_{CP} = 10 Hz), 27.9 – 27.8 (CH_{2Cy}), 27.2 (d, CH_{2Cy}, J_{CP} = 8 Hz), -1.1 (t, Si*Me*, J_{CP} = 9 Hz). $^{31}P\{^{1}H\}$ NMR (202.5 MHz, benzene-d_6): δ -8.0. ^{29}Si NMR (99.4 MHz, benzene-d_6): δ -24.2 ($^{1}J_{SiH}$ = 210 Hz).

([Cy-PSiP]RuCl)$_2$ (3-2). A solution of **3-1** (1.4 g, 2.4 mmol) in ca. 5 mL of THF was added to a slurry containing [(*p*-cymene)$RuCl_2$]$_2$ (0.73 g, 1.2 mmol) and PCy_3 (0.67 g, 2.4 mmol) in ca. 10 mL of THF at room temperature. Neat Et_3N (0.33 mL, 2.4 mmol) was added to the reaction mixture via syringe. The resulting orange solution was heated to 70 °C with stirring for a period of 24 h. The THF solvent was removed *in vacuo*, and the resulting residue was triturated with pentane (3 × 1 mL). The remaining solid was washed with ca. 150 mL of benzene. The benzene washes were combined and filtered through a medium porosity glass frit. The filtrate was collected and the volatile components were subsequently removed *in vacuo*. The remaining orange residue was washed with cold pentane (3 × 2 mL) and dried *in vacuo* to yield spectroscopically pure **3-2** (1.3 g, 74%) as an orange solid. ^{1}H NMR (300 K, 500 MHz, benzene-d_6): δ 7.82 (dbr, 2 H, H_{arom}, J = 7 Hz), 7.31 (m, 2 H, H_{arom}), 7.09 (t, 2 H, H_{arom}, J = 7 Hz), 6.93 (t, 2 H, H_{arom}, J = 7 Hz) 6.92 (br overlapping resonances, H_{arom}), 6.90 (apparent t, 2 H, H_{arom}, J = 17 Hz), 2.68 (br ms, 2 H, P*Cy*), 2.61 – 2.45 (br overlapping resonancess, 4 H, P*Cy*), 2.23 – 0.64 (br overlapping resonances, 41 H P*Cy* + Si*Me*; a singlet resonance at 1.56 ppm was assigned to the Si*Me* protons by use of a ^{1}H-^{13}C HSQC experiment), 1.62 (s, 3 H, Si*Me*), 1.56 – 0.66 (br overlapping resonances, P*Cy*). ^{13}C{^{1}H} NMR (333 K, 125.8 MHz, benzene-d_6): δ 159.5 (m, C_{arom}), 147.3 (br, C_{arom}), 132.0 - 134.7 (d, CH_{arom}, J = 15 Hz), 131.9 (overlapping resonances, CH_{arom}), 129.9 (CH_{arom}), 126.2 (CH_{arom}), 41.6 (br m, CH_{Cy}), 37.9 (br m, CH_{Cy}), 32.7 (CH_{2Cy}), 31.1 (CH_{2Cy}), 30.1 (CH_{2Cy}), 29.0 - 28.4 (overlapping resonances, CH_{2Cy}), 27.3 (CH_{2Cy}), 27.1 (CH_{2Cy}), 2.6 (Si*Me*). ^{31}P{^{1}H} NMR (300K, 202.5 MHz, benzene-d_6): δ 89.1. ^{29}Si NMR (300K, 99.4 MHz, benzene-d_6): δ 65.2. Anal. Calcd for $C_{74}H_{110}P_4Si_2Ru_2Cl_2$: C, 61.18; H, 7.63. Found: C, 61.12; H, 7.57. A

single crystal of **3-2**·$(C_6H_6)_{3.5}$ suitable for X-ray diffraction analysis was grown by vapor diffusion of pentane into a benzene solution of **3-2**.

[Cy-PSiP]RuO^{t}Bu (3-3). A slurry of KO^{t}Bu (0.023 g, 0.21 mmol) in ca. 1 mL of benzene was added to a slurry of **3-2** (0.15 g, 0.10 mmol) in ca. 3 mL of benzene at room temperature. The reaction mixture was stirred for 1 h at room temperature over which time a color change from orange to red was observed. The solution was then filtered through Celite and the filtrate was retained. The volatile components of the filtrate solution were removed *in vacuo* and the resulting residue was triturated with pentane (2 × 1 mL) to yield **3-3** (0.15 g, 97%) as a red solid. ^{1}H NMR (500 MHz, benzene-d_6): δ 7.88 (d, 2 H, H_{arom}, J = 7 Hz), 7.44 (m, 2 H, H_{arom}), 7.14 (m, 2 H, H_{arom}), 7.01 (t, 2 H, H_{arom}, J = 7 Hz), 2.52 (br s, 2 H, P*Cy*), 2.32 (m, 2 H, P*Cy*), 2.18 (m, 2 H, P*Cy*), 2.04 (br m, 4 H, P*Cy*), 1.95 (m, 2 H, P*Cy*), 1.74 – 1.15 (overlapping resonances, 40 H, P*Cy* + O^t*Bu* + Si*Me*; singlet resonances at 1.50 and 1.33 ppm were assigned to the O^t*Bu* and Si*Me* protons, respectively, by use of a ^{1}H-^{13}C HSQC experiment), 1.04 (br m, 2 H, P*Cy*), 0.62 (br s, 2 H, P*Cy*). ^{13}C{^{1}H} NMR (125.8 MHz, benzene-d_6): δ 160.6 (d, C_{arom}, J_{CP} = 42 Hz), 148.0 (d, C_{arom}, J_{CP} = 48 Hz), 131.7 (d, *C*H$_{arom}$, J = 20 Hz), 129.1 (*C*H$_{arom}$), 127.0 (d, *C*H$_{arom}$, J = 5 Hz), 126.4 (*C*H$_{arom}$), 75.1 (O*C*Me$_3$), 40.2 (d, *C*H$_{Cy}$, J = 17 Hz), 37.4 (d, *C*H$_{Cy}$, J = 27 Hz), 35.5 (OC*Me$_3$*), 30.9 (*C*H$_{2Cy}$), 29.2 – 27.7 (overlapping resonances, *C*H$_{2Cy}$), 27.1 (*C*H$_{2Cy}$), 26.8 (*C*H$_{2Cy}$), 4.9 (Si*Me*). ^{31}P{^{1}H} NMR (202.5 MHz, benzene-d_6): δ 110.5. ^{29}Si NMR (99.4 MHz, benzene-d_6): δ 65.5. Anal. Calcd for $C_{41}H_{64}P_2OSiRu$: C, 64.43; H, 8.44. Found: C, 64.34; H, 8.33. A single crystal of **3-3**·C_6H_6·(C_5H_{12})0.5 suitable for X-ray diffraction analysis was grown by vapor diffusion of pentane into a benzene solution of **3-3**.

[Cy-PSiP]RuN(SiMe$_3$)$_2$ (3-4). A slurry of NaN(SiMe$_3$)$_2$ (0.027 g, 0.14 mmol) in ca. 1 mL of benzene was added to a slurry of **3-2** (0.10 g, 0.07 mmol) in ca. 3 mL of benzene at room temperature. The reaction mixture was stirred for 30 minutes at room temperature over which time a color change from orange to red was observed along with the formation of a white precipitate. The solution was then filtered through Celite and the filtrate was collected. The volatile components of the filtrate solution were removed *in vacuo*, to give **3-4** as a red solid (0.086 g, 70%). ^{1}H NMR (500 MHz, benzene-d_6): δ 7.78 (d, 2 H, H_{arom}, J = 7 Hz), 7.39 (m, 2 H, H_{arom}), 7.11 (apparent t, 2 H, H_{arom}, J = 6 Hz), 6.99 (apparent t, 2 H, H_{arom}, J = 7 Hz), 2.33 (m, 2 H, P*Cy*), 2.15 (m, 2 H, P*Cy*), 2.06 (4 H, P*Cy*), 1.91 – 0.96 (broad overlapping resonances, 39 H, P*Cy* + Si*Me*; a singlet resonance at 1.33 ppm was assigned to the Si*Me* protons by use of a ^{1}H-^{13}C HSQC experiment), 0.65 (s, 9 H, NSi*Me$_3$*), 0.36 (s, 9 H, NSi*Me$_3$*). ^{13}C{^{1}H} NMR (125.8 MHz, benzene-d_6): δ 160.8 (d, C_{arom}, J = 41 Hz), 147.0 (d, C_{arom}, J = 48 Hz), 131.6 (d, CH_{arom}, J = 19 Hz), 129.2 (CH_{arom}), 127.2 (d, CH_{arom}, J = 4 Hz), 126.2 (CH_{arom}), 41.7 (d, CH_{Cy}, J = 17 Hz), 38.0 (d, CH_{Cy}, J = 27 Hz), 31.2 (CH_{2Cy}), 29.9 (CH_{2Cy}), 29.3 – 27.7 (overlapping resonances, CH_{2Cy}), 27.1 (CH_{2Cy}), 26.7 (CH_{2Cy}), 8.8 (NSi*Me$_3$*), 8.3 (NSi*Me$_3$*), 5.0 (Si*Me*). ^{31}P{^{1}H} NMR (202.5 MHz, benzene-d_6): δ 98.9. ^{29}Si NMR (99.4 MHz, benzene-d_6): δ 56.4 [P*Si*P], - 6.2 (N*Si*Me$_3$). Anal. Calcd for $C_{43}H_{73}P_2NSi_3Ru$: C, 60.67; H, 8.64; N, 1.64. Found: C, 60.59; H, 8.36; N, 1.41. A single crystal of **3-4** suitable for X-ray diffraction analysis was grown from a concentrated diethyl ether solution at -30 °C.

[Cy-PSiP]RuNHPh (3-5). A solution of LiNHPh (0.015 g, 0.15 mmol) in ca. 1 mL of benzene Et$_2$O was added to a slurry of **3-2** (0.11 g, 0.08 mmol) in ca. 5 mL of benzene Et$_2$O at room temperature. The reaction mixture was stirred for 1 h at room temperature

over which time a color change from orange to dark red was observed along with the formation of a white precipitate. The volatile components of the reaction mixture were removed in vacuo, and the remaining residue was washed with ca. 5 mL of benzene. The benzene solution was then filtered through Celite and the filtrate solution was retained. The volatile components of the filtrate solution were removed *in vacuo*. The resulting dark red residue was triturated with pentane (3 × 1 mL) to yield **3-5** (0.11 g, 92%) as a dark red solid. ^{1}H NMR (500 MHz, benzene-d_6): δ 7.81 (d, 2 H, H_{arom}, J = 7 Hz), 7.46 (m, 2 H, H_{arom}), 7.19 – 7.13 (overlapping resonances, 4 H, H_{arom} + NHPh_{meta}), 7.02 (t, 2 H, H_{arom}, J = 7 Hz), 6.93 (d, 2 H, NHPh_{ortho}, J = 8 Hz), 6.70 (t, 1 H, NHPh_{para}, J = 7 Hz), 6.35 (br s, 1 H, N*H*Ph), 2.54 (m, 2 H, P*Cy*), 2.29 – 2.08 (overlapping resonances, 6 H, P*Cy*), 1.91 – 1.06 (overlapping resonances, 34 H, P*Cy*), 1.00 (s, 3 H, Si*Me*), 0.71 (br s, 2 H, P*Cy*). ^{13}C{^{1}H} NMR (125.8 MHz, benzene-d_6): δ 159.3 (d, C_{arom}, J = 40 Hz), 157.3 (NH*Ph*, C_{ipso}), 147.5 (d, C_{arom}, J = 47 Hz), 131.7 (d, CH_{arom}, J = 19 Hz), 130.2 (CH_{arom}), 128.9 (NH*Ph*, C_{meta}), 127.2 (d, CH_{arom}, J = 4 Hz), 126.7 (CH_{arom}), 117.7 (NH*Ph*, C_{para}), 117.4 (NH*Ph*, C_{ortho}), 40.5 (d, CH_{Cy}, J = 14 Hz), 38.4 (d, CH_{Cy}, J = 28 Hz), 33.1 (CH_{2Cy}), 30.6 (CH_{2Cy}), 29.9 (CH_{2Cy}), 29.3 (CH_{2Cy}), 29.2 (CH_{2Cy}), 28.5 – 27.8 (overlapping resonances, CH_{2Cy}), 27.1 (CH_{2Cy}), 26.8 (CH_{2Cy}), -0.02 (Si*Me*). ^{31}P{^{1}H} NMR (202.5 MHz, benzene-d_6): δ 96.5. ^{29}Si NMR (99.4 MHz, benzene-d_6): δ 58.7. ^{15}N NMR (50.7 MHz, benzene-d_6): δ –220.5. Anal. Calcd for $C_{43}H_{61}P_2NSiRu$: C, 65.95; H, 7.85; N, 1.79. Found: C, 65.91; H, 7.48; N, 2.13.

[Cy-PSiP]RuNH(2,6-$Me_2C_6H_3$) (3-6). A slurry of LiNH(2,6-$Me_2C_6H_3$) (0.017 g, 0.14 mmol) in ca. 3 mL of benzene was added to a slurry of **3-2** (0.10 g, 0.07 mmol) in ca. 5 mL of benzene at room temperature. The reaction mixture was stirred for 1 h at

room temperature over which time a color change from orange to dark red was observed along with the formation of a white precipitate. The solution was then filtered through Celite and the filtrate solution was retained. The volatile components of the filtrate solution were removed *in vacuo* and the resulting residue was triturated with pentane (*ca.* 1 mL) to yield **3-6** (0.11 g, 96%) as a dark red solid. ^{1}H NMR (500 MHz, benzene-d_6): δ 7.92 (d, 2 H, H_{arom}, J = 7 Hz), 7.57 (br s, 1 H, N*H*), 7.49 (m, 2 H, H_{arom}), 7.24 – 7.18 (overlapping resonances, 4 H, H_{arom} + 2,6-$Me_2C_6H_3$), 7.05 (t, 2 H, H_{arom}, J = 7 Hz), 6.86 (t, 1 H, 2,6-$Me_2C_6H_3$, J = 7 Hz), 2.52 (m, 2 H, PCy), 2.31 (s, 6 H, 2,6-$Me_2C_6H_3$), 2.21 (m, 2 H, P*Cy*), 1.83 (m, 4 H, P*Cy*), 1.65 – 0.70 (overlapping resonances, 37 H, P*Cy* + Si*Me*; a singlet resonance at 1.25 ppm was assigned to the Si*Me* protons by use of a ^{1}H-^{13}C HSQC experiment), 0.62 (br m, 2 H, P*Cy*). ^{13}C{^{1}H} NMR (125.8 MHz, benzene-d_6): δ 158.4 (C_{arom}), 158.3 ($Me_2C_6H_3$, C_{ipso}), 148.1 (C_{arom}), 131.2 (d, CH_{arom}, J = 19 Hz), 128.3 (CH_{arom}), 127.7 (2,6-$Me_2C_6H_3$, CH_{meta}), 126.6 (d, CH_{arom}, J = 5 Hz), 125.8 (CH_{arom}), 122.9 (NC_{ipso}), 116.2 (2,6-$Me_2C_6H_3$, CH_{para}), 39.7 (d, CH_{Cy}, J = 13 Hz), 38.0 (d, CH_{Cy}, J = 25 Hz), 32.9 (CH_{2Cy}), 29.7 (CH_{2Cy}), 28.6 - 26.8 (overlapping resonances, CH_{2Cy}), 26.5 (CH_{2Cy}), 26.1 (CH_{2Cy}), 18.8 ($Me_2C_6H_3$), -1.7 (Si*Me*). ^{31}P{^{1}H} NMR (202.5 MHz, benzene-d_6): δ 94.2. ^{29}Si NMR (99.4 MHz, benzene-d_6): δ 57.2. ^{15}N NMR (50.7 MHz, benzene-d_6): δ -219.1. Anal. Calcd for $C_{45}H_{65}P_2NSiRu$: C, 66.63; H, 8.13; N, 1.76. Found: C, 66.50; H, 7.81; N, 1.68. A single crystal of **3-6** suitable for X-ray diffraction analysis was grown from a concentrated diethyl ether solution at -30 °C.

[Cy-PSiP]RuC(NH(2,6-$Me_2C_6H_3$))=N(2,6-$Me_2C_6H_3$) (3-7). A solution of 2,6-xylylisocyanide (0.012g g, 0.093 mmol) in 1 mL of benzene was added to a solution of **3-6** (0.075 g, 0.093 mmol) in 3 mL of benzene. Over the course of 16 h at room

temperature a color change from dark red to orange was observed. The volatile components of the reaction mixture were removed *in vacuo* and the remaining solid was triturated with pentane (2 × 1 mL) to yield **3-7** (0.087 g, 99%) as an orange powder. ^{1}H NMR (500 MHz, benzene-d_6): δ 8.21 (d, 2 H, H_{arom}, J = 7 Hz), 7.48 (d, 2 H, H_{arom}, J = 8 Hz), 7.27 (apparent t, 2 H, H_{arom}, J = 7 Hz), 7.19 - 7.14 (3 H, H_{arom}), 6.85 (m, 2 H, H_{arom}), 6.79 - 6.74 (2 H, H_{arom}), 6.36 (apparent t, 1 H, H_{arom}, J = 7 Hz), 2.71 (s, 3 H, NAr*Me*), 2.56 - 2.44 (8 H, NAr*Me* + P*Cy*; a broad singlet at 2.49 ppm was assigned as an NAr*Me* resonance on the basis of a ^{1}H-^{13}C HMQC experiment), 2.25 (m, 2 H, P*Cy*), 1.96 (m, 4 H, P*Cy*), 1.88 (m, 2 H, P*Cy*), 1.79 – 1.12 (overlapping resonances, 29 H, P*Cy* + NAr*Me*; a singlet at 1.35 ppm was assigned as an NAr*Me* resonance on the basis of a ^{1}H-^{13}C HMQC experiment), 1.10 – 0.87 (overlapping resonances, 6 H, P*Cy*), 0.85 (s, 3 H, Si*Me*), 0.78 - 0.64 (overlapping resonances, 3 H, P*Cy* + N*H*; a broad resonance at 0.72 ppm was assigned as an N*H* proton on the basis of a ^{1}H-^{15}N HMQC experiment). ^{13}C{^{1}H} NMR (125.8 MHz, benzene-d_6): δ 187.7 (t, N=*C*-N), 161.0 (C_{arom}), 157.7 (apparent t, C_{arom}, J = 21 Hz), 143.3 (apparent t, C_{arom}, J = 21 Hz), 133.3 (apparent t, *C*H$_{arom}$, J = 9 Hz), 132.8 (*C*H$_{arom}$), 129.8 (*C*H$_{arom}$), 129.0 - 128.4 (overlapping resonances, *C*H$_{arom}$), 127.3 (*C*H$_{arom}$), 124.8 (*C*H$_{arom}$), 124.0 (C_{arom}), 115.7 (C_{arom}), 108.7 (C_{arom}), 40.9 (m, *C*H$_{Cy}$), 35.3 (m, *C*H$_{Cy}$), 33.3 (*C*H$_{2Cy}$), 30.2 (*C*H$_{2Cy}$), 29.7 (d, *C*H$_{2Cy}$, J = 9 Hz), 29.1 (*C*H$_{2Cy}$), 28.3 (*C*H$_{2Cy}$), 28.0 (*C*H$_{2Cy}$), 27.6 (*C*H$_{2Cy}$), 27.1 (*C*H$_{2Cy}$), 26.5 (*C*H$_{2Cy}$), 19.9 (NAr*Me*), 18.7 (NAr*Me*), 11.4 (NAr*Me*), 10.5 (Si*Me*). ^{31}P{^{1}H} NMR (202.5 MHz, benzene-d_6): δ 48.38 (s, [Cy-PSiP]). ^{29}Si NMR (99.4 MHz, benzene-d_6): δ 56.9. ^{15}N NMR (50.7 MHz, benzene-d_6): δ -83.5. Anal. Calcd for $C_{54}H_{74}N_2P_2SiRu$: C, 68.83; H, 7.92; N, 2.97. Found: C, 68.50; H, 7.76; N, 2.56.

([Cy-PSiP]RuOH)$_2$ (3-8). A solution of **3-3** (0.21 g, 0.28 mmol) in ca. 3 mL of benzene was treated with degassed H_2O (0.005 mL,0.28 mmol). An immediate color change from red to orange was observed. The volatile components of the reaction mixture were removed *in vacuo* and the solid was triturated with pentane (2 × 1 mL) to yield **3-8** (0.19 g, 94%) as an orange solid. ^{1}H NMR (500 MHz, benzene-d_6): δ 8.02 (br s, 1 H, H_{arom}), 7.72 (br s, 1 H, H_{arom}), 7.72 (br s, 1 H, H_{arom}), 7.51 (br s, 1 H, H_{arom}), 7.24 (br s, 2 H, H_{arom}), 7.04 (br s, 2 H, H_{arom}), 6.94 (br s, 1 H, H_{arom}), 3.22 (br s, 1 H, P*Cy*), 3.03 (br s, 1 H, P*Cy*), 2.79 (br s, 1 H, P*Cy*), 2.64 (br s, 1 H, P*Cy*), 2.51 (br s, 1 H, P*Cy*), 2.42 (br s, 1 H, P*Cy*), 2.24 (m, 2 H, P*Cy*), 2.09 – 0.80 (overlapping resonances, 34 H, P*Cy* + Si*Me*; a singlet resonance at 1.52 ppm was assigned to the Si*Me* protons by use of a ^{1}H-^{13}C HSQC experiment), 0.65 (br m, 2 H, P*Cy*), 0.37 (br s, 1 H, P*Cy*), -0.13 (br s, 1 H, P*Cy*), -0.37 (br s, 1 H, P*Cy*), - 0.74 (s, 1 H, O*H*). ^{13}C{^{1}H} NMR (125.8 MHz, benzene-d_6): δ 160.4 (br, C_{arom}), 132.7 (m, CH_{arom}), 131.1 (m, CH_{arom}), 129.2 (CH_{arom}), 128.9 (CH_{arom}), 127.8 (CH_{arom}), 126.4 (CH_{arom}), 126.3 (CH_{arom}), 41.3 (m, CH_{Cy}), 39.9 (m, CH_{Cy}), 36.1 (m, CH_{Cy}), 34.8 – 26.7 (br overlapping resonances, CH_{2Cy}), 3.7 (Si*Me*). ^{31}P{^{1}H} NMR (300 K, 202.5 MHz, benzene-d_6): δ 91.2 (d, 2 P, $^2J_{PP}$ = 25 Hz), 86.5 (d, 2 P, $^2J_{PP}$ = 25 Hz). ^{31}P{^{1}H} NMR (363 K, 202.5 MHz, toluene-d_8): δ 94.8 (br s). ^{29}Si NMR (99.4 MHz, benzene-d_6): δ 68.7. Anal. Calcd for $C_{74}H_{112}P_4O_2Si_2Ru_2$: C, 62.77; H, 7.97. Found: C, 62.34; H, 8.15. A single crystal of **3-8**•C_7H_8 suitable for X-ray diffraction analysis was grown from a concentrated toluene solution.

[Cy-PSiP]Ru(η^5-*C*$_6$H$_5$O) (3-9). A solution of **3-3** (0.16 g, 0.21 mmol) in ca. 3 mL of benzene was treated with a solution of HOPh (0.020 g, 0.21 mmol) in ca. 1 mL of benzene at room temperature resulting in a color change from red to pale yellow. The

volatile components of the reaction mixture were removed *in vacuo* and the resulting residue was washed with pentane (3 × 1 mL) to yield **3-9** (0.14 g, 84%) as a white solid. ^{1}H NMR (500 MHz, benzene-d_6): δ 7.63 (br m, 2 H, H_{arom}), 7.27 (br s, 2 H, H_{arom}), 7.08 (br m, 2 H, H_{arom}), 6.97 (br m, 2 H, H_{arom}), 5.62 (br m, 2 H, Ru-η^5-C$_6H_5$O), 5.14 (br d, 2 H, Ru-η^5-C$_6H_5$O, J = 5 Hz), 3.98 (apparent t, 1 H, Ru-η^5-C$_6H_5$O, J = 5 Hz), 2.46 (br m, 4 H, P*Cy*), 1.92 (br s, 2 H, P*Cy*), 1.85 – 0.93 (br overlapping resonances, 37 H, P*Cy*), 0.89 (s, 3 H, Si*Me*), 0.62 (br s, 2 H, P*Cy*). ^{13}C{^{1}H} NMR (125.8 MHz, benzene-d_6): δ 169.9 (Ru-η^5-C_6H$_5$O), 158.7 (d, C_{arom}, J = 44 Hz), 147.2 (d, C_{arom}, J = 45 Hz), 132.2 (d, CH$_{arom}$, J = 19 Hz), 129.8 (CH$_{arom}$), 129.0 (CH$_{arom}$), 126.9 (CH$_{arom}$), 99.1 (Ru-η^5-C_6H$_5$O), 83.3 (Ru-η^5-C_6H$_5$O), 67.6 (Ru-η^5-C_6H$_5$O), 41.4 (br, CH$_{Cy}$), 38.9 (br, CH$_{Cy}$), 32.4 – 25.9 (br, CH$_{2Cy}$), 2.7 (Si*Me*). ^{31}P{^{1}H} NMR (300 K, 202.5 MHz, benzene-d_6): δ 74.7 (br m). ^{31}P{^{1}H} NMR (363 K, 202.5 MHz, toluene-d_8): δ 71.5 (s). ^{31}P{^{1}H} NMR (213 K, 101.3 MHz, toluene-d_8): δ 87.7 (br s, 1 P, Cy-*P*Si*P*), 66.7 (br s, 1 P, Cy-*P*Si*P*). ^{29}Si NMR (99.4 MHz, benzene-d_6): δ 57.4. Anal. Calcd for $C_{43}H_{60}OP_2SiRu$: C, 65.87; H, 7.71. Found: C, 65.85; H, 7.90. A single crystal of **3-9**•C_6H_6 suitable for X-ray diffraction analysis was grown from a concentrated benzene solution.

[Cy-PSiP]RuH(η^2:η^2-H$_2$BNH$_2$) (3-10). A solution of H_3B•NH_3 (0.004 g, 0.12 mmol) in ca. 2 mL of benzene was added to a room temperature solution of **3-3** (0.092 g, 0.12 mmol) in ca. 10 mL of benzene. An immediate color change from red to yellow was observed. The volatile components of the reaction mixture were removed *in vacuo* and the remaining solid was triturated with hexanes (2 × 1 mL) to yield **3-10** (0.070 g, 81%) as a yellow solid. ^{1}H NMR (500 MHz, benzene-d_6): δ 8.25 (d, 2 H, H_{arom}, J = 7 Hz), 7.51 (m, 2 H, H_{arom}), 7.30 (t, 2 H, H_{arom}, J = 7 Hz), 7.20 (t, 2 H, H_{arom}, J = 7 Hz), 2.44 (br s, 2

H, NH_2), 2.36 (m, 4 H, P*Cy*), 1.94 – 1.17 (overlapping resonances, 40 H, P*Cy*), 0.99 (s, 3 H, Si*Me*), - 3.36 (br s, 1 H, Ru*H*B), - 7.50 (br s, 1 H, Ru*H*B), - 12.62 (t, 1 H, Ru*H*, $^2J_{HP}$ = 26 Hz). $^{13}C\{^1H\}$ NMR (125.8 MHz, benzene-d_6): δ 161.6 (apparent t, C_{arom}, J = 26 Hz), 146.1 (apparent t, C_{arom}, J = 24 Hz), 133.1 (apparent t, CH_{arom}, J = 10 Hz), 129.2 (CH_{arom}), 129.1 (CH_{arom}), 126.8 (CH_{arom}), 42.1 (apparent t, CH_{Cy}, J = 8 Hz), 35.5 (apparent t, CH_{Cy}, J = 13 Hz), 31.0 (CH_{2Cy}), 30.4 (CH_{2Cy}), 30.0 (CH_{2Cy}), 29.0 (CH_{2Cy}), 28.5 – 27.7 (overlapping resonances, CH_{2Cy}), 9.7 (Si*Me*). $^{31}P\{^1H\}$ NMR (202.5 MHz, benzene-d_6): δ 90.1. ^{29}Si NMR (99.4 MHz, benzene-d_6): δ 63.5. $^{11}B\{^1H\}$ NMR (160 MHz, benzene-d_6): δ 44.1 (br). ^{15}N NMR (50.7 MHz, benzene-d_6): δ - 310.1. IR (Nujol, cm-1): ν 3499, 3399 (s, N-$H_{s,as}$); 1964 (m br, Ru-H); 1853, 1818 (w br, Ru-H-B); 1588 (s, N-H_{bend}). Anal. Calcd for $C_{37}H_{60}P_2NBSiRu$: C, 61.65; H, 8.39.; N, 1.94 Found: C, 61.31; H, 8.36; N, 1.69. A single crystal of **3-10** suitable for X-ray diffraction analysis was grown from a concentrated Et_2O solution at -35 °C.

[Cy-PSiP]RuH(η^2:η^2-H_2BNMe_2) (3-11). A solution of **3-3** (0.074 g, 0.097 mmol) in ca. 5 mL of benzene was treated with a solution of $H_3B{\bullet}NHMe_2$ (0.006 g, 0.097 mmol) in ca. 2 mL of benzene at room temperature. An immediate color change from red to yellow was observed. The volatile components of the reaction mixture were removed *in vacuo* and the remaining solid was washed with pentane (2 × 1 mL) to yield **3-11** (0.049 g, 67%) as a white solid. ^1H NMR (300 K, 500 MHz, benzene-d_6): δ 8.26 (d, 2 H, H_{arom}, J = 7 Hz), 7.53 (m, 2 H, H_{arom}), 7.31 (apparent t, 2 H, H_{arom}, J = 7 Hz), 7.20 (apparent t, 2 H, H_{arom}, J = 7 Hz), 2.59 (s, 6 H, NMe_2), 2.45 – 2.30 (overlapping resonances, 4 H, P*Cy*), 1.96 – 1.04 (overlapping resonances, 40 H, P*Cy*), 0.97 (s, 3 H, Si*Me*), - 3.29 (br s, 1 H, H_2B), - 7.49 (br s, 1 H, H_2B), - 13.07 (t, 1 H, Ru*H*, $^2J_{HP}$ = 25 Hz). $^{13}C\{^1H\}$ NMR (300 K,

125.8 MHz, benzene-d_6): δ 161.7 (apparent t, C_{arom}, J_{CP} = 26 Hz), 146.2 (apparent t, C_{arom}, J_{CP} = 24 Hz), 133.0 (apparent t, CH_{arom}, J = 10 Hz), 129.1 (CH_{arom}), 129.0 (CH_{arom}), 126.8 (CH_{arom}), 42.7 (apparent t, CH_{Cy}, J = 8 Hz), 40.9 (br s, NMe_2), 35.5 (apparent t, CH_{Cy}, J = 13 Hz), 31.3 (CH_{2Cy}), 30.4 (CH_{2Cy}), 30.1 (CH_{2Cy}), 29.1 (CH_{2Cy}), 28.4 (m, CH_{2Cy}), 28.1 (m, CH_{2Cy}), 27.9 – 27.7 (overlapping resonances, CH_{2Cy}), 27.2 (CH_{2Cy}), 10.5 (SiMe). $^{31}P\{^1H\}$ NMR (300 K, 202.5 MHz, benzene-d_6): δ 91.2. ^{29}Si NMR (300 K, 99.4 MHz, benzene-d_6): δ 63.7. ^{11}B NMR (300 K, 160 MHz, benzene-d_6): δ 43.9 (br). IR (thin film, cm^{-1}): ν 1966 (m br, Ru-H); the B-H stretches could not be unequivocally identified. Anal. Calcd for $C_{39}H_{64}P_2NBSiRu$: C, 62.55; H, 8.61; N, 1.87. Found: C, 62.34; H, 8.98; N, 1.68. A single crystal of **3-11** suitable for X-ray diffraction analysis was grown from a concentrated Et_2O solution at -35 °C.

[Cy-PSiP]RuH(η²:η²-H₂BNH^{t}Bu) (3-12). A solution of **3-3** (0.075 g, 0.098 mmol) in ca. 5 mL of benzene was treated with a solution of $H_3B{\bullet}NH_2{}^tBu$ (0.009 g, 0.098 mmol) in ca. 2 mL of benzene at room temperature. An immediate color change from red to yellow was observed. The volatile components of the reaction mixture were removed *in vacuo* and the remaining solid was washed with pentane (2 × 1 mL) to yield **3-12** (0.062 g, 82%) as a white solid. ^1H NMR (500 MHz, benzene-d_6): δ 8.26 (d, 2 H, H_{arom}, J = 7 Hz), 7.53 (m, 2 H, H_{arom}), 7.31 (apparent t, 2 H, H_{arom}, J = 7 Hz), 7.21 (apparent t, 2 H, H_{arom}, J = 7 Hz), 3.29 (br s, 1 H, NH), 2.33 (br m, 4 H, PCy), 2.06 – 1.13 (overlapping resonances, 40 H, PCy), 1.11 (s, 9 H, NCMe_3), 0.96 (s, 3 H, SiMe), - 3.34 (br s, 1 H, RuHB), - 7.56 (br s, 1 H, RuHB), - 12.66 (br s, 1 H, RuH). $^{13}C\{^1H\}$ NMR (125.8 MHz, benzene-d_6): δ 161.6 (apparent t, C_{arom}, J_{CP} = 25 Hz), 146.5 (apparent t, C_{arom}, J_{CP} = 23 Hz), 132.9 (apparent t, CH_{arom}, J = 10 Hz), 129.0 (CH_{arom}), 128.9 (CH_{arom}), 126.7

(CH_{arom}), 50.0 ($NCMe_3$), 42.8 (apparent t, CH_{Cy}, J = 8 Hz), 36.1 (br, CH_{Cy}), 32.4 ($NCMe_3$), 30.3 (CH_{2Cy}), 29.9 (CH_{2Cy}), 29.0 (CH_{2Cy}), 27.8 (CH_{2Cy}), 27.0 (CH_{2Cy}), 10.1 (Si*Me*). $^{31}P\{^1H\}$ NMR (202.5 MHz, benzene-d_6): δ 90.2. ^{29}Si NMR (99.4 MHz, benzene-d_6): δ 64.2. $^{11}B\{^1H\}$ NMR (160 MHz, benzene-d_6): δ 42.1 (br). IR (thin film, cm^{-1}): ν 3310 (br s, N-H); 1966 (m br, Ru-H); the B-H stretches could not be unequivocally identified. Anal. Calcd for $C_{41}H_{68}P_2NBSiRu$: C, 63.39; H, 8.82; N, 1.80. Found: C, 63.25; H, 8.80; N, 1.66.

3.4.4 Crystallographic Solution and Refinement Details

Crystallographic data for each of **3-2**·$(C_6H_6)_{3.5}$, **3-3**·C_6H_6·$(C_5H_{12})_{0.5}$, **3-4**, **3-6**, **3-8**·C_7H_8, **3-9**·C_6H_6, **3-10**, and **3-11** were obtained at 173(±2) K on a Bruker D8/APEX II CCD diffractometer using a graphite-monochromated Mo Kα (λ = 0.71073 Å) radiation, employing a sample that was mounted in inert oil and transferred to a cold gas stream on the diffractometer. Programs for diffractometer operation, data collection, and data reduction (including SAINT) were supplied by Bruker. Gaussian integration (face-indexed) was employed as the absorption correction method for **3-2**·$(C_6H_6)_{3.5}$, **3-3**·C_6H_6·$(C_5H_{12})_{0.5}$, **3-6**, **3-8**·C_7H_8, **3-9**·C_6H_6, **3-10**, and **3-11**, while SADABS (Bruker) was used for 3. The structures **3-2**·$(C_6H_6)_{3.5}$, **3-3**·C_6H_6·$(C_5H_{12})_{0.5}$, **3-6**, **3-9**·C_6H_6, and **3-11** were solved by use of the Patterson search/structure expansion, while the structures of **3-4**, **3-8**·C_7H_8, and **3-10** were solved by use of direct methods. All structures were refined by use of full-matrix least-squares procedures (on F^2) with R_1 based on F_o^2 ($2\sigma(F_o^2)$ and wR_2 based on F_o^2 ($-3\sigma(F_o^2)$. Anisotropic displacement parameters were employed for all the non-hydrogen atoms of **3-4**, **3-6**, **3-9**·C_6H_6, **3-10**, and **3-11**. During the structure

solution process for **3-2**·$(C_6H_6)_{3.5}$, 3.5 equivalents of benzene were located in the asymmetric unit. After location (and anisotropic refinement) of three equivalents of solvent benzene, attempts to refine peaks of residual electron density (located near the crystallographic inversion center [1/2, 1/2, 0]) as disordered or partial-occupancy benzene carbon atoms were unsuccessful. The data were corrected for disordered electron density through use of the SQUEEZE procedure as implemented in *PLATON*. A total solvent-accessible void volume of 426.0 $Å^3$ with a total electron count of 83 (consistent with one-half molecule per formula unit of the diruthenium complex) was found in the unit cell. All remaining non-hydrogen atoms for **3-2**·$(C_6H_6)_{3.5}$ were refined anisotropically. Disorder involving the O^{t}Bu ligand was identified during the solution process for **3-3**·C_6H_6·$(C_5H_{12})_{0.5}$. The carbon atoms of the disordered O^{t}Bu ligand were refined anisotropically over two positions (C3A, C4A, C5A, C3B, C4B, C5B), where each carbon atom has an occupancy factor of 0.5. Disordered benzene and *n*-pentane solvates were also identified during the structure solution process for **3-3**·C_6H_6·$(C_5H_{12})_{0.5}$. One molecule of benzene was modeled over two positions, where the carbon atoms (C11S – C16S and C21S – C26S) were refined anisotropically with an occupancy factor of 0.5. Restraints were applied during refinement to impose an idealized geometry upon the disordered solvent *n*-pentane molecule: d(C31S–C32S) = d(C32S–C33S) = d(C33S–C34S) = d(C34S–C35S) = 1.54(1) Å; d(C31S···C33S) = d(C32S···C34S) = d(C33S···C35S) = 2.52(1) Å. Atoms of the disordered *n*-pentane molecule were refined with a common isotropic displacement parameter an occupancy factor of 0.5. All remaining non-hydrogen atoms in **3-3**·C_6H_6·$(C_5H_{12})_{0.5}$ were refined anisotropically. During the structure solution process for **3-8**·C_7H_8 an equivalent of toluene was located in

the asymmetric unit. Carbon atoms of the disordered solvent toluene molecule were refined with an occupancy factor of 0.5 and a common isotropic displacement parameter. Distances involving the methyl carbon atom positions for the disordered solvent toluene molecule were given fixed idealized distances during refinement: d(C10S–C11S) = d(C20S–C21S) = 1.50(1) Å; d(C10S···C12S) = d(C10S···C16S) = d(C20S···C22S) = d(C20S···C26S) = 2.51(1) Å. The arene rings of the two conformers of this disordered molecule were modelled as regular hexagons with d(C–C) = 1.39 Å (*SHELXL-97* AFIX 66 instruction). Hydrogen atoms for **3-2**·$(C_6H_6)_{3.5}$, **3-3**·C_6H_6·$(C_5H_{12})_{0.5}$, **3-4**, **3-6**, **3-8**·C_7H_8 and **3-9**·C_6H_6 were added at calculated positions and refined by use of a riding model employing isotropic displacement parameters based on the isotropic displacement parameter of the attached atom. The Ru-*H* (H1) and two Ru-*H*-B (H1BA and H1BB) hydrogen atoms in **3-10** were located in the difference map and refined isotropically, where H1BA and H1BB were refined with an isotropic displacement parameter 120% of the U_{eq} for the attached B atom. Distance restraints were applied as follows during the refinement process for **3-10**: d(Ru–H1) = 1.55(1) Å; d(B–H1BA) = d(B–H1BB) = 1.12(2) Å; d(H1BA···H1BB) = 1.94(2) Å; d(P1···H1) = d(P2···H1) (within 0.03 Å). The Ru-*H* (H1) and two Ru-*H*-B (H1BA and H1BB) hydrogen atoms in **3-11** were located in the difference map and refined isotropically. All remaining hydrogen atoms in **3-10** and **3-11** were added at calculated positions and refined by use of a riding model employing isotropic displacement parameters based on the isotropic displacement parameter of the attached atom. Additional crystallographic information is provided in Appendix A.

Chapter 4: Synthesis and Characterization of Five-Coordinate, 16-electron Ru^{II} Complexes of the Type [Cy-PSiP]RuXL

4.1 Introduction

Among the most prominent examples of Ru-mediated reactivity are the Nobel Prize winning catalytic reactions for asymmetric transfer hydrogenation[2e] and olefin metathesis[2c] from the groups of Noyori and Grubbs, respectively. Both of these catalytic processes invoke electronically unsaturated Ru species, which serves to illustrate the utility of such unsaturated Ru complexes in organometallic catalysis. By far the most common and synthetically useful class of electronically and coordinatively unsaturated Ru organometallic complexes known are Ru^{II} 16-electron species with a ligand bond number of five.[109] Such complexes have found application both in catalytic transformations,[2c,2e,4,54-58,110] as well as in stoichiometric bond activation processes.[52,83b,84,111] Of particular interest are compounds of the type $Cp^*RuX(PR_3)$ ($Cp^* = \eta^5$-C_5Me_5; R = ^{i}Pr, Cy; X = halide, pseudo-halide, alkyl) reported by Tilley and co-workers,[110-112] which are well established in the activation of E-H bonds (E = main group element).[110-113] Compounds of this type thus serve as precursors to a number of unusual complexes (Scheme 4-1), including Ru-silylenes,[110,112] a Ru-germylene,[112] and a bis-σ-B-H Ru compound.[113] In addition to this remarkable stoichiometric reactivity, the silylene complex $Cp^*Ru(=SiHR)(P^iPr_3)(H)_2$ was shown to catalyze alkene hydrosilylation via an unprecedented pathway involving insertion of an alkene into the Si-H bond of the electrophilic silylene.[110]

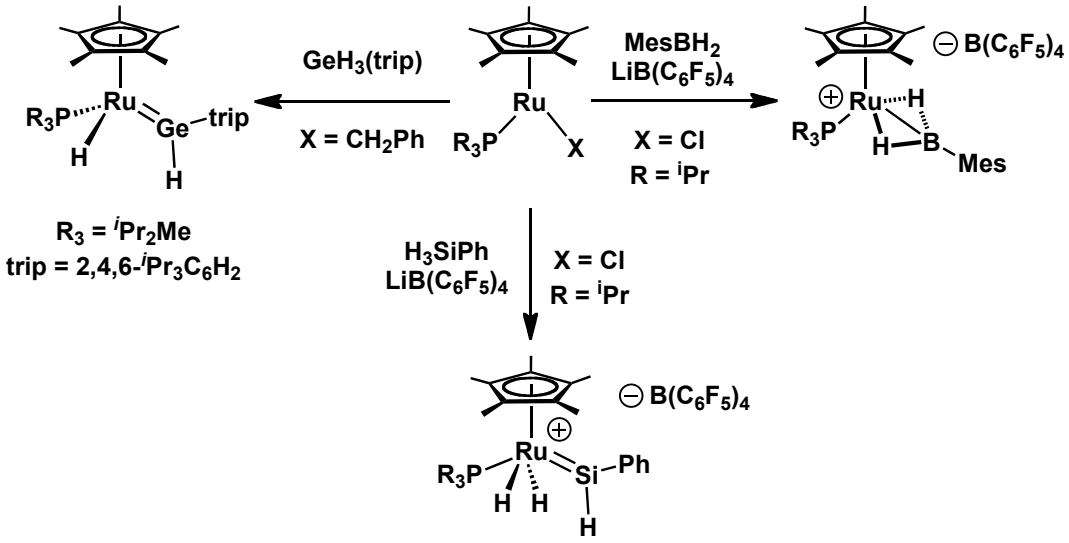

Scheme 4-1. Reactivity of Cp*RuX(PR_3) illustrating the variety of complexes stabilized by the "Cp*RuPR_3" fragment.

In this context, the synthesis of 16-electron complexes of the type [Cy-PSiP]RuX(PR_3) ([Cy-PSiP] = [κ^3-(2-$Cy_2PC_6H_4)_2SiMe$]$^-$) is of interest, as such electronically and coordinatively unsaturated species have the potential to engage in novel stoichiometric and/or catalytic bond activation processes. Like Cp*, [Cy-PSiP] is a strongly electron-donating ligand (as shown by computational studies described in Chapter 3) that offers significant steric protection to the metal center, as evidenced by the stabilization of an array of unusual four-coordinate, 14-electron Ru^{II} compounds of the type [Cy-PSiP]RuX' (X' = amido, alkoxo). In light of the reactivity seen for such four-coordinate, 14-electron Ru complexes, it is anticipated that extending the chemistry of [Cy-PSiP] to the synthesis of five-coordinate, 16-electron Ru^{II} complexes will lead to the discovery of new highly reactive Ru species.

4.2 Results and Discussion

4.2.1 Synthesis of 16-electron [Cy-PSiP]RuCl(PR_3) complexes.

It was expected that 16-electron [Cy-PSiP]Ru species could be accessed in a manner analogous to that previously utilized for the synthesis of [Ph-PSiP]RuCl(PR_3). However, reaction of a benzene solution of [Cy-PSiP]H with one equiv $RuCl_2(PPh_3)_3$ in the presence of Et_3N (Scheme 4-2) afforded more than one product (by ^{31}P NMR) after 24 h at 70 °C. The room temperature $^{31}P\{^1H\}$ NMR spectrum of the reaction mixture (toluene-d_8) features three resonances in a 1:1:1 ratio at 104.4 (br s), 72.4 (br d, J = 264 Hz), and 42.6 (br d, J = 264 Hz) ppm corresponding to the C_1-symmetric product [Cy-PSiP]RuCl(PPh_3) (**4-1**), as well as a singlet at 94.5 ppm corresponding to ([Cy-PSiP]RuCl)$_2$ (**3-2**), and a broad singlet at 0.5 ppm corresponding to free PPh_3. Variable temperature $^{31}P\{^1H\}$ NMR spectroscopy is consistent with a temperature-dependent equilibrium process involving reversible dissociation of PPh_3 from **4-1** to form **3-2**, where at high temperature the dinuclear complex **3-2** is the sole [Cy-PSiP]-containing Ru complex in solution, while at low temperatures the major species in solution is the mononuclear complex **4-1** (Scheme 4-2, Figure 4-1). Thus, heating the solution to 323K led to the disappearance of the signals corresponding to **4-1**, with the only remaining resonances being those that correspond to **3-2** and free PPh_3 (broad). Upon cooling the solution below room temperature the resonances corresponding to **4-1** sharpen, revealing further PP coupling (at 193K: 105.5 ppm, apparent t, J = 20 Hz; 70.5 ppm, dd, $^2J_{PPtrans}$ = 276 Hz, $^2J_{PPcis}$ = 20 Hz; 46.0 ppm, dd, $^2J_{PPtrans}$ = 276 Hz, $^2J_{PPcis}$ = 22 Hz). These temperature-dependent NMR line shape changes may arise due to intramolecular rearrangement processes (e.g., pseudorotation) in **4-1** and/or Ru-P dissociation.

Concomitant with these line shape changes, the ratio of **3-2**:**4-1** decreases significantly upon cooling, such that at 193K the ratio is 1:10. Interestingly, no similar temperature-dependent equilibrium was observed for the analogous complex [Ph-PSiP]RuCl(PPh_3) (**2-2**), suggesting that the cyclohexyl phosphino donors of [Cy-PSiP] exert increased steric pressure in the Ru coordination sphere relative to the phenyl phosphino derivative, resulting in the dissociation of PPh_3. Complex **3-2** could be isolated from the equilibrium mixture by crystallization from diethyl ether at -30 °C, however yields were low and irreproducible. An alternative synthetic route to **3-2** was developed using [(*p*-cymene)$RuCl_2$]$_2$ as the source of Ru in order to avoid contamination with PPh_3 (see Chapter 3).

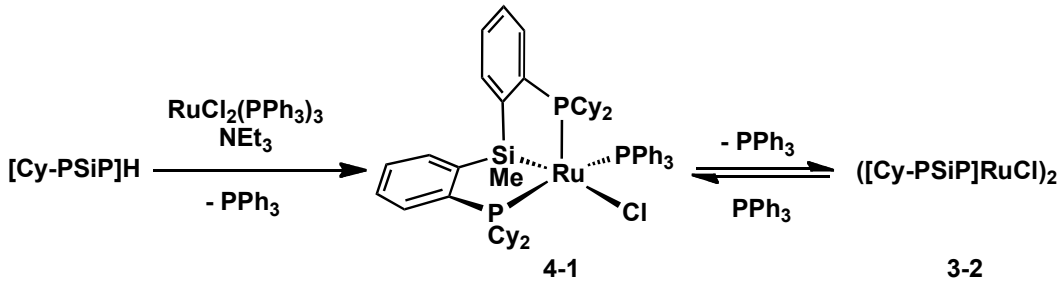

Scheme 4-2. Reaction of [Cy-PSiP]H with $RuCl_2(PPh_3)_3$ in the presence of NEt_3 to give an equilibrium mixture of [Cy-PSiP]RuCl(PPh_3) (**4-1**), ([Cy-PSiP]RuCl)$_2$ (**3-2**), and PPh_3.

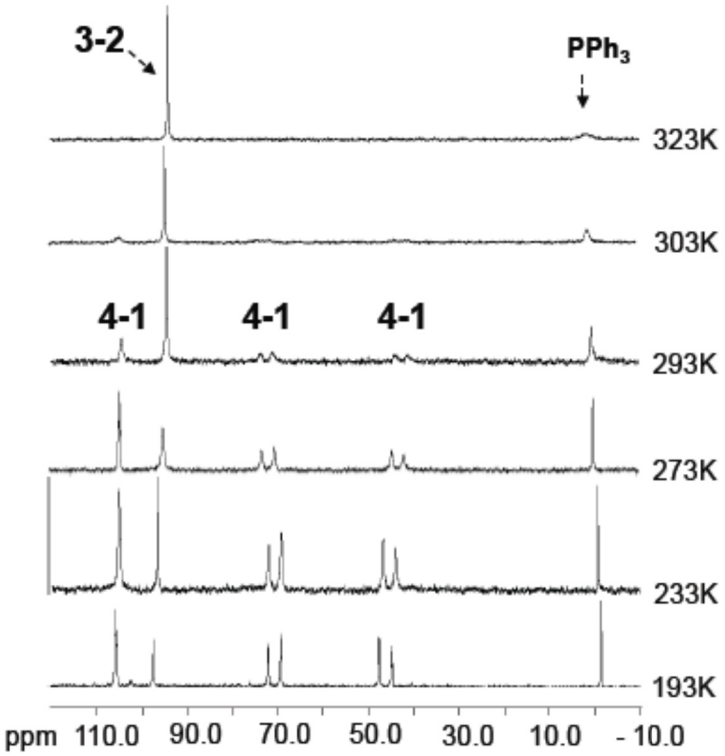

Figure 4-1. Variable-temperature ^{31}P NMR spectra of a sample containing **4-1**, **3-2**, and PPh_3 showing the temperature-dependent equilibrium involving the reversible dissociation of PPh_3 from **4-1**.

Substitution of PPh_3 with a smaller, more electron-donating phosphine was expected to lead to the formation of an isolable five-coordinate [Cy-PSiP]Ru complex analogous to **4-1**. Indeed, addition of PMe_3 to a solution containing an equilibrium mixture of **4-1** and **3-2** resulted in the quantitative formation (by ^{31}P NMR) of the five-coordinate, 16-electron complex [Cy-PSiP]RuCl(PMe_3) (**4-2**). Alternatively, complex **4-2** was isolated in 97% yield by addition of PMe_3 to a benzene solution of **3-2** (Scheme 4-3). The X-ray crystal structure of **4-2** (Figure 4-2) confirms the formation of a five-coordinate, *fac*-[Cy-PSiP] complex with "Y-shaped" geometry at Ru, as indicated by the acute P2-Ru-Si angle of 78.630(13)°.[66] The Ru-Si distance of 2.3010(4) Å is comparable to that observed for the related complexes **2-2** (2.3361(6) Å) and **2-6** (2.2944(11) Å).

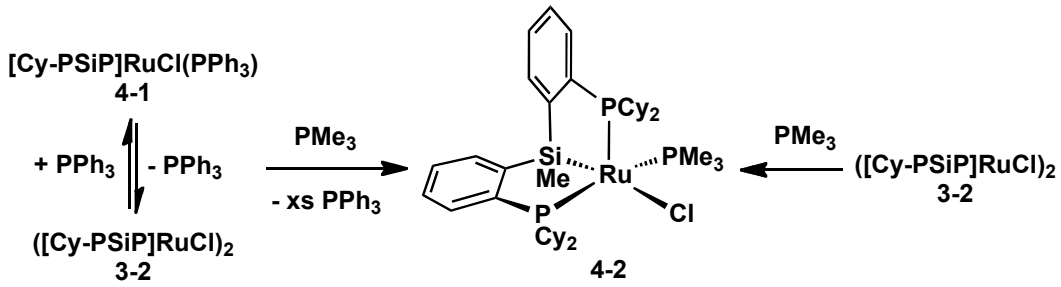

Scheme 4-3. Synthesis of the five-coordinate, 16-electron complex [Cy-PSiP]RuCl(PMe_3) (**4-2**).

The room temperature $^{31}P\{^1H\}$ NMR spectrum of **4-2** (toluene-d_8) features three resonances in a 1:1:1 ratio, consisting of a broad singlet at 100.4 ppm, a broad doublet at 64.7 ppm (J = 265 Hz), and a doublet at -0.5 ppm (J = 249 Hz). Upon cooling to 263K these resonances sharpen significantly, revealing further PP coupling (105.6 ppm, apparent t, $^2J_{PPcis}$ = 20 Hz, $^2J_{PPcis}$ = 28 Hz; 70.5 ppm, dd, $^2J_{PPcis}$ = 19 Hz, $^2J_{PPtrans}$ = 276 Hz; 5.9 ppm, dd, $^2J_{PPcis}$ = 19 Hz, $^2J_{PPtrans}$ = 276 Hz). No further decoalescence phenomena were observed below 263K. The resonances observed at low temperature in the ^{31}P NMR spectrum of **4-2** are consistent with the solid-state structure, which features the three inequivalent phosphine donors in a T-type configuration. As in the case of **4-1**, the temperature-dependent NMR line shape changes observed for **4-2** likely arise due to intramolecular rearrangement processes (e.g. pseudorotation), or possibly due to phosphine dissociation.

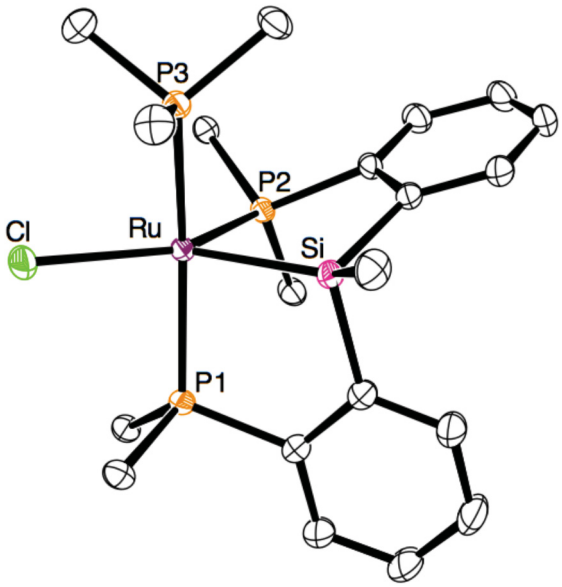

Figure 4-2. The crystallographically determined structure of **4-2** shown with 50% ellipsoids; H atoms and the cyclohexyl carbon atoms have been omitted for clarity. Selected interatomic distances (Å) and angles (deg): Ru-Si 2.3010(4), Ru-Cl 2.4435(4), P2-Ru-Si 78.630(13), Si-Ru-Cl 137.742(14), P2-Ru-Cl 143.618(13), P1-Ru-P2 97.170(13).

4.2.2 Attempted synthesis of [Cy-PSiP]Ru alkyl species.

In an attempt to generate a coordinatively unsaturated [Cy-PSiP]Ru^{II} alkyl complex, complex **4-2** was reacted with one equiv of MeMgBr (eq 4-1). In situ ^{1}H NMR analysis of the reaction mixture indicated loss of CH_4 and the formation of a new [Cy-PSiP]-containing Ru product (**4-3**). A single crystal of **4-3** suitable for X-ray diffraction was obtained by vapor diffusion of pentane into a benzene solution of the crude product. The solid state structure of **4-3** (Figure 4-3) indicated the formation of a distorted octahedral complex that features *fac*-[Cy-PSiP] ligation as well as a dehydrogenated cyclohexyl substituent bound in an η^3-fashion to Ru. The PMe_3 ligand is positioned *trans* to the cyclometalated phosphine donor of the [Cy-PSiP] ligand (P1). The Ru-Si bond

distance of 2.3518(4) Å is slightly elongated in comparison to the Ru-Si distance of 2.3010(4) Å in **4-2**.

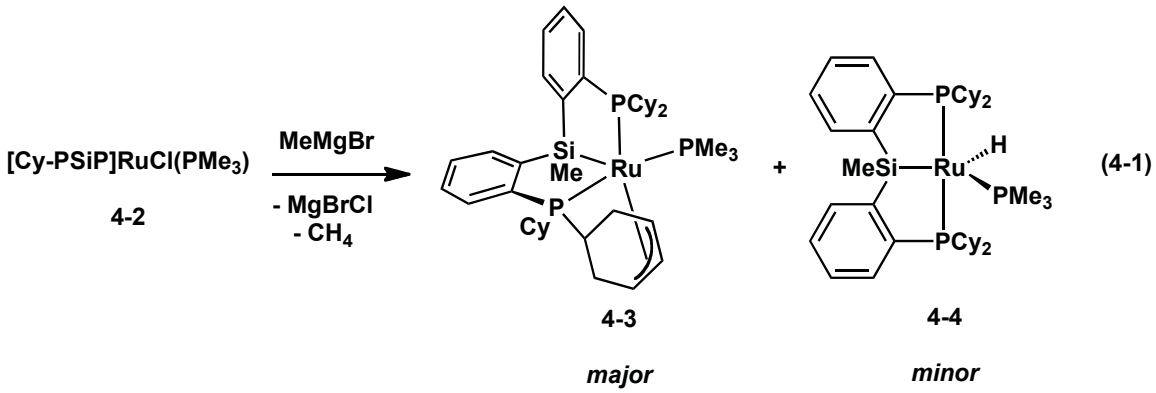

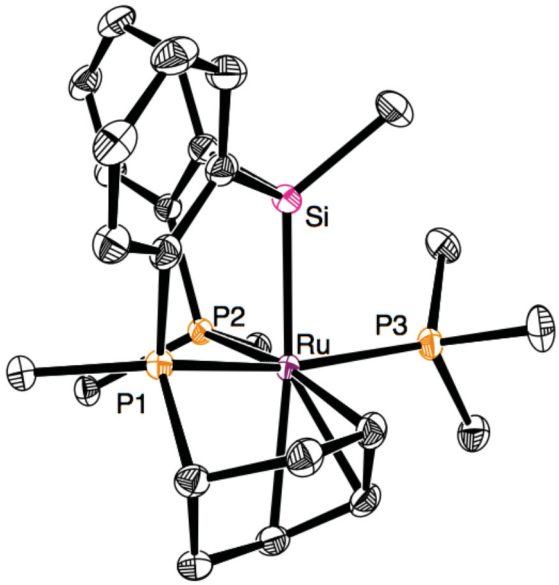

Figure 4-3. The crystallographically determined structure of **4-3** shown with 50% ellipsoids; H atoms and the cyclohexyl carbon atoms have been omitted for clarity. Selected interatomic distances (Å) and angles (deg): Ru-Si 2.3518(4), Ru-C33 2.2713(15), Ru-C34 2.1926(15), Ru-C35 2.3999(15), P1-Ru-P3 162.459(15), P1-Ru-C33 78.65(4), Si-Ru-C35 156.70(4), P2-Ru-C33 171.24(4).

The room temperature $^{31}P\{^{1}H\}$ NMR spectrum of **4-3** features three resonances at 104.0 (dd, $^{2}J_{PPcis}$ = 23 Hz, $^{2}J_{PPtrans}$ = 230 Hz), 83.7 (apparent t, J = 26 Hz), and -3.7 (dd,

$^2J_{PPcis}$ = 31 Hz, $^2J_{PPtrans}$ = 230 Hz) ppm in a 1:1:1 ratio. Unlike previously described five-coordinate, 16-electron [R-PSiP]Ru complexes, **4-3** is a six-coordinate, 18-electron complex that is non-fluxional at room temperature. The ^{1}H NMR spectrum (benzene-d_6) of **4-3** exhibits diagnostic resonances at 4.65, 4.21, and 2.54 ppm corresponding to the allylic protons of the dehydrogenated cyclohexyl substituent.

Although no intermediates were observed by NMR spectroscopy en route to **4-3**, a minute quantity of X-ray quality crystals of a minor product (**4-4**) were obtained by vapor diffusion of pentane into a benzene solution of the crude product resulting from the attempted methylation of **4-2**. The solid-state structure of **4-4** (Figure 4-4) indicates a five-coordinate [Cy-PSiP]Ru(H)PMe_3 complex that features distorted trigonal bipyramidal geometry at Ru. The [Cy-PSiP] ligand is coordinated to the metal center in a *mer*-type binding mode featuring *trans*-disposed phosphine donors (P1-Ru-P1' = 149.01(3)°). Attempts to independently synthesize **4-4** by exposing a benzene solution of **4-3** to 1 atm H_2 were not successful, despite prolonged reaction times (3-4 days) and elevated temperature (80 °C). Similarly, the reaction of **4-2** with $LiEt_3BH$ led to the formation of an intractable reaction mixture that featured multiple phosphorus-containing products.

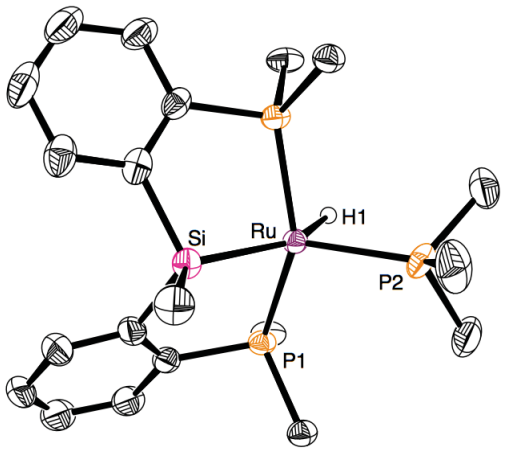

Figure 4-4. The crystallographically determined structure of **4-4**·$(C_5H_{12})_{0.875}$ shown with 50% ellipsoids; selected H atoms, cyclohexyl carbon atoms, and solvent atoms have been omitted for clarity. The crystallographically unique atoms are labeled. Selected interatomic distances (Å) and angles (deg): Ru-Si 2.3729(9), Si-Ru-P2 127.93(4), Si-Ru-H1 149.1(15), P2-Ru-H1 83.0(15), P1-Ru-P1' 149.01(3).

A proposed mechanism for the formation of **4-3** and **4-4** is outlined in Scheme 4-4. The initial step is proposed to be the formation of the (unobserved) 16-electron methyl intermediate [Cy-PSiP]Ru(Me)(PMe_3) (**4-5**). This reactive 16-electron alkyl species can undergo C-H activation of a PCy group with concomitant elimination of methane to form the cyclometalated, 16-electron alkyl intermediate **4-6**. Complex **4-6** can subsequently undergo β-hydride elimination to give the alkene hydride complex **4-7.** Activation of a C-H bond in **4-7** and loss of H_2 leads to the formation of **4-3**. The Ru-mediated dehydrogenation of cyclohexylphosphino ligands is well precedented.[114] In light of the observation that the reaction of **4-3** with 1 atm of H_2 does not produce **4-4**, it is likely that H_2 generated from the dehydrogenation of **4-7** instead reacts with proposed intermediate **4-6** to afford **4-4** (Scheme 4-4).

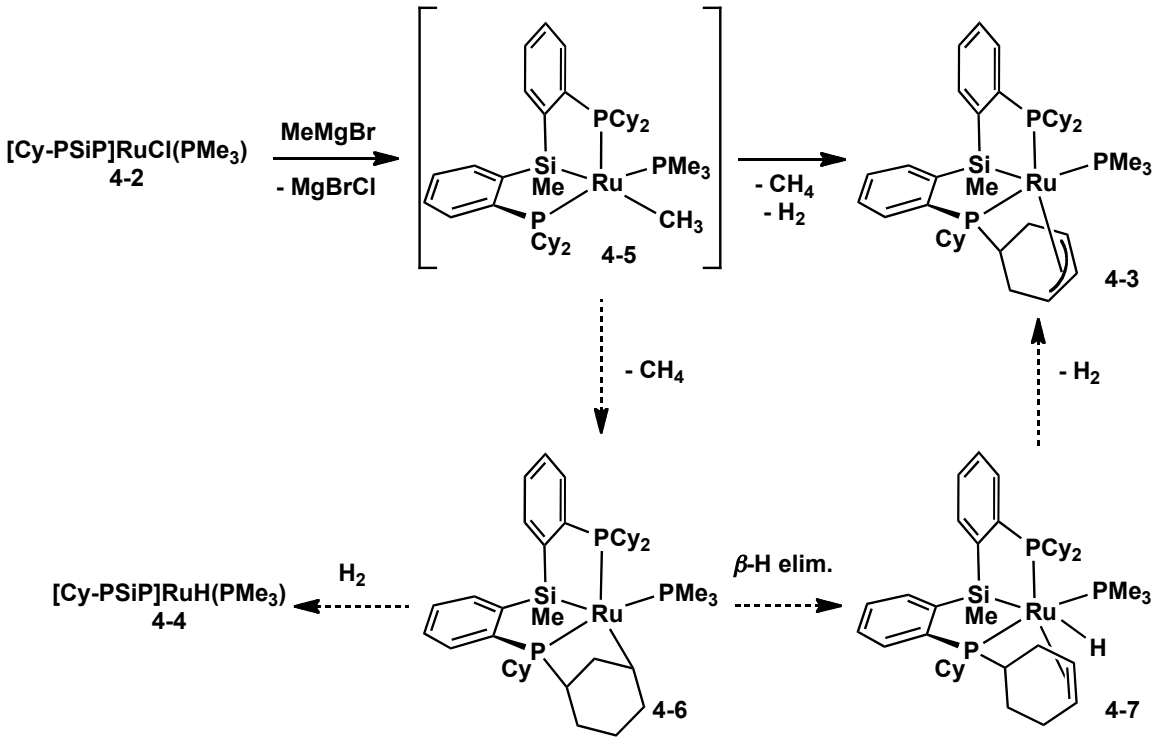

Scheme 4-4. Proposed mechanism for the formation of the cyclometalated product [MeSi($C_6H_4PCy_2$)($C_6H_4PCy(\eta^3$-$C_6H_8)$)]RuPMe$_3$ (**4-3**) and [Cy-PSiP]Ru(H)(PMe$_3$) (**4-4**).

In an effort to access a stable 16-electron [Cy-PSiP]Ru(alkyl) complex, ([Cy-PSiP]RuCl)$_2$ (**3-2**) was treated with one equiv of (C_3H_5)MgCl, which resulted in the formation of the Ru(η^3-allyl) complex **4-8** (79% yield; eq 4-2). Vapor diffusion of pentane into a benzene solution of **4-8** provided a single crystal suitable for X-ray diffraction analysis. The solid-state structure of **4-8** (Figure 4-5) confirms the formation of a five-coordinate, distorted square-pyramidal [Cy-PSiP]Ru(η^3-C_3H_5) complex in which the silyl donor occupies the apical position while the [Cy-PSiP] ligand phosphines and the η^3-allyl ligand occupy basal sites of the square pyramid. Since the silyl donor in **4-8** is trans to a vacant coordination site, it is not surprising that the Ru-Si distance of

2.2727(4) Å is shorter than the Ru-Si distance in **4-3** (2.3518(4) Å), which features the silyl donor *trans* to an allylic carbon.

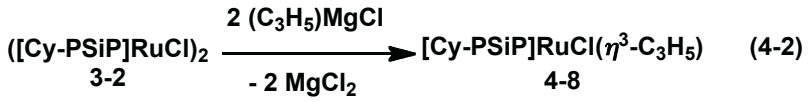

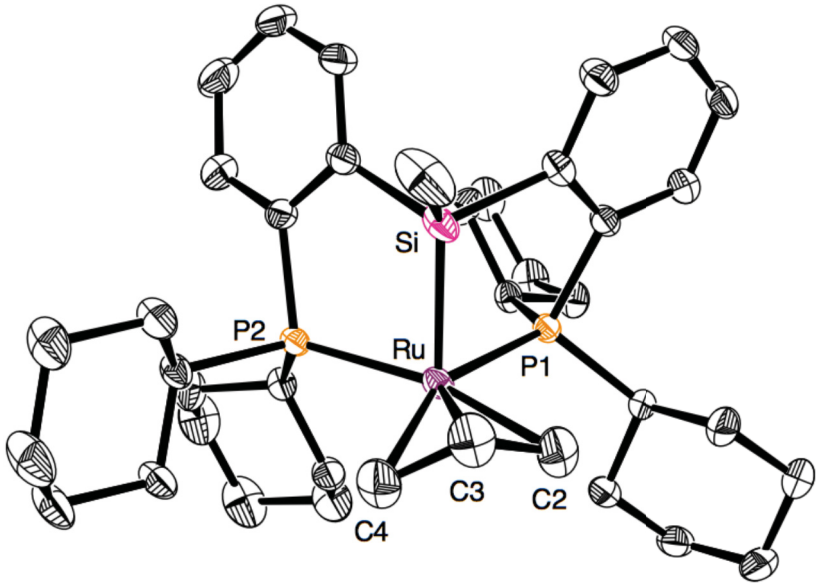

Figure 4-5. The crystallographically determined structure of **4-8** shown with 50% ellipsoids; H atoms have been omitted for clarity. Selected interatomic distances (Å) and angles (deg): Ru-Si 2.2727(4), Ru-C2 2.2018(16), Ru-C3 2.1731(15), Ru-C4 2.2072(15), P2-Ru-C2 164.42(5), P1-Ru-C4 155.70(5), P2-Ru-P1 104.411(12).

The room temperature ^{31}P NMR spectrum of complex **4-8** exhibits a single resonance at 69.9 ppm, which is indicative of an averaged C_s-symmetric structure in solution. The ^{1}H and ^{13}C NMR spectra of **4-8** (benzene-d_6) exhibit resonances diagnostic

of an η^3-allyl fragment (^{1}H NMR: 4.90, 3.83, and 1.35 ppm; ^{13}C NMR: 98.1 and 54.4 ppm; the third allyl carbon resonance was not observed at room temperature despite prolonged acquisition times). At 203K the $^{31}P\{^1H\}$ NMR signal for **4-8** has decoalesced into two peaks in a 1:1 ratio at 74.6 (d, J_{PP} = 6 Hz) and 65.1 (d, J_{PP} = 6 Hz) ppm (decoalescence temperature = 263K), indicative of inequivalent ligand phosphine environments at low temperature. Although it is very common for allyl complexes to exhibit fluxional behavior,[79d] the observed decoalescence in the ^{31}P NMR spectrum of **4-8** cannot be attributed to allyl dynamics. Rather, it is likely that at the low temperature limit complex **4-8** adopts a κ^3-mer structure resulting in a C_1-symmetric η^3-allyl complex (Figure 4-6) that is structurally analogous to the previously reported Ni^{II} species [Cy-PSiP]Ni(η^3-C_3H_5).[79d]

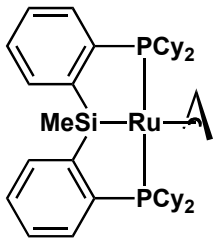

4-8

Figure 4-6. Proposed conformation of **4-8** at 193K.

4.2.3 Synthesis of [Cy-PSiP]RuN$_3$ complexes

Caulton and co-workers have recently demonstrated that [PNP]RuN_3 (PNP = $N(SiMe_2CH_2P^tBu_2)_2$) serves as a source of the novel d^4 terminal nitrido complex (PNP)Ru≡N.[115] In an attempt to prepare [Cy-PSiP]RuN_3 species, complex **4-2** was treated with one equiv of Me_3SiN_3 (Scheme 4-5). However, addition of Me_3SiN_3 to a

benzene solution of **4-2** resulted in no reaction, even after heating at 80 °C for 3 days. Reaction of **4-2** with NaN_3 led to formation of a new product that featured ^{31}P NMR resonances at 99, 68, and 0.5 ppm (in a 1:1:1 ratio), however after heating at 80 °C for 14 days only 10% conversion was obtained. Alternatively, complex **3-3** reacted with one equiv of Me_3SiN_3 in benzene solution resulting in an immediate color change from orange to red and complete conversion (by ^{31}P NMR) to a new product (**4-9**) that gives rise to a singlet resonance at 82.3 ppm in the ^{31}P NMR spectrum of the reaction mixture (eq 4-3). Upon attempted isolation, **4-9** proved insoluble in common organic solvents including THF and CH_2Cl_2, which made its unambiguous characterization difficult. However, **4-9** does exhibit an IR stretch at 2081 cm^{-1}, which is consistent with a Ru azide. Based on this IR data as well as the poor solubility of **4-9**, this compound is tentatively formulated as $([Cy\text{-}PSiP]RuN_3)_2$.

$$\underset{\textbf{3-3}}{[Cy\text{-}PSiP]RuO^tBu} + Me_3SiN_3 \xrightarrow[-\ Me_3SiO^tBu]{\text{benzene}} \underset{\textbf{4-9}}{([Cy\text{-}PSiP]RuN_3)_2} \qquad (4\text{-}3)$$

In an attempt to obtain a more soluble Ru azide complex, **4-9** was treated with excess PMe_3, resulting in complete conversion (by ^{31}P NMR) to the monomeric 16-electron complex $[Cy\text{-}PSiP]Ru(N_3)(PMe_3)$ (**4-10**, Scheme 4-5). Crystallographic characterization of **4-10** indicated formation of a "Y-shaped" five-coordinate complex featuring *fac*-[Cy-PSiP] coordination to the metal center (Figure 4-7). In benzene-d_6 solution the ^{31}P NMR spectrum of **4-10** exhibits resonances at 97.6, 67.0 (br d, J = 260 Hz), and -1.1 (d, J = 245 Hz) ppm in a 1:1:1 ratio. The IR spectrum of **4-10** exhibits a

band at 2042 cm^{-1}, which is consistent with the formulation of a Ru-azide as opposed to a Ru-nitride.

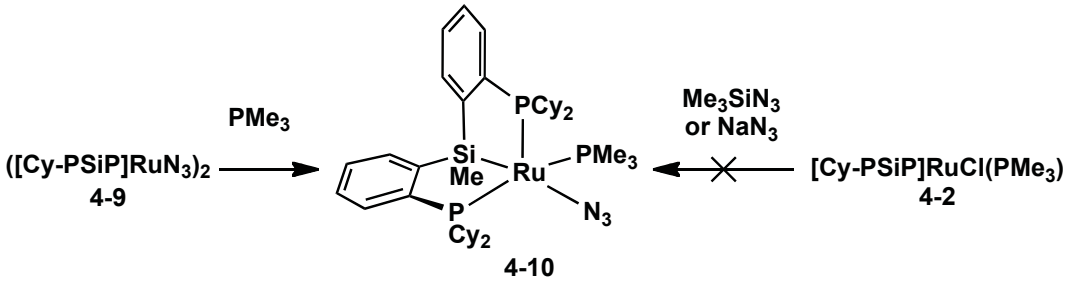

Scheme 4-5. Synthesis of the five-coordinate Ru-azide [Cy-PSiP]$RuN_3(PMe_3)$ **4-10**.

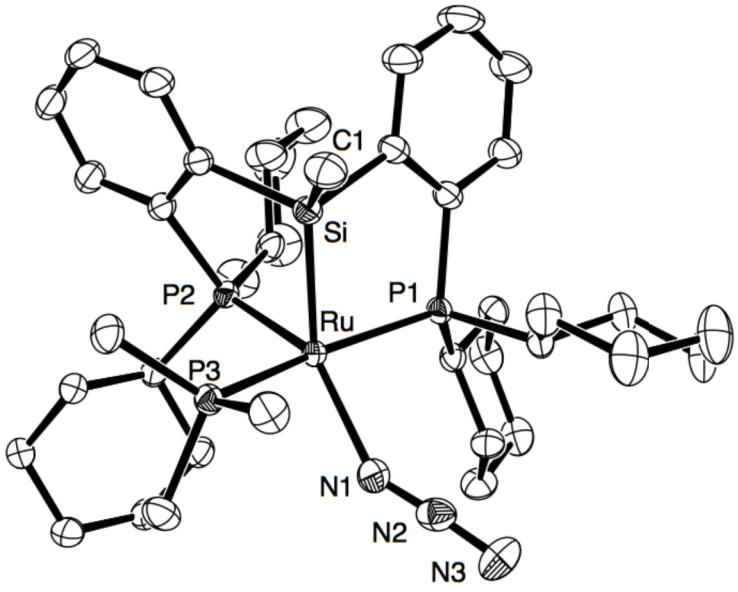

Figure 4-7. The crystallographically determined structure of **4-10** shown with 50% ellipsoids; H atoms have been omitted for clarity. Selected interatomic distances (Å) and angles (deg): Ru-Si 2.3049(5), Ru-N1 2.1433(16), P2-Ru-N1 143.7(5), Si-Ru-N1 137.56(5), P2-Ru-Si 78.590(16), P3-Ru-P1 160.663(16).

4.2.4 Synthesis of a cationic 16-electron [Cy-PSiP]Ru complex.

Treatment of **3-2** with the halide abstraction reagent $LiB(C_6F_5)_4 \cdot 2.5Et_2O$ in acetonitrile solution provided a convenient route for the synthesis of the cationic complex $\{[Cy\text{-}PSiP]Ru(CH_3CN)_2\}^+[B(C_6F_5)_4]^-$ (**4-11**), which was isolated as a yellow solid in 83% yield (eq 4-4). The room temperature ^{31}P NMR spectrum of **4-11** exhibits a sharp singlet at 56.1 ppm, while the ^1H NMR spectrum (benzene-d_6) features two peaks (1.37 and -0.08 ppm) corresponding to the methyl groups of the coordinated acetonitrile ligands. Attempts to obtain a single crystal suitable for X-ray diffraction have thus far proven unsuccessful. In the absence of acetonitrile, the reaction of **3-2** with $LiB(C_6F_5)_4 \cdot 2.5Et_2O$ in fluorobenzene as solvent resulted in the formation of a new product that exhibited a broad resonance in the *in situ* ^{31}P NMR spectrum. However, the product is unstable in the absence of a coordinating solvent, and thus was not amenable to isolation.

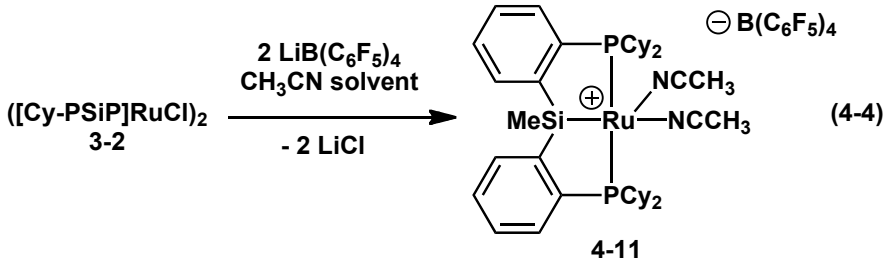

4.3 Conclusions

In summary we have shown that the [Cy-PSiP] ligand is able to support a variety of five-coordinate, 16-electron Ru^{II} complexes. Unlike the analogous complex [Ph-PSiP]RuCl(PPh_3) (**2-2**) which is readily isolable, [Cy-PSiP]RuCl(PPh_3) is in equilibrium with the dinuclear species $([Cy\text{-}PSiP]RuCl)_2$ and free PPh_3. This result highlights the

increased steric demand of [Cy-PSiP] ligation relative to [Ph-PSiP]. The less sterically demanding phosphine PMe_3 binds irreversibly to Ru, facilitating the isolation of [Cy-PSiP]RuCl(PMe_3) (**4-2**). Attempts to form an alkyl complex of the type [Cy-PSiP]RuR(PMe_3) led to the dehydrogenation and cyclometalation of a cyclohexyl phosphino group to give the 18-electron complex **4-3**. A minor product in this dehydrogenative process was the hydride [Cy-PSiP]RuH(PMe_3) (**4-4**), which is proposed to form upon reaction of the H_2 gas produced during the formation of **4-3** with the cyclometalated alkyl intermediate **4-6**. Although 16-electron alkyl complexes proved elusive, the allyl complex [Cy-PSiP]Ru(η^3-C_3H_5) (**4-8**) was synthesized upon reaction of **3-2** with $(C_3H_5)MgCl$. While the reaction of Me_3SiN_3 or NaN_3 with **4-2** did not lead to the formation of five-coordinate azide species, the insoluble complex $([Cy\text{-}PSiP]RuN_3)_2$ (**4-9**) reacted with one equiv of PMe_3 to yield the five-coordinate azide complex [Cy-PSiP]Ru(N_3)(PMe_3) (**4-10**). Finally, the synthesis of the 16-electron cationic complex $\{[Cy\text{-}PSiP]Ru(CH_3CN)_2\}^+[B(C_6F_5)_4]^-$ (**4-11**) was achieved by reacting **3-2** with $LiB(C_6F_5)_4 \cdot (OEt_2)_{2.5}$ in acetonitrile solvent. These results demonstrate the rich Ru coordination chemistry accessible with [Cy-PSiP] ligation. It is anticipated that future studies will address the reactivity of such coordinatively and electronically unsaturated 16-electron Ru complexes with E-H bonds.

4.4 Experimental Section

4.4.1 General considerations.

All experiments were conducted under argon in an MBraun glovebox or using standard Schlenk techniques. Dry, oxygen-free solvents were used unless otherwise

indicated. Benzene and pentane solvents were deoxygenated and dried by sparging with nitrogen and subsequent passage through a double-column solvent purification system (one activated alumina column and one column packed with activated Q-5) purchased from MBraun Inc. Tetrahydrofuran and diethyl ether were purified by distillation from Na/benzophenone ketyl. All purified solvents were sparged with argon prior to use and stored over 4 Å molecular sieves. Benzene-d_6 and toluene-d_8 were degassed via three freeze-pump-thaw cycles and stored over 4 Å molecular sieves. Triethylamine was distilled from CaH_2. All other reagents were purchased from Aldrich and used without further purification. Unless otherwise stated, ^{1}H, ^{13}C, ^{31}P, and ^{29}Si NMR characterization data were collected at 300 K on a Bruker AV-500 spectrometer operating at 500.1, 125.8, 202.5, and 99.4 MHz (respectively) with chemical shifts reported in parts per million downfield of $SiMe_4$ (for ^{1}H, ^{13}C, and ^{29}Si) or 85% H_3PO_4 in D_2O (for ^{31}P). ^{1}H and ^{13}C NMR chemical shift assignments are based on data obtained from ^{13}C-DEPTQ, ^{1}H-^{1}H COSY, ^{1}H-^{13}C HSQC, and ^{1}H-^{13}C HMBC NMR experiments. ^{29}Si NMR assignments are based on ^{1}H-^{29}Si HMBC experiments. In some cases, fewer than expected unique ^{13}C NMR resonances were observed, despite prolonged acquisition times. Elemental analyses were performed by Canadian Microanalytical Service Ltd. of Delta, British Columbia, Canada and Columbia Analytical Services of Tucson, Arizona. Infrared spectra were recorded using a Bruker VECTOR 22 FT-IR spectrometer at a resolution of 4 cm^{-1}. X-ray data collection, solution, and refinement were carried out by Drs. Robert MacDonald and Michael J. Ferguson at the University of Alberta X-ray Crystallography Laboratory, Edmonton, Alberta.

4.4.2 Synthetic details and characterization data.

Formation of equilibrium mixture containing [Cy-PSiP]RuCl(PPh_3) (4-1) and ([Cy-PSiP]RuCl)$_2$ (3-2). A solution of [Cy-PSiP]H (0.20 g, 0.34 mmol) in 2 mL of benzene was added to a slurry of $RuCl_2(PPh_3)_3$ (0.33 g, 0.34 mmol) in 3 mL of benzene at room temperature. Et_3N (0.05 mL, 0.34 mmol) was added to the reaction mixture via syringe. The resulting red solution was heated to 70 °C with stirring for a period of 24 h, over the course of which a white precipitate was observed. The reaction mixture was filtered through Celite, and the volatile components were removed *in vacuo* to yield a red-orange solid consisting of **4-1**, **3-2**, and PPh_3. $^{31}P\{^1H\}$ NMR (300K, benzene-d_6): δ 104.4 (br s, 1 P, [Cy-PSiP]), 94.5 (br s, 2 P, ([Cy-PSiP]RuCl)$_2$), 72.4 (br d, 1 P, [Cy-PSiP], $^2J_{PP}$ = 264 Hz), 42.6 (br d, 1 P, [Cy-PSiP], $^2J_{PP}$ = 264 Hz), 0.5 (br s, PPh_3). $^{31}P\{^1H\}$ NMR (193K, toluene-d_8): δ 105.5 (apparent t, 1 P, [Cy-PSiP], $^2J_{PPcis}$ = 20 Hz), 97.2 (s, 2 P, ([Cy-PSiP]RuCl)$_2$), 70.5 (dd, 1 P, [Cy-PSiP], $^2J_{PPcis}$ = 19 Hz, $^2J_{PPtrans}$ = 276 Hz), 46.0 (dd, [Cy-PSiP], $^2J_{PPcis}$ = 22 Hz, $^2J_{PPtrans}$ = 276 Hz), -1.6 (s, PPh_3).

[Cy-PSiP]RuCl(PMe_3) (4-2). PMe_3 (0.046 mL, 0.44 mmol) was added via syringe to a solution of ([Cy-PSiP]RuCl)$_2$ (0.32 g, 0.22 mmol) in 5 mL of benzene. An immediate color change from orange to red was observed. The volatile components were removed *in vacuo*, and the residue was triturated with pentane (2 × 1 mL) to yield **4-2** as a red solid (0.34 g, 97%). ^1H NMR (500 MHz, benzene-d_6): δ 7.9 – 7.6 (br resonance, H_{arom}), 7.40 – 7.35 (m, H_{arom}), 7.06 – 7.00 (m, H_{arom}), 3.2 – 1.2 (P*Cy*), 1.16 (d, 9 H, PMe_3, $^2J_{PH}$ = 7 Hz), 1.12 (s, 3 H, Si*Me*), 0.4 – - 0.2 (P*Cy*). ^1H NMR (263 K, 250 MHz, toluene-d_8): δ 7.78 (d, H_{arom}, J = 7 Hz), 7.64 (d, H_{arom}, J = 5 Hz), 7.4 – 6.8 (br overlapping resonances, H_{arom}), 3.2 – 2.8 (br, P*Cy*), 2.7 – 1.3 (P*Cy*), 1.26 (PMe_3), 1.12 (s, Si*Me*), 1.1 –

0.7 (P*Cy*), 0.2 – 0.0 (P*Cy*). $^{13}C\{^1H\}$ NMR (300K, 125.8 MHz, benzene-d_6): δ 160.4 (C_{arom}), 132.0 (d, CH_{arom}, J = 21 Hz), 128.9 (CH_{arom}), 128.6 (CH_{arom}), 126.5 (d, CH_{arom}, J = 4 Hz), 32.5 (br resonance, CH_{2Cy}), 32.0 (m, CH_{2Cy}), 28.7 (m, CH_{2Cy}), 28.4 – 27.9 (br overlapping resonances, CH_{2Cy}), 26.9 (CH_{2Cy}), 18.2 (d, P*Me*$_3$, J = 26 Hz), 4.0 (Si*Me*). $^{13}C\{^1H\}$ NMR (333K, 125.8 MHz, benzene-d_6): δ 160.4 (d, C_{arom}, J = 46 Hz), 138.6 (d, C_{arom}, J = 13 Hz), 134.5 (d, CH_{arom}, J = 20 Hz), 132.1 (d, CH_{arom}, J = 20 Hz), 129.8 (br, CH_{arom}), 129.2 (CH_{arom}), 129.1 (CH_{arom}), 129.0 (CH_{arom}), 126.6 (d, CH_{arom}, J = 5 Hz), 32.8 (CH_{2Cy}), 30.4 (CH_{2Cy}), 28.9 (d, CH_{2Cy}, J = 11 Hz), 28.3 (d, CH_{2Cy}, J = 9 Hz), 28.1 (d, CH_{2Cy}, J = 12 Hz), 27.1 (CH_{2Cy}), 18.4 (d, P*Me*$_3$, $^2J_{CP}$ = 26 Hz), 4.0 (Si*Me*). $^{31}P\{^1H\}$ NMR (300K, 202.5 MHz, benzene-d_6): δ 100.4 (br s, 1 P, [Cy-PSiP]), 64.7 (br d, 1 P, [Cy-PSiP], $^2J_{PP}$ = 265 Hz), -0.5 (d, 1 P, PMe_3, $^2J_{PP}$ = 249 Hz). $^{31}P\{^1H\}$ NMR (263K, 101.2 MHz, toluene-d_8): δ 105.6 (m, 1 P, [Cy-PSiP], $^2J_{PPcis}$ = 20 Hz, $^2J_{PPcis}$ = 28 Hz), 70.5 (dd, 1 P, [Cy-PSiP], $^2J_{PPcis}$ = 19 Hz, $^2J_{PPtrans}$ = 276 Hz), 5.9 (dd, 1 P, [Cy-PSiP], $^2J_{PPcis}$ = 19 Hz, $^2J_{PPtrans}$ = 276 Hz). ^{29}Si NMR (99.4 MHz, benzene-d_6): δ 59.8. Anal. Calcd for $C_{40}H_{64}P_3SiRuCl$: C, 59.87; H, 8.04. Found: C, 59.93; H, 8.22. A single crystal of **4-2** suitable for X-ray diffraction analysis was grown from benzene solution at room temperature.

[MeSi($C_6H_4PCy_2$)($C_6H_4PCy(\eta^3$-$C_6H_8)$)]RuPMe$_3$ (4-3). MeMgCl (0.045 mL, 3.0 M in THF) was added via syringe to a solution of **4-2** (0.11 g, 0.14 mmol) in 3 mL of benzene. The reaction mixture was allowed to stand at room temperature for a period of 20 h, after which time a white precipitate was observed. The solution was filtered through Celite and the volatile components were removed *in vacuo*. Diethyl ether was added to the orange residue resulting in the formation of a white precipitate. The

supernatant was removed by pipette, and the remaining residue was dried *in vacuo* to yield **4-3** (0.081 g, 78%) as a white solid. ^{1}H NMR (500 MHz, benzene-d_6): δ 8.19 (d, 1 H, H_{arom}, J = 7 Hz), 8.12 (d, 1 H, H_{arom}, J = 7 Hz), 7.96 (m, 1 H, H_{arom}), 7.35 (apparent t, 1 H, H_{arom}, J = 7 Hz), 7.27 (apparent t, 1 H, H_{arom}, J = 7 Hz), 7.18 (apparent t, 1 H, H_{arom}, J = 7 Hz), 7.06 (apparent t, 2 H, H_{arom}), 4.65 (br m, 1 H, η^3-C_6H_8), 4.21 (m, 1 H, η^3-C_6H_8), 2.94 - 2.91 (br overlapping resonances, 2 H, P*Cy*), 2.54 (s, 1 H, η^3-C_6H_8), 2.48 (br m, 1 H, P*Cy*), 2.42 – 1.10 (br overlapping resonances, P*Cy*), 1.08 (s, 3 H, Si*Me*), 0.99 (d, 9 H, P*Me*$_3$, J = 6 Hz), 0.94 (m, 2 H, P*Cy*), 0.81 (m, 1 H, P*Cy*), 0.67 (m, 2 H, P*Cy*), 0.25 (br m, 1 H, P*Cy*), - 0.14 (m, 1 H, P*Cy*). ^{13}C{^{1}H} NMR (125.8 MHz, benzene-d_6): δ 164.8 (C_{arom}), 163.9 (C_{arom}), 150.2 (C_{arom}), 145.9 (C_{arom}), 133.5 (d, CH_{arom}, J = 19 Hz), 132.1 (CH_{arom}), 131.9 (CH_{arom}), 131.8 (CH_{arom}), 125.7 (d, CH_{arom}, J = 5 Hz), 125.2 (d, CH_{arom}, J = 3 Hz), 80.7 (CH_{allyl}), 61.9 (CH_{allyl}), 45.8 (br m, CH_{Cy}), 42.4 (d, CH_{Cy}, J = 10 Hz), 40.0 (d, CH_{allyl}, J = 27 Hz), 34.7 (CH_{2Cy}), 34.0 (d, CH_{Cy}, J = 21 Hz), 32.5 (d, CH_{2Cy}, J = 6 Hz), 31.9 (d, CH_{2Cy}, J = 6 Hz), 30.6 (CH_{2Cy}), 30.4 (CH_{2Cy}), 30.3 (CH_{2Cy}), 29.3 (CH_{2Cy}), 29.1 (d, CH_{2Cy}, J = 5 Hz), 29.0 (d, CH_{2Cy}, J = 6 Hz), 28.8 (CH_{2Cy}), 28.7 (CH_{2Cy}), 28.6 (CH_{2Cy}), 28.3 (d, CH_{2Cy}, J = 6 Hz), 27.3 – 26.5 (CH_{2Cy}), 21.6 (d, P*Me*$_3$, J_{CP} = 23 Hz), 5.6 (Si*Me*). ^{31}P{^{1}H} NMR (202.5 MHz, benzene-d_6): δ 104.0 (dd, 1 P, [Cy-PSiP], $^{2}J_{PPcis}$ = 23 Hz, $^{2}J_{PPtrans}$ = 230 Hz), 83.7 (apparent t, 1 P, [Cy-PSiP], J = 26 Hz), - 3.7 (dd, 1 P, *P*Me$_3$, $^{2}J_{PPcis}$ = 31 Hz, $^{2}J_{PPtrans}$ = 230 Hz). ^{29}Si NMR (99.4 MHz, benzene-d_6): δ 51.4. A single crystal of **4-3** suitable for X-ray diffraction analysis was grown by diffusion of pentane into a solution of benzene containing the product.

[Cy-PSiP]Ru(η^3-C_3H_5) (4-8). A cold (-30 °C) solution of **3-2** (0.14 mg, 0.10 mmol) in ca. 5 mL of THF was treated with (C_3H_5)MgCl (2.0 M in THF, 0.10 mL, 0.20

mmol). The reaction mixture was allowed to warm to room temperature over the course of 20 minutes and was subsequently concentrated to dryness under vacuum. The residue was redissolved in benzene and filtered through Celite. The volatile components of the filtrate solution were removed *in vacuo* and the resulting residue was triturated with pentane (2 × 1 mL) to yield **4-8** (0.11 g, 79%) as an orange solid. ^{1}H NMR (500 MHz, benzene-d_6): δ 7.59 (d, 2 H, H_{arom}, J = 7 Hz), 7.54 (m, 2 H, H_{arom}), 7.11 – 7.06 (br overlapping resonances, 4 H, H_{arom}), 4.90 (m, 1 H, η^3-C$_3H_5$), 3.83 (br s, 2 H, η^3-C$_3H_5$), 2.63 (m, 2 H, P*Cy*), 2.14 (m, 2 H, P*Cy*), 2.05 (br m, 4 H, P*Cy*), 1.89 (m, 2 H, P*Cy*), 1.79 – 0.93 (overlapping resonances, 36 H, P*Cy* + η^3-C$_3H_5$; a resonance at 1.35 ppm was assigned to two η^3-C$_3H_5$ protons by use of a ^{1}H-^{1}H COSY experiment), 0.44 (s, 3 H, Si*Me*). ^{13}C{^{1}H} NMR (125.8 MHz, benzene-d_6): δ 160.0 (d, C_{arom}, J_{CP} = 50 Hz), 131.7 (d, CH_{arom}, J_{CP} = 21 Hz), 128.5 (CH_{arom}), 126.9 (CH_{arom}), 126.8 (CH_{arom}), 98.1 (RuCH$_2$*C*HCH$_2$), 54.4 (br, Ru*C*H$_2$CHCH$_2$), 41.9 (d, CH_{Cy}, J_{CP} = 11 Hz), 40.1 (br, CH_{Cy}), 32.5 (d, *C*HCy, J_{CP} = 19 Hz), 32.0 (d, CH_{2Cy}, J_{CP} = 13 Hz), 30.6 – 30.4 (overlapping resonances, CH_{2Cy}), 29.3 – 29.0 (overlapping resonances, CH_{2Cy}), 28.7 (d, CH_{2Cy}, J_{CP} = 7 Hz), 28.4 (d, CH_{2Cy}, J_{CP} = 9 Hz), 28.1 (d, CH_{2Cy}, J_{CP} = 10 Hz), 27.8 (d, CH_{2Cy}, J_{CP} = 12 Hz), 27.3 (CH_{2Cy}), 27.2 (CH_{2Cy}),1.4 (Si*Me*). ^{31}P{^{1}H} NMR (202.5 MHz, benzene-d_6): δ 69.9. ^{29}Si NMR (99.4 MHz, benzene-d_6): δ 59.2. Anal. Calcd for $C_{40}H_{61}P_2SiRu$: C, 65.54; H, 8.39. Found: C, 65.90; H, 8.59. A single crystal of **4-8** suitable for X-ray diffraction analysis was grown by vapor diffusion of pentane into a benzene solution of **4-8**.

([Cy-PSiP]RuN$_3$)$_2$ (4-9). A solution of **3-3** (0.063 g, 0.08 mmol) in ca. 3 mL of benzene was treated with Me_3SiN_3 (0.011 mL, 0.08 mmol). An immediate color change

from red to orange was observed along with the formation of a red precipitate. The volatile components were removed *in vacuo*, and the residue was triturated with pentane (2 × 1 mL) to yield **4-9** as an orange solid (0.05 g, 87%). Complex **4-9** is insoluble in common organic solvents and thus NMR characterization was limited. $^{31}P\{^{1}H\}$ NMR (101.2 MHz, benzene): δ 82.3 (s). IR (Film from THF, cm^{-1}): ν(Ru-N_3) 2081.0 (strong).

[Cy-PSiP]Ru(N_3)(PMe_3) (4-10). A slurry of **4-9** (0.04 g, 0.06 mmol) in ca. 3 mL of THF was treated with PMe_3 (0.006 mL, 0.06 mmol). An immediate color change from orange to red was observed and the solution became homogeneous. The volatile components were removed *in vacuo*, and the residue was triturated with pentane (2 × 1 mL) to yield **4-10** as a red solid (0.05 g, 94%). ^{1}H NMR (500 MHz, benzene-d_6): δ 7.64 (br s, 2 H, H_{arom}), 7.11 (br s, 4 H, H_{arom}), 6.96 (br m, 2 H, H_{arom}), 2.81 – 0.53 (br overlapping resonances, P*Cy* + Si*Me* + P*Me*$_3$; resonances at 1.09 and 1.02 ppm were assigned as the Si*Me* and P*Me*$_3$ protons on the basis of a ^{1}H-^{13}C HMQC experiment), 0.13 (br s, 2 H, P*Cy*). $^{13}C\{^{1}H\}$ NMR (125.8 MHz, benzene-d_6): δ 159.7 (d, C_{arom}, J = 46 Hz), 132.1 (d, CH_{arom}, J = 21 Hz), 129.1 (CH_{arom}), 127.6 (CH_{arom}), 127.2 (CH_{arom}), 126.7 (CH_{arom}), 32.9 (br s, CH_{2Cy}), 32.2 (br s, CH_{2Cy}), 30.9 (CH_{2Cy}), 28.8 (CH_{2Cy}), 28.7 (CH_{2Cy}), 28.3 (br s, CH_{Cy}), 27.0 (CH_{Cy}), 26.9 (CH_{2Cy}), 17.8 (d, P*Me*$_3$, J = 24 Hz), 3.9 (Si*Me*). $^{31}P\{^{1}H\}$ NMR (202.5 MHz, benzene-d_6): δ 97.6 (br s, 1 P, [Cy-PSiP]), 67.0 (br d, 1 P, [Cy-PSiP], J_{PP} = 260 Hz), -1.1 (d, 1 P, PMe_3, J_{PP} = 245 Hz). ^{29}Si NMR (99.4 MHz, benzene-d_6): δ 60.7. IR (Film from THF, cm^{-1}): ν(Ru-N_3) 2042 (strong). A single crystal of **4-10** suitable for X-ray diffraction analysis was grown from benzene at room temperature.

{[Cy-PSiP]Ru(CH$_3$CN)$_2$}$^+$[B(C$_6$F$_5$)$_4$]$^-$ (4-11). A solution of LiB(C$_6$F$_5$)$_4$·2.5Et$_2$O (0.31 g, 0.36 mmol) in ca. 5 mL of CH$_3$CN was added to a room temperature solution of **3-2** (0.26 g, 0.18 mmol) in ca. 5 mL of CH$_3$CN. An immediate color change from orange to yellow was observed. The solvent was removed *in vacuo* and the residue was dissolved in fluorobenzene and filtered through Celite. The filtrate was pumped down to dryness to yield **4-11** as a yellow solid (0.43 g, 83%). ^{1}H NMR (500 MHz, benzene-d_6): δ 8.04 (d, 2 H, H_{arom}, J = 7 Hz), 7.36 (m, 2 H, H_{arom}), 7.24 (m, 2 H, H_{arom}), 7.18 (m, 2 H, H_{arom}), 2.69 (br m, 2 H, PC*H*), 2.05 – 0.61 (overlapping resonances, 48 H, P*Cy* + C*H*$_3$CN + Si*Me*; resonances at 1.37 and 0.70 ppm were assigned to C*H*$_3$CN and Si*Me* protons, respectively, by use of a ^{1}H-^{13}C HSQC experiment), -0.08 (s, 3 H, C*H*$_3$CN). ^{13}C{^{1}H} NMR (125.8 MHz, benzene-d_6): δ 160.8 (apparent t, C_{arom}, J_{CP} = 22 Hz), 150.5 (B(*C*$_6$F$_5$)$_4$), 148.6 (B(*C*$_6$F$_5$)$_4$), 140.3 (br, B(*C*$_6$F$_5$)$_4$), 139.5 (apparent t, C_{arom}, J_{CP} = 20 Hz), 138.3 (B(*C*$_6$F$_5$)$_4$), 136.5 (B(*C*$_6$F$_5$)$_4$), 133.6 (apparent t, *C*H$_{arom}$, J = 9 Hz), 130.8 (*C*H$_{arom}$), 129.3 (*C*H$_{arom}$), 127.6 (*C*H$_{arom}$), 125.0 (RuN*C*CH$_3$), 124.6 (RuN*C*CH$_3$), 36.2 (t, P*C*H, J_{CP} = 10 Hz), 35.7 (t, P*C*H, J_{CP} = 9 Hz), 31.1 (*C*H$_{2Cy}$), 29.2 (*C*H$_{2Cy}$), 28.3 (br m, *C*H$_{2Cy}$), 27.9 – 27.4 (br overlapping resonances, *C*H$_{2Cy}$), 26.7 (*C*H$_{2Cy}$), 7.2 (Si*Me*), 2.6 (RuNC*C*H$_3$), 1.6 (RuNC*C*H$_3$). ^{31}P{^{1}H} NMR (202.5 MHz, benzene-d_6): δ 56.1. ^{29}Si NMR (99.4 MHz, benzene-d_6): δ 53.4. Anal. Calcd for C$_{65}$H$_{61}$F$_{20}$P$_2$N$_2$BSiRu: C, 53.76; H, 4.23; N, 1.93. Found: C, 53.71; H, 4.44; N, 2.06.

4.4.2 Crystallographic solution and refinement details for 4-2, 4-3, 4-4·(C$_5$H$_{12}$)$_{0.875}$, 4-8, and 4-10.

Crystallographic data for **4-2**, **4-3**, **4-4**·(C$_5$H$_{12}$)$_{0.875}$, and **4-8** were obtained at 173(±2) K on a Bruker D8/APEX II CCD diffractometer using graphite-monochromated

Mo Kα (λ = 0.71073 Å) radiation, employing a sample that was mounted in inert oil and transferred to a cold gas stream on the diffractometer. Crystallographic data for **4-10** were obtained at 173(±2) K on a Bruker PLATFORM/APEX II CCD diffractometer using graphite-monochromated Mo Kα (λ = 0.71073 Å) radiation, employing a sample that was mounted in inert oil and transferred to a cold gas stream on the diffractometer. Programs for diffractometer operation, data collection, and data reduction (including SAINT) were supplied by Bruker. Gaussian integration (face-indexed) was employed as the absorption correction method for **4-2**, **4-8**, and **4-10**, while SADABS (Bruker) was used for **4-3** and **4-4**·$(C_5H_{12})_{0.875}$. The structures of complexes **4-2** and **4-10** were solved by use of the Patterson search/structure expansion, while the structures of complexes **4-3**, **4-4**·$(C_5H_{12})_{0.875}$, and **4-8** were solved by direct methods. The structures were refined by use of full-matrix least-squares procedures (on F^2) with R_1 based on $F_o^2 \geq 2\sigma(F_o^2)$ and wR_2 based on $F_o^2 \geq -3\sigma(F_o^2)$. Anisotropic displacement parameters were employed throughout for all non-hydrogen atoms. During the structure solution process for **4-4**·$(C_5H_{12})_{0.875}$, attempts to refine peaks of residual electron density as disordered or partial-occupancy solvent pentane carbon atoms were unsuccessful. The data were corrected for disordered electron density through use of the SQUEEZE procedure as implemented in *PLATON*. A total solvent-accessible void volume of 1229 Å^3 with a total electron count of 300 (consistent with 7 molecules of solvent pentane, or 0.875 molecules per formula unit of the ruthenium complex) was found in the unit cell. Disorder involving the PMe_3 ligand in **4-4**·$(C_5H_{12})_{0.875}$ was also identified. The carbon atoms of the disordered PMe_3 ligand were refined anisotropically over two positions with an occupancy factor of 0.5. The Ru-*H* in **4-4**·$(C_5H_{12})_{0.875}$ was located in the difference map

and refined isotropically. Otherwise, all hydrogen atoms were added at calculated positions and refined by use of a riding model employing isotropic displacement parameters based on the isotropic displacement parameter of the attached atom. Additional crystallographic information is provided in Appendix A.

Chapter 5: Synthesis and Characterization of Palladium Complexes Supported by an NPN-Phosphido Ancillary Ligand

5.1 Introduction

Monoanionic tridentate ligands comprised of a central anionic X-type donor fragment flanked by two neutral L-type donors (i.e. κ^3-LXL, where X is typically C or N) have proven to be particularly useful in supporting platinum-group metal complexes that exhibit unique reactivity and structural features.[5,13,28,36,40,43,45,46] Given this progress, it is surprising that the exploration of such ligand architectures featuring alternative central donor atoms including silicon[39,61,62,79] and phosphorus[59,116,117] has received relatively little attention; indeed, despite the remarkable advancements that have been achieved by use of tridentate bis(phosphino)amido [PNP] ligands in platinum-group metal chemistry,[5c,13,40,43,48,115] the synthesis and characterization of related complexes supported by phosphido-based (i.e. R_2P^-) pincer ancillary ligands is limited to the work of Mazzeo *et al.*,[116a] in which complexes of the type [κ^3-PPP]PdCl are reported for use in the allylation of aldehydes. Given that the incorporation of phosphido fragments into pincer ligand frameworks is likely to promote the formation of late metal complexes that may exhibit new and unusual reactivity, it is evident that the further development of platinum-group metal complexes supported by phosphido-based multidentate ligands is warranted. To complement our investigations into late-metal complexes supported by pincer type bis(phosphino)silyl ligands,[39,79] and encouraged by the rich and diverse chemistry exhibited by platinum-group metal complexes featuring bis(phosphino)amido ligation, [5c,13,40,43,48,115] a synthetic and reactivity study of platinum-group metal complexes

featuring phosphido-based NPN ligands, including $[(2\text{-}Me_2NC_6H_4)_2P]^-$ ($[NPN]^-$), has been initiated by the Turculet group. In this context, the ability of $[(2\text{-}Me_2NC_6H_4)_2P]^-$ and the BPh_3 adduct $[(2\text{-}Me_2NC_6H_4)_2P{\cdot}BPh_3]^-$ to support monodentate, bidentate, and tridentate coordination complexes of Pd^{II}, and the application of dimeric, phosphido-bridged (κ^2-[*NP*N]PdX)$_2$ (X = Cl, OAc, OTf) species of this type as pre-catalysts for the Heck arylation of olefins are described herein.

5.2 Results and Discussion

5.2.1 Synthesis of dimeric [κ^1-N*P*N]Pd and [κ^2-*NP*N]Pd species.

Treatment of 2-Li-*N*,*N*-dimethylaniline with 0.5 equiv. of PCl_3 followed by reduction with $LiAlH_4$ afforded the desired secondary phosphine $[(2\text{-}Me_2NC_6H_4)_2P]H$ (**5-1**, [NPN]H) in 79% isolated yield. The ^{1}H NMR spectrum of **5-1** exhibits a characteristic doublet at 5.52 ppm ($^1J_{PH}$ = 221 Hz) corresponding to the P-*H* resonance, while the ^{31}P NMR spectrum of **5-1** features a doublet at -59.3 ppm ($^1J_{PH}$ = 220 Hz).

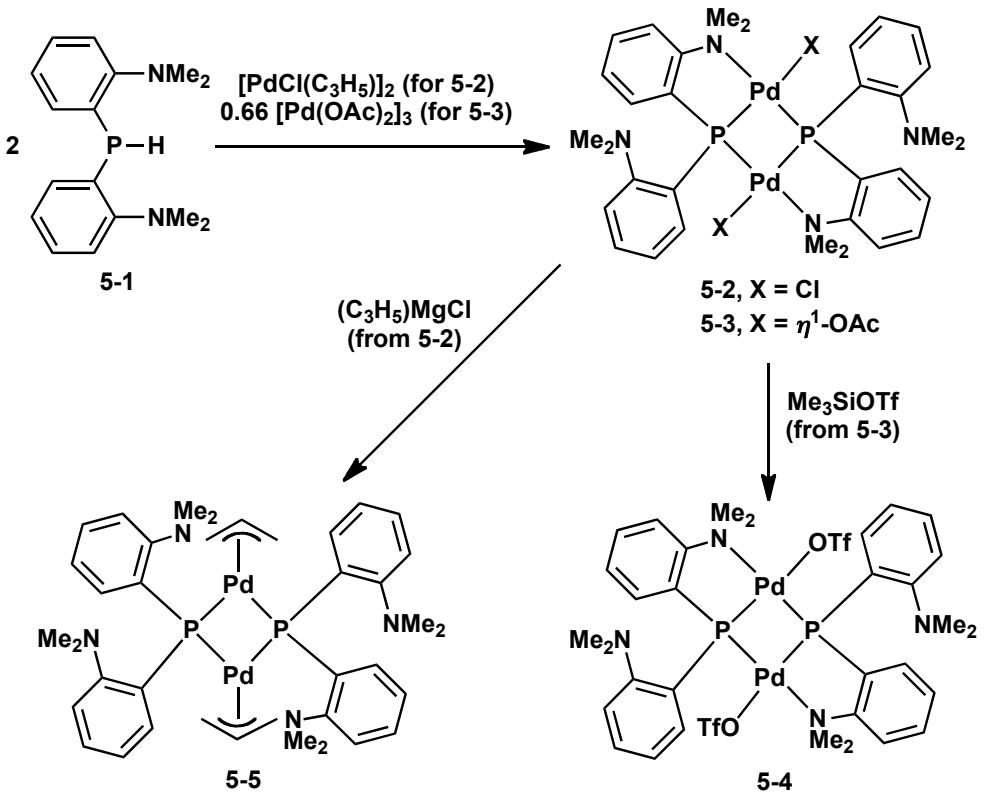

Scheme 5-1. Synthesis of the palladium complexes **5-2** – **5-5**.

The reaction of **5-1** directly with Pd^{II} starting materials led to the isolation of phosphido-bridged dimeric complexes of the type $[\kappa^2\text{-}[NPN]PdX]_2$ (**5-2**, X = Cl; **5-3**, X = η^1-OAc). Treatment of **5-1** with half an equivalent of $[PdCl(C_3H_5)]_2$ in benzene at 65 °C led to the precipitation of red crystalline **5-2**, which was isolated in 96% yield (Scheme 5-1). The X-ray crystal structure of **5-2** confirms the formation of a phosphido-bridged dimeric Pd complex in which the [NPN] ligand is coordinated to the metal center in a κ^2-*NP*N fashion (Figure 5-1). Each Pd center in **5-2** also features a terminal chloride ligand, resulting in approximate square planar coordination geometry at the metal center. The dimer features a slightly unsymmetrical puckered Pd_2P_2 core, such that the dihedral angle

between the two square planes defined by the coordination sphere of each Pd center in the dimeric structure is 83.78(4)°. The Pd···Pd distance of 3.196 Å in **5-2** is long,[118] suggesting that Pd-Pd bonding does not play a significant role in the observed structure.[119] The Pd-P distances in **5-2** (2.2166(5) – 2.2495(5) Å) are comparable to the Pd-phosphido distance of 2.2533(9) Å found in the monomeric phosphido complex [κ^3-(2-^{i}Pr$_2$*P*C$_6$H$_4$)$_2$*P*]PdCl.[116a] By comparison with the latter monomeric κ^3-PPP complex, the dinuclear bridged structure adopted by **5-2** establishes that phosphido-bridging within a dinuclear species is preferred over a monomeric κ^3-NPN motif, owing to the comparatively poor donor ability of the dimethylamino fragments within the NPN ligand.

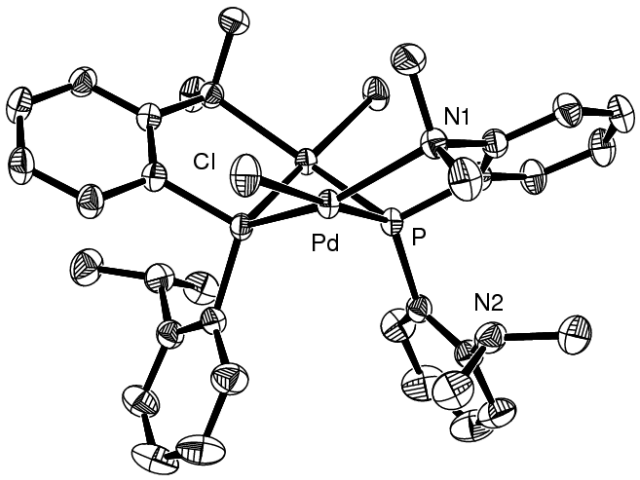

Figure 5-1. ORTEP diagram for **5-2** shown with 50% displacement ellipsoids; hydrogen atoms have been removed for clarity. The crystallographically unique atoms are labeled. Selected interatomic distances (Å) and angles (º): Pd-P 2.2213(5); Pd-P′ 2.2462(5); Pd′-P 2.2166(5); Pd′-P′ 2.2495(5); Cl-Pd-P 175.65(2); Cl-Pd-P′ 101.18(2); Cl-Pd-N 95.15(4); P-Pd-P′ 76.00(2); P-Pd-N 86.34(4); P′-Pd-N 153.53(5).

The room temperature ^{1}H NMR spectrum of **5-2** (methylene chloride-d_2) features a single resonance corresponding to the ligand dimethylamino protons at 2.76 ppm, as well as one set of aromatic proton resonances. The observed spectrum suggests two possible scenarios: (a) compound **5-2** is monomeric in solution and features C_s symmetry; or (b) compound **5-2** is dimeric in solution as in the solid state and is fluxional, giving rise to an averaged ^{1}H NMR spectrum at room temperature. Variable temperature ^{1}H NMR spectroscopy of **5-2** (Figure 5-2, methylene chloride-d_2) revealed substantial line-shape changes. In particular, three decoalescence events were observed at low temperature for the resonance corresponding to the dimethylamino protons, consistent with rapid exchange of free and bound NMe_2 groups in a dimeric complex, as well as slowed C_{aryl}-N bond rotation and inversion at both free and bound NMe_2 nitrogen donors. Upon cooling the solution to -55 °C, the resonance corresponding to the dimethylamino protons decoalesced into two broad resonances centered at 3.25 and 2.10 ppm (*ca.* 1:1 ratio), respectively, consistent with the slowed exchange of free and bound NMe_2 groups. The value of $\Delta G^{\ddagger}$ was estimated as ~10 kcal·mol^{-1} for this process.[120] At -70 °C decoalescence of the resonance centered at 3.25 ppm was observed, giving rise to two singlets at 3.35 and 3.11 ppm (*ca.* 1:1 ratio, Figure 5-2), respectively. Lastly, at -80 °C decoalescence of the resonance centered at 2.10 ppm was observed, giving rise to two broad peaks centered at 2.58 and 1.45 ppm (*ca.* 1:1 ratio, Figure 5-2), respectively. The latter processes are consistent with slowed C_{aryl}-N bond rotation and inversion at both the free and bound NMe_2 nitrogen donors. Thus, at the low-temperature limit the ^{1}H NMR spectrum of **5-2** is in agreement with the C_2-symmetric structure observed in the solid state, suggesting that **5-2** is likely dimeric and fluxional in solution, resulting in an

averaged spectrum at elevated temperatures. Further support for this structural assignment was provided by variable temperature ^{31}P NMR spectroscopy. The ^{31}P NMR spectrum of **5-2** (methylene chloride-d_2) features a single resonance at -54.0 ppm, and no line-shape changes were observed when the spectrum was acquired at low temperature; these data are consistent with an absence of monomer-dimer equilibrium for **5-2**, suggesting that the line-shape changes that are observed in the variable temperature ^{1}H NMR spectra of this compound are indeed due to fluxional processes within the dipalladium complex.

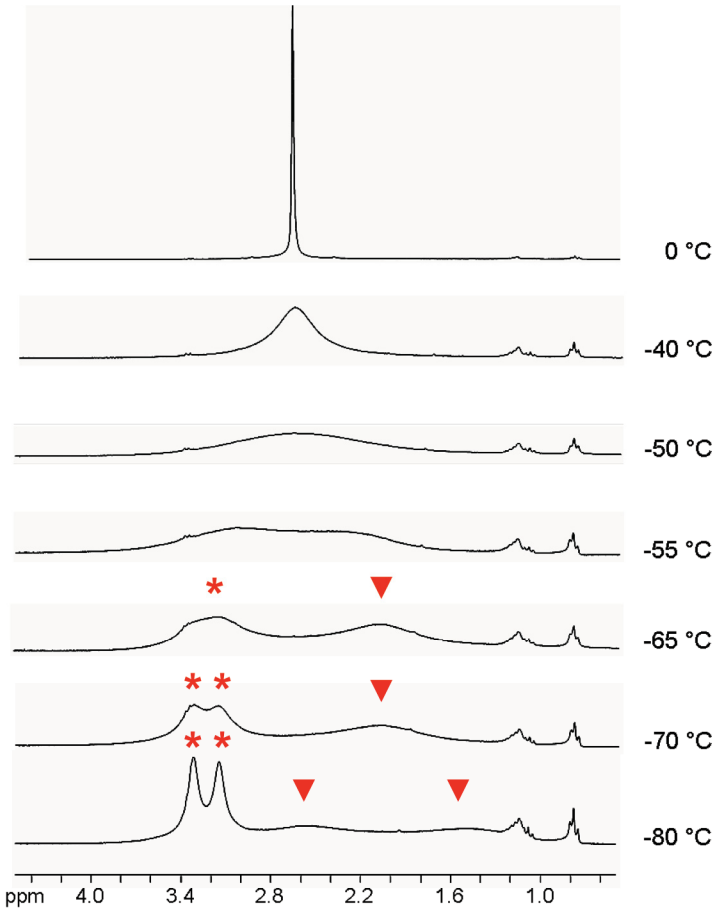

Figure 5-2. Variable temperature ^{1}H NMR spectra of **5-2** (methylene chloride-d_2) showing line-shape changes in the dimethylamino proton region of the spectrum (* and ▼correspond to unique NMe resonances observed at low temperature).

The reaction of **5-1** with a third of an equiv of $[Pd(OAc)_2]_3$ in benzene at room temperature resulted in the formation of **5-3** in 98% isolated yield (Scheme 5-1) with the apparent loss of acetic acid. The X-ray crystal structure of **5-3**·C_6H_6 (Figure 5-3) indicates the formation of a phosphido-bridged dimeric Pd complex that is analogous to **5-2** (Pd1···Pd2 3.1897(4) Å). As in the case of **5-2**, the ^{1}H NMR spectrum of **5-3** (benzene-d_6) is consistent with an averaged structure at room temperature, as indicated by the presence of only one NMe_2 resonance at 2.60 ppm, as well as only one set of aromatic proton resonances. The reaction of **5-3** with Me_3SiOTf in benzene solution resulted in precipitation of the presumptive triflate analog **5-4,** which was isolated in 78% yield.

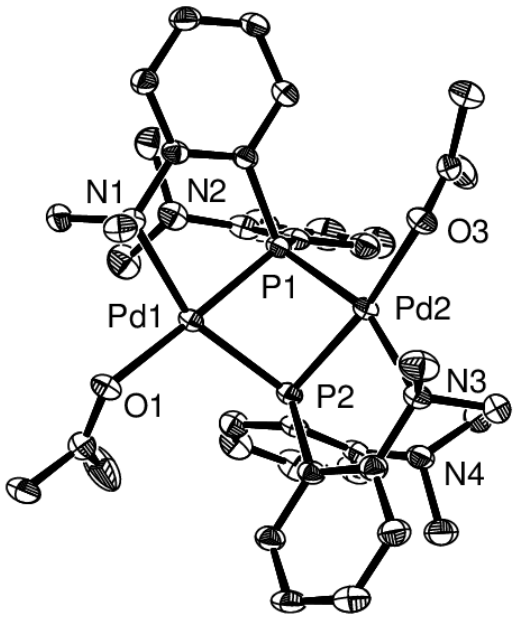

Figure 5-3. ORTEP diagram for **5-3**·C_6H_6 shown with 50% displacement ellipsoids; hydrogen atoms have been removed for clarity. Selected interatomic distances (Å) and angles (º): Pd1-P1 2.2091(8); Pd1-P2 2.2670(8); Pd2-P1 2.2488(8); Pd2-P2 2.2163(8); P1-Pd1-P2 75.26(3); Pd1-P1-Pd2 91.37(3); P1-Pd1-O1 172.77(6); P2-Pd1-N1 155.71(6); P1-Pd2-P2 75.48(3); Pd1-P2-Pd2 90.70(3); P2-Pd2-O3 167.16(7); P1-Pd2-N3 158.96(7).

Attempts to generate a Pd-H complex by the reaction of **5-2** with $LiEt_3BH$ were not successful and led to the formation of intractable reaction mixtures. However, **5-2** reacted cleanly with $(C_3H_5)MgCl$ to form a new thermally sensitive allyl-Pd complex **5-5** (Scheme 5-1). The X-ray crystal structure of **5-5** confirms the formation of a phosphido-bridged dimeric η^3-allyl Pd complex that features κ^1-N*P*N coordination (Figure 5-4). As in the case of **5-2** and **5-3**, the dimer features a puckered Pd_2P_2 core (Pd1···Pd2 3.47 Å). However, unlike the former complexes, η^3-allyl coordination in **5-5** results in a κ^1-N*P*N bonding motif in which both N-donor fragments remain uncoordinated to Pd.

The room temperature ^{1}H NMR spectrum of **5-5** (toluene-d_8) features broad resonances that are consistent with fluxional character. A single broad resonance corresponding to the ligand dimethylamino protons is observed at 2.52 ppm, and a broad resonance corresponding to the terminal allylic protons is observed at 3.09 ppm. Upon cooling the solution to -50 °C, the resonance corresponding to the dimethylamino protons decoalesced into two resonances at 2.71 and 2.30 ppm (*ca.* 1:1 ratio). Line-shape changes were also observed for the allylic protons upon cooling; however, these resonances remained quite broad down to -80 °C and exhibited substantial overlap with each other as well as with the resonances corresponding to the dimethylamino protons, and as such it is not possible to comment definitively on the nature of the dynamic properties of **5-5**. Complex **5-5** decomposed in room temperature benzene solution over the course of several hours to form a mixture of unidentified products (^{1}H, ^{31}P NMR).

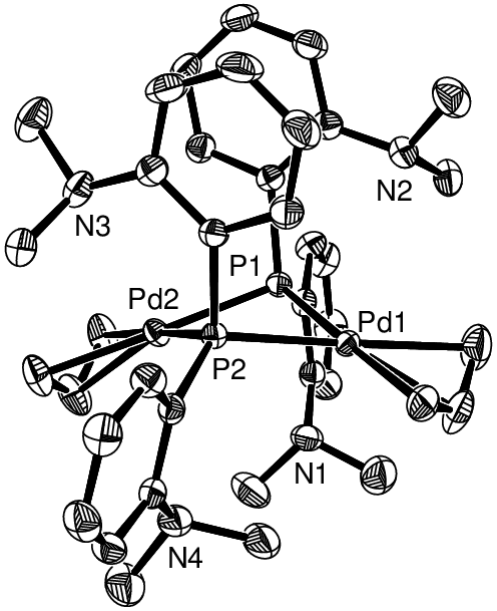

Figure 5-4. ORTEP diagram for **5-5** shown with 50% displacement ellipsoids; hydrogen atoms have been removed for clarity, and only the major component of the disordered allyl fragment is shown. Selected interatomic distances (Å) and angles (º): Pd1-P1 2.3418(5); Pd2-P1 2.3192(5); Pd1-P2 2.3440(5); Pd2-P2 2.3181(5); Pd1-C1 2.205(2); Pd1-C2 2.154(2); Pd1-C3 2.177(2); Pd1-P1-Pd2 96.197(19); P1-Pd2-P2 78.798(18); Pd1-P2-Pd2 96.165(19); P1-Pd1-P2 77.827(18); P1-Pd1-C3 176.83(6); P2-Pd1-C1 170.26(8).

5.2.2 Heck olefin arylation studies using $([NPN]PdX)_2$ as catalyst.

The utility of [PCP]Pd^{II} pincer complexes as catalysts in C-C coupling reactions is well-established[5,33] and amido-centered monomeric [PNP]Pd^{II} complexes have also recently been shown to act as effective pre-catalysts for the Heck arylation of olefins.[121,122] In a preliminary effort to assess the catalytic efficacy of dimeric κ^2-[*NP*N]Pd^{II} phosphido species such as **5-2**, **5-3**, and **5-4,** the utility of these complexes as pre-catalysts in the Heck coupling of aryl halides and ethyl acrylate was probed (eq 5-1). Catalytic runs were carried out at Pd loadings of 0.5 mol % (0.25 mol % pre-catalyst), between 110–140 °C, and for reaction times ranging from 2–20 h. As a control, no

degradation was observed (^{31}P NMR) after heating **5-2** at 140 °C for over 14 h under the catalytic reaction conditions. Selected catalytic results are listed in Table 5-1.

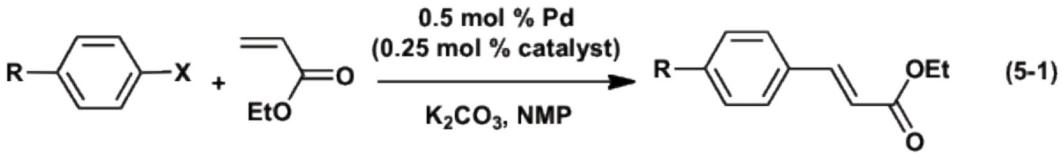

(5-1)

The coupling of ethyl acrylate and substituted iodo-, bromo-, and chloro arenes was investigated in the course of these studies. With 4-iodonitrobenzene, conversions of >98 % were achieved after 5 h at 140 °C using either **5-2**, **5-3**, or **5-4** as the pre-catalyst, and the desired Heck coupling product was the only arene-containing product formed on the basis of ^{1}H NMR spectroscopic analysis of the crude reaction mixtures. Similarly high conversions were observed when using 4-iodotoluene after either 20 h at 110 °C or 10 h at 140 °C, using **5-2** as the pre-catalyst. With 4-bromonitrobenzene, >90% conversions to the desired Heck product were observed under similar reaction conditions. By comparison, the coupling of 4-bromotoluene and ethyl acrylate required heating to 140 °C in order to attain high conversions. For the significantly less reactive 4-chloronitrobenzene, 87% conversion was obtained after 10 h at 140 °C, while the relatively deactivated substrate 4-chlorotoluene gave no conversion even after heating for 20 h at 140 °C. Attempts to couple ethyl acrylate and bromobenzene under these reaction conditions using **5-2** as the catalyst resulted in nearly exclusive formation of biphenyl (^{1}H NMR), presumably arising from homocoupling of bromobenzene. In addition, attempts to reduce the catalyst loading to 0.1 and 0.05 mol % Pd in the coupling of ethyl acrylate and 4-iodonitrobenzene resulted in the formation of nitrobenzene (^{1}H NMR; > 98 %

conversion to nitrobenzene after 20 h at 140 °C using **5-2** as the catalyst at a loading of 0.05 mol % Pd). Overall, the performance of (κ^2-[*NP*N]PdX)$_2$ complexes as pre-catalysts for the Heck arylation of olefins was comparable to that previously determined for related monomeric κ^3-[PNP]PdX complexes, as reported by Ozerov and co-workers.[121a] While compounds **5-2**, **5-3**, and **5-4** are clearly dinuclear species in the solid state (as evidenced by the crystal structures of **5-2** and **5-3**) it is not currently known whether mononuclear variants of these compounds play a role in the generation of catalytically active Pd species *in situ*.

Table 5-1. Catalytic performance of **5-2**, **5-3**, and **5-4** in the Heck arylation of olefins.

Entry	Catalyst[a]	X	R	Temp. (°C)	Time (h)	Yield (%)[b]
1	**5-2**	I	NO_2	110	10	>98
2	**5-2**	I	NO_2	140	5	>98
3	**5-2**	I	NO_2	140	2	62
4	**5-2**	I	Me	110	20	>98
5	**5-2**	I	Me	140	10	>98
6	**5-2**	Br	NO_2	110	20	>98
7	**5-2**	Br	NO_2	110	10	91
8	**5-2**	Br	Me	110	20	20
9	**5-2**	Br	Me	140	10	>98
10	**5-2**	Cl	NO_2	140	10	87
11	**5-2**	Cl	Me	140	20	0
12	**5-3**	I	NO_2	140	5	>98
13	**5-4**	I	NO_2	140	5	>98

[a] 0.5 mol % Pd (0.25 mol % catalyst); [b] Determined on the basis of ^{1}H NMR data; no conversion was observed in the absence of catalyst.

5.2.3 Synthesis of a κ^3-[NPN]Pd complex

In an effort to further explore the coordination chemistry of NPN-type ligation, the pre-coordination of a Lewis acid to the phosphido donor was investigated as a means

to encourage the formation of monomeric κ^3-[NPN]Pd complexes. In this regard, treatment of **5-1** with KCH_2Ph followed by BPh_3 led to the formation of the BPh_3 adduct **5-6** (Scheme 5-2). The ^1H NMR spectrum of **5-6** (benzene-d_6) is consistent with the formation of a phosphido species, as indicated by the disappearance of the P-*H* resonance in **5-1**, and is consistent with the formation of a 1:1 [NPN]·BPh_3 adduct. The observation of a single ^1H NMR resonance corresponding to the NMe_2 protons in **5-6** (2.25 ppm) supports a formulation where BPh_3 is coordinated to the phosphido P atom, rather than to an NMe_2 group. The $^{31}P\{^1H\}$ NMR spectrum of **5-6** features a resonance at -36.4 ppm, while the $^{11}B\{^1H\}$ NMR spectrum features a slightly broad resonance at -6.0 ppm (*cf.* free BPh_3 at 68.0 ppm).[123] On the basis of these NMR data **5-6** is tentatively formulated as an adduct of the type [N(P·BPh_3)N]K that features coordination of the phosphido group to boron. Although X-ray quality crystals of **5-6** were not accessible, the related complex [N(P·BH_3)N]H (**5-7**), which was prepared by treatment of **5-1** with BH_3·THF (Scheme 5-2), was crystallographically characterized. The solid state structure of **5-7** (Figure 5-5) confirmed the preferential coordination of the NPN ligand phosphorus to BH_3.

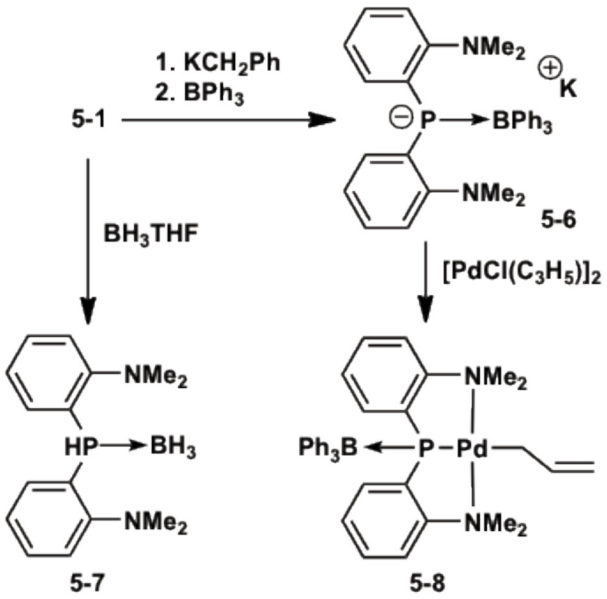

Scheme 5-2. Synthesis of compounds **5-6** – **5-8**.

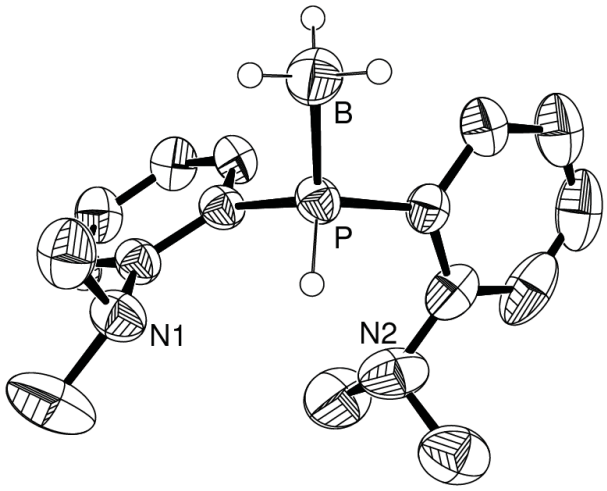

Figure 5-5. ORTEP diagram for **5-7** shown with 50% displacement ellipsoids; selected hydrogen atoms have been removed for clarity.

Treatment of **5-6** with half an equivalent of $[PdCl(C_3H_5)]_2$ led to the formation of a new Pd allyl complex **5-8** (Scheme 5-2). Complex **5-8** is formulated as [κ^3-*N*(*P*·BPh_3)*N*]Pd(η^1-C_3H_5) on the basis of solution NMR characterization. The ^{1}H NMR spectrum of **5-8** (benzene-d_6) is consistent with a 1:1 (NPN)·BPh_3 adduct. The ^{11}B{^{1}H}

NMR spectrum of **5-8** features a broadened resonance at 16.5 ppm, that is consistent with coordinated BPh_3 (*vide supra*). The η^1-coordination of the allyl ligand is supported by the observation of the allyl ^{13}C NMR resonances (benzene-d_6) at 132.6, 118.3 (d, J_{CP} = 12 Hz), and 32.8 ppm (d, J_{CP} = 17 Hz).[124] Such η^1-allyl coordination is consistent with the formation of a [κ^3-*N(P*·BPh_3)*N*]Pd species, as alternative formulations, including [κ^2-*N(P*·BPh_3)N]Pd(C_3H_5) and the dinuclear, phosphido-bridged complex {[κ^1-(N·BPh_3)*P*N]Pd(C_3H_5)}$_2$, require η^3-allyl coordination in order to achieve a 16-electron configuration. The coordination of the allyl fragment to Pd rather than B is supported by the observation of C-P coupling, which is consistent with coordination of both the NPN ligand as well as the allyl ligand to Pd. The isolation of **5-8** establishes the coordination of a Lewis acid to the phosphido donor of the [NPN] ligand as a viable strategy for encouraging the formation of mononuclear complexes of such multidentate phosphido ligands.

5.3 Conclusions

The facile synthesis of a phosphine precursor to an [NPN] diaminophosphido ligand has been accomplished, and preliminary coordination chemistry studies with Pd have been conducted. In the course of these studies [(2-$Me_2NC_6H_4)_2P$]$^-$ ligation has been shown to support monodentate and bidentate coordination complexes of Pd^{II}. Complexes of the type [κ^2-(*NP*N)PdX]$_2$ (X = Cl, OAc, OTf) serve as pre-catalysts for the Heck arylation of olefins and exhibit catalytic performance that is comparable (on a per-Pd basis) to that of related monomeric κ^3-[*PNP*]PdX species. In solution these dinuclear complexes exhibit dynamic behavior, likely resulting from exchange of free and bound

NMe_2 ligand arms. The complex (κ^2-[*NP*N]PdCl)$_2$ serves as a precursor for the η^3-allyl species (κ^1-[N*P*N]Pd(η^3-C_3H_5))$_2$, in which η^3-allyl coordination has displaced an NMe_2 donor from the Pd coordination sphere. This phenomenon is in contrast to the κ^2-*NP*N binding mode observed for the acetate complex **5-3**, which features monodentate acetate ligands, and likely reflects the more favorable interaction between the electron-rich Pd center and the η^3-allyl ligand relative to the hard acetate ligands. In an effort to discourage the formation of phosphido-bridged dinuclear complexes, pre-coordination of BPh_3 to [NPN] was pursued. Upon reaction of [N(P·BPh_3)N]K with [PdCl(C_3H_5)]$_2$, the η^1-allyl complex [κ^3-*N(P*·BPh_3)*N*]Pd(η^1-C_3H_5) (**5-8**) was isolated, which establishes the coordination of a Lewis acid to the phosphido donor of the [NPN] ligand as a viable strategy for encouraging the formation of mononuclear κ^3-*NPN* complexes. These studies establish the versatility of NPN ligation, which has proven capable of adopting κ^1-, κ^2-, and pincer-like κ^3-NPN binding motifs.

5.4 Experimental Section

5.4.1 General considerations.

All experiments were conducted under nitrogen in an MBraun glovebox or using standard Schlenk techniques. Dry, oxygen-free solvents were used unless otherwise indicated. All non-deuterated solvents were deoxygenated and dried by sparging with nitrogen and subsequent passage through a double-column solvent purification system provided by MBraun Inc. Tetrahydrofuran and diethyl ether were purified over two activated alumina columns, while benzene and pentane were purified over one activated alumina column and one column packed with activated Q-5. All purified solvents were

stored over 4 Å molecular sieves. Benzene-d_6, toluene-d_8, and methylene chloride-d_2 were degassed via three freeze-pump-thaw cycles and stored over 4 Å molecular sieves. The compounds $[(C_3H_5)PdCl]_2$ and $[Pd(OAc)_2]_3$ were purchased from Strem and used as received. 2-Li-*N*,*N*-dimethylaniline was prepared according to a previously published procedure.[125] $LiAlH_4$ was purified by extraction into Et_2O, followed by filtration to remove insoluble components. Distilled water was deoxygenated by sparging with nitrogen for ca. 40 min. All other reagents were purchased from Aldrich and used without further purification. Unless otherwise stated, ^1H, ^{13}C, ^{31}P, and ^{11}B NMR characterization data were collected at 300K on a Bruker AV-500 spectrometer operating at 500.1, 125.8, 202.5, and 160.5 MHz (respectively) with chemical shifts reported in parts per million downfield of $SiMe_4$ (for ^1H and ^{13}C), 85% H_3PO_4 in D_2O (for ^{31}P), or $BF_3 \cdot OEt_2$ (for ^{11}B). Variable-temperature NMR data were collected on a Bruker AC-250 spectrometer. ^1H and ^{13}C NMR chemical shift assignments are based on data obtained from ^{13}C-DEPT, ^1H-^1H COSY, ^1H-^{13}C HSQC, and ^1H-^{13}C HMBC NMR experiments. In some cases, fewer than expected unique ^{13}C NMR resonances were observed, despite prolonged acquisition times. Elemental analyses were performed by Desert Analytics, Inc. of Tucson, Arizona and Canadian Microanalytical Service Ltd. of Delta, British Columbia, Canada. X-ray data collection, solution, and refinement were carried out by Drs. Robert MacDonald and Michael J. Ferguson at the University of Alberta X-ray Crystallography Laboratory, Edmonton, Alberta.

5.4.2 Synthetic details and characterization data.

[NPN]H (5-1). A solution of 2-Li-*N*,*N*-dimethylaniline (4.13 g, 32.5 mmol) in ca. 50 mL of Et_2O was added dropwise via cannula to a precooled (-78 °C), stirring solution of PCl_3 (1.42 mL, 2.23 g, 16.3 mmol) in ca. 50 mL of Et_2O. The resulting reaction mixture was allowed to warm to room temperature over the course of 3 h. An off-white precipitate formed during this time. The reaction mixture was cooled once again to -78 °C and a solution of $LiAlH_4$ (0.65 g, 17.0 mmol) in ca. 30 mL of Et_2O was added via cannula. The reaction mixture was allowed to warm to room temperature and stir for an additional 4 h. The mixture was then cooled to 0 °C and the reaction was quenched by drop-wise addition of 40 mL of degassed water. The organic fraction was cannula transferred away from the aqueous layer, which was extracted with diethyl ether (2 × 100 mL). All organic fractions were combined and dried over anhydrous $MgSO_4$ under a nitrogen atmosphere. Following filtration, the volatile components were removed *in vacuo* affording **5-1** (3.50 g, 79%) as a colorless oil that solidified upon standing at -35 °C. ^{1}H NMR (500 MHz, benzene-d_6): δ 7.34 (m, 2 H, H_{arom}), 7.11 (m, 2 H, H_{arom}), 6.94 (m, 2 H, H_{arom}), 6.85 (t, 2 H, H_{arom}, J = 7 Hz), 5.52 (d, 1 H, P*H*, $^1J_{PH}$ = 221 Hz), 2.56 (s, 12 H, NMe_2). ^{13}C{^{1}H} NMR (125.8 MHz, benzene-d_6): δ 158.1 (d, C_{arom}, J_{CP} = 14 Hz), 136.4 (d, CH_{arom}, J_{CP} = 4 Hz), 133.2 (d, C_{arom}, J_{CP} = 13 Hz), 129.9 (CH_{arom}), 124.6 (CH_{arom}), 120.4 (CH_{arom}), 45.6 (NMe_2). ^{31}P{^{1}H} NMR (202.5 MHz, benzene-d_6): δ -59.3. Anal. Calcd for $C_{16}H_{21}N_2P$: C, 70.57; H, 7.77; N, 10.29. Found: C, 70.85; H, 7.72; N, 10.51.

([κ^2-*NP*N]PdCl)$_2$ (5-2). A room temperature solution of **5-1** (0.20 g, 0.74 mmol) in ca. 5 mL of benzene was added to a room temperature solution of $[(C_3H_5)PdCl]_2$ (0.13

g, 0.37 mmol) in ca. 2 mL of benzene. The resulting orange solution was transferred to a 250 mL thick-walled resealable Schlenk tube adapted with a Teflon stopcock, and the reaction mixture was heated at 65 °C for 2.5 h. The formation of a red crystalline precipitate was observed. The reaction mixture was cooled to room temperature, and in the glove box, the supernatant solution was removed by pipette. The remaining crystalline residue was washed with pentane (3 × 5 mL) and subsequently dried *in vacuo* to give **5-2** as a microcrystalline red-orange solid (0.29 g, 96%). ^{1}H NMR (500 MHz, methylene chloride-d_2): δ 8.02 (m, 2 H, H_{arom}), 7.35 – 7.29 (4 H, H_{arom}), 7.00 (t, 2 H, H_{arom}, J = 7 Hz), 2.76 (s, 12 H, NMe_2). ^{13}C{^{1}H} NMR (methylene chloride-d_2): δ 158.3 (C_{arom}), 139.7 (m, CH$_{arom}$), 132.6 (CH$_{arom}$), 132.4 (apparent t, C_{arom}, J_{CP} = 18 Hz), 126.7 (CH$_{arom}$), 122.9 (CH$_{arom}$), 49.2 (NMe_2). ^{31}P{^{1}H} NMR (methylene chloride-d_2): δ -54.0. Anal. Calcd for $C_{32}H_{40}Cl_2N_4P_2Pd_2$: C, 46.51; H, 4.88; N, 6.78. Found: C, 46.49; H, 4.75; N, 6.58. A single crystal of **5-2** suitable for X-ray diffraction analysis was grown from benzene solution at room temperature.

([κ^2-*NP*N]PdOAc)$_2$ (5-3). A room temperature solution of **5-1** (0.15 g, 0.55 mmol) in ca. 5 mL of benzene was added to a room temperature solution of $[Pd(OAc)_2]_3$ (0.12 g, 0.18 mmol) in ca. 2 mL of benzene. The resulting bright orange solution was allowed to stand at room temperature for 20 min. The volatile components were removed *in vacuo* and the remaining residue was washed with pentane (3 × 5 mL) and dried *in vacuo* to afford **5-3** as a bright yellow-orange solid (0.23 g, 98%). ^{1}H NMR (500 MHz, benzene-d_6): δ 8.38 (br s, 2 H, H_{arom}), 6.88 (t, 2 H, H_{arom}, J = 7 Hz), 6.80 (t, 2 H, H_{arom}, J = 7 Hz), 6.74 (d, 2 H, H_{arom}, J = 8 Hz), 2.60 (s, 12 H, NMe_2), 2.13 (s, 3 H, CH_3CO$_2$). ^{13}C{^{1}H} NMR (125.8 MHz, benzene-d_6): δ 175.8 (CH$_3$$CO_2$), 158.2 ($C_{arom}$), 139.7

(CH_{arom}), 132.8 (m, C_{arom}), 131.5 (CH_{arom}), 126.9 (CH_{arom}), 123.3 (CH_{arom}), 48.8 (NMe_2), 23.5 (CH_3CO_2). $^{31}P\{^1H\}$ NMR (202.5 MHz, benzene-d_6): δ -52.0. Anal. Calcd for $C_{36}H_{46}N_4O_4P_2Pd_2$: C, 49.50; H, 5.31; N, 6.41. Found: C, 50.03; H, 5.56; N, 5.66. A single crystal of **5-3**·C_6H_6 suitable for X-ray diffraction analysis was grown from benzene solution at room temperature.

([κ^2-*NP*N]PdOTf)$_2$ (5-4). Neat Me_3SiOTf (0.083 mL, 0.10 g, 0.46 mmol) was added via syringe to a room temperature solution of **5-3** (0.20 g, 0.23 mmol) in *ca.* 5 mL of benzene. A yellow precipitate formed immediately upon addition. The resulting reaction mixture was allowed to stir at room temperature for 30 min. The volatile components were then removed *in vacuo*, and the remaining residue was washed with benzene (5 mL), followed by pentane (3 × 7 mL), and dried *in vacuo* to afford **5-4** as a yellow solid (0.19 g, 78%). ^1H NMR (250 MHz, methylene chloride-d_2): δ 8.00 (m, 2 H, H_{arom}), 7.45 – 7.35 (4 H, H_{arom}), 7.01 (m, 2 H, H_{arom}), 2.75 (s, 12 H, NMe_2). $^{13}C\{^1H\}$ NMR (125.8 MHz, methylene chloride-d_2): δ 158.0 (C_{arom}), 138.9 (CH_{arom}), 133.9 (m, CH_{arom}), 129.8 (C_{arom}), 127.6 (m, CH_{arom}), 123.3 (m, CH_{arom}), 49.0 (NMe_2). $^{31}P\{^1H\}$ NMR (101.3 MHz, methylene chloride-d_2): δ -31.3. $^{19}F\{^1H\}$ NMR (235.4 MHz, methylene chloride-d_2): δ -77.2. Anal. Calcd for $C_{34}H_{40}F_6N_4O_6P_2Pd_2S_2$: C, 38.76; H, 3.83; N, 5.32. Found: C, 38.77; H, 3.73; N, 5.12.

([κ^1-N*P*N]Pd(η^3-C_3H_5))$_2$ (5-5). A precooled (-30 °C) solution of **5-2** (0.14 g, 0.17 mmol) in *ca.* 5 mL THF was treated with (C_3H_5)MgCl (2.0 M in THF, 0.17 mL, 0.34 mmol). The resulting reaction mixture was allowed to warm to room temperature over the course of 25 min. The volatile components were removed *in vacuo* and the remaining residue was extracted into benzene (ca. 10 mL). The benzene extract was

filtered through Celite and evaporated to dryness to afford a yellow solid that was recrystallized from *ca.* 10 mL of Et_2O at -30 °C to afford **5-5** (0.12 g, 87%) as a yellow microcrystalline solid. ^{1}H NMR (500 MHz, toluene-d_8): δ 7.68 (br s, 2 H, H_{arom}), 6.95 (m, 2 H, H_{arom}), 6.80 (m, 2 H, H_{arom}), 6.63 (m, 2 H, H_{arom}), 5.13 (quin, 1 H, η^3-C_3H_5, J = 10 Hz), 3.09 (br s, 4 H, η^3-C_3H_5), 2.52 (br s, 12 H, NMe_2). ^{13}C{^{1}H} NMR (125.8 MHz, toluene-d_8): δ 128.4 (CH$_{arom}$), 122.8 (CH$_{arom}$), 120.1 (CH$_{arom}$), 117.0 (t, η^3-C_3H$_5$, J = 5 Hz), 46.2 (NMe_2). ^{31}P{^{1}H} NMR (202.5 MHz, methylene chloride-d_2): δ -103.1. Repeated attempts to obtain satisfactory elemental analysis for **5-5** were not successful, likely due to the thermally sensitive nature of this compound. A single crystal of **5-5** suitable for X-ray diffraction analysis was grown from Et_2O solution at -30 °C.

[N(P·BPh$_3$)N]K (5-6). A precooled (-30 °C) solution of **5-1** (0.20 g, 0.74 mmol) in ca. 7 mL of THF was treated with a precooled (-30 °C) solution of KCH_2Ph (0.096 g, 0.74 mmol) in *ca.* 3 mL of THF. The resulting red-orange solution was allowed to warm to room temperature over the course of 20 min. The reaction mixture was cooled to -30 °C and a solution of BPh_3 (0.18 g, 0.74 mmol) in *ca.* 3 mL of THF was added, resulting in a color change to bright yellow. The reaction mixture was allowed to warm to room temperature over the course of 20 min. The volatile components of the reaction mixture were removed *in vacuo* to afford a yellow solid that was washed with pentane (5 × 5 mL) to give **5-6** (0.36 g, 88%) as a bright yellow powder. ^{1}H NMR (500 MHz, benzene-d_6): δ 7.70 (d, 6 H, BPh_{ortho}), 7.32 (m, 2 H, H_{arom}), 7.06 (t, 6 H, BPh_{meta}, J = 7 Hz), 6.91 – 6.80 (7 H, BPh_{para} + H_{arom}), 6.59 (t, 2 H, H_{arom}, J = 7 Hz), 2.25 (s, 12 H, NMe_2). ^{13}C{^{1}H} NMR (125.8 MHz, benzene-d_6): δ 158.1 (d, C_{arom}, J = 16 Hz), 141.5 (d, C_{arom}, J = 20 Hz), 139.0 (CH$_{arom}$), 136.1 (d, BPh_{ortho}, J = 9 Hz), 127.9 (BPh_{ipso}), 127.5 (BPh_{meta} + CH$_{arom}$),

123.9 (B*Ph*$_{para}$), 123.7 (*C*H$_{arom}$), 119.7 (*C*H$_{arom}$), 46.0 (N*Me*$_2$). ^{31}P{^{1}H} NMR (202.5 MHz, benzene-d_6): δ -36.4. ^{11}B{^{1}H} NMR (160.5 MHz, benzene-d_6): δ -6.0 (br s). Anal. Calcd for $C_{34}H_{35}BKN_2P$: C, 73.91; H, 6.38; N 5.07. Found: C, 73.59; H, 6.58; N, 4.77.

[N(P·BH$_3$)N]H (5-7). A solution of **5-1** (0.10 g, 0.37 mmol) in *ca.* 5 mL of THF was treated with BH_3·THF (1.0 M in THF, 0.37 mL, 0.37 mmol). The reaction mixture was allowed to stand at room temperature for 1 h. The volatile components of the reaction mixture were subsequently removed *in vacuo* to afford **5-7** (0.10 g, 98%) as a white solid. ^{1}H NMR (500 MHz, benzene-d_8): δ 7.79 (m, 2 H, *H*$_{arom}$), 7.06 (d of quart, 1 H, P*H*, $^1J_{PH}$ = 410 Hz, $^3J_{HH}$ = 7 Hz), 7.04 (t, 2 H, *H*$_{arom}$, *J* = 8 Hz), 6.84 – 6.81 (4 H, *H*$_{arom}$), 2.21 (s, 12 H, N*Me*$_2$), 2.07 (br m, 3 H, B*H*$_3$). ^{13}C{^{1}H} NMR (125.8 MHz, benzene-d_6): δ 157.6 (*C*$_{arom}$), 135.2 (d, *C*H$_{arom,}$ *J* = 13 Hz), 132,5 (*C*H$_{arom}$). 127.6 (*C*$_{arom}$), 125.5 (d, *C*H$_{arom,}$ *J* = 12 Hz), 122.2 (d, *C*H$_{arom,}$ *J* = 5 Hz), 45.7 (N*Me*$_2$). ^{31}P{^{1}H} NMR (202.5 MHz, benzene-d_6): δ -23.2 (d, $^1J_{PB}$ = 56 Hz). ^{11}B{^{1}H} NMR (160.5 MHz, benzene-d_6): δ -37.8. Anal. Calcd for $C_{16}H_{24}BN_2P$: C, 67.16; H, 8.45; N 9.79. Found: C, 67.35; H, 8.37; N, 9.70. A single crystal of **5-7** suitable for X-ray diffraction analysis was grown from Et_2O solution at -30 °C.

[κ^3-*N(P*·BPh$_3$)*N*]Pd(η^1-C$_3$H$_5$) (5-8). A solution of **5-6** (0.10 g, 0.18 mmol) in *ca.* 5 mL of benzene was treated with a solution of [Pd(C$_3$H$_5$)Cl]$_2$ (0.033 g, 0.090 mmol) in *ca.* 2 mL of benzene. The resulting dark red reaction mixture was allowed to stand at room temperature for 5 minutes. The reaction mixture was filtered through Celite and the volatile components were removed *in vacuo*. The remaining residue was extracted into Et_2O (*ca.* 10 mL) and the Et_2O extracts were filtered through Celite to afford a dark red solution that was concentrated *in vacuo* to *ca.* 5 mL and refrigerated at -30 °C to give **5-8**

(0.054 g, 45%) as a dark red microcrystalline solid. ^{1}H NMR (500 MHz, benzene-d_8): δ 7.57 (m, 6 H, B*Ph*$_{ortho}$), 7.26 – 7.19 (9 H, B*Ph*$_{meta}$ + B*Ph*$_{para}$), 6.99 (m, 2 H, *H*$_{arom}$), 6.88 (m, 2 H, *H*$_{arom}$), 6.75 (m, 4 H, *H*$_{arom}$), 5.62 (m, 1 H, η^1-C$_3$*H*$_5$), 4.55 (m, 1 H, η^1-C$_3$*H*$_5$), 4.45 (m, 1 H, η^1-C$_3$*H*$_5$), 2.58 (m, 2 H, η^1-C$_3$*H*$_5$), 1.98 (s, 12 H, N*Me*$_2$). ^{13}C{^{1}H} NMR (125.8 MHz, benzene-d_6): δ 157.5 (d, *C*$_{arom}$, *J* = 13 Hz), 142.2 (B*Ph*$_{ipso}$), 137.0 (d, *C*$_{arom}$, *J* = 38 Hz), 132.6 (η^1-*C*$_3$H$_5$), 132.0 (B*Ph*$_{ortho}$), 131.8 (*C*H$_{arom}$), 130.6 (*C*H$_{arom}$), 127.9 (B*Ph*$_{meta}$), 126.7 (d, *C*H$_{arom}$, *J* = 5 Hz), 126.1 (B*Ph*$_{para}$), 123.4 (*C*H$_{arom}$), 118.3 (d, η^1-*C*$_3$H$_5$, J_{CP} = 12 Hz), 47.5 (N*Me*$_2$), 32.8 (d, η^1-*C*$_3$H$_5$, J_{CP} = 17 Hz). ^{31}P{^{1}H} NMR (202.5 MHz, benzene-d_6): δ -0.8. ^{11}B{^{1}H} NMR (160.5 MHz, benzene-d_6): δ 16.5 (br s). Anal. Calcd for $C_{37}H_{40}BN_2PPd$: C, 67.24; H, 6.10; N 4.24. Found: C, 66.95; H, 5.74; N, 4.38.

5.4.3 Crystallographic solution and refinement details for 5-2, 5-3·C$_6$H$_6$, 5-5, and 5-7.

Crystallographic data for each of **5-2, 5-3**·C$_6$H$_6$, **5-5**, and **5-7** were obtained at 193(±2) K on either a Bruker PLATFORM/SMART 1000 CCD diffractometer or a Bruker D8/APEX II CCD diffractometer using a graphite-monochromated Mo Kα (λ = 0.71073 Å) radiation, employing a sample that was mounted in inert oil and transferred to a cold gas stream on the diffractometer. Programs for diffractometer operation, data collection, and data reduction (including SAINT) were supplied by Bruker. Gaussian integration (face-indexed) was employed as the absorption correction method for **5-3**·C$_6$H$_6$ and **5-5**, while for **5-2** and **5-7** SADABS (Bruker) was employed as the absorption correction method. For each of **5-2** and **5-3**·C$_6$H$_6$, the structure was solved by use of the Patterson search/structure expansion, whereas direct methods were employed for **5-5** and **5-7**. All structures were refined by use of full-matrix least-squares procedures

(on F^2) with R_1 based on $F_o^2 \geq 2\sigma(F_o^2)$ and wR_2 based on $F_o^2 \geq -3\sigma(F_o^2)$. Anisotropic displacement parameters were employed throughout for the non-hydrogen atoms, and all hydrogen-atoms were added at calculated positions and refined by use of a riding model employing isotropic displacement parameters based on the isotropic displacement parameter of the attached atom. During the structure solution process for **5-2**, two crystallographically independent half molecules of the target complex were located in the asymmetric unit and refined in a satisfactory manner; for simplicity, discussion of metrical parameters is limited to one of the crystallographically independent half molecules. During the structure solution process for **5-3**·C_6H_6, attempts to refine peaks of residual electron density as solvent benzene carbon atoms were unsuccessful. The data were corrected for disordered electron density through use of the SQUEEZE procedure as implemented in PLATON. A total solvent-accessible void volume of 374.8 $Å^3$ with a total electron count of 99 (consistent with two molecules of solvent benzene, or one molecule per formula unit of **5-3**) was found in the unit cell. During the structure solution process for **5-5**, one of the allyl fragments was found to exhibit a conformational disorder that was modeled in a satisfactory manner by using a 55:45 split occupancy. Distances within the two conformers of the disordered allyl group in **5-5** were constrained to be equal (within 0.01 Å) during refinement: d(C4A–C5A) = d(C4B–C5B); d(C5A–C6A) = d(C5B–C6B); d(C4A···C6A) = d(C4B···C6B). Disorder within the dimethylamino fragments in **5-7** were modeled in a satisfactory manner by using a 65:35 split occupancy; the N1–C17A, N1–C18A, N1–C17B, N1–C18B, N2–C27A, N2–C28A, N2–C27B, and N2–C28B were constrained to be equal (within 0.05 Å) during refinement. Additional crystallographic information can be found in Appendix A.

5.4.4 Representative procedure for the catalytic Heck arylation of olefins.

All catalytic runs were conducted under a nitrogen atmosphere in 100 mL resealable Schlenk tubes adapted with a Teflon stopcock. The Pd catalyst **5-2** (2.1 mg, 0.005 mmol), K_2CO_3 (0.21 g, 1.5 mmol), haloarene (1.00 mmol), and ethyl acrylate (0.14 ml, 1.3 mmol) were dissolved in 3 mL of *N*-methylpyrrolidone in a reaction tube containing a magnetic stir bar. The reaction vessel was placed in a temperature controlled oil bath set at the desired temperature. Conversions were determined on the basis of ^{1}H NMR spectroscopic data (average of at least two runs).

Chapter 6: Conclusions

6.1 Summary and Conclusions

The syntheses of Ru^{II} complexes supported by bis(phosphino)silyl ligation and Pd^{II} complexes supported by a bis(amino)phosphido ligand have been detailed. In Chapter 2 of this thesis, the coordination chemistry of [Ph-PSiP]Ru^{II} ([Ph-PSiP] = [κ^3-(2-$Ph_2PC_6H_4)_2SiMe]^-$) complexes, including the synthesis of the bis(phosphino)silane precursor [Ph-PSiP]H (**2-1**), was outlined. The metalation of [Ph-PSiP]H to Ru was achieved by reacting the tertiary silane with $RuCl_2(PPh_3)_3$ and NEt_3 to produce the five-coordinate complex *fac*-[Ph-PSiP]RuCl(PPh_3) (**2-2**). Attempts to form alkyl derivatives of **2-2** led to the metalation of a C-H bond of the PPh_3 ligand along with loss of alkane to furnish the cyclometalated complex[Ph-PSiP]Ru(κ^2-$C_6H_4PPh_2$) (**2-3)**. Exposure of **2-3** to an atmosphere of CO resulted in the formation of the six-coordinate, octahedral CO adduct *mer*-[Ph-PSiP]RuCl(PPh_3)(CO). This result highlights the conformational flexibility of [Ph-PSiP] ligation, which can accommodate both *fac*- (*cis*-P-Ru-P) and *mer*-type (*trans*-P-Ru-P) coordination. In an effort to side-step metalation of the PPh_3 ligand in **2-2**, the PEt_3 complex [Ph-PSiP]RuCl(PEt_3) (**2-5**) was readily prepared, as it was anticipated that the C(sp^3)-H bonds of the PEt_3 ligand would be more difficult to activate. Indeed, it appears that the methyl derivative [Ph-PSiP]RuMe(PEt_3) is isolable. The generation of [Ph-PSiP]Ru^{II} hydride complexes was achieved by reaction of **2-2** with $LiEt_3BH$, resulting in the formation of a mixture of Ru hydride products, including [Ph-PSiP]RuH(PPh_3)(N_2) (**2-8a**) and [Ph-PSiP]RuH(PPh_3)(H_2) (**2-8b**). Complex **2-8a** was readily isolated, however, **2-8b** readily loses coordinated H_2 and is only observable under an H_2 atmosphere. The synthesis of amido and alkoxo complexes of the type [Ph-

PSiP]RuX was attempted. Although the amido derivative [Ph-PSiP]RuN($SiMe_3$)$_2$ proved isolable, the *tert*-butoxy complex [Ph-PSiP]RuO^tBu was only observed *in situ* as it reacted rapidly with PPh_3 generated from the reaction of **2-2** with KO^tBu to form **2-3** with loss of HO^tBu.

The cyclometalated complex **2-3** was shown to activate E-H bonds of secondary silanes, amine-boranes, and H_2. Reaction with H_2 led to the formation of **2-8b**, while reactions with R_2SiH_2 (R = Ph, Mes) and $H_3B{\bullet}NRH_2$ (R = ^{t}Bu, H) resulted in the formation of **2-8a**. Complexes **2-2** and **2-8a** also serve as precatalysts for the transfer hydrogenation of ketones in basic isopropanol, which demonstrates that [R-PSiP]Ru complexes are viable in catalysis.

The cyclohexylphosphino derivative [Cy-PSiP] ([Cy-PSiP] = [κ^3-(2-$Cy_2PC_6H_4)_2SiMe]^-$) was also utilized for the synthesis of bis(phosphino)silyl Ru^{II} complexes. Cyclohexylphosphino donors were anticipated to be more electron donating relative to phenylphosphino groups, as well as more sterically encumbering. As such, [Cy-PSiP] has the potential to support more reactive, coordinatively unsaturated Ru species. Indeed, the utilization of [Cy-PSiP] ligation facilitated the synthesis and isolation of a series of rare examples of four-coordinate, formally 14-electron diamagnetic complexes of the type [Cy-PSiP]RuX (X = O^tBu, N($SiMe_3$)$_2$, NHPh, NH(2,6-$Me_2C_6H_3$)) that feature an unusual trigonal pyramidal geometry at Ru. Interestingly, the solid-state structures of the monomeric O^tBu and N($SiMe_3$)$_2$ complexes showed no evidence of agostic interactions to stabilize the Ru center (all Ru$\cdots$C > 3 Å). Examples of such four-coordinate Ru complexes that lack agostic stabilization are exceedingly rare. The Ru anilido complex [Cy-PSiP]RuNH(2,6-$Me_2C_6H_3$) (**3-6)** does

feature a short Ru···C contact of 2.749(3) Å in the solid-state, such that the presence of an agostic interaction cannot be ruled out. However, computational studies and the persistence of the O^{t}Bu and NSi(Me$_3$)$_2$ derivatives in the absence of agostic stabilization indicate that this interaction is very weak. Computational studies confirmed the key role of the strongly σ-donating silyl group of the Cy-PSiP ligand in facilitating the synthesis of such low-coordinate Ru species and enforcing the unusual trigonal pyramidal geometry. Although previous examples of four-coordinate square planar Ru complexes that lack agostic interactions were stabilized by adopting a triplet spin state, in the case of [Cy-PSiP]RuX complexes calculations indicated that the triplet spin state, which also adopts a trigonal pyramidal geometry, is higher in energy by more than 24 kcal mol^{-1}. Thus, the stability of the diamagnetic [Cy-PSiP]RuX complexes outlined in this document cannot be attributed to a triplet spin state, but rather appears to be a consequence of the highly electron releasing Cy-PSiP ligand set. Computational studies of analogues of [Cy-PSiP]RuX that have the silyl group replaced with C(sp^3)-Me, phosphido, and amido groups revealed the following order of descending donating ability of the central donor atom: PSiP > PPP > PCP > PNP.

Although silyl ligation serves to afford stability to [Cy-PSiP]RuX complexes, these low-coordinate species are still reactive, as demonstrated by their ability to undergo insertion reactions, as well as E-H bond activation chemistry. Thus, complex **3-6** was shown to undergo insertion of xylyl isocyanide into the Ru-N bond to give the insertion product [Cy-PSiP]RuC(NHAr)=NAr (Ar = 2,6-Me$_2$C$_6$H$_3$). The O^{t}Bu and N(SiMe$_3$)$_2$ Ru derivatives (**3-3** and **3-4**, respectively) were shown to react with H$_2$O to yield a dinuclear Ru hydroxide complex (**3-9**) that features bridging hydroxide ligands in the solid state. A

comparison of the diffusion coefficients for **3-3** and **3-9** (measured using ^{1}H NMR diffusion spectroscopy (DOSY)) also supports a dinuclear structure for **3-9** in solution, which highlights the importance of steric bulk for the formation of mononuclear [Cy-PSiP]RuX complexes. The reaction of **3-3** and **3-4** with PhOH resulted in the formation of the 18-electron η^5-oxocyclohexadienyl complex **3-10**, while reactions of **3-3** and **3-4** with a selection of amine-boranes led to the formation of unusual bis(σ-B-H)complexes of the type [Cy-PSiP]Ru(H)(η^2:η^2-H_2BNRR') (R = R' = H, **3-11**; R = R' = Me, **3-12**; R = H, R' = ^{t}Bu, **3-13**). These complexes result from the net dehydrogenation of the corresponding amine-borane. The mechanism of dehydrogenation of amine-boranes by complexes **3-3** and **3-4** was investigated computationally and it was determined to most likely proceed in a stepwise fashion via intramolecular deprotonation of ammonia and subsequent borane B–H bond oxidative addition. These studies confirm that such four-coordinate, formally 14-electron [Cy-PSiP]RuX complexes are capable of promoting multiple bond activation steps in a manner that may be synthetically useful in the transformation of main group substrates.

In addition to the four-coordinate complexes described above, a series of five-coordinate, 16-electron [Cy-PSiP]Ru^{II} complexes was also investigated. While [Ph-PSiP]RuCl(PPh_3) is readily isolable, the analogous [Cy-PSiP]Ru complex is in equilibrium with the dinuclear species ([Cy-PSiP]RuCl)$_2$ and free PPh_3. This result highlights the increased steric demand of [Cy-PSiP] ligation relative to [Ph-PSiP]. The less sterically demanding phosphine PMe_3 binds irreversibly to Ru, facilitating the isolation of [Cy-PSiP]RuCl(PMe_3) (**4-2**). Attempts to form an alkyl complex of the type [Cy-PSiP]RuR(PMe_3) led to the dehydrogenation and cyclometalation of a cyclohexyl

phosphino group to give the 18-electron complex [MeSi($C_6H_4PCy_2$)($C_6H_4PCy(\eta^3$-C_6H_8))]$RuPMe_3$. By comparison, the 16-electron allyl complex [Cy-PSiP]Ru(η^3-C_3H_5) was readily isolated. Although the reaction of **4-5** with Me_3SiN_3 and NaN_3 did not lead did not lead to the formation of five-coordinate azide species, the insoluble complex ([Cy-PSiP]RuN_3)$_2$ (**4-9**) reacted with one equiv of PMe_3 to yield the five-coordinate azide complex [Cy-PSiP]Ru(N_3)(PMe_3) (**4-10**). Finally, the synthesis of the 16-electron cationic complex {[Cy-PSiP]Ru(CH_3CN)$_2$}$^+$[$B(C_6F_5)_4$]$^-$ was achieved by reacting ([Cy-PSiP]RuCl)$_2$ with $(Et_2O)_{2.5}LiB(C_6F_5)_4$ in acetonitrile solvent. These results demonstrate the rich Ru coordination chemistry accessible with [Cy-PSiP] ligation. It is anticipated that future studies will address the reactivity of such coordinatively and electronically unsaturated 16-electron Ru complexes with E-H bonds.

To complement investigations into late-metal complexes supported by bis(phosphino)silyl ligands, a synthetic and reactivity study of Pd^{II} complexes featuring the phosphido-based ligand [(2-$Me_2NC_6H_4$)$_2$P]$^-$ ([NPN]) was conducted. Examples of κ^1-, κ^2-, and κ^3-NPN coordination to Pd were described. Complexes of the type [κ^2-(*NP*N)PdX]$_2$ (X = Cl, OAc, OTf) exhibit dynamic behavior in solution, likely resulting from exchange of free and bound NMe_2 ligand arms. These dinuclear complexes serve as pre-catalysts for the Heck arylation of olefins and exhibit catalytic performance that is comparable (on a per-Pd basis) to that of related monomeric κ^3-[*PNP*]PdX species. The complex (κ^2-[*NP*N]PdCl)$_2$ serves as a precursor for the η^3-allyl species (κ^1-[N*P*N]Pd(η^3-C_3H_5))$_2$, in which η^3-allyl coordination has displaced an NMe_2 donor from the Pd coordination sphere. This phenomenon is in contrast to the κ^2-*NP*N binding mode observed for the acetate complex [κ^2-(*NP*N)PdOAc]$_2$, which features monodentate

acetate ligands, and likely reflects the more favorable interaction between the electron-rich Pd center and the η^3-allyl ligand relative to the hard acetate ligands. In an effort to discourage the formation of phosphido-bridged dinuclear complexes, pre-coordination of BPh_3 to [NPN] was pursued. Upon reaction of [N(P·BPh_3)N]K with $[PdCl(C_3H_5)]_2$, the η^1-allyl complex [κ^3-*N(P*·BPh_3)*N*]Pd(η^1-C_3H_5) (**5-8**) was isolated, which establishes the coordination of a Lewis acid to the phosphido donor of the [NPN] ligand as a viable strategy for encouraging the formation of mononuclear κ^3-*NPN* complexes. These studies establish the versatility of NPN ligation, which has proven capable of adopting κ^1-, κ^2-, and pincer-like κ^3-NPN binding motifs.

6.2 Future Work

Although efforts to isolate a [Ph-PSiP]RuR(PR_3) (R = Ph, Et) alkyl complex proved challenging, future synthetic targets should include allyl and benzyl derivatives. Allyl and benzyl ligands can adopt η^3-coordination modes and thus satisfy the electronic requirements of a metal complex without necessarily forfeiting reactivity. As such, the synthesis of allyl or benzyl complexes may be a more viable route toward the formation of stable alkyl complexes of [Ph-PSiP]Ru that are sufficiently reactive.

Chapter 3 has established the viability of a series of rare four-coordinate species of the type [Cy-PSiP]RuX in which X is an amido, anilido, or alkoxo ligand. It is highly likely that the electron density provided by π-donation of a lone pair on the heteroatomic ligand plays a large part in stabilizing such species. Expanding the scope of heteroatomic ligands to include phosphide and thiolate donors may be challenging due to the diminished π-donation from P and S, however, the synthesis of [Cy-PSiP]RuX complexes

in which X = PR_2 or SR (R = bulky aryl or alkyl group) is worthy of pursuit. Such complexes are poised to exhibit different reactivity relative to the amido and alkoxide analogues described herein due to diminished π-donation from the X ligand. The synthesis of silyl analogues can also be pursued by pursuing either Si-H oxidative addition to $([Cy\text{-}PSiP]RuCl)_2$, or by utilizing a silyl anion reagent such as $(THF)_2LiSiHMes_2$.[126]

It was shown that four-coordinate [Cy-PSiP]RuX species react with E-H bonds, however studies on the insertion chemistry of these complexes were limited to one example involving xylyl isocyanide. Further studies are warranted to study the insertion chemistry of additional substrates such as CO, CO_2, nitriles, isocyanates, carbodiimides, and aldehydes. The catalytic functionalization of such molecules may be possible, as a cycle can be envisioned whereby insertion of an unsaturated substrate into the Ru-X bond would give a new four-coordinate complex, while subsequent protonation by HX would release the organic fragment and regenerate [Cy-PSiP]RuX, completing the catalytic cycle (Scheme 6-1).

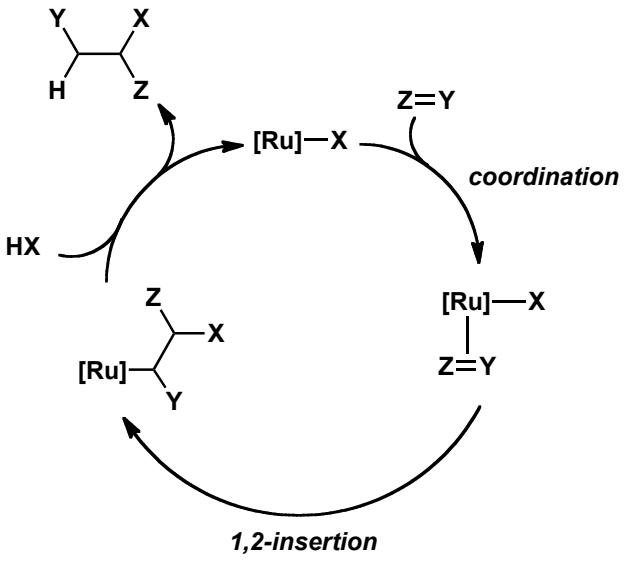

Scheme 6-1. Proposed catalytic cycle for the functionalization of unsaturated substrates by [Cy-PSiP]RuX.

Reactions of [Cy-PSiP]RuX with amine-boranes have shown that the [Cy-PSiP]Ru fragment is capable of stabilizing bis(σ-BH) complexes upon net dehydrogenation of the amine-borane. Interestingly, preliminary reactions of [Cy-PSiP]RuX with trialkylamine-boranes of the type $H_3B{\bullet}NR_3$ (R = alkyl) indicate loss of NR_3 and transfer of X to B to give [Cy-PSiP]Ru(H)(η^2:η^2-H_2BX) (Scheme 6-2). Since there are only a few examples of bis(σ-BH) complexes known, a greater understanding of this bonding motif is of interest. A priority moving forward will be to probe the scope of this reaction in order to gain a better understanding of the factors leading to isolable bis(σ-BH) complexes and to examine any potential reactivity these species may exhibit.

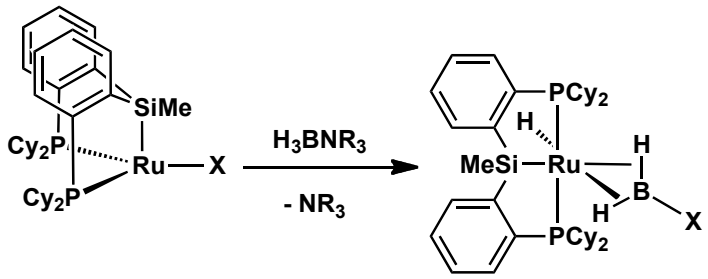

Scheme 6-2. Reaction of [Cy-PSiP]RuX with trialkylamine-boranes to generate substituted bis(σ-B-H) complexes [Cy-PSiP]Ru(H)(η^2:η^2-H_2BX).

Future directions for research involving [R-PSiP]Ru^{II} 16-electron complexes should focus on further exploring the coordination chemistry of this system. In particular, the pursuit of complexes supported by [^{i}Pr-PSiP] ligation is of interest, as such complexes would be significantly less susceptible to metalation and dehydrogenation. Such an isopropylphosphino derivative may facilitate the synthesis of isolable alkyl complexes of the type [^{i}Pr-PSiP]Ru(R)(PMe_3) (R = alkyl). The E-H bond activation chemistry of [R-PSiP]RuCl(PMe_3) also needs to be investigated. Furthermore, the synthesis and reactivity of cationic Ru^{II} complexes should be pursued, as such species are known to be highly reactive. A preliminary reaction targeting the synthesis of {[Cy-PSiP]Ru(PMe_3)}$^+$[X]$^-$ complexes led to the observation of one very broad signal in the ^{31}P NMR spectrum. Indications are that this complex is not isolable, however, it is possible that this cationic fragment will survive *in situ*, which would allow for subsequent reactivity studies.

Building on initial investigations of [NPN] ligation, initiatives for future investigation include studying the coordination chemistry of related [N(P=X)N] (X = O, S, Se) ligands, where the central anionic donor has been oxidized. This represents another strategy that may inhibit bridging of the central phosphido donor. Additionally,

the incorporation of amino donors that bind more strongly to electron-rich late metal centers may facilitate the synthesis of mononuclear complexes. One such possibility would be a quinolyl-based ligand, as shown in Figure 6-1.

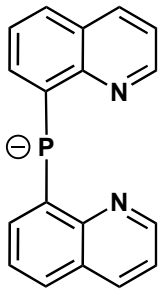

Figure 6-1. A quinolyl-based [NPN]-phosphido pincer ligand.

Appendix A: Crystallographic Experimental Details

Table A1. Crystallographic Experimental Details for [Ph-PSiP]RuCl(PPh$_3$)·(OEt$_2$)$_{1.5}$ (**2-2**·(OEt$_2$)$_{1.5}$).

A. Crystal Data	
formula	$C_{61}H_{61}ClO_{1.5}P_3RuSi$
formula weight	1075.62
crystal dimensions (mm)	0.56 ×· 0.24 × 0.10
crystal system	triclinic
space group	$P\bar{1}$ (No. 2)
unit cell parameters	
a (Å)	11.2541 (9)
b (Å)	13.4722 (11)
c (Å)	17.6235 (14)
α (deg)	85.0100 (11)
β (deg)	85.5172 (11)
γ (deg)	85.8870 (11)
V (Å^3)	2648.1 (4)
Z	2
ρcalcd (g cm^{-3})	1.349
μ (mm^{-1})	0.502
B. Data Collection and Refinement Conditions	
diffractometer	Bruker PLATFORM/SMART 1000 CCD[b]
radiation (λ [Å])	graphite-monochromated Mo Kα (0.71073)
temperature (°C)	–80
scan type	ω scans (0.3°) (20 s exposures)
data collection 2θ limit (deg)	54.94
total data collected	23268 (-14 ≤ h ≤ 14, -17 ≤ k ≤ 17, -22 ≤ l ≤ 22)
independent reflections	11995 (R_{int} = 0.0212)
number of observed reflections (*NO*)	10044 [$F_o^2 \geq 2\sigma(F_o^2)$]
structure solution method	Patterson search/structure expansion (*DIRDIF–99*)
refinement method	full-matrix least-squares on F^2 (*SHELXL–97*)
absorption correction method	Gaussian integration (face-indexed)
range of transmission factors	0.9515–0.7663
data/restraints/parameters	11995 [$F_o^2 \geq -3\sigma(F_o^2)$] / 0 / 641
goodness-of-fit (S)	1.050 [$F_o^2 \geq -3\sigma(F_o^2)$]
final R indices	
R_1 [$F_o^2 \geq 2\sigma(F_o^2)$]	0.0369
wR_2 [$F_o^2 \geq -3\sigma(F_o^2)$]	0.0975
largest difference peak and hole	1.099 and –0.473 e Å^{-3}

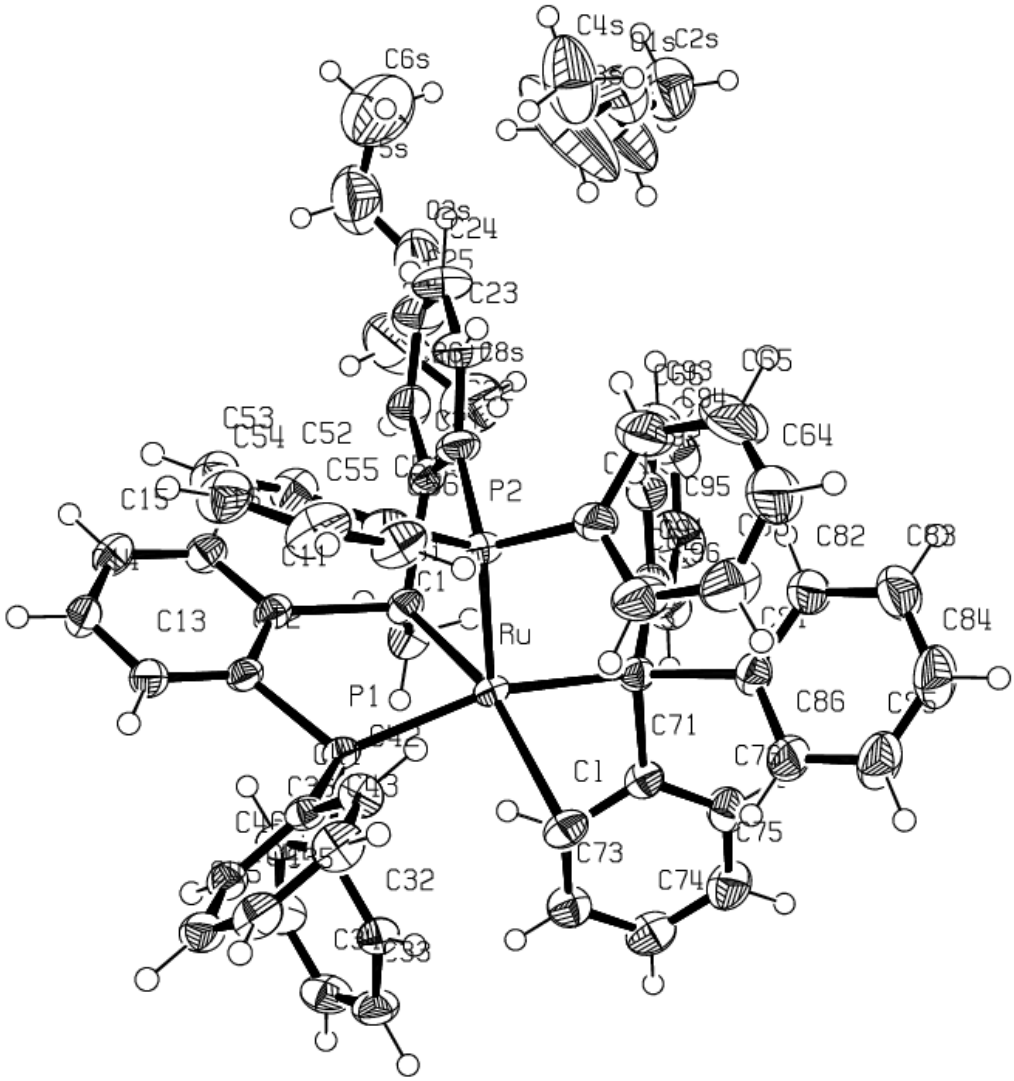

Figure A1. ORTEP diagram of [Ph-PSiP]RuCl(PPh_3)·$(OEt_2)_{1.5}$ (**2-2**·$(OEt_2)_{1.5}$).

Table A2. Crystallographic Experimental Details for [Ph-PSiP]Ru(κ^2-C_6H_4PPh$_2$)·OEt$_2$ (**2-3**·OEt$_2$).

A. Crystal Data	
formula	$C_{59}H_{55}OP_3RuSi$
formula weight	1002.10
crystal dimensions (mm)	0.70 × 0.31 × 0.12
crystal system	triclinic
space group	$P\bar{1}$ (No. 2)
unit cell parameters	
a (Å)	11.727 (2)
b (Å)	13.231 (3)
c (Å)	15.949 (3)
α (deg)	86.801 (3)
β (deg)	89.923 (3)
γ (deg)	86.074 (3)
V (Å^3)	2465.1 (9)
Z	2
ρ_{calcd} (g cm^{-3})	1.350
μ (mm^{-1})	0.481
B. Data Collection and Refinement Conditions	
diffractometer	Bruker PLATFORM/SMART 1000 CCD
radiation (λ [Å])	graphite-monochromated Mo Kα (0.71073)
temperature (°C)	–80
scan type	ω scans (0.3°) (20 s exposures)
data collection 2θ limit (deg)	55.08
total data collected	21690 ($-15 \le h \le 15$, $-17 \le k \le 17$, $-20 \le l \le 20$)
independent reflections	11175 (R_{int} = 0.0365)
number of observed reflections (*NO*)	8618 [$F_o^2 \ge 2\sigma(F_o^2)$]
structure solution method	direct methods (*SHELXS–97*)
refinement method	full-matrix least-squares on F^2 (*SHELXL–97*)
absorption correction method	Gaussian integration (face-indexed)
range of transmission factors	0.9446–0.7296
data/restraints/parameters	11175 [$F_o^2 \le -3\sigma(F_o^2)$] / 0 / 586
goodness-of-fit (S)	1.070 [$F_o^2 \le -3\sigma(F_o^2)$]
final R indices	
R_1 [$F_o^2 \le 2\sigma(F_o^2)$]	0.0637
wR_2 [$F_o^2 \le -3\sigma(F_o^2)$]	0.1791
largest difference peak and hole	2.563 and –3.265 e Å^{-3}

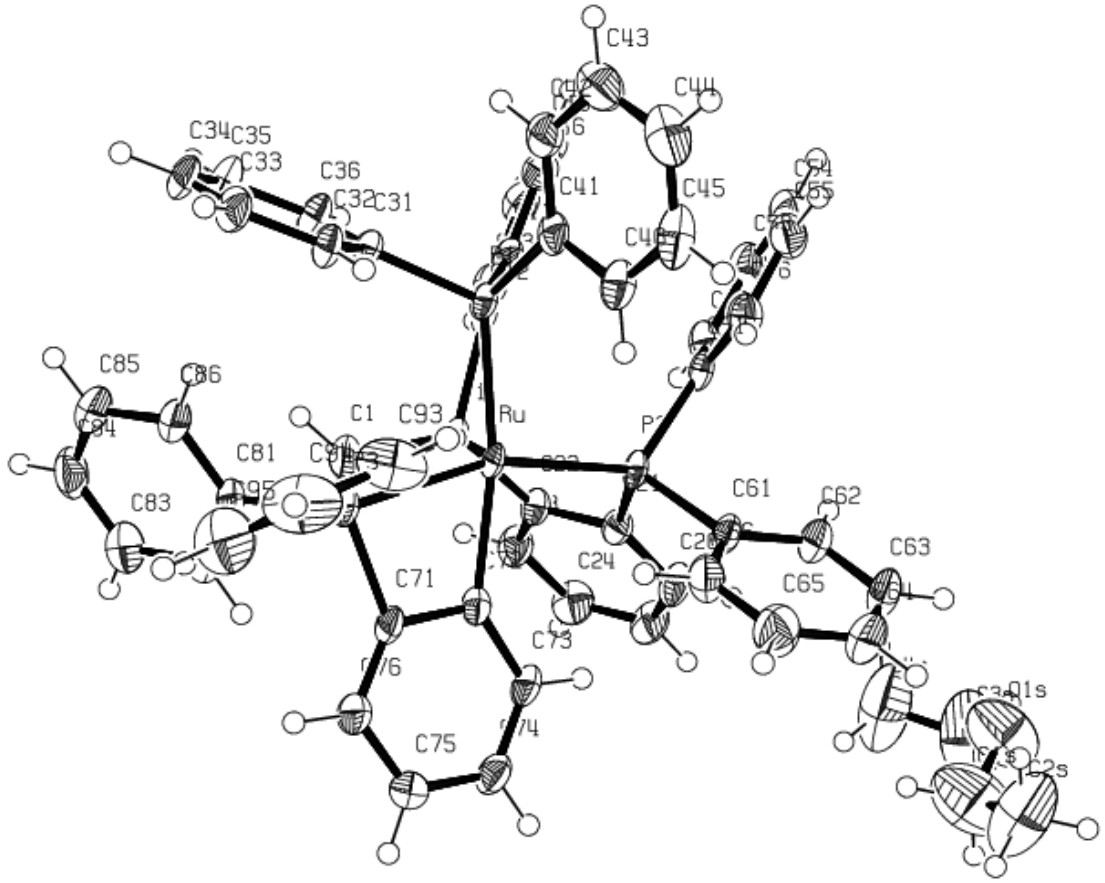

Figure A2. ORTEP diagram of [Ph-PSiP]RuCl(κ^2-C_6H_4PPh$_2$)·OEt$_2$ (**2-3**·OEt$_2$).

Table A3. Crystallographic Experimental Details for [Ph-PSiP]Ru(CO)(κ^2-$C_6H_4PPh_2$) (**2-5**).

A. Crystal Data	
formula	$C_{56}H_{45}OP_3RuSi$
formula weight	955.99
crystal dimensions (mm)	0.45 × 0.39 × 0.11
crystal system	monoclinic
space group	$P2_1/n$ (an alternate setting of $P2_1/c$ [No. 14])
unit cell parameters	
a (Å)	13.7133 (15)
b (Å)	15.9762 (18)
c (Å)	21.015 (2)
α (deg)	90.8000 (16)
V (Å^3)	4603.7 (9)
Z	4
ρ_{calcd} (g cm^{-3})	1.379
μ (mm^{-1})	0.511
B. Data Collection and Refinement Conditions	
diffractometer	Bruker PLATFORM/SMART 1000 CCD
radiation (λ [Å])	graphite-monochromated Mo Kα (0.71073)
temperature (°C)	–80
scan type	ω scans (0.3°) (15 s exposures)
data collection 2θ limit (deg)	55.04
total data collected	39691 ($-17 \le h \le 17$, $-20 \le k \le 20$, $-27 \le l \le 27$)
independent reflections	10576 (R_{int} = 0.0363)
number of observed reflections (*NO*)	8729 [$F_o^2 \ge 2\sigma(F_o^2)$]
structure solution method	Patterson search/structure expansion (*DIRDIF–99*)
refinement method	full-matrix least-squares on F^2 (*SHELXL–97*)
absorption correction method	multi-scan (*SADABS*)
range of transmission factors	0.9459–0.8026
data/restraints/parameters	10576 [$F_o^2 \ge -3\sigma(F_o^2)$] / 0 / 559
goodness-of-fit (S)	1.058 [$F_o^2 \ge -3\sigma(F_o^2)$]
final R indices	
R_1 [$F_o^2 \ge 2\sigma(F_o^2)$]	0.0302
wR_2 [$F_o^2 \ge -3\sigma(F_o^2)$]	0.0767
largest difference peak and hole	0.649 and –0.231 e Å^{-3}

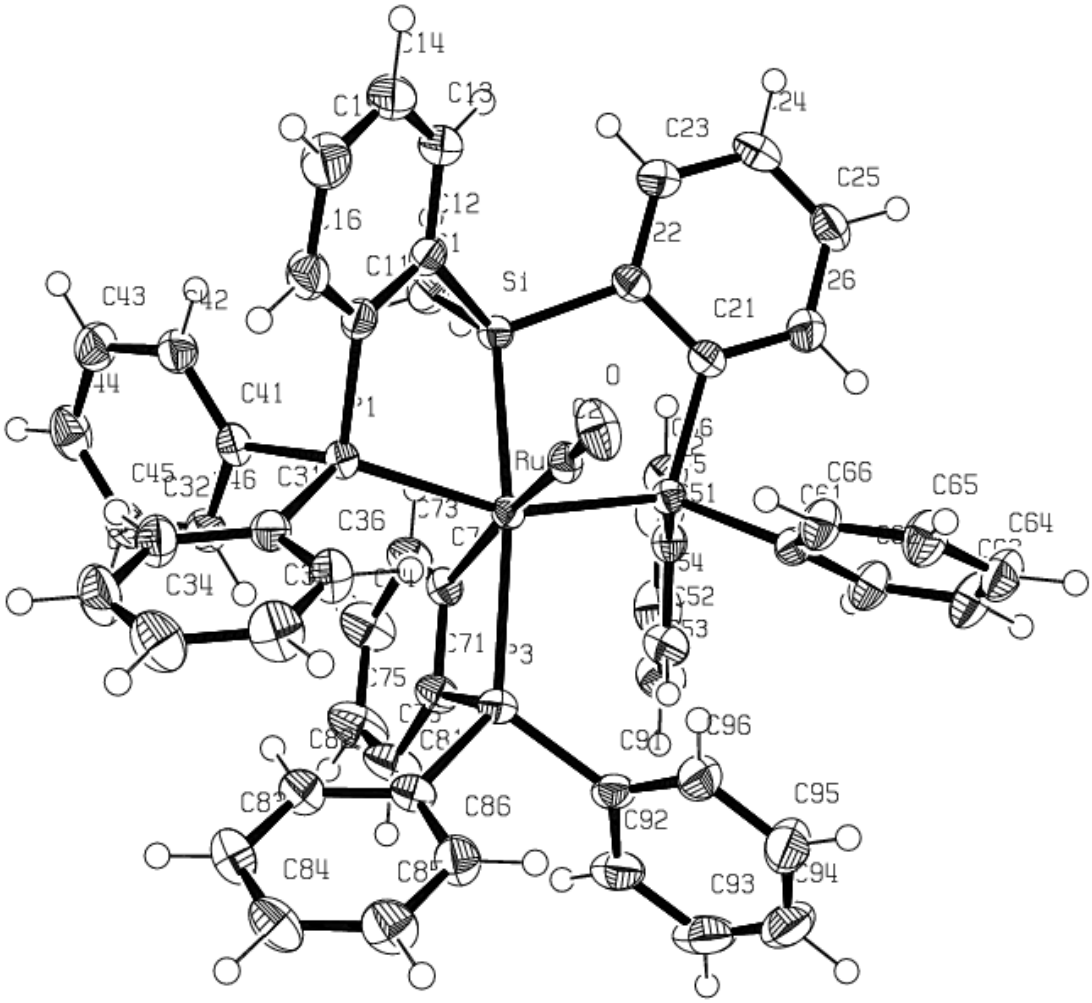

Figure A3. ORTEP diagram of [Ph-PSiP]RuCl(CO)(κ^2-$C_6H_4PPh_2$) (**2-5**).

Table A4. Crystallographic Experimental Details for [Ph-PSiP]RuCl(PEt$_3$)·(CH$_2$Cl$_2$)$_{1.17}$·OEt$_2$ (**2-6**·(CH$_2$Cl$_2$)$_{1.17}$·OEt$_2$).

A. Crystal Data	
formula	$C_{48.17}H_{58.33}Cl_{3.33}OP_3RuSi$
formula weight	993.52
crystal dimensions (mm)	0.43 × 0.28 × 0.22
crystal system	trigonal
space group	$R\bar{3}$ (No. 148)
unit cell parameters	
a (Å)	33.202 (3)
c (Å)	22.654 (2)
V (Å^3)	21627 (3)
Z	18
ρ_{calcd} (g cm^{-3})	1.373
μ (mm^{-1})	0.671
B. Data Collection and Refinement Conditions	
diffractometer	Bruker D8/APEX II CCD
radiation (λ [Å])	graphite-monochromated Mo Kα (0.71073)
temperature (°C)	–100
scan type	ω scans (0.3°) (20 s exposures)
data collection 2θ limit (deg)	52.92
total data collected	58143 (-41 ≤ h ≤ 41, -41 ≤ k ≤ 41, -28 ≤ l ≤ 28)
independent reflections	9936 (R_{int} = 0.0839)
number of observed reflections (*NO*)	6876 [$F_o^2 \geq 2\sigma(F_o^2)$]
structure solution method	direct methods (*SHELXS–97*)
refinement method	full-matrix least-squares on F^2 (*SHELXL–97*)
absorption correction method	Gaussian integration (face-indexed)
range of transmission factors	0.8675–0.7626
data/restraints/parameters	9047 / 2[a] / 512
goodness-of-fit (*S*) [all data]	1.063
final *R* indices	
R_1 [$F_o^2 \geq 2\sigma(F_o^2)$]	0.0510
wR_2 [all data]	0.1465
largest difference peak and hole	0.767 and –0.770 e Å^{-3}

[a] One ethyl group of the triethylphosphine ligand was found to be disordered and required the following distances to be restrained to be equal (within 0.03 Å) during refinement: d(P3–C6A) = d(P3–C6B); d(C6A–C7A) = d(C6B–C7B).

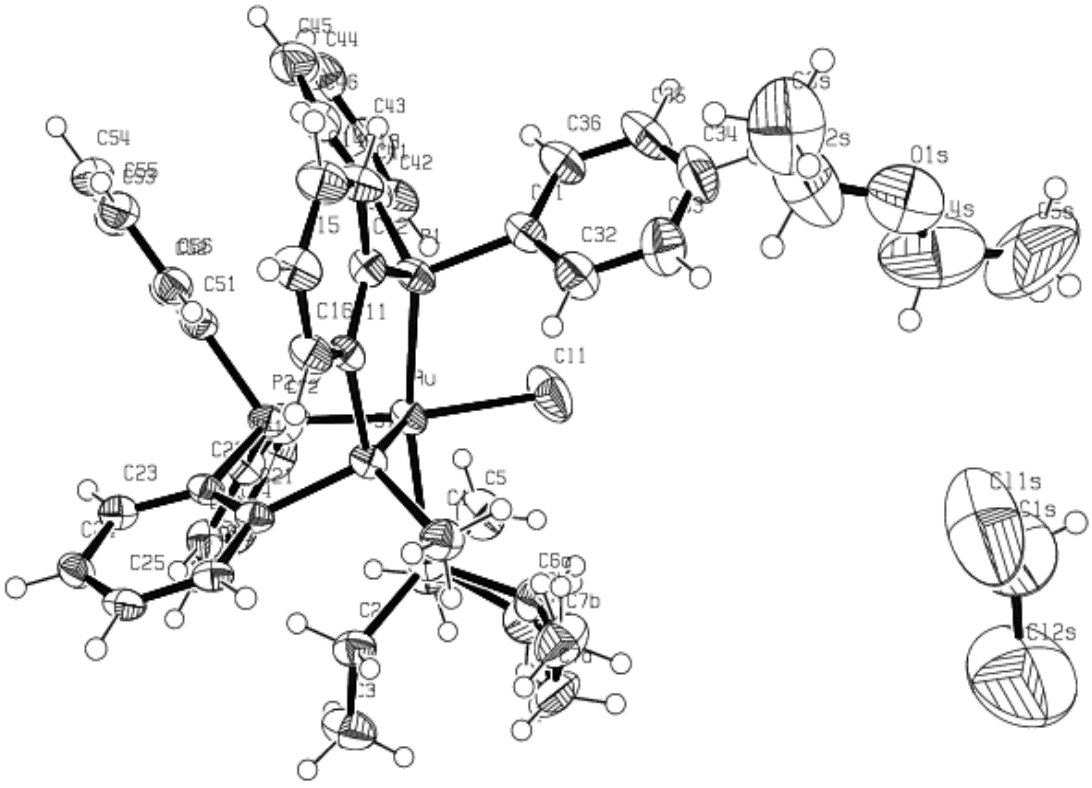

Figure A4. ORTEP diagram of [Ph-PSiP]RuCl(PEt$_3$) $\cdot(CH_2Cl_2)_{1.17}\cdot OEt_2$ (**2-6**$\cdot(CH_2Cl_2)_{1.17}\cdot OEt_2$).

Table A5. Crystallographic Experimental Details for ([Cy-PSiP]RuCl)$_2$·$(C_6H_6)_{3.5}$ (**3-2**·$(C_6H_6)_{3.5}$).

A. Crystal Data

formula	$C_{95}H_{131}Cl_2P_4Ru_2Si_2$
formula weight	1726.10
crystal dimensions (mm)	0.44 × 0.40 × 0.24
crystal system	triclinic
space group	$P\bar{1}$ (No. 2)
unit cell parameters	
a (Å)	14.6187 (6)
b (Å)	17.3802 (7)
c (Å)	20.6810 (9)
α (deg)	109.0018 (5)
β (deg)	98.3716 (5)
γ (deg)	107.0762 (5)
V (Å^3)	4576.9 (3)
Z	2
ρ_{calcd} (g cm^{-3})	1.252
μ (mm^{-1})	0.527

B. Data Collection and Refinement Conditions

diffractometer	Bruker D8/APEX II CCD
radiation (λ [Å])	graphite-monochromated Mo Kα (0.71073)
temperature (°C)	–100
scan type	ω scans (0.4°) (10 s exposures)
data collection 2θ limit (deg)	55.04
total data collected	40048 (-18 ≤ h ≤ 18, -22 ≤ k ≤ 22, -26 ≤ l ≤ 26)
independent reflections	20697 (R_{int} = 0.0219)
number of observed reflections (*NO*)	16550 [$F_o^2 \geq 2\sigma(F_o^2)$]
structure solution method	Patterson/structure expansion (*DIRDIF–2008*)
refinement method	full-matrix least-squares on F^2 (*SHELXL–97*)
absorption correction method	Gaussian integration (face-indexed)
range of transmission factors	0.8847–0.7992
data/restraints/parameters	20697 [$F_o^2 \geq -3\sigma(F_o^2)$] / 0 / 919
goodness-of-fit (S)	1.118 [$F_o^2 \geq -3\sigma(F_o^2)$]
final R indices	
R_1 [$F_o^2 \geq 2\sigma(F_o^2)$]	0.0380
wR_2 [$F_o^2 \geq -3\sigma(F_o^2)$]	0.1029
largest difference peak and hole	0.665 and –0.722 e Å^{-3}

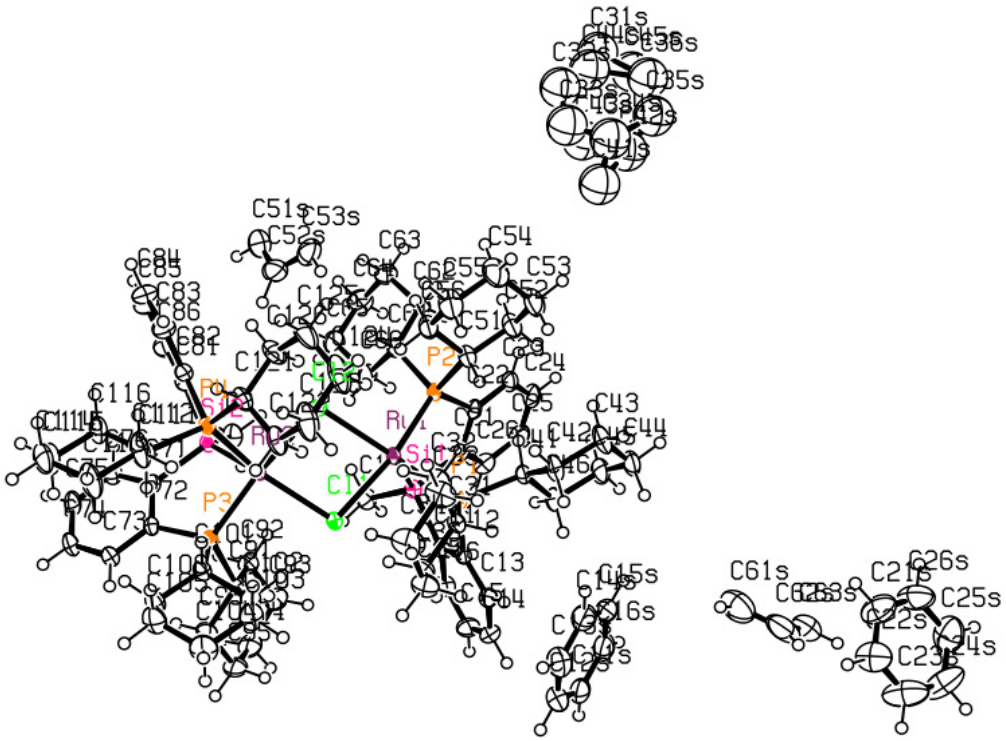

Figure A5. ORTEP diagram of $([Cy\text{-}PSiP]RuCl)_2 \cdot (C_6H_6)_{3.5}$ (**3-2**$\cdot (C_6H_6)_{3.5}$).

Table A6. Crystallographic Experimental Details for [Cy-PSiP]RuO^{t}Bu·C_6H_6·$(C_5H_{12})_{0.5}$ (**3-3**·C_6H_6·$(C_5H_{12})_{0.5}$).

A. Crystal Data	
formula	$C_{49.5}H_{76}OP_2RuSi$
formula weight	878.20
crystal dimensions (mm)	0.21 × 0.16 × 0.14
crystal system	triclinic
space group	$P\bar{1}$ (No. 2)
unit cell parameters	
a (Å)	9.6834 (3)
b (Å)	10.7231 (3)
c (Å)	23.2229 (7)
α (deg)	98.9179 (4)
β (deg)	90.9953 (4)
γ (deg)	98.6300 (4)
V (Å^3)	2353.21 (12)
Z	2
ρ_{calcd} (g cm^{-3})	1.239
μ (mm^{-1})	0.461
B. Data Collection and Refinement Conditions	
diffractometer	Bruker D8/APEX II CCD
radiation (λ [Å])	graphite-monochromated Mo Kα (0.71073)
temperature (°C)	–100
scan type	ω scans (0.3°) (20 s exposures)
data collection 2θ limit (deg)	54.92
total data collected	20859 ($-12 \le h \le 12$, $-13 \le k \le 13$, $-30 \le l \le 30$)
independent reflections	10680 (R_{int} = 0.0245)
number of observed reflections (*NO*)	9221 [$F_o^2 \ge 2\sigma(F_o^2)$]
structure solution method	Patterson/structure expansion (*DIRDIF–2008*)
refinement method	full-matrix least-squares on F^2 (*SHELXL–97*)
absorption correction method	Gaussian integration (face-indexed)
range of transmission factors	0.9383–0.9091
data/restraints/parameters	10680 / 7[a] / 567
goodness-of-fit (*S*) [all data]	1.051
final *R* indices	
R_1 [$F_o^2 \ge 2\sigma(F_o^2)$]	0.0335
wR_2 [all data]	0.0846
largest difference peak and hole	0.959 and –0.704 e Å^{-3}

[a] Restraints were applied during refinement to impose an idealized gemetry upon the disordered solvent *n*-pentane molecule: d(C31S–C32S) = d(C32S–C33S) = d(C33S–C34S) = d(C34S–C35S) = 1.54(1) Å; d(C31S…C33S) = d(C32S…C34S) = d(C33S…C35S) = 2.52(1) Å.

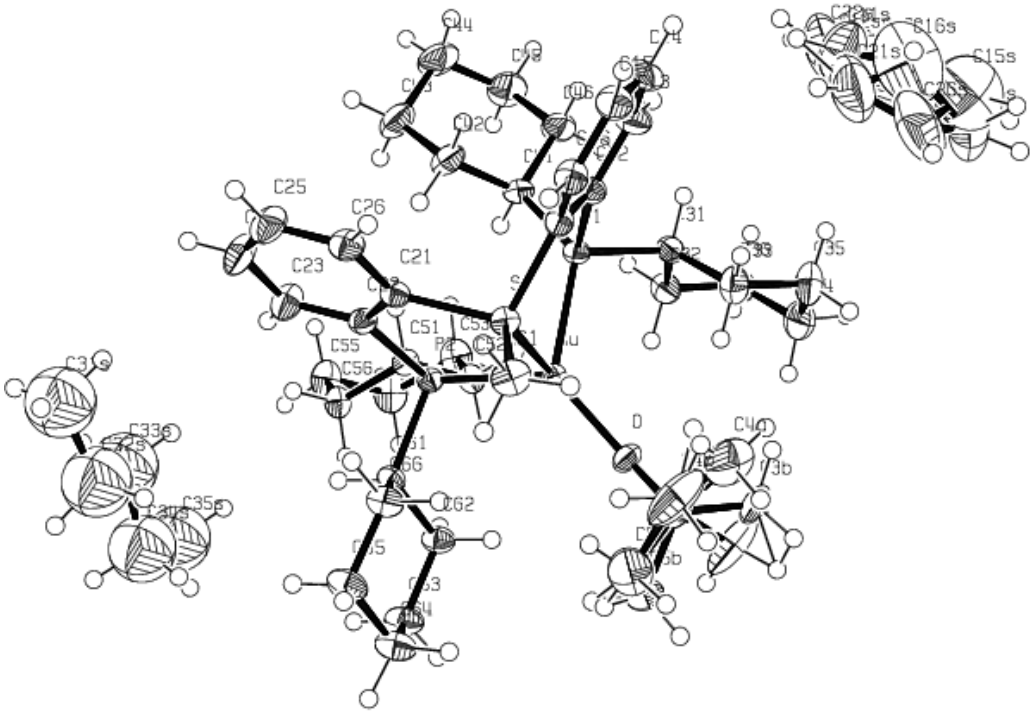

Figure A6. ORTEP diagram of [Cy-PSiP]RuO^{t}Bu·C_6H_6·$(C_5H_{12})_{0.5}$ (**3-3**·C_6H_6·$(C_5H_{12})_{0.5}$).

Table A7. Crystallographic Experimental Details for [Cy-PSiP]RuN($SiMe_3$)$_2$ (**3-4**).

A. Crystal Data	
formula	$C_{43}H_{73}NP_2RuSi_3$
formula weight	851.30
crystal dimensions (mm)	0.39 × 0.31 × 0.28
crystal system	orthorhombic
space group	$P2_12_12_1$ (No. 19)
unit cell parameters	
a (Å)	11.2207 (4)
b (Å)	18.6724 (7)
c (Å)	21.6126 (8)
V (Å^3)	4528.2 (3)
Z	4
ρ_{calcd} (g cm^{-3})	1.249
μ (mm^{-1})	0.526
B. Data Collection and Refinement Conditions	
diffractometer	Bruker D8/APEX II CCD
radiation (λ [Å])	graphite-monochromated Mo Kα (0.71073)
temperature (°C)	–100
scan type	ω scans (0.3°) (20 s exposures)
data collection 2θ limit (deg)	55.12
total data collected	40041 (-14 ≤ h ≤ 14, -24 ≤ k ≤ 24, -28 ≤ l ≤ 27)
independent reflections	10431 (R_{int} = 0.0207)
number of observed reflections (*NO*)	10195 [$F_o^2 \geq 2\sigma(F_o^2)$]
structure solution method	direct methods (*SIR*97)
refinement method	full-matrix least-squares on F^2 (*SHELXL–97*)
absorption correction method	multi-scan (*SADABS*)
range of transmission factors	0.8664–0.8217
data/restraints/parameters	10431 [$F_o^2 \leq -3\sigma(F_o^2)$] / 0 / 451
Flack absolute structure parameter	–0.019(11)
goodness-of-fit (*S*)	1.047 [$F_o^2 \leq -3\sigma(F_o^2)$]
final R indices	
R_1 [$F_o^2 \leq 2\sigma(F_o^2)$]	0.0186
wR_2 [$F_o^2 \leq -3\sigma(F_o^2)$]	0.0497
largest difference peak and hole	0.364 and –0.184e Å^{-3}

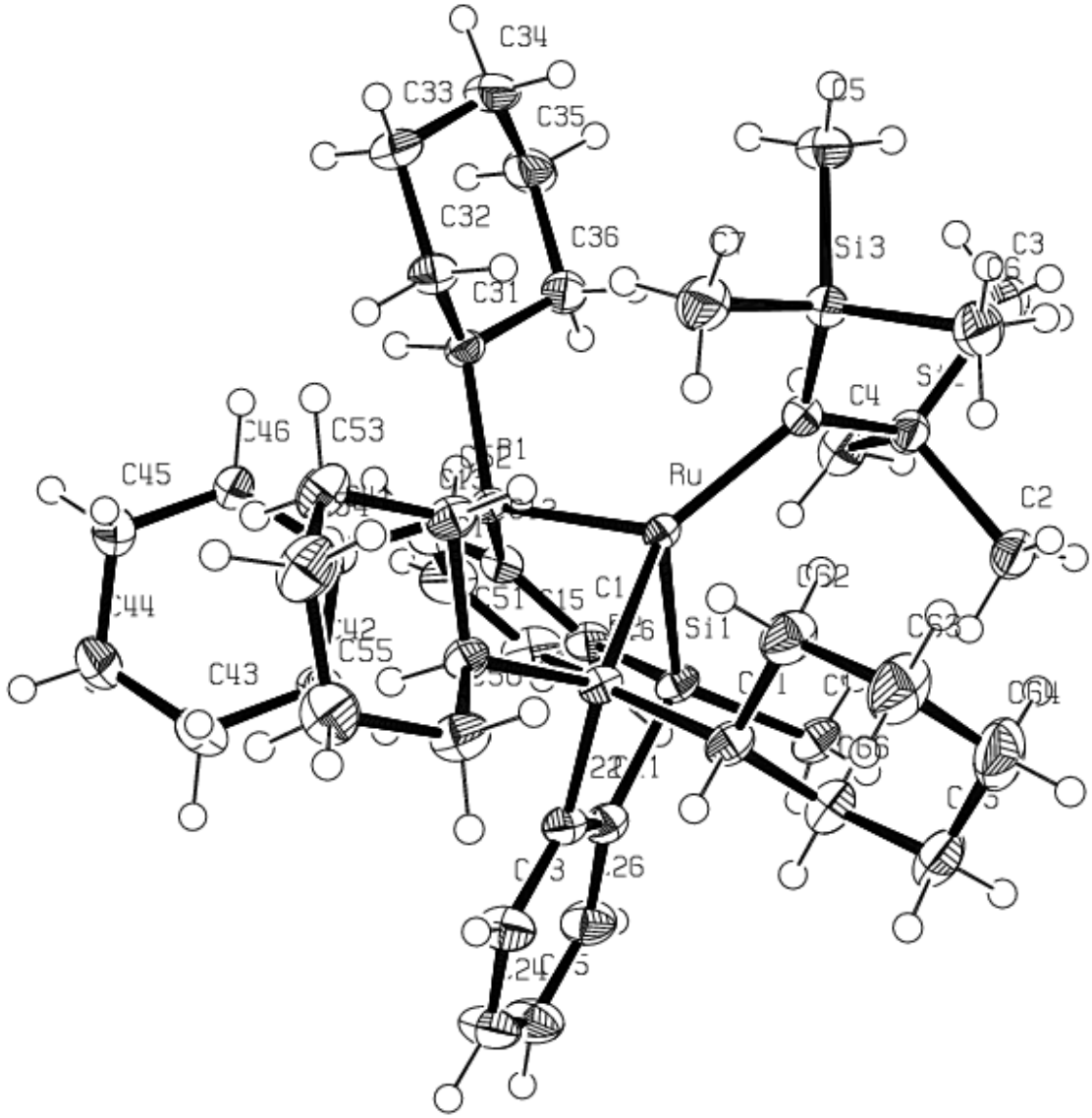

Figure A7. ORTEP diagram of [Cy-PSiP]RuN($SiMe_3$)$_2$ (**3-4**).

Table A8. Crystallographic Experimental Details for [Cy-PSiP]RuNH(2,6-$Me_2C_6H_3$) (**3-6**).

A. Crystal Data	
formula	$C_{45}H_{65}NP_2RuSi$
formula weight	811.08
crystal dimensions (mm)	0.46 × 0.20 × 0.10
crystal system	monoclinic
space group	$P2_1/n$ (an alternate setting of $P2_1/c$ [No. 14])
unit cell parameters	
a (Å)	13.686 (5)
b (Å)	17.529 (6)
c (Å)	17.303 (6)
β (deg)	95.650 (5)
V (Å^3)	4131 (2)
Z	4
ρ_{calcd} (g cm^{-3})	1.304
μ (mm^{-1})	0.518
B. Data Collection and Refinement Conditions	
diffractometer	Bruker D8/APEX II CCD
radiation (λ [Å])	graphite-monochromated Mo Kα (0.71073)
temperature (°C)	–100
scan type	ω scans (0.3°) (25 s exposures)
data collection 2θ limit (deg)	51.36
total data collected	30048 (-16 ≤ h ≤ 16, -21 ≤ k ≤ 21, -21 ≤ l ≤ 21)
independent reflections	7809 (R_{int} = 0.0769)
number of observed reflections (*NO*)	5620 [$F_o^2 \geq 2\sigma(F_o^2)$]
structure solution method	Patterson/structure expansion (*DIRDIF–2008*)
refinement method	full-matrix least-squares on F^2 (*SHELXL–97*)
absorption correction method	Gaussian integration (face-indexed)
range of transmission factors	0.9481–0.7981
data/restraints/parameters	7809 [$F_o^2 \geq -3\sigma(F_o^2)$] / 0 / 453
goodness-of-fit (S)	1.008 [$F_o^2 \geq -3\sigma(F_o^2)$]
final R indices	
R_1 [$F_o^2 \geq 2\sigma(F_o^2)$]	0.0379
wR_2 [$F_o^2 \geq -3\sigma(F_o^2)$]	0.0847
largest difference peak and hole	0.468 and –0.468 e Å^{-3}

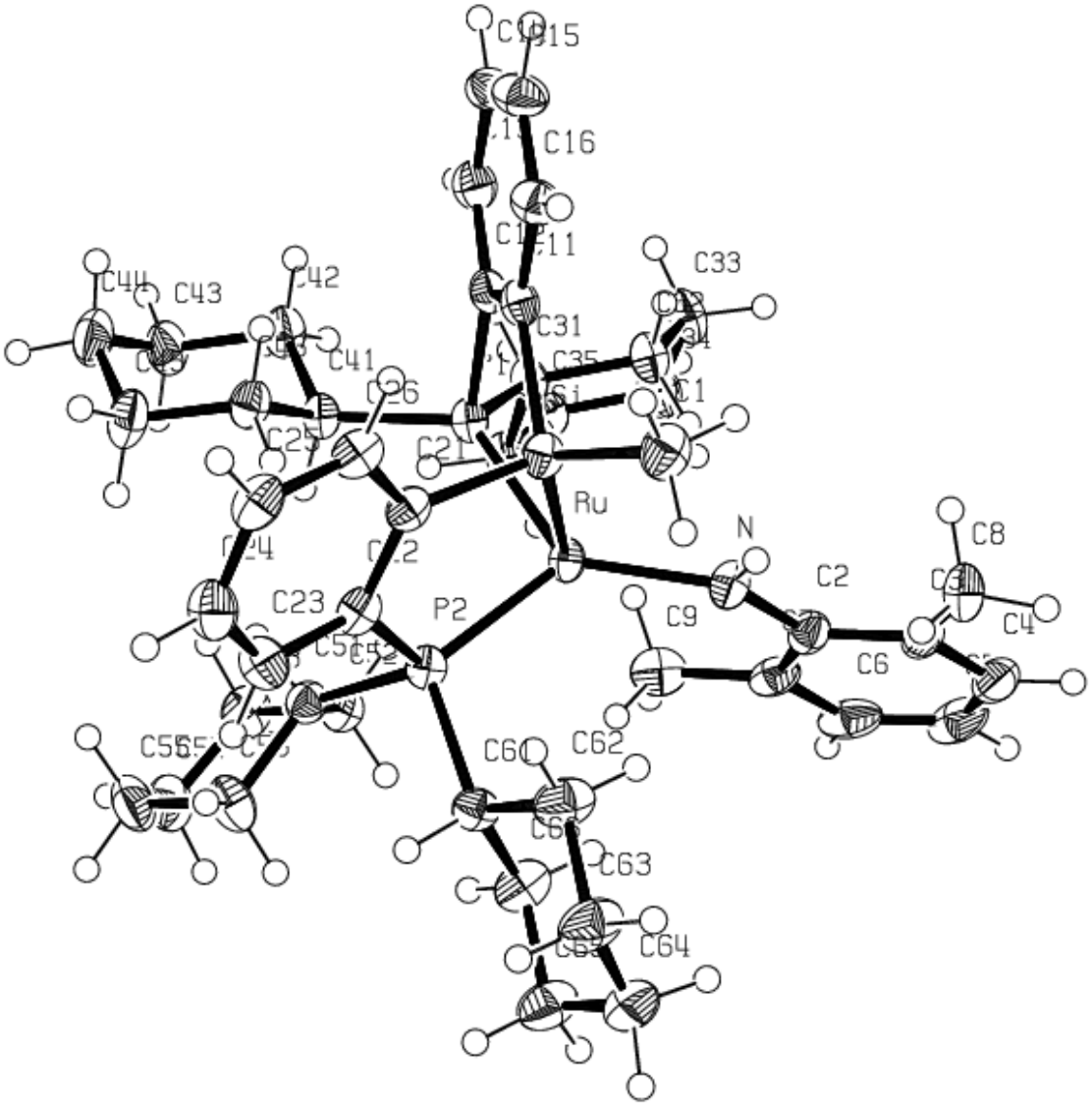

Figure A8. ORTEP diagram for [Cy-PSiP]RuNH(2,6-$Me_2C_6H_3$) (**3-6**).

Table A9. Crystallographic Experimental Details for ([Cy-PSiP]RuOH)$_2$·C_7H_8 (**3-8**·C_7H_8).

A. Crystal Data	
formula	$C_{81}H_{120}O_2P_4Ru_2Si_2$
formula weight	1507.97
crystal dimensions (mm)	0.27 × 0.19 × 0.12
crystal system	monoclinic
space group	$P2_1/c$ (No. 14)
unit cell parameters	
a (Å)	16.9400 (8)
b (Å)	17.7122 (8)
c (Å)	26.4360 (13)
β (deg)	102.8828 (7)
V (Å^3)	7732.3 (6)
Z	4
ρ_{calcd} (g cm^{-3})	1.295
μ (mm^{-1})	1.295
B. Data Collection and Refinement Conditions	
diffractometer	Bruker D8/APEX II CCD
radiation (λ [Å])	graphite-monochromated Mo Kα (0.71073)
temperature (°C)	–100
scan type	ω scans (0.3°) (30 s exposures)
data collection 2θ limit (deg)	51.80
total data collected	58033 (-20 ≤ h ≤ 20, -21 ≤ k ≤ 21, -32 ≤ l ≤ 32)
independent reflections	15024 (R_{int} = 0.0319)
number of observed reflections (*NO*)	12959 [$F_o^2 \geq 2\sigma(F_o^2)$]
structure solution method	direct methods (*SHELXS–97*)
refinement method	full-matrix least-squares on F^2 (*SHELXL–97*)
absorption correction method	Gaussian integration (face-indexed)
range of transmission factors	0.9361–0.8668
data/restraints/parameters	15024 / 6[a] / 779
goodness-of-fit (*S*) [all data]	1.244
final *R* indices	
R_1 [$F_o^2 \geq 2\sigma(F_o^2)$]	0.0490
wR_2 [all data]	0.1231
largest difference peak and hole	1.354 and –1.119 e Å^{-3}

[a] Distances involving the methyl carbon atom positions for the disordered solvent toluene molecule were given fixed idealized distances during refinement: d(C10S–C11S) = d(C20S–C21S) = 1.50(1) Å; d(C10S…C12S) = d(C10S…C16S) = d(C20S…C22S) =

d(C20S…C26S) = 2.51(1) Å. The arene rings of the two conformers of this disordred molecule were modelled as regular hexagons with d(C–C) = 1.39 Å (*SHELXL-97* AFIX 66 instruction).

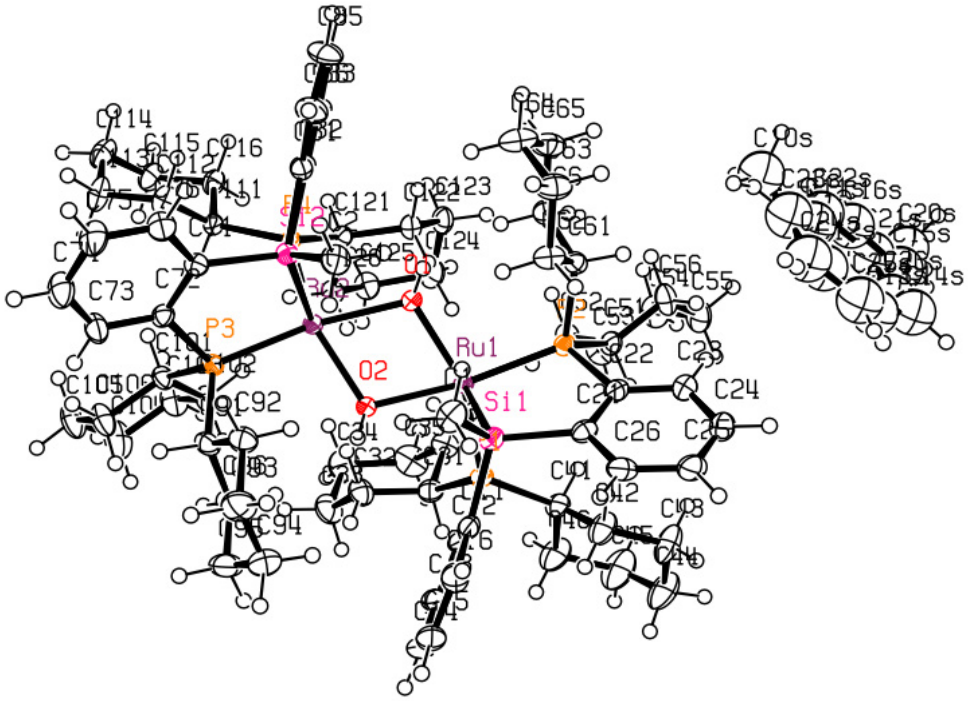

Figure A9. ORTEP diagram for ([Cy-PSiP]RuOH)$_2$·C_7H_8 (**3-8**·C_7H_8).

Table A10. Crystallographic Experimental Details for [Cy-PSiP]Ru(η^5-C_6H_5O)·C_6H_6 (**3-9**·C_6H_6).

A. Crystal Data	
formula	$C_{49}H_{66}OP_2RuSi$
formula weight	862.12
crystal dimensions (mm)	0.39 × 0.26 × 0.26
crystal system	monoclinic
space group	*C*2/*c* (No. 15)
unit cell parameters	
a (Å)	24.2475 (7)
b (Å)	11.0287 (3)
c (Å)	33.2893 (9)
β (deg)	103.5036 (4)
V (Å^3)	8656.1 (4)
Z	8
ρ_{calcd} (g cm^{-3})	1.323
μ (mm^{-1})	0.500
B. Data Collection and Refinement Conditions	
diffractometer	Bruker D8/APEX II CCD
radiation (λ [Å])	graphite-monochromated Mo Kα (0.71073)
temperature (°C)	–100
scan type	ω scans (0.3°) (15 s exposures)
data collection 2θ limit (deg)	55.26
total data collected	38294 (-31 ≤ *h* ≤ 31, -14 ≤ *k* ≤ 14, -43 ≤ *l* ≤ 43)
independent reflections	10048 (R_{int} = 0.0213)
number of observed reflections (*NO*)	9377 [$F_o^2 \geq 2\sigma(F_o^2)$]
structure solution method	Patterson/structure expansion (*DIRDIF–2008*)
refinement method	full-matrix least-squares on F^2 (*SHELXL–97*)
absorption correction method	Gaussian integration (face-indexed)
range of transmission factors	0.8827–0.8286
data/restraints/parameters	10048 / 0 / 487
goodness-of-fit (*S*) [all data]	1.238
final *R* indices	
R_1 [$F_o^2 \geq 2\sigma(F_o^2)$]	0.0300
wR_2 [all data]	0.0731
largest difference peak and hole	0.352 and –0.439 e Å^{-3}

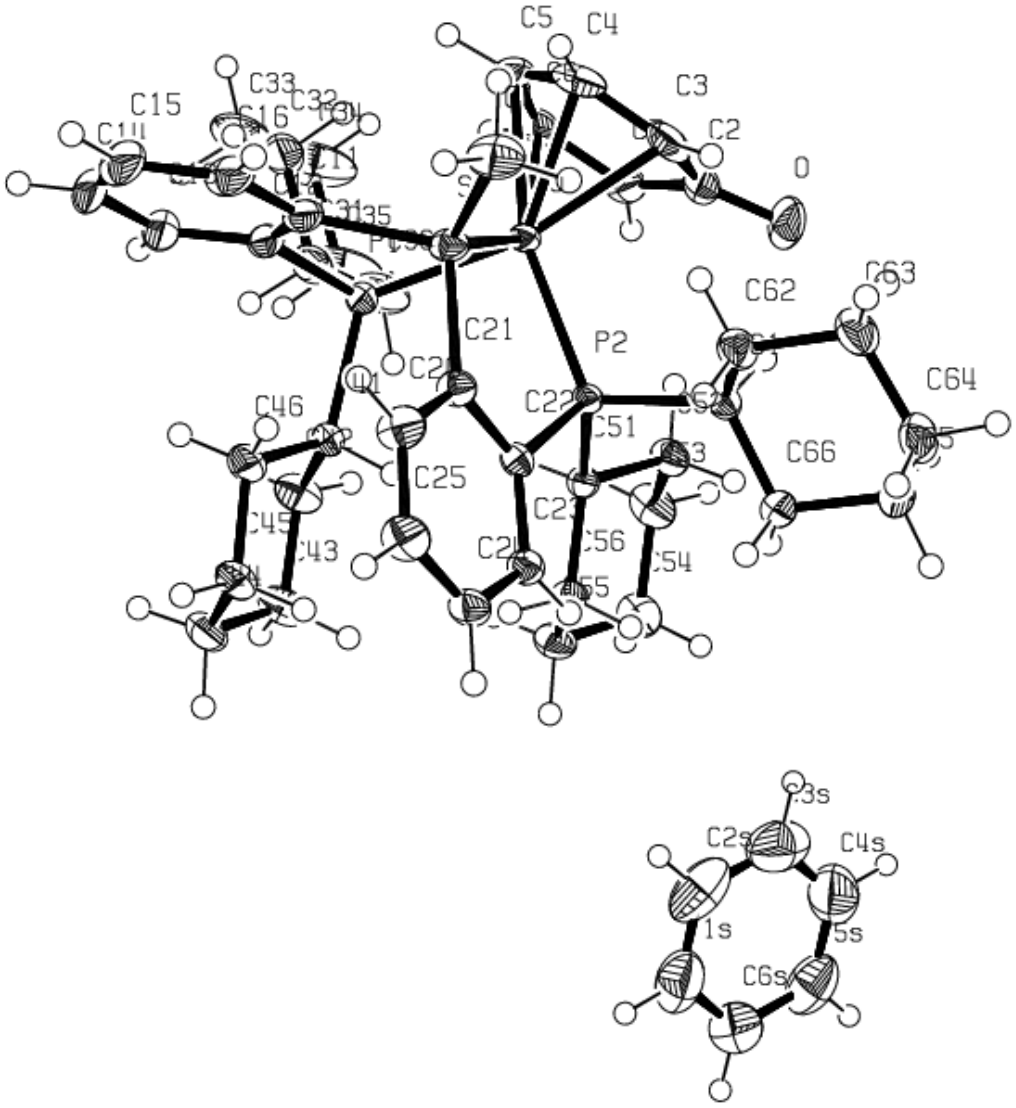

Figure A10. ORTEP diagram of [Cy-PSiP]Ru(η^5-C_6H_5O)·C_6H_6 (**3-9**·C_6H_6).

Table A11. Crystallographic Experimental Details for [Cy-PSiP]Ru(H)(η^2:η^2-H_2BNH_2) (**3-10**).

A. Crystal Data	
formula	$C_{37}H_{60}BNP_2RuSi$
formula weight	720.77
crystal dimensions (mm)	0.25 × 0.13 × 0.09
crystal system	monoclinic
space group	*Ia* (an alternate setting of *Cc* [No. 9])
unit cell parameters	
a (Å)	16.250 (3)
b (Å)	13.600 (3)
c (Å)	17.563 (4)
β (deg)	98.434 (3)
V (Å^3)	3839.7 (14)
Z	4
ρ_{calcd} (g cm^{-3})	1.247
μ (mm^{-1})	0.548
B. Data Collection and Refinement Conditions	
diffractometer	Bruker D8/APEX II CCD
radiation (λ [Å])	graphite-monochromated Mo Kα (0.71073)
temperature (°C)	–100
scan type	ω scans (0.3°) (45 s exposures)
data collection 2θ limit (deg)	52.90
total data collected	14909 (-20 ≤ *h* ≤ 20, -17 ≤ *k* ≤ 16, -21 ≤ *l* ≤ 21)
independent reflections	7824 (R_{int} = 0.0610)
number of observed reflections (*NO*)	6477 [$F_o^2 \geq 2\sigma(F_o^2)$]
structure solution method	direct methods (*SHELXS–97*)
refinement method	full-matrix least-squares on F^2 (*SHELXL–97*)
absorption correction method	Gaussian integration (face-indexed)
range of transmission factors	0.9503–0.8770
data/restraints/parameters	7824 / 5[a] / 398
Flack absolute structure parameter	–0.03(4)
goodness-of-fit (*S*) [all data]	1.006
final *R* indices	
R_1 [$F_o^2 \geq 2\sigma(F_o^2)$]	0.0452
wR_2 [all data]	0.1152
largest difference peak and hole	2.077 and –1.313 e Å^{-3}

[a] Distance restraints applied during refinement: d(Ru–H1) = 1.55(1) Å; d(B–H1BA) = d(B–H1BB) = 1.12(2) Å; d(H1BA…H1BB) = 1.94(2) Å; d(P1…H1) = d(P2…H1)

(within 0.03 Å).

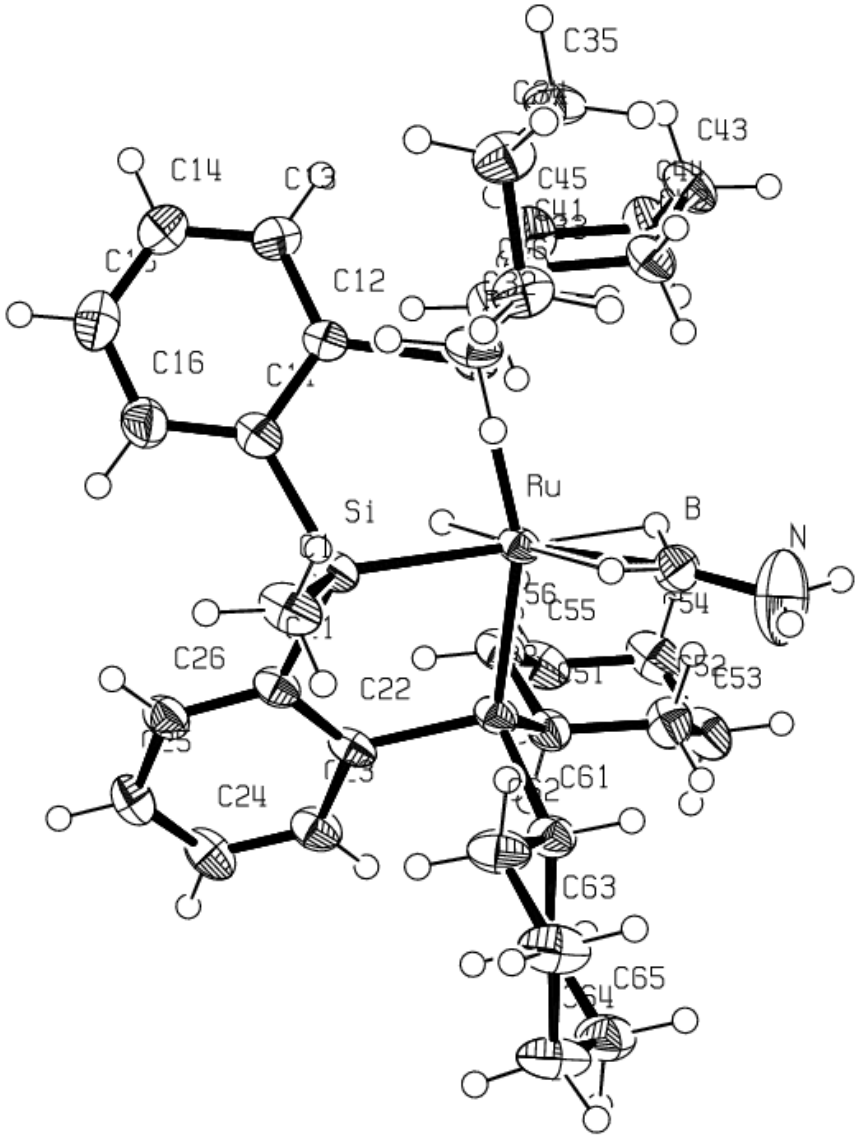

Figure A11. ORTEP diagram for [Cy-PSiP]Ru(H)(η^2:η^2-H_2BNH_2) (**3-10**).

Table A12. Crystallographic Experimental Details for [Cy-PSiP]Ru(H)(η^2:η^2-H_2BNMe_2) (**3-11**).

A. Crystal Data	
formula	$C_{39}H_{64}BNP_2RuSi$
formula weight	748.82
crystal dimensions (mm)	0.26 × 0.22 × 0.14
crystal system	monoclinic
space group	$P2_1/n$ (an alternate setting of $P2_1/c$ [No. 14])
unit cell parameters	
a (Å)	15.8401 (5)
b (Å)	14.1034 (4)
c (Å)	17.5564 (5)
β (deg)	93.3341 (4)
V (Å^3)	3915.4 (2)
Z	4
ρ_{calcd} (g cm^{-3})	1.270
μ (mm^{-1})	0.540
B. Data Collection and Refinement Conditions	
diffractometer	Bruker D8/APEX II CCD
radiation (λ [Å])	graphite-monochromated Mo Kα (0.71073)
temperature (°C)	–100
scan type	ω scans (0.3°) (20 s exposures)
data collection 2θ limit (deg)	55.04
total data collected	34171 (-20 ≤ h ≤ 20, -18 ≤ k ≤ 18, -22 ≤ l ≤ 22)
independent reflections	9002 (R_{int} = 0.0290)
number of observed reflections (*NO*)	7713 [$F_o^2 \geq 2\sigma(F_o^2)$]
structure solution method	Patterson/structure expansion (*DIRDIF–2008*)
refinement method	full-matrix least-squares on F^2 (*SHELXL–97*)
absorption correction method	Gaussian integration (face-indexed)
range of transmission factors	0.9287–0.8737
data/restraints/parameters	9002 / 0 / 420
goodness-of-fit (*S*) [all data]	1.034
final R indices	
R_1 [$F_o^2 \geq 2\sigma(F_o^2)$]	0.0249
wR_2 [all data]	0.0635
largest difference peak and hole	0.411 and –0.356 e Å^{-3}

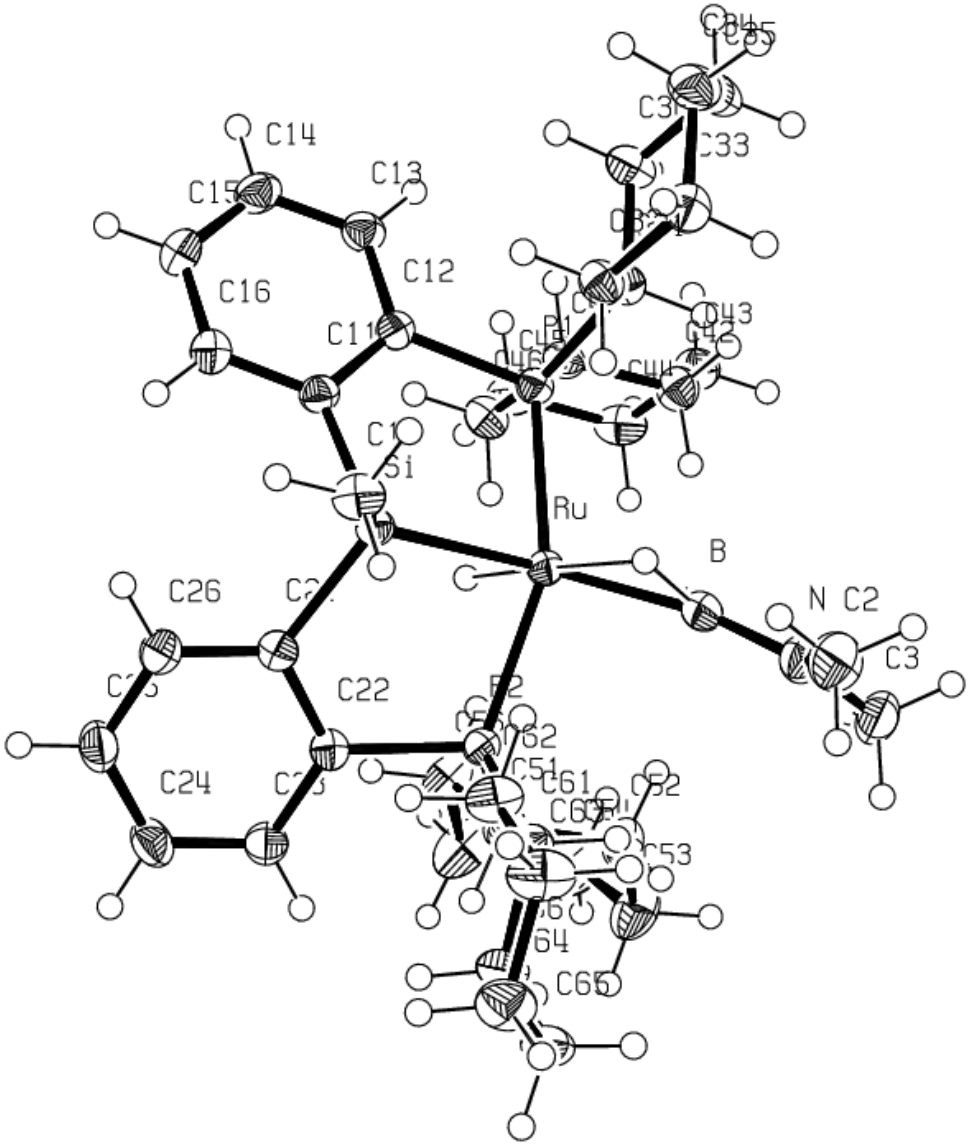

Figure A12. ORTEP diagram for [Cy-PSiP]Ru(H)(η^2:η^2-H_2BNMe_2) (**3-11**).

Table A13. Crystallographic Experimental Details for [Cy-PSiP]RuCl(PMe_3) (**4-2**).

A. Crystal Data	
formula	$C_{40}H_{64}ClP_3RuSi$
formula weight	802.43
crystal dimensions (mm)	0.41 × 0.39 × 0.22
crystal system	triclinic
space group	$P\bar{1}$ (No. 2)
unit cell parameters	
a (Å)	10.3409 (5)
b (Å)	10.5020 (5)
c (Å)	18.9852 (9)
α (deg)	95.6088 (5)
β (deg)	92.0827 (5)
γ (deg)	101.5544 (5)
V (Å^3)	2007.03 (17)
Z	2
ρ_{calcd} (g cm^{-3})	1.328
μ (mm^{-1})	0.634
B. Data Collection and Refinement Conditions	
diffractometer	Bruker D8/APEX II CCD
radiation (λ [Å])	graphite-monochromated Mo Kα (0.71073)
temperature (°C)	–100
scan type	ω scans (0.3°) (20 s exposures)
data collection 2θ limit (deg)	55.30
total data collected	17730 (-13 ≤ h ≤ 13, -13 ≤ k ≤ 13, -24 ≤ l ≤ 24)
independent reflections	9159 (R_{int} = 0.0112)
number of observed reflections (*NO*)	8596 [$F_o^2 \geq 2\sigma(F_o^2)$]
structure solution method	Patterson/structure expansion (*DIRDIF–2008*)
refinement method	full-matrix least-squares on F^2 (*SHELXL–97*)
absorption correction method	Gaussian integration (face-indexed)
range of transmission factors	0.8706–0.7803
data/restraints/parameters	9159 [$F_o^2 \geq -3\sigma(F_o^2)$] / 0 / 415
goodness-of-fit (S)	1.041 [$F_o^2 \geq -3\sigma(F_o^2)$]
final R indices	
R_1 [$F_o^2 \geq 2\sigma(F_o^2)$]	0.0211
wR_2 [$F_o^2 \geq -3\sigma(F_o^2)$]	0.0549
largest difference peak and hole	0.504 and –0.343 e Å^{-3}

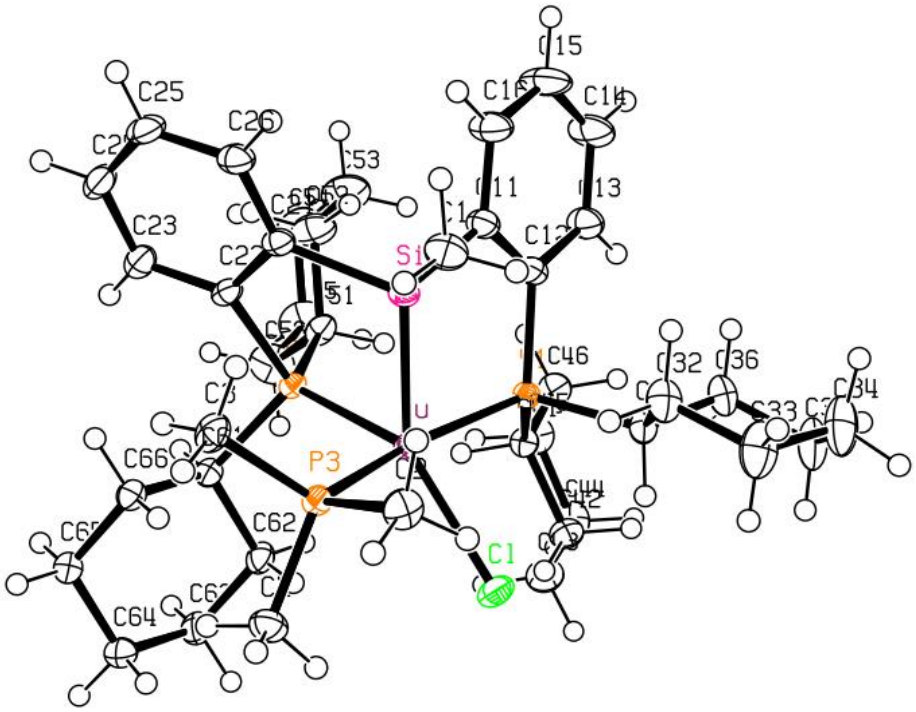

Figure A13. ORTEP diagram for [Cy-PSiP]RuCl(PMe$_3$) (**4-2**).

Table A14. Crystallographic Experimental Details for [MeSi($C_6H_4PCy_2$)($C_6H_4PCy(\eta^3$-$C_6H_8)$)]$RuPMe_3$ (**4-3**).

A. Crystal Data	
formula	$C_{40}H_{61}P_3RuSi$
formula weight	763.96
crystal dimensions (mm)	0.46 × 0.36 × 0.31
crystal system	triclinic
space group	$P\bar{1}$ (No. 2)
unit cell parameters	
a (Å)	10.5218 (5)
b (Å)	12.5407 (6)
c (Å)	15.2414 (7)
α (deg)	87.6054 (5)
β (deg)	70.3495 (5)
γ (deg)	89.9268 (5)
V (Å^3)	1892.16 (15)
Z	2
ρ_{calcd} (g cm^{-3})	1.341
μ (mm^{-1})	0.600
B. Data Collection and Refinement Conditions	
diffractometer	Bruker D8/APEX II CCD
radiation (λ [Å])	graphite-monochromated Mo Kα (0.71073)
temperature (°C)	–100
scan type	ω scans (0.3°) (15 s exposures)
data collection 2θ limit (deg)	55.08
total data collected	16781 (-13 ≤ h ≤ 13, -16 ≤ k ≤ 16, -19 ≤ l ≤ 19)
independent reflections	8620 (R_{int} = 0.0121)
number of observed reflections (*NO*)	8106 [$F_o^2 \geq 2\sigma(F_o^2)$]
structure solution method	direct methods (*SIR*97)
refinement method	full-matrix least-squares on F^2 (*SHELXL–97*)
absorption correction method	multi-scan (*SADABS*)
range of transmission factors	0.8367–0.7686
data/restraints/parameters	8620 [$F_o^2 \geq -3\sigma(F_o^2)$] / 0 / 410
goodness-of-fit (S)	1.071 [$F_o^2 \geq -3\sigma(F_o^2)$]
final R indices	
R_1 [$F_o^2 \geq 2\sigma(F_o^2)$]	0.0225
wR_2 [$F_o^2 \geq -3\sigma(F_o^2)$]	0.0647
largest difference peak and hole	0.880 and –0.477 e Å^{-3}

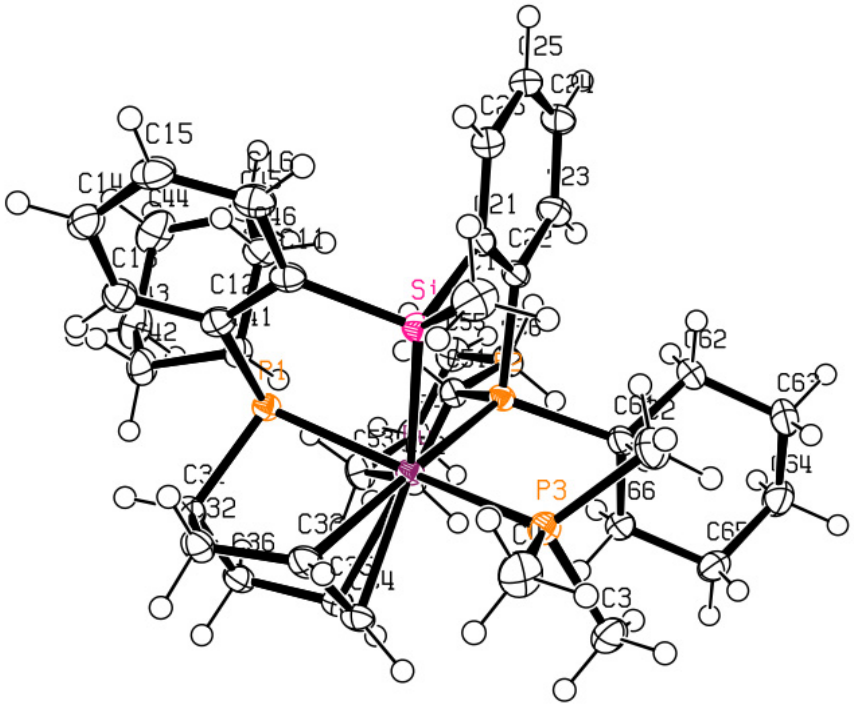

Figure A14. ORTEP diagram for [MeSi($C_6H_4PCy_2$)($C_6H_4PCy(\eta^3$-$C_6H_8)$)]RuPMe_3 (**4-3**).

Table A15. Crystallographic Experimental Details for [Cy-PSiP]RuH(PMe_3)·$(C_5H_{12})_{0.875}$ (**4-4**·$(C_5H_{12})_{0.875}$).

A. Crystal Data	
formula	$C_{44.375}H_{75.50}P_3RuSi$
formula weight	831.12
crystal dimensions (mm)	0.36 × 0.35 × 0.05
crystal system	tetragonal
space group	$I\bar{4}2m$ (No. 121)
unit cell parameters[a]	
a (Å)	22.5341 (9)
c (Å)	17.3711 (7)
V (Å^3)	8820.8 (6)
Z	8
ρ_{calcd} (g cm^{-3})	1.252
μ (mm^{-1})	0.520
B. Data Collection and Refinement Conditions	
diffractometer	Bruker D8/APEX II CCD
radiation (λ [Å])	graphite-monochromated Mo Kα (0.71073)
temperature (°C)	–100
scan type	ω scans (0.3°) (20 s exposures)
data collection 2θ limit (deg)	52.90
total data collected	35591 (-28 ≤ h ≤ 28, -28 ≤ k ≤ 28, -21 ≤ l ≤ 21)
independent reflections	4722 (R_{int} = 0.0447)
number of observed reflections (*NO*)	4371 [$F_o^2 \geq 2\sigma(F_o^2)$]
structure solution method	direct methods (*SHELXS–97*)
refinement method	full-matrix least-squares on F^2 (*SHELXL–97*)
absorption correction method	multi-scan (*SADABS*)
range of transmission factors	0.9724–0.8344
data/restraints/parameters	4722 [$F_o^2 \geq -3\sigma(F_o^2)$] / 0 / 233
Flack absolute structure parameter	–0.03(2)
goodness-of-fit (*S*)	1.058 [$F_o^2 \geq -3\sigma(F_o^2)$]
final R indices	
R_1 [$F_o^2 \geq 2\sigma(F_o^2)$]	0.0251
wR_2 [$F_o^2 \geq -3\sigma(F_o^2)$]	0.0619
largest difference peak and hole	0.990 and –0.202 e Å^{-3}

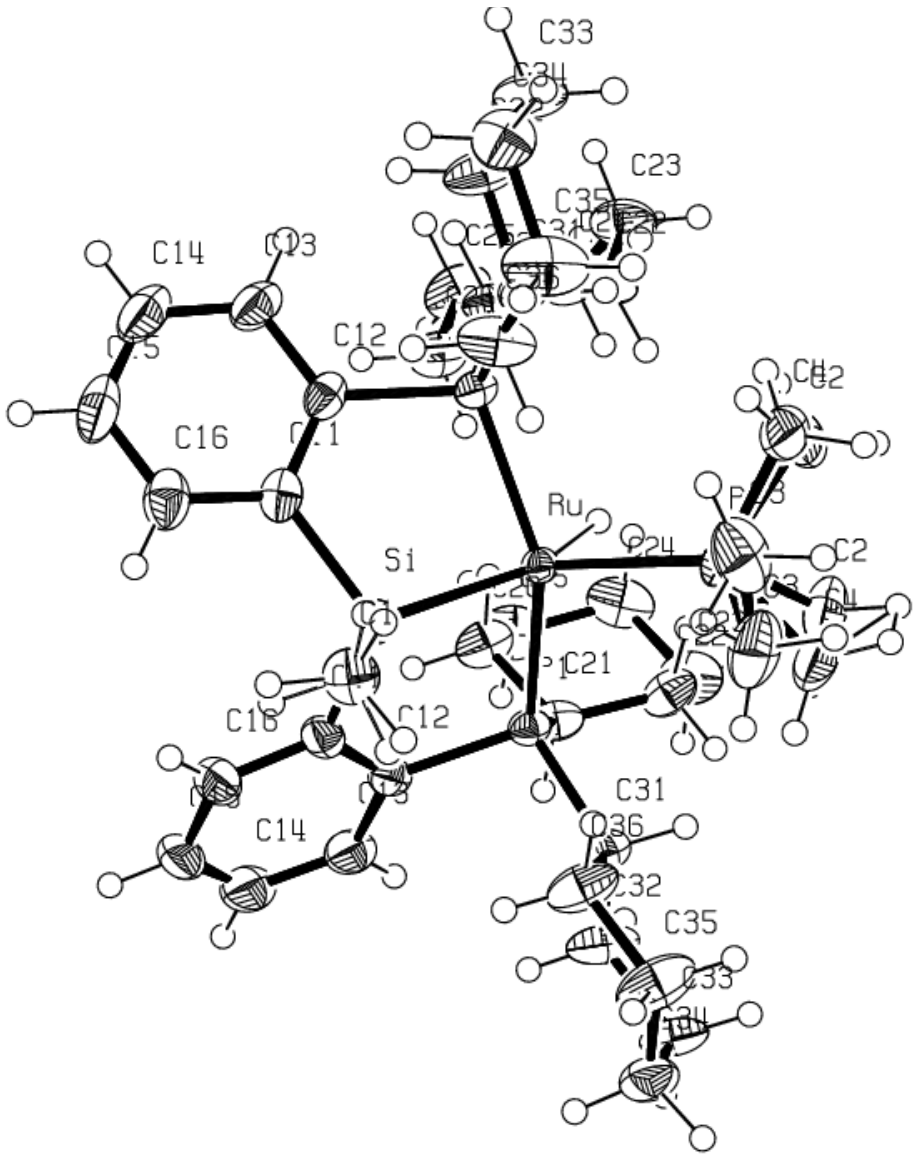

Figure A15. ORTEP diagram for [Cy-PSiP]RuH(PMe_3)·$(C_5H_{12})_{0.875}$ (**4-4**·$(C_5H_{12})_{0.875}$).

Table A16. Crystallographic Experimental Details for [Cy-PSiP]Ru(η^3-C_3H_5) (**4-8**).

A. Crystal Data	
formula	$C_{40}H_{60}P_2RuSi$
formula weight	731.98
crystal dimensions (mm)	0.37 × 0.36 × 0.12
crystal system	triclinic
space group	$P\bar{1}$ (No. 2)
unit cell parameters	
a (Å)	9.8037 (3)
b (Å)	10.8919 (3)
c (Å)	18.5073 (5)
α (deg)	73.1497 (3)
β (deg)	84.6217 (3)
γ (deg)	79.5330 (3)
V (Å^3)	1858.13 (9)
Z	2
ρ_{calcd} (g cm^{-3})	1.308
μ (mm^{-1})	0.567
B. Data Collection and Refinement Conditions	
diffractometer	Bruker D8/APEX II CCD
radiation (λ [Å])	graphite-monochromated Mo Kα (0.71073)
temperature (°C)	–100
scan type	ω scans (0.3°) (20 s exposures)
data collection 2θ limit (deg)	55.12
total data collected	16463 ($-12 \le h \le 12$, $-14 \le k \le 14$, $-23 \le l \le 24$)
independent reflections	8480 (R_{int} = 0.0100)
number of observed reflections (*NO*)	8053 [$F_o^2 \ge 2\sigma(F_o^2)$]
structure solution method	direct methods (*SIR*97)
refinement method	full-matrix least-squares on F^2 (*SHELXL–97*)
absorption correction method	Gaussian integration (face-indexed)
range of transmission factors	0.9330–0.8185
data/restraints/parameters	8480 / 0 / 398
goodness-of-fit (*S*) [all data]	1.121
final *R* indices	
R_1 [$F_o^2 \ge 2\sigma(F_o^2)$]	0.0202
wR_2 [all data]	0.0626
largest difference peak and hole	0.361 and –0.401 e Å^{-3}

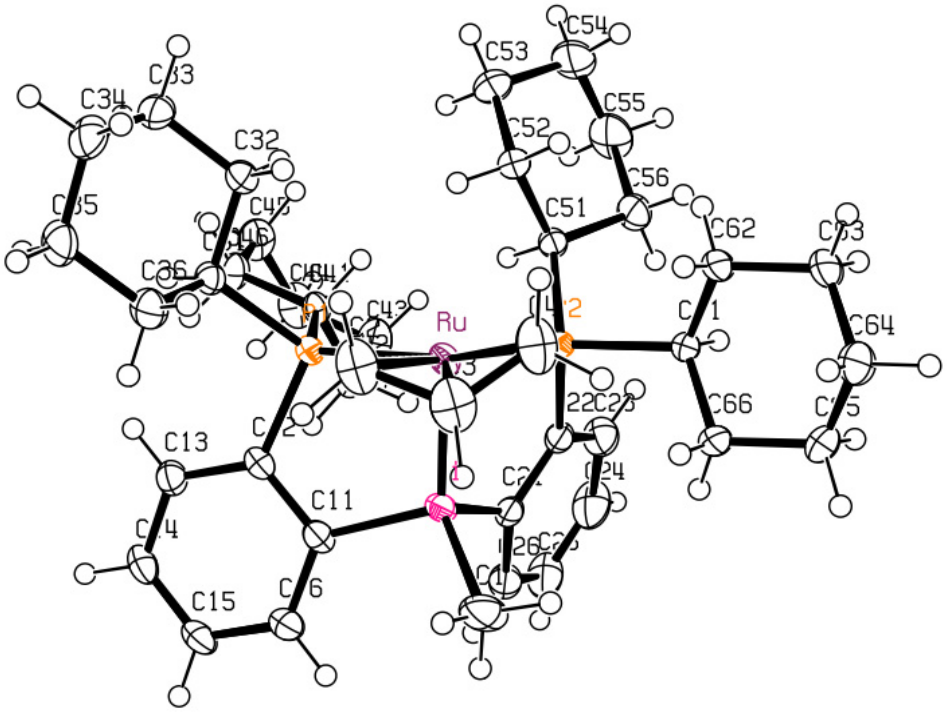

Figure A16. ORTEP diagram for [Cy-PSiP]Ru(η^3-C_3H_5) (**4-8**).

Table A17. Crystallographic Experimental Details for [Cy-PSiP]Ru(N_3)(PMe_3) (**4-10**).

A. Crystal Data	
formula	$C_{40}H_{64}N_3P_3RuSi$
formula weight	809.01
crystal dimensions (mm)	0.44 × 0.38 × 0.04
crystal system	triclinic
space group	$P\bar{1}$ (No. 2)
unit cell parameters	
a (Å)	10.3984 (4)
b (Å)	10.5102 (4)
c (Å)	19.0001 (8)
α (deg)	95.6660 (5)
β (deg)	92.3748 (5)
γ (deg)	102.1706 (5)
V (Å^3)	2015.78 (14)
Z	2
ρ_{calcd} (g cm^{-3})	1.333
μ (mm^{-1})	0.569
B. Data Collection and Refinement Conditions	
diffractometer	Bruker PLATFORM/APEX II CCD
radiation (λ [Å])	graphite-monochromated Mo Kα (0.71073)
temperature (°C)	–100
scan type	ω scans (0.3°) (15 s exposures)
data collection 2θ limit (deg)	55.08
total data collected	17901 ($-13 \le h \le 13$, $-13 \le k \le 13$, $-24 \le l \le 24$)
independent reflections	9205 (R_{int} = 0.0184)
number of observed reflections (*NO*)	8209 [$F_o^2 \ge 2\sigma(F_o^2)$]
structure solution method	Patterson/structure expansion (*DIRDIF–2008*)
refinement method	full-matrix least-squares on F^2 (*SHELXL–97*)
absorption correction method	Gaussian integration (face-indexed)
range of transmission factors	0.9787–0.7878
data/restraints/parameters	9205 / 0 / 433
goodness-of-fit (S) [all data]	1.041
final R indices	
R_1 [$F_o^2 \ge 2\sigma(F_o^2)$]	0.0252
wR_2 [all data]	0.0650
largest difference peak and hole	0.475 and –0.444 e Å^{-3}

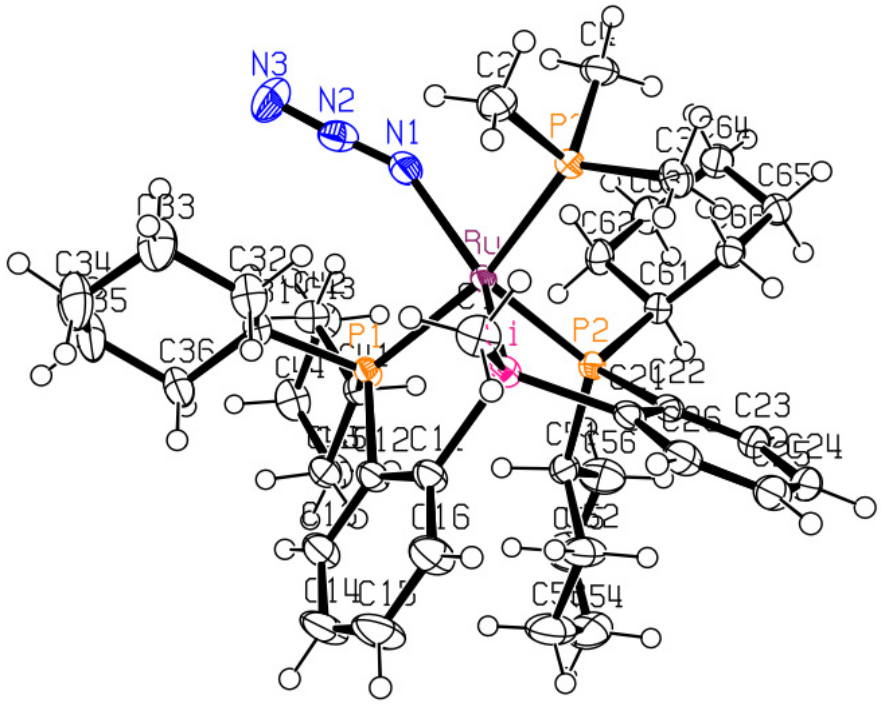

Figure A17. ORTEP diagram for [Cy-PSiP]Ru(N_3)(PMe_3) (**4-10**).

Table A18. Crystallographic Experimental Details for ([κ^2-*NP*N]PdCl)$_2$ (**5-2**).

A. Crystal Data	
formula	$C_{32}H_{40}Cl_2N_4P_2Pd_2$
formula weight	826.32
crystal dimensions (mm)	0.31 × 0.26 × 0.22
crystal system	monoclinic
space group	*P*2/*n* (an alternate setting of *P*2/*c* [No. 13])
unit cell parameters	
a (Å)	19.7889 (14)
b (Å)	9.4338 (7)
c (Å)	20.2742 (15)
β (deg)	114.9868 (10)
V (Å^3)	3430.6 (4)
Z	4
ρ_{calcd} (g cm^{-3})	1.600
μ (mm^{-1})	1.325
B. Data Collection and Refinement Conditions	
diffractometer	Bruker PLATFORM/SMART 1000 CCD
radiation (λ [Å])	graphite-monochromated Mo Kα (0.71073)
temperature (°C)	–80
scan type	ω scans (0.3°) (15 s exposures)
data collection 2θ limit (deg)	54.96
total data collected	28274 (-25 ≤ *h* ≤ 25, -12 ≤ *k* ≤ 12, -26 ≤ *l* ≤ 26)
independent reflections	7861 (R_{int} = 0.0257)
number of observed reflections (*NO*)	6906 [$F_o^2 \geq 2\sigma(F_o^2)$]
structure solution method	Patterson search/structure expansion (*DIRDIF–99*)
refinement method	full-matrix least-squares on F^2 (*SHELXL–97*)
absorption correction method	multi-scan (*SADABS*)
range of transmission factors	0.7592–0.6841
data/restraints/parameters	7861 [$F_o^2 \geq -3\sigma(F_o^2)$] / 0 / 379
goodness-of-fit (*S*)	1.055 [$F_o^2 \geq -3\sigma(F_o^2)$]
final *R* indices	
R_1 [$F_o^2 \geq 2\sigma(F_o^2)$]	0.0220
wR_2 [$F_o^2 \geq -3\sigma(F_o^2)$]	0.0592
largest difference peak and hole	0.558 and –0.249 e Å^{-3}

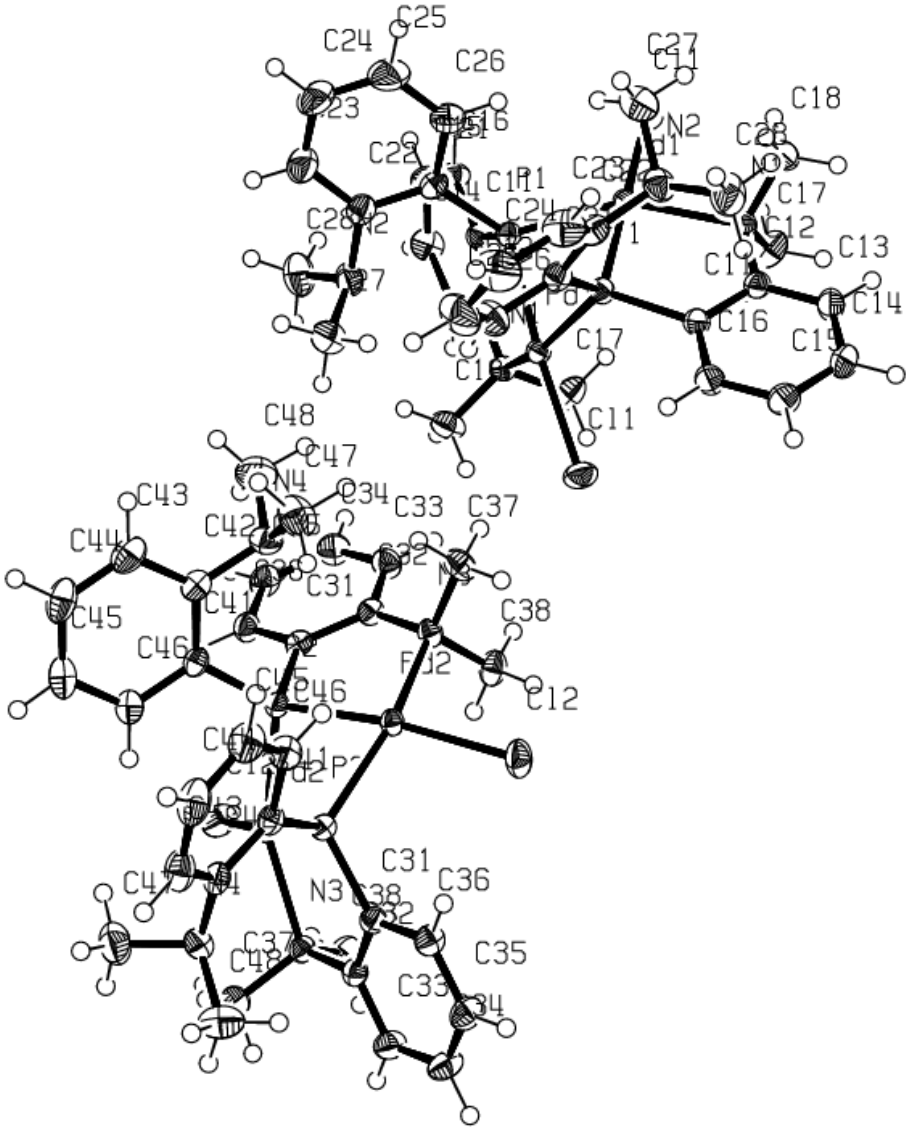

Figure A18. ORTEP diagram for ([κ^2-*NP*N]PdCl)$_2$ (**5-2**).

Table A19. Crystallographic Experimental Details for ([κ^2-*NP*N]PdOAc)$_2$·C_6H_6(**5-3**·C_6H_6).

A. Crystal Data	
formula	$C_{42}H_{52}N_4O_4P_2Pd_2$
formula weight	951.62
crystal dimensions (mm)	0.38 × 0.24 × 0.21
crystal system	triclinic
space group	$P\bar{1}$ (No. 2)
unit cell parameters	
a (Å)	11.7857 (15)
b (Å)	11.8320 (15)
c (Å)	15.682 (2)
α (deg)	91.9195 (18)
β (deg)	96.8964 (18)
γ (deg)	95.3691 (17)
V (Å^3)	2159.3 (5)
Z	2
ρ_{calcd} (g cm^{-3})	1.464
μ (mm^{-1})	0.951
B. Data Collection and Refinement Conditions	
diffractometer	Bruker PLATFORM/SMART 1000 CCD
radiation (λ [Å])	graphite-monochromated Mo Kα (0.71073)
temperature (°C)	–80
scan type	ω scans (0.4°) (10 s exposures)
data collection 2θ limit (deg)	52.84
total data collected	14929 (-14 ≤ h ≤ 14, -14 ≤ k ≤ 14, -19 ≤ l ≤ 19)
independent reflections	8723 (R_{int} = 0.0271)
number of observed reflections (*NO*)	6448 [$F_o^2 \geq 2\sigma(F_o^2)$]
structure solution method	Patterson search/structure expansion (*DIRDIF–99*)
refinement method	full-matrix least-squares on F^2 (*SHELXL–93*)
absorption correction method	Gaussian integration (face-indexed)
range of transmission factors	0.8253–0.7140
data/restraints/parameters	8723 [$F_o^2 \geq -3\sigma(F_o^2)$] / 0 / 435
goodness-of-fit (S)	0.946 [$F_o^2 \geq -3\sigma(F_o^2)$]
final R indices	
R_1 [$F_o^2 \geq 2\sigma(F_o^2)$]	0.0314
wR_2 [$F_o^2 \geq -3\sigma(F_o^2)$]	0.0759
largest difference peak and hole	0.516 and –0.280 e Å^{-3}

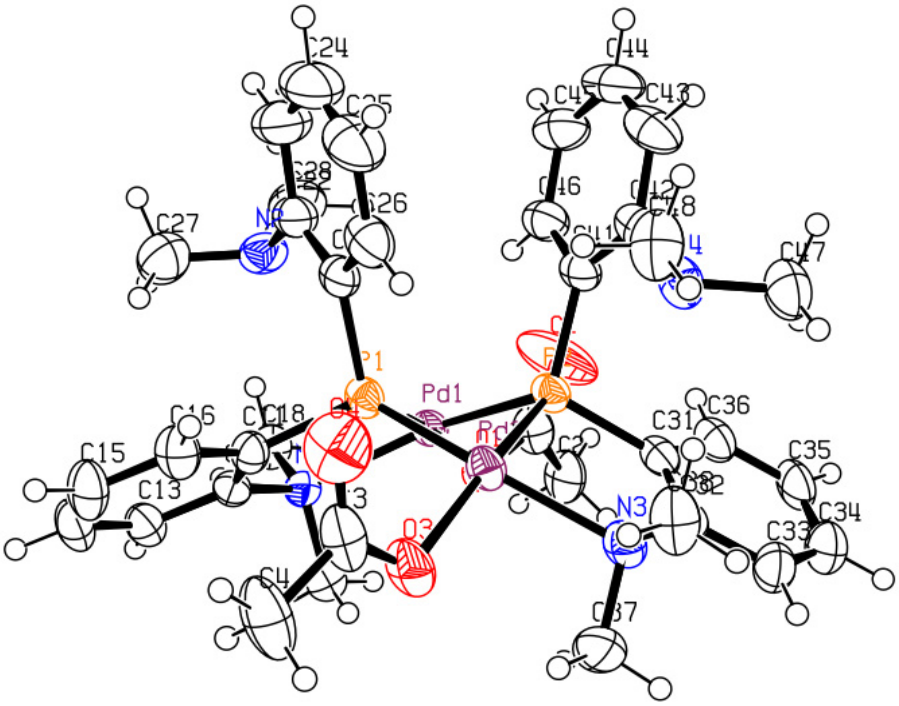

Figure A19. ORTEP diagram for $([\kappa^2\text{-}NP\text{N}]\text{PdOAc})_2 \cdot C_6H_6$ (**5-3**).

Table A20. Crystallographic Experimental Details for ([κ^1-N*P*N]Pd(η^3-C_3H_5))$_2$ (**5-5**).

A. Crystal Data	
formula	$C_{38}H_{50}N_4P_2Pd_2$
formula weight	837.56
crystal dimensions (mm)	0.32 × 0.16 × 0.08
crystal system	monoclinic
space group	$P2_1/n$ (an alternate setting of $P2_1/c$ [No. 14])
unit cell parameters	
a (Å)	9.8192 (4)
b (Å)	18.1484 (7)
c (Å)	20.4887 (8)
β (deg)	92.9071 (4)
V (Å^3)	3646.4 (2)
Z	4
ρ_{calcd} (g cm^{-3})	1.526
μ (mm^{-1})	1.106
B. Data Collection and Refinement Conditions	
diffractometer	Bruker D8/APEX II CCD
radiation (λ [Å])	graphite-monochromated Mo Kα (0.71073)
temperature (°C)	–100
scan type	ω scans (0.3°) (20 s exposures)
data collection 2θ limit (deg)	54.90
total data collected	31701 (-12 ≤ h ≤ 12, -23 ≤ k ≤ 23, -26 ≤ l ≤ 26)
independent reflections	8325 (R_{int} = 0.0304)
number of observed reflections (*NO*)	7184 [$F_o^2 \geq 2\sigma(F_o^2)$]
structure solution method	direct methods (*SHELXS–97*)
refinement method	full-matrix least-squares on F^2 (*SHELXL–97*)
absorption correction method	Gaussian integration (face-indexed)
range of transmission factors	0.9177–0.7198
data/restraints/parameters	8325 [$F_o^2 \geq -3\sigma(F_o^2)$] / 3[a] / 443
goodness-of-fit (S)	1.034 [$F_o^2 \geq -3\sigma(F_o^2)$]
final R indices	
R_1 [$F_o^2 \geq 2\sigma(F_o^2)$]	0.0227
wR_2 [$F_o^2 \geq -3\sigma(F_o^2)$]	0.0567
largest difference peak and hole	0.738 and –0.493 e Å^{-3}

[a] Distances within the two conformers of the disordered allyl group were constrained to be equal (within 0.01 Å) during refinement: d(C4A–C5A) = d(C4B–C5B); d(C5A–C6A)

= d(C5B–C6B); d(C4A…C6A) = d(C4B…C6B).

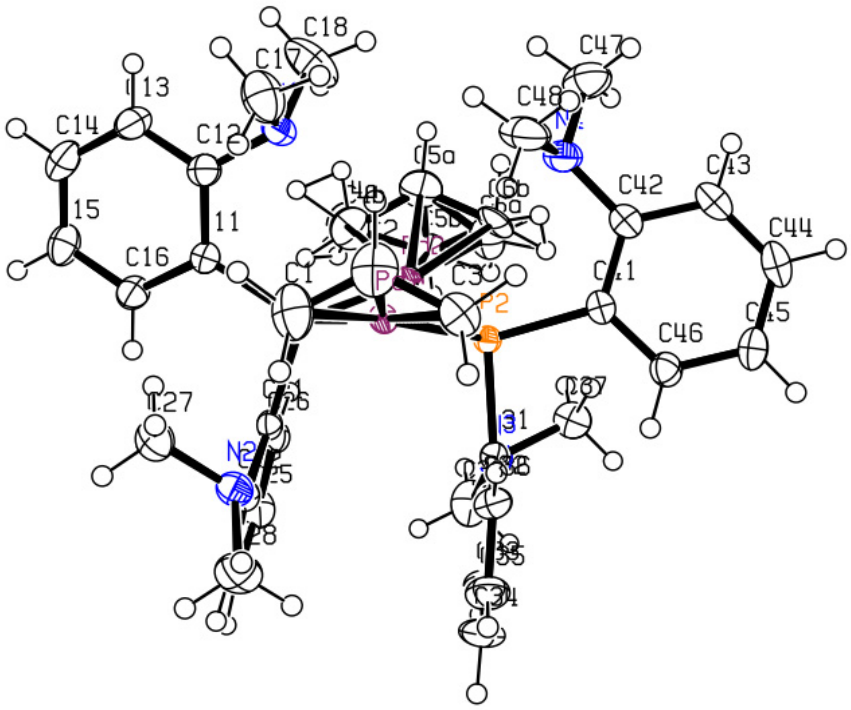

Figure A20. ORTEP diagram for ([κ^2-N*P*N]Pd(η^3-C_3H_5))$_2$ (**5-5**).

Table A21. Crystallographic Experimental Details for [N(P·BH_3)N]H (**5-7**).

A. Crystal Data	
formula	$C_{16}H_{24}BN_2P$
formula weight	286.15
crystal dimensions (mm)	0.54 × 0.09 × 0.08
crystal system	orthorhombic
space group	*Pbca* (No. 61)
unit cell parameters	
a (Å)	13.8992 (16)
b (Å)	14.8869 (17)
c (Å)	16.4172 (19)
V (Å^3)	3397.0 (7)
Z	8
ρcalcd (g cm^{-3})	1.119
μ (mm^{-1})	0.154
B. Data Collection and Refinement Conditions	
diffractometer	Bruker PLATFORM/SMART 1000 CCD
radiation (λ [Å])	graphite-monochromated Mo Kα (0.71073)
temperature (°C)	–80
scan type	ω scans (0.3°) (25 s exposures)
data collection 2θ limit (deg)	51.00
total data collected	23216 (-16 ≤ *h* ≤ 16, -18 ≤ *k* ≤ 18, -19 ≤ *l* ≤ 19)
independent reflections	3154 (R_{int} = 0.0915)
number of observed reflections (*NO*)	2074 [$F_o^2 \geq 2\sigma(F_o^2)$]
structure solution method	direct methods (*SHELXS–97*)
refinement method	full-matrix least-squares on F^2 (*SHELXL–97*)
absorption correction method	multi-scan (*SADABS*)
range of transmission factors	0.9878–0.9214
data/restraints/parameters	3154 [$F_o^2 \geq -3\sigma(F_o^2)$] / 8[a] / 209
goodness-of-fit (*S*)	1.012 [$F_o^2 \geq -3\sigma(F_o^2)$]
final *R* indices	
R_1 [$F_o^2 \geq 2\sigma(F_o^2)$]	0.0574
wR_2 [$F_o^2 \geq -3\sigma(F_o^2)$]	0.1550
largest difference peak and hole	0.308 and –0.211 e Å^{-3}

[a] The N1–C17A, N1–C18A, N1–C17B, N1–C18B, N2–C27A, N2–C28A, N2–C27B, and N2–C28B were constrained to be equal (within 0.05 Å) during refinement.

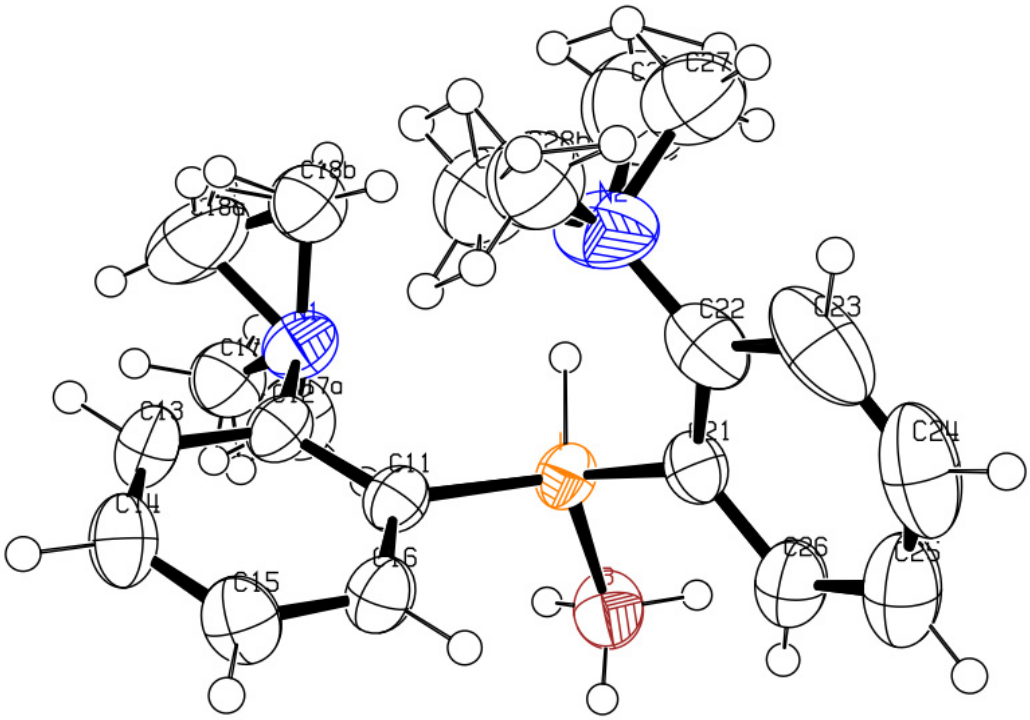

Figure A21. ORTEP diagram for [N(P·BH_3)N]H (**5-7**).

Appendix B: Computational Data

The study of four-coordinate, 14-electron [Cy-PSiP]RuX (X = amido, alkoxo) complexes described in Chapter 3 was complemented by DFT (TPSS/SDD+TZVP) studies of the structural and electronic features of the four-coordinate complexes **3-3**, **3-4**, and **3-6**. In addition, the mechanism of the activation of ammonia-borane by such low-coordinate [R-PSiP]RuX species was also studied computationally All computational studies were carried out by Dr. Sven Tobisch of the University of St. Andrews.

Structural Validation. In order to build more confidence in the applied computational methodology, optimized structures of complexes **3-3**, **3-4** and **3-6** were compared with available X-ray diffraction data. Figure B1 summarizes main structural aspects of the computed (singlet state) and X-ray geometries of the slightly distorted trigonal pyramidal four-coordinate complexes **3-3**, **3-4** and **3-6** featuring a *fac*-κ^3-[Cy-PSiP]Ru^{II} ligation.

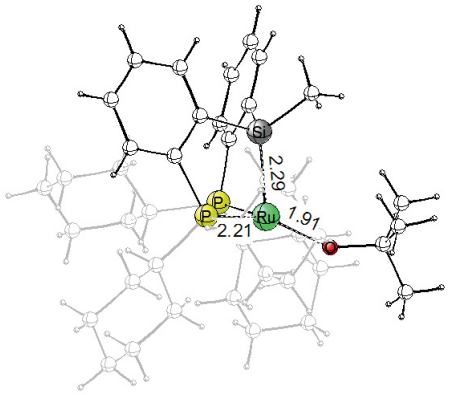

X-ray structure of **3-3**

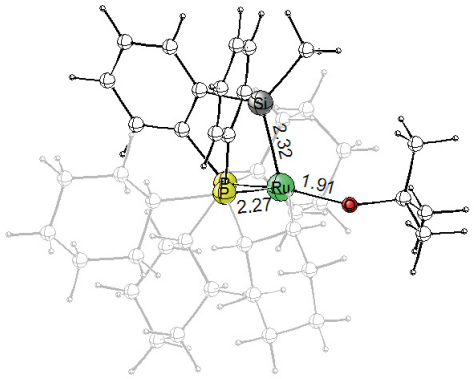

DFT optimised structure of **3-3**

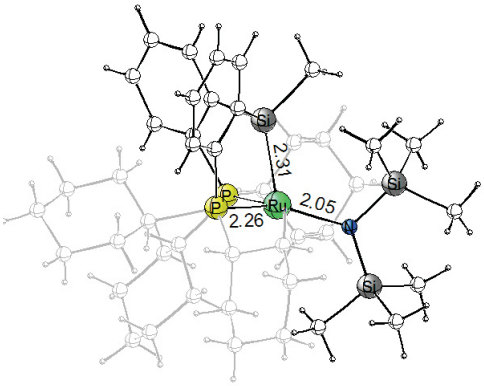

X-ray structure of **3-4**

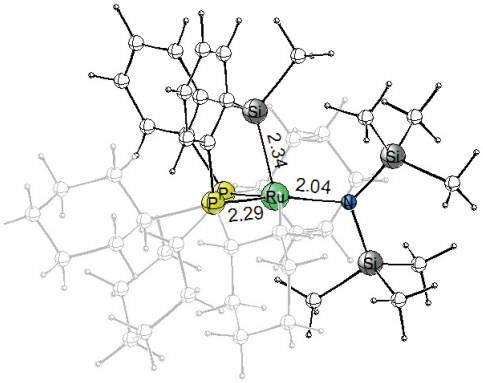

DFT optimised structure of **3-4**

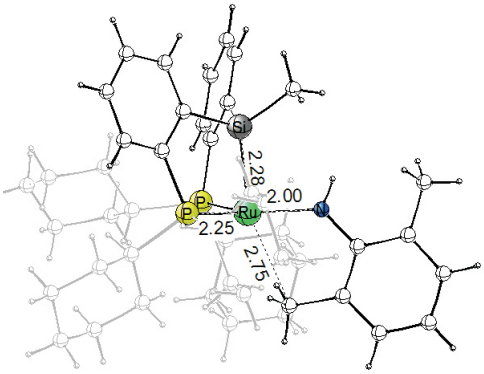

X-ray structure of **3-6**

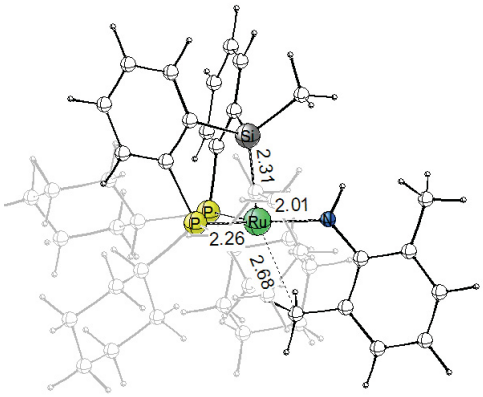

DFT optimised structure of **3-6**

Figure B1. DFT (singlet state) optimized and X-ray geometries of complexes **3-3**, **3-4** and **3-6**.

Singlet–Triplet Energy Gap – Comparison of Approximate DFT Methods. The accurate calculation of spin-state energetics can be a challenging task. As has been previously demonstrated in numerous benchmark applications, the amount of Hartree–Fock exchange included in a DFT functional critically determines its ability to reliably reproduce spin-state energy gaps. Specifically, hybrid functionals that include a variable portion of exact Hartee–Fock exchange (for instance, B3LYP with 20% exchange) tend to favor the higher spin state, whilst GGA functionals (for instance, BP86, PBE), which do not contain any exchange at all, favour the lower spin state. The known inadequacy of the B3LYP method to correctly describe relative energies of spin states of iron complexes led Reiher and co-workers[130a] to propose a modified B3LYP* functional, which has the amount of exchange reduced from 20%, as in the original parameterization, to 15%. It led to a significant improvement for a variety of iron complexes.[130b] Likewise, the TPSSh DFT method (i.e. TPSS with 10% exchange)[131-133] was recently reported to accurately describe spin-state energetics for transition metal complexes.[134] We have therefore compared two flavors of approximate DFT, the TPSS[131] and TPSSh functionals in conjunction with flexible basis sets of triple-ζ quality. Stationary points of **3-3**, **3-4** and **3-6** and their analogues described in Chapter 3 were located for the singlet and triplet spin states. Unrestricted calculations were performed in all cases to avoid singlet instabilities. In order to keep the calculations affordable, we started by examining the ΔE(S–T) gap at TPSS and TPSSh levels of approximation for (Me-PSiP)RuX model compounds **3-3'**, **3-4'**, and **3-6'**, where the PCy_2 ligand was substituted by PMe_2. Somewhat fortunately, TPSSh, which is deemed superior, and TPSS DFT methods predict singlet-triplet gaps that are almost identical (*cf.* Table B1), thereby reassuring one that both methods are

equally capable of adequately describing spin-state energetics for the herein studied four-coordinate 14-electron Ru^{II} complexes. We will therefore refer to the TPSS method for assessing the ΔE(S–T) gap for complexes **3-3**, **3-4**, **3-6** and related analogues.

Table B1. Assessed ΔE(S–T) gap [kcal mol^{-1}] for complexes **3-3'**, **3-4'** and **3-6'**

	3-3'	**3-4'**	**3-6'**
TPSS	30.4	27.7	29.2
TPSSh	29.7	27.4	28.4

Table B2. Assessed ΔE(S–T) gap (TPSS) [kcal mol^{-1}] for **3-4** and analogues

3-4	**3-4p**	**3-4c**	**3-4n**
24.2	23.6	22.7	20.5

Agostic C–H Interactions in Complex 3-6. As shown in Figure B1 the close contact between the methyl substituent on the anilido ligand and the vacant coordination site at the Ru center is indicative of a C–H agostic interaction. Further evidence of the existence of such an agostic interaction comes from an analysis of the bonding situation. It was performed with the aid of Wiberg bond orders (WBO) that are known to provide a good measure of the covalent bond order between interacting atoms. Agostic contacts between the C–H bonds involved and the Ru centre give rise to a diminished bond order (WBO(C–H) = 0.759 relative to 0.926 for a remote Me substituent) together with weak covalent Ru–H (WBO = 0.108) and Ru–C (WBO = 0.253) interactions.

The strength of the agostic C–H interaction was further assessed for the (Cy-PSiP)Ru(NH(2-MeC_6H_4)) model complex **3-6***, with an unsymmetrically substituted

anilido ligand, by comparison of the two isomers having the methyl substituent positioned proximal or distal to the vacant coordination site at Ru.

Table B3. Assessed strength of the C–H agostic interaction [kcal mol^{-1}] in (Cy-PSiP)Ru(NH(2-MeC_6H_4)) complex **3-6*** and analogues

3-6*	**3-6*p**	**3-6*c**	**3-6*n**
2.3	3.8	4.4	7.3

Table B4. Assessed NBO charge distribution of complexes **3-3**, **3-4**, **3-6** and analogues

complex	q_{Ru} [e]	q_{PXP} [e]	q_L [e]
3-6	–0.489	0.799	–0.310
3-6c	–0.207	0.527	–0.320
3-6p	–0.378	0.661	–0.283
3-6n	–0.088	0.332	–0.244
3-4	–0.433	0.849	–0.416
3-4c	–0.170	0.618	–0.447
3-4p	–0.341	0.726	–0.385
3-4n	–0.079	0.392	–0.313
3-3	–0.367	0.757	–0.390
3-3c	–0.102	0.520	–0.418
3-3p	–0.248	0.637	–0.390
3-3n	0.014	0.376	–0.391

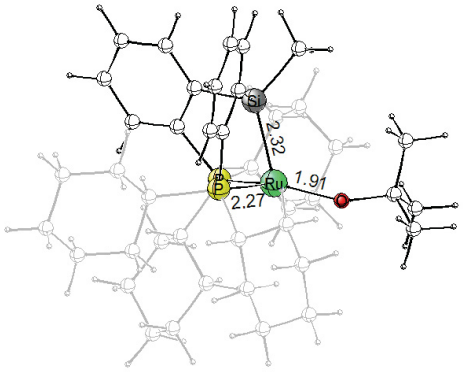

fac-κ^3 **3-3** (0.0)

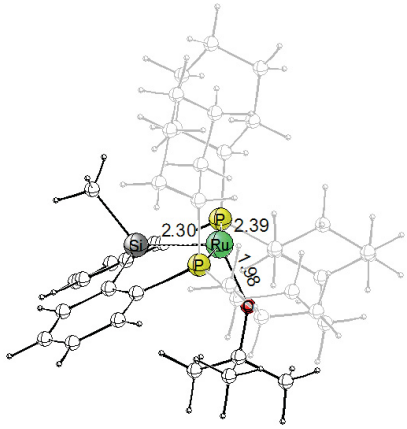

mer-κ^3 **3-3** (28.8)

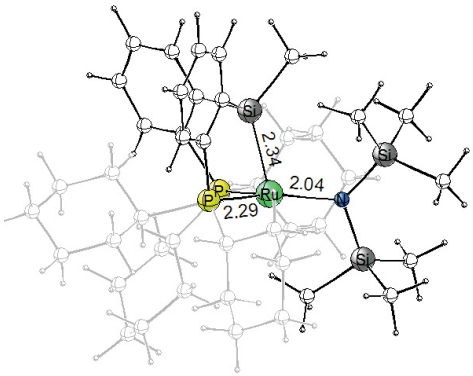

fac-κ^3 **3-4** (0.0)

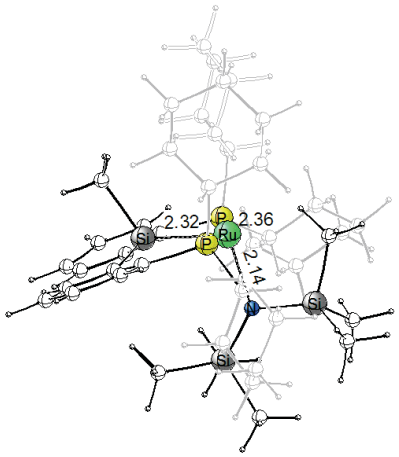

mer-κ^3 **3-4** (34.2)

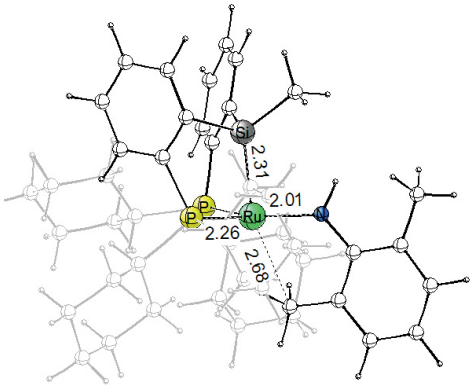

fac-κ^3 **3-6** (0.0)

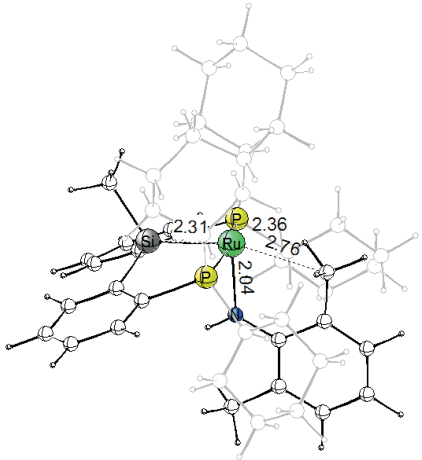

mer-κ^3 **3-6** (32.0)

Figure B2. DFT (singlet state) optimized geometry of *fac*-κ^3 and *mer*-κ^3-pincer–Ru^{II} forms of complexes **3-3**, **3-4** and **3-6**, together with relative stabilities [kcal mol^{-1}]

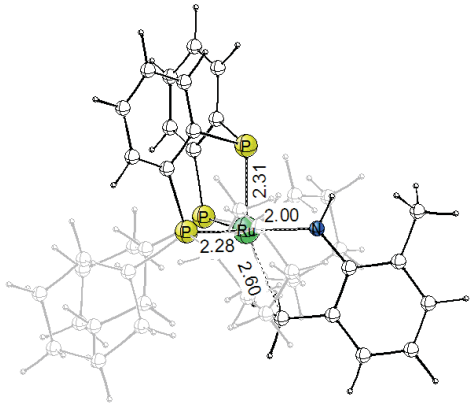

fac-κ^3 **3-6p** (0.0)

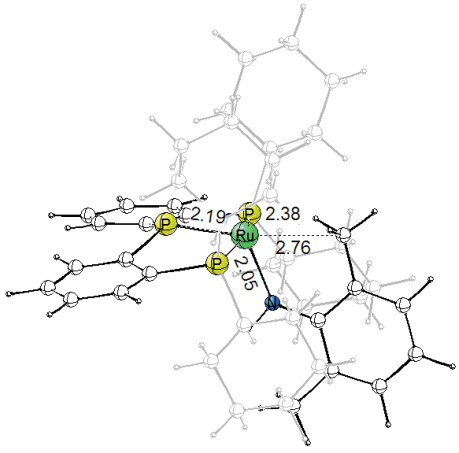

mer-κ^3 **3-6p** (25.3)

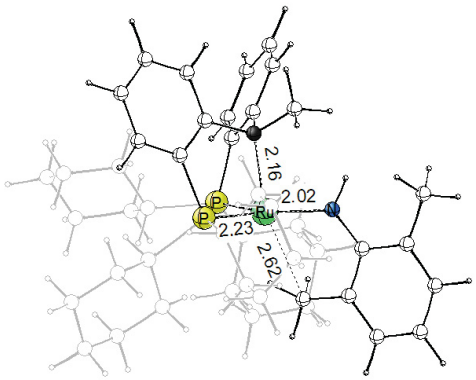

fac-κ^3 **3-6c** (0.0)

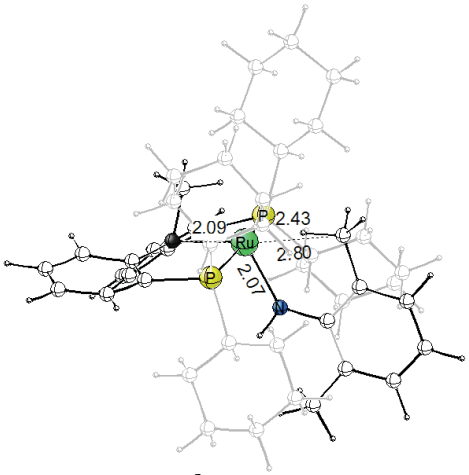

mer-κ^3 **3-6c** (17.5)

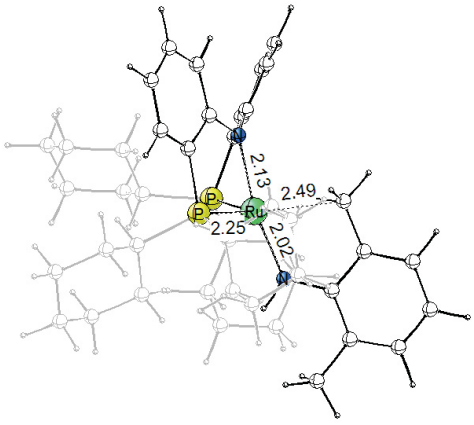

fac-κ^3 **3-6n** (0.0)

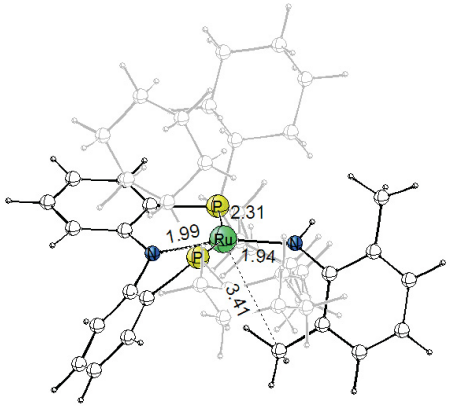

mer-κ^3 **3-6n** (10.8)

Figure B3. DFT (singlet state) optimized geometry of *fac*-κ^3 and *mer*-κ^3-pincer–Ru^{II} forms of analogues of **3-6**, together with relative stabilities [kcal mol^{-1}]

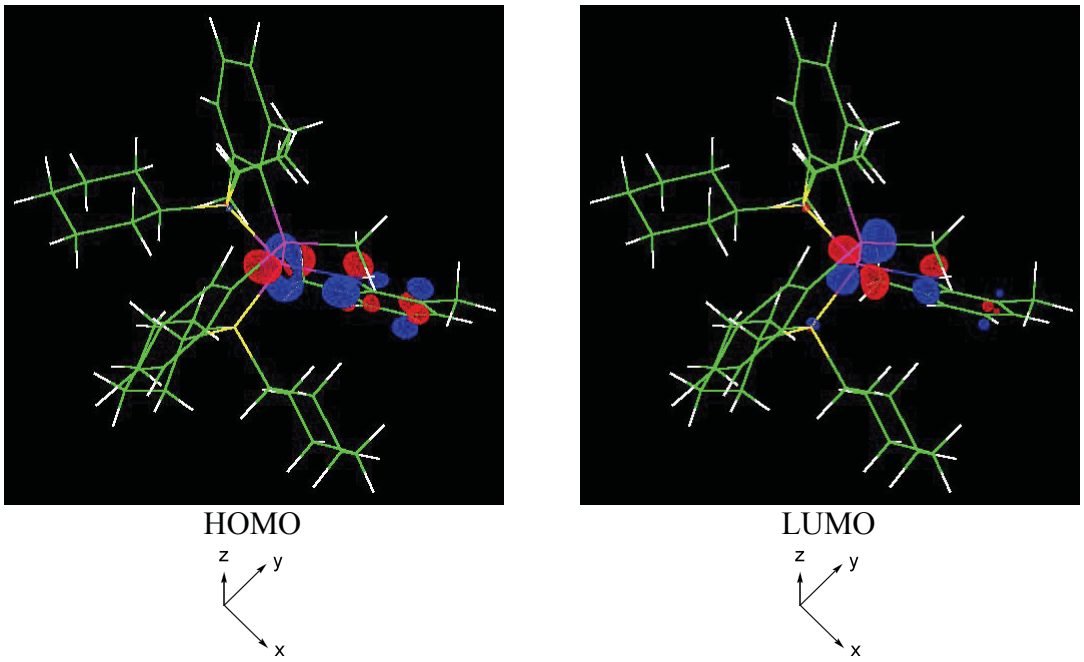

Figure B4. Shape of frontier orbitals of *fac*-κ^3-(Cy-PSiP)Ru(NH(2,6-$Me_2C_6H_3$)) **3-6** in the singlet state.

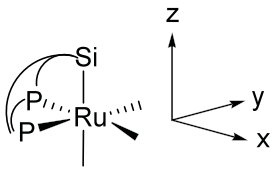

The HOMO features strong metal d_{xx-yy} character, together with a small metal d_{xz} component that is involved in some Ru–X π bonding. The LUMO is primarily d_{xy} in character and exhibits a Ru–X antibonding interaction.

Mechanism of $H_3B{\cdot}NH_3$ Activation by 3-4'. The four coordinate (Me-PSiP)RuN($SiMe_3$)$_2$ compound **3-4'** readily binds $H_3B{\cdot}NH_3$ to form the adduct **3-4'**·AB that features a weakly associated AB unit (d(Ru–N) = 2.772 Å) bound in an η^2-B-H fashion (Figure B5). Wiberg bond indices in **3-4'** support this view (Figure B6). Ammonia-borane association at the Ru^{II} centre does not involve a significant barrier[135a]

and is found to be somewhat uphill at the Δ*H* surface (Δ*H* = 2.7 kcal mol^{-1} relative to {**3-4'** + AB}) and even more so when free energies are considered (Figure B7).

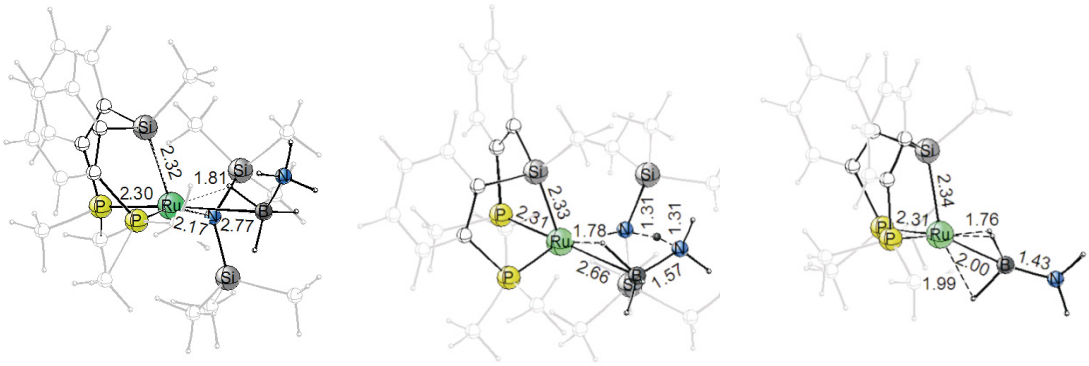

3-4'·AB TS[**3-4'**·AB–**3-13'**·HX] **3-13'**

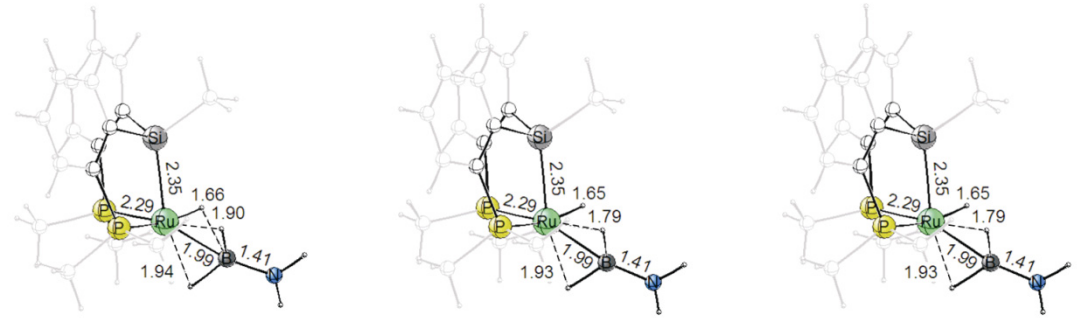

TS[**3-13'**–**3-10'**] **3-10'** (*fac*-κ^3-pincer–Ru^{II}) **3-10'** (*mer*-κ^3-pincer–Ru^{II})

Figure B5. Selected metric parameters (Å) of the optimized structures of key stationary points for consecutive N–H and B–H bond activation of ammonia-borane (AB) by the four-coordinate (Me-PSiP)RuN(SiMe$_3$)$_2$ complex **3-4'** (*cf*. route A in Scheme 3-3).

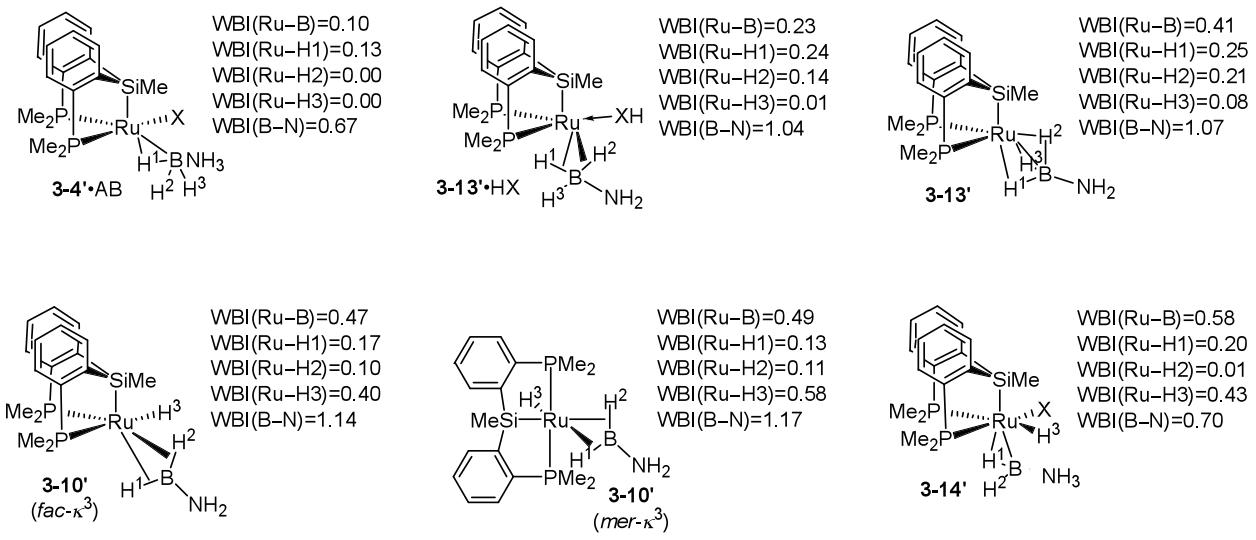

Figure B6. Wiberg bond indices for Ru and B centers in the compounds shown in Scheme 3-3 (X = $N(SiMe_3)_2$).

Focusing on route A (Scheme 3-3), protonolytic Ru–N(amido) bond cleavage via N–H bond activation proceeds whilst traversing a metathesis-type transition state (TS) structure TS[**3-4'**·AB–**3-13'**·HX] featuring the concomitant N(ammonia)–H bond rupture and N(amido)–H bond formation together with strengthened/weakened B(borane)–N(ammonia) and Ru–N(amido) bonds, respectively (Figure B7). Because the increase in strength for several bonds overcompensates for partially attenuated bonds in TS[**3-4'**·AB–**3-13'**·HX], it comes as no surprise that the TS is low in free energy and only 2.0 kcal mol^{-1} above {**3-4'** + AB}. The initially formed intermediate **3-13'**·HX is stabilized thereafter through $HN(SiMe_3)_2$ release. The kinetically facile ammonia-borane N–H activation is moreover driven by a thermodynamic force of substantial magnitude (ΔG = 41.6 kcal mol^{-1}) and can thus be expected to furnish **3-13'** instantaneously in an irreversible fashion (Figure B7).

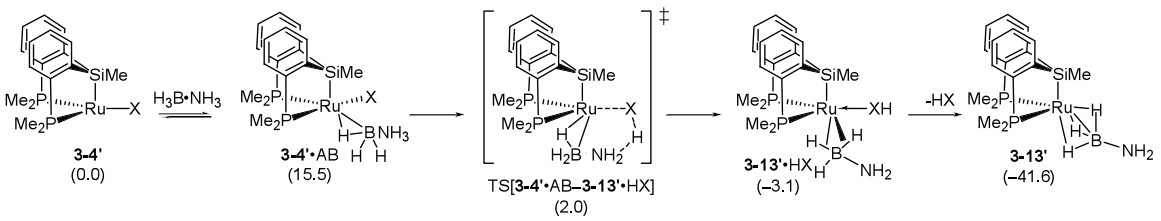

Figure B7. Free energies (kcal mol^{-1}) associated with the most accessible pathway for protonolytic Ru^{II}–N(amido) bond cleavage by ammonia-borane N–H activation in **3-4'**·AB (X = N(SiMe$_3$)$_2$).[135b]

Given the substantial energy gap between **3-13'**·HX and **3-13',** borane oxidative addition at the Ru^{II} centre preferably proceeds from **3-13'**, whereas a pathway commencing from **3-13'**·HX via key structures having the HN(SiMe$_3$)$_2$ molecule weakly associated is found to be less favorable. Borane B–H bond oxidative addition is moderately exergonic and has a rather small activation barrier to overcome in the process of traversing TS[**3-13'**–**3-10'**] (Figure B8). Although all the key species involved along the most accessible pathway for consecutive N–H and B–H bond activation adopt a *fac*-κ^3-(Me-PSiP)Ru^{II} ligation, *fac*-κ^3 and *mer*-κ^3 forms of **3-10'** are energetically close, with the latter being somewhat more stable.

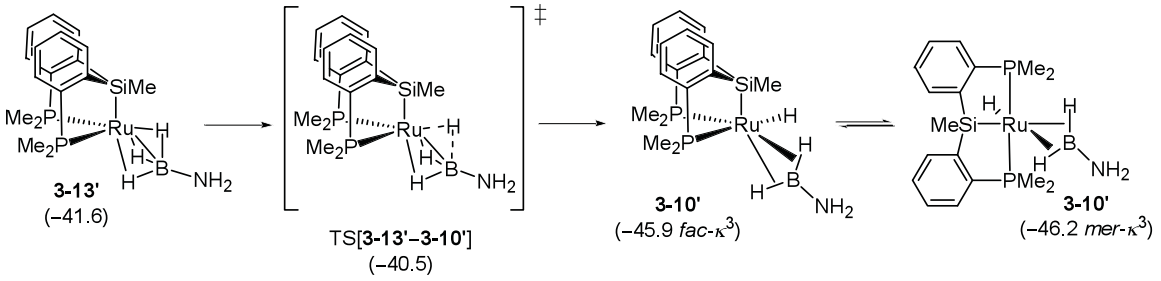

Figure B8. Free energies (kcal mol^{-1}) associated with the most accessible pathway for B–H oxidative addition of the H$_3$B–NH$_2$ fragment in **3-13'**.[135b]

The alternate route that initiates through borane oxidative addition to the Ru^{II} centre in **3-4'**·AB has a prohibitively high barrier of 33.1 kcal mol^{-1} to overcome (Figure B9) and is thus at odds with the observed smooth activation of ammonia-borane by **3-4**.

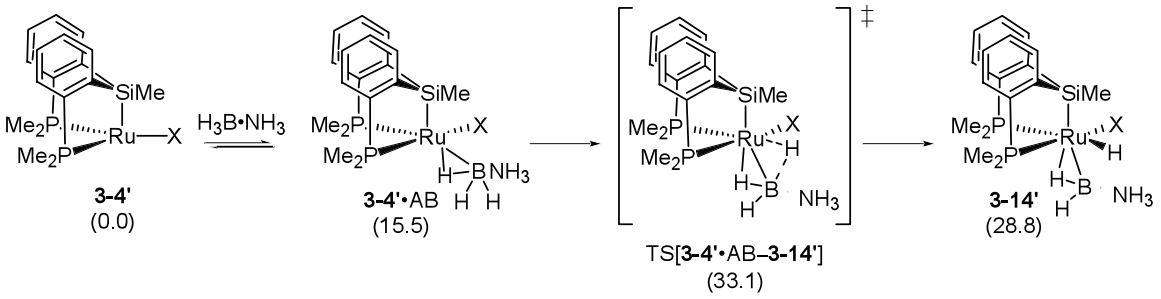

Figure B9. Free energies (kcal mol^{-1}) associated with the most accessible pathway for B–H oxidative addition of ammonia-borane in **3-4'**·AB (with X = $N(SiMe_3)_2$).[135b]

Optimized structures and total electronic energies (hartree) of all species described.

$H_3B–NH_3$

E = -83.264425

N	0,8344	-0,0001	0,2289
B	-0,7750	0,0001	-0,2123
H	1,4434	-0,0273	-0,5905
H	1,0603	-0,8105	0,8084
H	1,0730	0,8371	0,7631
H	-1,3799	0,0343	0,8371
H	-0,9225	-1,0320	-0,8302
H	-0,9064	0,9983	-0,8871

$HN(SiMe_3)_2$

E = -874.147612

Si	-1,6070	0,0770	0,2374
N	0,0386	0,7137	0,2197
Si	1,6131	0,0369	-0,2020
C	-1,9527	-0,9421	1,8039
C	-1,9010	-1,0260	-1,2787
C	-2,7787	1,5697	0,1994
H	0,0947	1,6814	0,5290
C	1,8694	-0,0320	-2,0835
C	1,7879	-1,7194	0,4969
C	2,9235	1,1770	0,5631
H	-2,6453	2,1569	-0,7167
H	-2,6054	2,2357	1,0542
H	-3,8268	1,2494	0,2430
H	-1,7971	-0,3377	2,7058
H	-1,2874	-1,8115	1,8694
H	-2,9862	-1,3113	1,8206
H	-1,2215	-1,8866	-1,2984
H	-1,7611	-0,4659	-2,2102
H	-2,9247	-1,4209	-1,2718
H	1,0271	-2,3981	0,0927
H	1,6939	-1,7230	1,5888
H	2,7682	-2,1404	0,2403
H	1,7775	0,9665	-2,5274
H	1,1254	-0,6781	-2,5647
H	2,8632	-0,4231	-2,3365
H	2,8344	1,2085	1,6554
H	2,8308	2,2039	0,1874
H	3,9356	0,8313	0,3197

3-4'

E = -2602.851864

Ru	0,0029	-0,5798	-0,3748
P	-1,3457	-0,8189	1,3993
P	-1,6578	-0,3694	-1,8965
Si	-0,4577	1,6831	-0,0200
C	0,6777	3,1487	-0,5133
H	0,1765	4,0966	-0,2735
H	0,8603	3,1461	-1,5940
H	1,6452	3,1386	-0,0046
C	-0,8697	1,8684	1,8514
C	-1,3239	0,6929	2,4793
C	-1,7201	0,6956	3,8223
H	-2,0759	-0,2139	4,3025
C	-1,6484	1,8756	4,5649
H	-1,9442	1,8775	5,6112
C	-1,1888	3,0493	3,9618
H	-1,1259	3,9670	4,5423
C	-0,8106	3,0444	2,6172
H	-0,4551	3,9686	2,1655
C	-2,1271	2,1347	-0,9024
C	-2,6810	1,1662	-1,7574
C	-3,8842	1,3957	-2,4401
H	-4,3041	0,6416	-3,1028
C	-4,5589	2,6038	-2,2635
H	-5,4979	2,7836	-2,7814
C	-4,0243	3,5809	-1,4176
H	-4,5527	4,5209	-1,2754
C	-2,8187	3,3495	-0,7534
H	-2,4222	4,1228	-0,0979
C	-0,7208	-2,1684	2,5284
C	-3,1659	-1,2451	1,3812
C	-2,9075	-1,7220	-2,2178
C	-0,9338	-0,2175	-3,6150
Si	3,3301	0,1304	0,1864
Si	2,2207	-2,6267	-0,7360
N	1,9972	-0,9407	-0,2727

C	4,9419	-0,8048	0,6136
C	2,9107	1,0975	1,7646
C	3,7627	1,2798	-1,2652
C	3,3697	-2,8467	-2,2369
C	0,5072	-3,3186	-1,2515
C	2,8499	-3,7332	0,6804
H	2,8810	1,7991	-1,6515
H	4,1904	0,6936	-2,0885
H	4,5042	2,0345	-0,9734
H	2,8674	0,4096	2,6185
H	1,9465	1,6107	1,7146
H	3,6866	1,8438	1,9795
H	5,3002	-1,4533	-0,1939
H	4,8357	-1,4149	1,5179
H	5,7331	-0,0685	0,8101
H	4,4042	-2,5612	-2,0178
H	3,0254	-2,2373	-3,0808
H	3,3778	-3,8963	-2,5595
H	2,2040	-3,6524	1,5625
H	3,8689	-3,4748	0,9856
H	2,8553	-4,7849	0,3640
H	0,3194	-3,1871	-2,3225
H	-0,3397	-2,8571	-0,7042
H	0,4589	-4,3936	-1,0306
H	-3,3083	-2,2288	0,9232
H	-3,7086	-0,4927	0,8025
H	-3,5637	-1,2647	2,4012
H	0,3171	-1,9534	2,7924
H	-0,7621	-3,1260	2,0006
H	-1,3249	-2,2390	3,4396
H	-3,6011	-1,8022	-1,3784
H	-2,3779	-2,6721	-2,3324
H	-3,4743	-1,5236	-3,1335
H	-0,3878	-1,1332	-3,8623
H	-0,2357	0,6228	-3,6328
H	-1,7213	-0,0512	-4,3582

3-4'–AB

E = -2686.113372

Ru	0,1334	-0,4974	0,4304
P	-1,6715	-0,4541	-0,9889
P	-1,0491	-0,6751	2,3728
Si	-0,4469	1,7360	0,6950
C	0,8550	3,0793	1,1354
H	0,3797	4,0639	1,2405
H	1,3360	2,8581	2,0972
H	1,6343	3,1596	0,3710
C	-1,3761	2,3081	-0,8832
C	-1,9800	1,2710	-1,6175
C	-2,7676	1,5522	-2,7408
H	-3,2401	0,7520	-3,3064
C	-2,9410	2,8727	-3,1588
H	-3,5409	3,0882	-4,0397
C	-2,3356	3,9122	-2,4492
H	-2,4618	4,9406	-2,7801
C	-1,5682	3,6295	-1,3177
H	-1,1037	4,4520	-0,7767
C	-1,8302	1,9203	2,0486
C	-2,1721	0,7530	2,7546
C	-3,2046	0,7493	3,7031
H	-3,4628	-0,1588	4,2448
C	-3,9171	1,9221	3,9550
H	-4,7282	1,9223	4,6791
C	-3,5845	3,0966	3,2723
H	-4,1391	4,0117	3,4688
C	-2,5509	3,0936	2,3344
H	-2,3204	4,0158	1,8036
C	-1,5809	-1,4668	-2,5436
C	-3,3935	-0,9257	-0,4354
C	-2,0875	-2,2062	2,6440
C	-0,1264	-0,7244	4,0147
Si	2,3786	0,1371	-2,1702
Si	1,7055	-2,7127	-1,2515
N	1,4231	-0,9896	-1,2454
C	3,4237	-0,7086	-3,5349
C	1,3357	1,4202	-3,1168
C	3,6387	1,1369	-1,1304

3-13'-HX

E = -2686.143766

Ru	0,2656	-0,7616	-0,6585
P	-1,2455	-0,9254	1,1365
P	-1,3132	-0,6455	-2,2573
Si	-0,3944	1,5484	-0,3388
C	0,4933	3,1685	-0,8833
H	-0,1376	4,0353	-0,6445
H	0,6455	3,1706	-1,9690
H	1,4663	3,3194	-0,4082
C	-0,8504	1,7795	1,5279
C	-1,2695	0,6083	2,1939
C	-1,6929	0,6484	3,5286
H	-2,0223	-0,2553	4,0369
C	-1,6753	1,8557	4,2304
H	-1,9855	1,8831	5,2723
C	-1,2516	3,0234	3,5915
H	-1,2310	3,9637	4,1382
C	-0,8548	2,9834	2,2523
H	-0,5325	3,9050	1,7707
C	-2,1224	1,7622	-1,2044
C	-2,5448	0,7228	-2,0511
C	-3,7761	0,7785	-2,7206
H	-4,0931	-0,0293	-3,3765
C	-4,6121	1,8805	-2,5398
H	-5,5723	1,9239	-3,0483
C	-4,2115	2,9260	-1,7016
H	-4,8640	3,7843	-1,5575
C	-2,9794	2,8662	-1,0488
H	-2,6896	3,6866	-0,3944
C	-1,1294	-2,3260	2,3699
C	-3,0749	-1,1302	0,7961
C	-2,3679	-2,1360	-2,6630
C	-0,6431	-0,2173	-3,9462
Si	3,5140	0,7474	0,2779
Si	2,7402	-1,7775	2,0308
N	2,5338	-0,7613	0,5443
C	5,3857	0,4417	0,4871
C	3,0118	2,0464	1,5580
C	3,3545	1,3008	-1,5232

3-13'

E = -1812.024423

Ru	1,2107	-1,2122	-0,3090
P	-0,1484	-1,3279	1,5444
P	-0,3767	-1,0149	-1,9754
Si	0,8565	1,0867	-0,0443
C	2,2879	2,3110	-0,3881
H	1,9818	3,3557	-0,2442
H	2,6391	2,2066	-1,4211
H	3,1336	2,1100	0,2794
C	0,2461	1,4123	1,7584
C	-0,2341	0,2894	2,4598
C	-0,7411	0,4116	3,7609
H	-1,1152	-0,4589	4,2969
C	-0,7583	1,6570	4,3893
H	-1,1414	1,7502	5,4027
C	-0,2745	2,7807	3,7138
H	-0,2802	3,7519	4,2037
C	0,2171	2,6560	2,4134
H	0,5915	3,5437	1,9063
C	-0,6216	1,6326	-1,1740
C	-1,1898	0,6558	-2,0158
C	-2,2713	0,9644	-2,8550
H	-2,7044	0,2060	-3,5041
C	-2,8033	2,2533	-2,8638
H	-3,6442	2,4909	-3,5109
C	-2,2510	3,2367	-2,0373
H	-2,6644	4,2429	-2,0412
C	-1,1731	2,9262	-1,2077
H	-0,7619	3,7053	-0,5679
C	0,4931	-2,5198	2,8256
C	-1,9476	-1,8296	1,5084
C	-1,7979	-2,2118	-2,1745
C	0,3571	-1,1371	-3,6872
H	1,5165	-2,2378	3,0835
H	0,5029	-3,5251	2,3940
H	-0,1271	-2,5215	3,7283
H	-2,4725	-2,1396	-1,3191
H	-1,3874	-3,2255	-2,2126
H	-2,3614	-2,0230	-3,0944

C	3,4624	-3,3088	-0,7829
C	0,5520	-3,5140	0,0609
C	1,3582	-3,5951	-2,9162
H	3,1538	1,6546	-0,2945
H	4,4121	0,4810	-0,7147
H	4,1341	1,8948	-1,7522
H	0,6250	0,9376	-3,7986
H	0,7625	2,0778	-2,4573
H	1,9979	2,0512	-3,7252
H	4,0964	-1,4858	-3,1569
H	2,7932	-1,1555	-4,3122
H	4,0470	0,0544	-4,0203
H	4,2325	-2,9113	-1,4535
H	3,7235	-3,0184	0,2394
H	3,5071	-4,4053	-0,8473
H	0,3646	-3,3836	-3,3236
H	2,0962	-3,3120	-3,6748
H	1,4376	-4,6820	-2,7761
H	1,0116	-3,5017	1,0557
H	-0,4262	-3,0126	0,1362
H	0,3526	-4,5624	-0,1990
H	-3,4371	-2,0015	-0,2387
H	-3,6584	-0,3766	0,4710
H	-4,1130	-0,6812	-1,2234
H	-0,6689	-1,2091	-3,0813
H	-1,5409	-2,5239	-2,2685
H	-2,4607	-1,2968	-3,1720
H	-2,8497	-2,2913	1,8689
H	-1,4315	-3,0797	2,5879
H	-2,5710	-2,1888	3,6259
H	0,6555	-1,4878	3,9880
H	0,3071	0,2647	4,2001
H	-0,8217	-0,9371	4,8329
N	3,0135	0,2397	3,0188
B	2,5270	-0,7657	1,8026
H	2,2679	0,4218	3,6949
H	3,3230	1,1386	2,6424
H	3,7997	-0,1717	3,5260
H	1,6848	-0,0265	1,2419
H	3,4829	-0,8897	1,0941
H	2,1341	-1,7749	2,3238
C	4,5572	-2,1286	2,4869
C	2,0256	-3,4930	1,6551
C	1,9808	-0,8937	3,5237
H	2,3225	1,4570	-1,8382
H	3,7956	0,5417	-2,1813
H	3,9177	2,2325	-1,6664
H	3,4424	1,8046	2,5370
H	1,9284	2,1280	1,6792
H	3,3998	3,0304	1,2673
H	5,7291	-0,4187	-0,0987
H	5,6991	0,2926	1,5240
H	5,9173	1,3250	0,1079
H	5,0748	-1,2668	2,9189
H	5,1432	-2,4839	1,6320
H	4,5648	-2,9266	3,2423
H	1,0296	-0,4017	3,3058
H	2,6709	-0,1253	3,8908
H	1,8235	-1,6036	4,3455
H	2,7089	-4,0247	0,9811
H	1,0478	-3,4622	1,1720
H	1,9467	-4,0831	2,5767
H	-3,2532	-2,1179	0,3595
H	-3,4266	-0,3595	0,1092
H	-3,6262	-1,0530	1,7386
H	-0,1804	-2,3183	2,9047
H	-1,2159	-3,2667	1,8194
H	-1,9515	-2,2643	3,0902
H	-3,0849	-2,3113	-1,8587
H	-1,7263	-3,0180	-2,7431
H	-2,9079	-2,0015	-3,6061
H	0,1388	-0,9271	-4,2278
H	-0,2091	0,7839	-3,8897
H	-1,4493	-0,2197	-4,6875
N	1,2409	-2,8768	-3,1549
B	1,5192	-2,1704	-1,9145
H	0,3174	-3,1100	-3,4916
H	1,9692	-3,3837	-3,6377
H	2,7864	-1,3866	-0,2374
H	1,3749	-0,7485	-1,9875
H	2,6861	-2,3159	-1,6015
H	0,6875	-2,4909	-0,9185
H	-2,0370	-2,8371	1,0909
H	-2,5039	-1,1290	0,8802
H	-2,3747	-1,8169	2,5165
H	0,7981	-2,1307	-3,8133
H	1,1467	-0,3885	-3,7847
H	-0,4027	-0,9713	-4,4580
N	4,3887	-2,4328	-0,6091
B	3,0179	-2,0575	-0,4996
H	5,1424	-1,7589	-0,6052
H	4,6995	-3,3850	-0,4810
H	2,6400	-1,2589	0,6647
H	2,1255	-2,9738	-0,5042
H	2,5748	-1,1115	-1,4183

TS[**3-4'-AB–3-13'-HX**]

E = -2686.141863

Ru	0,0891	-0,7235	0,4483
P	-1,5475	0,0031	-1,0067
P	-1,3192	-1,7124	1,9288
Si	-0,5816	1,1926	1,5864
C	0,5632	2,0876	2,8333
H	0,0477	2,9427	3,2907
H	0,8376	1,3999	3,6415
H	1,4844	2,4522	2,3697
C	-1,1934	2,4459	0,2605
C	-1,6611	1,8631	-0,9354
C	-2,1899	2,6557	-1,9615
H	-2,5541	2,2056	-2,8825
C	-2,2354	4,0443	-1,8183
H	-2,6282	4,6597	-2,6241
C	-1,7679	4,6383	-0,6440
H	-1,7978	5,7201	-0,5340
C	-1,2614	3,8430	0,3868
H	-0,9032	4,3232	1,2960
C	-2,1865	0,7981	2,6057
C	-2,5433	-0,5586	2,7117
C	-3,6922	-0,9574	3,4104
H	-3,9603	-2,0090	3,4909
C	-4,5095	0,0044	4,0050
H	-5,4087	-0,2983	4,5362
C	-4,1689	1,3581	3,9149
H	-4,8062	2,1080	4,3784
C	-3,0173	1,7468	3,2279
H	-2,7749	2,8061	3,1640
C	-1,4292	-0,3664	-2,8305
C	-3,3480	-0,4517	-0,7823
C	-2,3170	-3,1821	1,3566

3-10' (*fac*-κ^3)

E = -1812.031337

Ru	1,1635	-1,2904	-0,2119
P	-0,4587	-0,9173	-1,7836
P	-0,1168	-1,4307	1,7631
Si	0,9634	1,0286	0,0946
C	2,5100	2,0929	0,4674
H	2,2571	3,1515	0,6131
H	3,0052	1,7419	1,3801
H	3,2293	2,0239	-0,3564
C	0,1083	1,7808	-1,4646
C	-0,5594	0,8649	-2,3011
C	-1,2564	1,2964	-3,4381
H	-1,7763	0,5839	-4,0764
C	-1,2781	2,6514	-3,7703
H	-1,8090	2,9859	-4,6584
C	-0,6082	3,5735	-2,9613
H	-0,6167	4,6295	-3,2225
C	0,0706	3,1401	-1,8211
H	0,5858	3,8757	-1,2059
C	-0,2856	1,3492	1,5444
C	-0,7809	0,2370	2,2559
C	-1,6935	0,4044	3,3091
H	-2,0701	-0,4563	3,8581
C	-2,1296	1,6798	3,6659
H	-2,8407	1,8046	4,4792
C	-1,6474	2,7944	2,9737
H	-1,9845	3,7916	3,2478
C	-0,7360	2,6250	1,9311
H	-0,3771	3,5060	1,4015
C	-0,1462	-1,8316	-3,3746
C	-2,2574	-1,3324	-1,5065
C	-1,5791	-2,5736	1,9926

3-10' (*mer*-κ^3)

E = -1812.033319

Ru	1,4364	0,0032	-0,1442
H	0,6172	0,5276	-1,4445
P	0,8615	-1,9991	-1,1357
Si	-0,7325	-0,1872	0,7667
P	1,1362	2,2382	0,4171
C	-0,9330	-0,8210	2,5718
C	-0,9783	-2,2707	-1,1481
C	-1,7420	-1,4418	-0,3012
C	-3,1313	-1,6573	-0,2606
C	-3,7418	-2,6368	-1,0448
C	-2,9680	-3,4459	-1,8804
C	-1,5856	-3,2693	-1,9236
H	-3,7556	-1,0521	0,3929
H	-4,8201	-2,7726	-1,0043
H	-3,4384	-4,2117	-2,4922
H	-0,9886	-3,9095	-2,5704
C	-0,6601	2,6550	0,6406
C	-1,5465	1,5668	0,7780
C	-2,9068	1,8597	0,9844
C	-3,3732	3,1743	1,0310
C	-2,4788	4,2388	0,8917
C	-1,1215	3,9782	0,7062
H	-3,6228	1,0507	1,1092
H	-4,4329	3,3711	1,1784
H	-2,8366	5,2648	0,9298
H	-0,4299	4,8123	0,6062
H	-0,5126	-1,8283	2,6770
H	-0,4111	-0,1619	3,2756
H	-1,9894	-0,8632	2,8690
C	1,7290	3,4771	-0,8397
C	1,9042	2,9278	1,9724

C	-0,5420	-2,4693	3,4441
H	-0,5100	0,0556	-3,2361
H	-1,4092	-1,4524	-2,9591
H	-2,2895	0,0356	-3,3749
H	-2,9797	-2,9042	0,5360
H	-1,6188	-3,9472	1,0040
H	-2,9103	-3,5994	2,1771
H	-3,4976	-1,5027	-1,0483
H	-3,6526	-0,2914	0,2542
H	-3,9649	0,1709	-1,4383
H	0,1761	-3,2378	3,1478
H	-0,0092	-1,6968	4,0018
H	-1,3210	-2,9067	4,0777
N	3,3858	-0,9299	1,0697
B	2,1962	-1,6624	1,7778
H	2,7507	-0,6011	-0,0321
H	4,1839	-1,5359	0,8851
H	3,7300	-0,1246	1,5914
H	1,9169	-2,6795	1,1767
H	2,3460	-1,8368	2,9656
H	1,2511	-0,7771	1,7899
Si	2,4975	1,1163	-1,6835
Si	2,0035	-1,9192	-1,9544
N	1,8782	-0,4116	-0,9956
C	4,2941	0,8702	-2,2906
C	1,5210	1,8512	-3,1388
C	2,5802	2,4517	-0,3411
C	3,6677	-2,8032	-1,6583
C	0,6318	-3,1421	-1,4251
C	1,9067	-1,7009	-3,8483
H	1,5818	2,7548	-0,0126
H	3,1458	2,1224	0,5375
H	3,0827	3,3406	-0,7434
H	1,4558	1,1739	-3,9971
H	0,5094	2,1514	-2,8486
H	2,0450	2,7554	-3,4765
H	4,9428	0,5082	-1,4836
H	4,3768	0,1647	-3,1252
H	4,7017	1,8304	-2,6334
H	4,5311	-2,1587	-1,8590
H	3,7475	-3,1886	-0,6359
H	3,7375	-3,6651	-2,3355
H	0,9607	-1,2792	-4,2002
H	2,7193	-1,0784	-4,2389
H	2,0112	-2,6944	-4,3057
H	1,0512	-3,9727	-0,8480
H	-0,1446	-2,6668	-0,7932
H	0,1125	-3,5561	-2,2992

C	0,8723	-1,9071	3,2742
H	0,8371	-1,5436	-3,7522
H	-0,1438	-2,9054	-3,1646
H	-0,9118	-1,6126	-4,1264
H	-2,3708	-2,3105	1,2880
H	-1,2473	-3,5945	1,7792
H	-1,9770	-2,5365	3,0123
H	-2,3514	-2,3992	-1,2826
H	-2,6323	-0,7522	-0,6593
H	-2,8554	-1,0945	-2,3923
H	1,2446	-2,9285	3,1486
H	1,7262	-1,2309	3,3614
H	0,2660	-1,8467	4,1842
N	4,0872	-2,9577	-0,5278
B	2,8098	-2,4130	-0,3021
H	4,2353	-3,7829	-1,0924
H	4,9406	-2,4690	-0,2923
H	1,7512	-3,1072	-0,4889
H	2,6957	-1,5294	0,6820
H	2,1389	-0,8588	-1,4738

C	1,3440	-2,1712	-2,9265
C	1,4862	-3,6213	-0,4553
H	1,5596	2,3399	2,8270
H	2,9926	2,8374	1,9008
H	1,6339	3,9784	2,1235
H	2,5798	-3,6271	-0,5032
H	1,1814	-3,7049	0,5912
H	1,0901	-4,4750	-1,0156
H	0,9112	-1,3384	-3,4855
H	2,4341	-2,1116	-2,9984
H	1,0064	-3,1202	-3,3557
H	2,8086	3,3507	-0,9662
H	1,2393	3,2683	-1,7936
H	1,5214	4,5082	-0,5348
N	4,5690	-1,1200	0,6289
B	3,3203	-0,5476	0,3228
H	4,7585	-1,6017	1,4982
H	5,3585	-1,0959	-0,0025
H	2,4427	-0,5230	1,2826
H	3,2152	0,1578	-0,7462

TS[**3-13'–3-10**]

E = -1812.023272

Ru	1,1954	-1,2609	-0,2148
P	-0,4631	-0,9363	-1,7603
P	-0,0569	-1,4377	1,7673
Si	0,9243	1,0495	0,0971
C	2,4426	2,1586	0,4573
H	2,1612	3,2105	0,5997
H	2,9530	1,8259	1,3685
H	3,1585	2,1061	-0,3707
C	0,0365	1,7766	-1,4555
C	-0,6139	0,8415	-2,2845
C	-1,3276	1,2520	-3,4187
H	-1,8335	0,5250	-4,0519
C	-1,3838	2,6048	-3,7557
H	-1,9269	2,9226	-4,6425
C	-0,7322	3,5461	-2,9541
H	-0,7677	4,6006	-3,2191
C	-0,0364	3,1334	-1,8163
H	0,4649	3,8834	-1,2069
C	-0,3198	1,3322	1,5590
C	-0,7712	0,2041	2,2745
C	-1,6774	0,3405	3,3376
H	-2,0206	-0,5328	3,8886
C	-2,1507	1,6010	3,7002
H	-2,8572	1,7019	4,5207

TS[**3-4'-AB–3-14'**]

E = -2686.084003

Ru	0,6470	-0,0333	-0,1365
P	-0,7484	-0,0236	1,7001
P	-0,7956	0,3428	-2,0242
Si	0,2101	2,3191	0,1015
C	1,2715	3,7930	-0,5367
H	0,6626	4,7061	-0,5259
H	1,6015	3,6328	-1,5701
H	2,1635	3,9679	0,0736
C	-0,0452	2,6403	1,9772
C	-0,4419	1,5086	2,7134
C	-0,6550	1,5838	4,0951
H	-0,9699	0,7098	4,6610
C	-0,4474	2,7923	4,7649
H	-0,5936	2,8476	5,8410
C	-0,0481	3,9244	4,0512
H	0,1147	4,8649	4,5732
C	0,1426	3,8477	2,6689
H	0,4557	4,7392	2,1283
C	-1,4887	2,6904	-0,7588
C	-1,9159	1,7934	-1,7575
C	-3,1039	2,0146	-2,4690
H	-3,4278	1,3200	-3,2407
C	-3,8911	3,1299	-2,1791
H	-4,8199	3,2941	-2,7202

3-14'

E = -2686.090632

Ru	0,3849	-0,4665	-0,7748
P	-1,1400	-0,7099	1,0833
P	-1,1578	-0,5459	-2,4592
Si	-0,5995	1,7653	-0,4519
C	0,2428	3,3837	-1,0478
H	-0,4843	4,2064	-1,0343
H	0,6054	3,2800	-2,0763
H	1,0897	3,6708	-0,4163
C	-1,2302	2,0446	1,3359
C	-1,5910	0,8562	1,9927
C	-2,2184	0,8870	3,2443
H	-2,5123	-0,0316	3,7475
C	-2,4472	2,1123	3,8749
H	-2,9112	2,1377	4,8578
C	-2,0654	3,3011	3,2478
H	-2,2309	4,2535	3,7466
C	-1,4753	3,2668	1,9818
H	-1,1974	4,2029	1,5009
C	-2,2889	1,7377	-1,4063
C	-2,5627	0,6497	-2,2524
C	-3,7850	0,5508	-2,9352
H	-3,9902	-0,2941	-3,5896
C	-4,7548	1,5393	-2,7732
H	-5,7075	1,4576	-3,2911

C	-1,7130	2,7310	3,0035
H	-2,0797	3,7166	3,2818
C	-0,8078	2,5923	1,9510
H	-0,4840	3,4848	1,4180
C	-0,1564	-1,8501	-3,3530
C	-2,2489	-1,3888	-1,4546
C	-1,4745	-2,6324	2,0103
C	0,9689	-1,8889	3,2614
H	0,8117	-1,5388	-3,7508
H	-0,1218	-2,9223	-3,1380
H	-0,9411	-1,6555	-4,0915
H	-2,2850	-2,3940	1,3182
H	-1,1098	-3,6399	1,7873
H	-1,8591	-2,6137	3,0356
H	-2,3200	-2,4595	-1,2402
H	-2,6184	-0,8240	-0,5946
H	-2,8675	-1,1522	-2,3266
H	1,3722	-2,8968	3,1235
H	1,8017	-1,1861	3,3411
H	0,3731	-1,8542	4,1794
N	4,2053	-2,7281	-0,6747
B	2,9006	-2,2697	-0,3993
H	4,3850	-3,5393	-1,2502
H	5,0295	-2,1715	-0,4919
H	1,8896	-3,0472	-0,5289
H	2,7539	-1,4468	0,6429
H	2,1987	-0,8732	-1,4792

C	-3,4848	4,0294	-1,1896
H	-4,1010	4,8956	-0,9584
C	-2,2914	3,8142	-0,4974
H	-1,9925	4,5240	0,2724
C	-0,4756	-1,3946	2,9239
C	-2,6098	0,0880	1,6059
C	-1,8753	-0,9093	-2,8747
C	0,2326	0,8695	-3,4920
Si	2,3709	-2,9670	-0,8020
Si	-0,4599	-3,6178	-0,4293
N	0,7554	-2,3744	-0,5940
C	2,6020	-4,7384	-1,5101
C	3,3130	-3,0875	0,8922
C	3,4667	-2,0369	-2,0860
C	-0,7737	-4,6316	-2,0298
C	-2,2115	-3,0235	0,0521
C	-0,0980	-4,9277	0,9349
H	3,5943	-0,9568	-1,9795
H	3,0207	-2,1959	-3,0765
H	4,4619	-2,5026	-2,1064
H	3,0663	-4,0704	1,3133
H	2,9688	-2,3574	1,6369
H	4,4111	-3,0523	0,8223
H	2,3205	-4,7891	-2,5682
H	2,0556	-5,5220	-0,9773
H	3,6719	-4,9837	-1,4463
H	0,1162	-5,1575	-2,3873
H	-1,1310	-3,9977	-2,8510
H	-1,5496	-5,3861	-1,8396
H	0,0152	-4,4604	1,9214
H	0,8091	-5,5130	0,7493
H	-0,9343	-5,6373	1,0031
H	-2,9171	-3,8234	-0,2068
H	-2,5319	-2,1208	-0,4722
H	-2,3125	-2,8490	1,1282
H	-3,0342	-0,7956	1,1299
H	-2,8675	0,9741	1,0205
H	-3,0172	0,1951	2,6166
H	0,5230	-1,2798	3,3523
H	-0,5187	-2,3505	2,4017
H	-1,2246	-1,3788	3,7219
H	-2,7630	-1,1281	-2,2785
H	-1,2965	-1,8272	-2,9953
H	-2,1833	-0,5434	-3,8594
H	0,8703	0,0312	-3,7882
H	0,8661	1,7116	-3,2061
H	-0,4083	1,1604	-4,3307
N	3,8741	0,0074	0,4295
B	2,5217	0,7865	-0,1233
H	1,6742	-0,2739	1,1234
H	3,7550	-1,0128	0,4785
H	4,0869	0,3405	1,3736
H	4,6879	0,2135	-0,1566
H	2,9258	1,9120	-0,2249
H	2,1328	0,2110	-1,2152

C	-4,4966	2,6346	-1,9423
H	-5,2507	3,4081	-1,8152
C	-3,2773	2,7302	-1,2722
H	-3,1013	3,5822	-0,6180
C	-0,6152	-1,8049	2,4801
C	-2,8178	-1,4506	0,7435
C	-1,9690	-2,1877	-2,7893
C	-0,6828	-0,1115	-4,2157
Si	2,9898	0,3068	1,5475
Si	2,6066	-2,6859	1,1406
N	2,2375	-1,0219	0,6613
C	4,7277	-0,1065	2,2548
C	1,9957	0,9554	3,0333
C	3,3720	1,7695	0,3824
C	4,3782	-3,1971	0,5805
C	1,5337	-4,0300	0,3172
C	2,6037	-3,0606	3,0204
H	2,5098	2,0741	-0,2143
H	4,1899	1,5170	-0,3066
H	3,7071	2,6365	0,9660
H	1,8993	0,1880	3,8118
H	0,9909	1,2888	2,7590
H	2,5211	1,8088	3,4819
H	5,4555	-0,3135	1,4608
H	4,7488	-0,9491	2,9536
H	5,0893	0,7759	2,8005
H	5,1535	-2,4885	0,8880
H	4,4562	-3,3286	-0,5075
H	4,6275	-4,1696	1,0247
H	1,6024	-3,0762	3,4603
H	3,2057	-2,3473	3,5934
H	3,0426	-4,0553	3,1758
H	1,5888	-3,9697	-0,7754
H	0,4733	-3,9898	0,5828
H	1,9221	-5,0114	0,6242
H	-2,6895	-2,4832	0,4050
H	-3,3325	-0,8756	-0,0293
H	-3,4209	-1,4446	1,6569
H	0,2734	-1,3845	2,9487
H	-0,3829	-2,7976	2,0914
H	-1,4187	-1,8868	3,2188
H	-2,4989	-2,5309	-1,8993
H	-1,1789	-2,9067	-3,0216
H	-2,6661	-2,1307	-3,6316
H	-0,0417	-0,8842	-4,6445
H	-0,1486	0,8415	-4,2310
H	-1,5976	-0,0212	-4,8095
N	3,2749	-1,0380	-1,7924
B	1,8086	-0,7121	-2,2823
H	0,0655	-2,0741	-0,7134
H	3,1269	-1,0405	-0,6948
H	3,5937	-1,9557	-2,1071
H	3,9758	-0,3541	-2,0880
H	1,7602	-0,7301	-3,4806
H	1,4849	0,4871	-1,7428

References

(1) J. F. Hartwig, *Organotransition Metal Chemistry: From Bonding to Catalysis*, University Science Books, Sausalito, **2010**.

(2) (a) Chauvin, Y. *Angew. Chem. Int. Ed.* **2006**, *45*, 3740. (b) Schrock, R. R. *Angew. Chem. Int. Ed.* **2006**, *45*, 3748. (c) Grubbs, R. H. *Angew. Chem. Int. Ed.* **2006**, *45*, 3760. (d) Knowles, W. S. *Angew. Chem. Int. Ed.* **2002**, *45*, 1998. (e) Noyori, R. *Angew. Chem. Int. Ed.* **2002**, *45*, 2008. (f) Sharpless, K. B. *Angew. Chem. Int. Ed.* **2002**, *45*, 2024. (g) Wu, X. F.; Anbarasan, P.; Neumann, H.; Beller, M. *Angew. Chem. Int. Ed.* **2010**, *48*, 9047.

(3) Jensen, C. M. *Chem. Commun.* **1999**, 2443.

(4) Gunanathan, C.; Ben-David, Y.; Milstein, D. *Science*, **2007**, *317*, 790.

(5) (a) Albrecht, M.; van Koten, G. *Angew. Chem. Int. Ed.* **2001**, *40*, 3750. (b) van der Boom, M. E.; Milstein, D. *Chem. Rev.* **2003**, *103*, 1759. (c) Morales-Morales, D.; Jensen, C. M.; Eds. The Chemistry of Pincer Compounds, Elsevier: Oxford: 2007. (d) Selander, N.; Szabo, K. J.; *Chem. Rev.* **2011**, *111*, 2048.

(6) Ma, L.; Wobser, S. D.; Protasciewicz, J. D. *J. Organomet. Chem.* **2007**, *692*, 5331.

(7) (a) Bibal, C.; Pink, M.; Smurnyy, Y. D.; Tomaszewski, J.; Caulton, K. G. *J. Am. Chem. Soc.* **2004**, *126*, 2312. (b) Jones, N. D., Cavell, R. G. *J. Organomet. Chem.* **2005**, *690*, 5485.

(8) Slagt, M. Q.; van Zwieten D. A. P.; Moerkerk, A. J. C. M.; Klein Gebbink, R. J. M.; van Koten, G. Coord. *Chem. Rev.* **2004**, *248*, 2275.

(9) Pugh, D.; Danopoulos, A. A. *Coord. Chem. Rev.* **2007**, *251*, 610.

(10) (a) Espinet, P.; Garcia-Orodea, E.; Miguel, J. A. *Chem. Mater.* **2004**, *16*, 551. (b) Zim, D.; Gruber, A. S.; Ebeling, G.; Dupont, J.; Monteiro, A. L. *Org. Lett.* **2000**, *2*, 2881.

(11) Fischer, J.; Schürmann, M.; Mehring, M.; Zachwieja, U.; Jurkschat, K. *Organometallics* **2006**, *25*, 2886.

(12) (a) Yao, Q.; Sheets, M. *J. Org. Chem.* **2006**, *71*, 5384. (b) Olsson, V. J.; Sevelius, S.; Selander, N.; Szabó, K. J. *J. Am. Chem. Soc.* **2006**, *128*, 4588.

(13) Liang, L.-C. Coord. *Chem. Rev.* **2006**, *250*, 1152.

(14) (a) Moulton, C. J.; Shaw, B. L. *J. Chem. Soc. Dalton Trans.* **1976**, 1020. (b) Empsall, H. D.; Hyde, E. M.; Markham, R.; McDonald, W. S.; Norton, M. C.; Shaw, B. L.; Weeks, B. *J. Chem. Soc. Chem. Commun.* **1977**, 589. (c) Crocker, C.; Errington, R. J.; McDonald, W. S.; Odell, K. J.; Shaw, B. L. *J. Chem. Soc. Chem. Commun.* **1979**, 498. (d) Crocker, C.; Errington, R. J.; Markham, R.; Moulton, C. J.; Odell, K. J.; Shaw, B. L. *J. Am. Chem. Soc.* **1980**, 4373. (e) Al-Salem, N. A.; Empsall, H. D.; Markham, R.; Shaw, B. L.; Weeks, B. *J. Chem. Soc. Dalton Trans.* **1979**, 1972.

(15) van der Zeijden, A. A. H.; van Koten, G.; Luijk, R.; Nordemann, R. A.; Spek, A. L. *Organometallics* **1988**, *7*, 1549.

(16) Kleij, A. W.; Gossage, R. A.; Klein Gebbink, R. J. M.; Brinkmann, N.; Reijerse, E. J.; Kragl, U.; Lutz, M.; Spek, A. L.; van Koten, G. *J. Am. Chem. Soc.* **2000**, *122*, 12112

(17) (a) Grove, D. M.; van Koten, G.; Louwen, J. N.; Noltes, J. G.; Spek, A. L.; Ubbels, H. J. C. *J. Am. Chem. Soc.* **1982**, *104*, 6609. (b) Terheijden, J.; van Koten, G.; Muller, F.; Grove, D. M.; Vrieze, K.; Nielsen, E.; Stam, C. H. *J. Organomet. Chem.* **1986**, *315*, 401.

(18) Sutter, J.-P.; James, S. L.; Steenwinkel, P.; Karlen, T.; Grove, D. M.; Veldman, N.; Smeets, W. J. J.; Spek, A. L.; van Koten, G. *Organometallics*, **1996**, *15*, 941.

(19) Rybtchinski, B.; Vigalok, A.; Ben-David, Y.; Milstein, D. *J. Am. Chem. Soc.* **1996**, *118*, 12406.

(20) Steenwinkel, P.; Gossage, R. A.; van Koten, G. *Chem. Eur. J.* **1998**, *4*, 759.

(21) Albrecht, M.; Dani, P.; Lutz, M.; Spek, A.L.; van Koten, G. *J. Am. Chem. Soc.* **2000**, *122*, 11822.

(22) Maassarani, F.; Davidson, M. F.; Wehman-Ooyevaar, I. C. M.; Grove, D. M.; van Koten, M. A.; Smeets, W. J. J.; Spek, A. L.; van Koten, G. *Inorg. Chim. Acta* **1995**, *235*, 327.

(23) (a) Labinger, J. A.; Bercaw, J. E. *Nature* **2002**, *417*, 507. (b) Arndtsen, B. A.; Bergman, R. G.; Mobley, T. A.; Peterson, T. H. *Acc. Chem. Res.* **1995**, *28*, 154.

(24) Arnstden, B. A.; Bergman, R. G. *Science*, **1995**, *270*, 1970.

(25) (a) Burk, M. W.; Crabtree, R. H. *J. Am. Chem. Soc.* **1987**, *109*, 8025. (b) Belli, J.; Jensen, C. M. *Organometallics*, **1996**, *15*, 1532.

(26) Liu, F.; Pak, E. B.; Singh, B.; Jensen, C. M.; Goldman, A. S. *J. Am. Chem. Soc.* **1999**, *121*, 4086.

(27) Liu, F.; Goldman, A. S. *Chem. Commun.* **1999**, 655.

(28) (a) Göttker-Schnettman, I.; White, P.; Brookhart, M. *J. Am. Chem. Soc.* **2004**, *126*, 1804. (b) Göttker-Schnettman, I.; White, P.; Brookhart, M. *Organometallics*, **2004**, *23*, 1766. (c) Göttker-Schnettman, I.; Brookhart, M. *J. Am. Chem. Soc.* **2004**, *126*, 9330.

(29) (a) Noyori, R.; Hashiguchi, S. *Acc. Chem. Res.* **1997**, *30*, 97. (b) Ikariya, T.; Murata, K.; Noyori, R. *Org. Biomol. Chem.* **2006**, *4*, 393. (c) Clapham, S. E.; Hadzovic, A.; Morris, R. H. *Coord. Chem. Rev.* **2004**, *248*, 2201. (d) Gladiali, S.; Alberico, E. *Chem. Soc. Rev.* **2006**, *35*, 226. (e) Samec, J. S. M.; Bäckvall, J. E.; Andersson, P. G.; Brandt, P. *Chem. Soc. Rev.* **2006**, *35*, 237.

(30) (a) Medici, S.; Gagliardo, M.; Williams, S. B.; Chase, P. A.; Gladiali, S.; Lutz, M.; Spek, A. L.; van Klink, G. P. M.; van Koten, G. *Helv. Chim. Acta* **2005**, *88*, 694. (b) Gagliardo, M.; Chase, P. A.; Brouwer, S.; van Klink, G. P. M.; van Koten, G. *Organometallics* **2007**, *26*, 2219. (c) Dani, P.; Karlen, T.; Gossage, R. A.; Gladiali, S.; van Koten, G. *Angew. Chem. Int. Ed.* **2000**, *39*, 743.

(31) (a) Baratta, W.; Chelucci, G.; Gladiali, S.; Siega, K.; Toniutti, M.; Zanette, M.; Zangrando, E.; Rigo, P. *Angew. Chem. Int. Ed.* **2005**, *44*, 6214. (b) Baratta, W.; Da Ros, P.; Del Zotto, A.; Sechi, A.; Zangrando, E.; Rigo, P. *Angew. Chem. Int. Ed.* **2004**, *43*, 3584. (c) Lundgren, R. J.; Rankin, M. A.; McDonald, R.; Schatte, G.; Stradiotto, M. *Angew. Chem. Int. Ed.* **2007**, *46*, 4732.

(32) (a) Beletskaya, I. P.; Cheprakov, A. V. *Chem. Rev.* **2000**, *100*, 3009. (b) Alonso, F.; Beletskaya, I. P; Yus, M. *Tetrahedron* **2005**, *61*, 11771. (c) Trzeciak, A. M.; Ziółkowski, J. J. *Coord. Chem. Rev.* **2005**, *249*, 2308. (d) Singleton, J. *Tetrahedron* **2003**, *59*, 1837.

(33) (a) Ohff, M.; Ohff, A.; van der Boom, M. E.; Milstein, D. *J. Am. Chem. Soc.* **1997**, *119*, 11687. (b) Morales-Morales, D.; Redo´n, R.; Yung, C.; Jensen, C. M. *Chem. Commun.* **2000**, 1619.

(34) Kiewel, K.; Liu, Y. S.; Bergbreiter, D. E.; Sulikowski, G. A. *Tetrahedron Lett.* **1999**, *40*, 8945.

(35) Haggin, J. *Chem. Eng. News* **1993**, *71*, 23.

(36) Zhao, J.; Goldman, A. S.; Hartwig, J. F. *Science* **2005**, *307*, 1080.

(37) Kanzelberger, M.; Zhang, X.; Emge, T. J.; Goldman, A. S.; Zhao, J.; Incarvito, C.; Hartwig, J. F. *J. Am. Chem. Soc.* **2003**, *125*, 13644.

(38) Huang, Z.; Zhou, J.; Hartwig, J. F. *J. Am. Chem. Soc.* **2010**, *132*, 11458.

(39) Morgan, E.; MacLean, D. F.; McDonald, R.; Turculet, L. *J. Am. Chem. Soc.* **2009**, *131*, 14234.

(40) (a) Ozerov, O. V.; Guo, C.; Fan, L.; Foxman, B. M. *Organometallics* **2004**, *23*, 5573. (b) Ozerov, O. V.; Guo, C.; Papkov, V. A.; Foxman, B. M. *J. Am. Chem. Soc.* **2004**, *126*, 4792.

(41) (a) Fryzuk, M. D.; MacNeil, P. A. *J. Am. Chem. Soc.* **1981**, *103*, 3592. (b) Fryzuk, M. D.; MacNeil, P. A.; Rettig, S. J.; Secco, A. S.; Trotter, J. *Organometallics* **1982**, *1*, 918. (c) Fryzuk, M. D.; MacNeil, P. A.; *Organometallics* **1983**, *2*, 682. (d) Fryzuk, M. D.; *Can. J. Chem.* **1992**, *70*, 2839.

(42) Cohen, J. D.; Fryzuk, M. D.; Loehr, T. M.; Mylvaganam, M.; Rettig, S. J. *Inorg. Chem.* **1998**, *37*, 112.

(43) Watson, L. A.; Ozerov, O. V.; Pink, M.; Caulton, K. G. *J. Am. Chem. Soc.* **2003**, *125*, 8426.

(44) Liang, L.-C.; Lin, J.-M.; Lee, W.-Y. *Chem. Commun.* **2005**, 2462.

(45) Fout, A. R.; Basuli, F.; Fan, H.; Tomaszewski, J.; Huffman, J. C.; Baik, M.-H.; Mindiola, D. J. *Angew. Chem. Int. Ed.* **2006**, *45*, 3291.

(46) Csok, Z.; Vechorkin, O.; Harkins, S. B.; Scopelliti, R.; Hu, X. J. Am. Chem. Soc. 2008, 130, 8156.

(47) Wei, W.; Qin, Y.; Luo, M.; Xia, P.; Wong, M. S. *Organometallics* **2008**, *27*, 2268.

(48) Askevold, B.; Khusniyarov, M. M.; Herdtweck, E.; Meyer, K.; Schneider, S. *Angew Chem. Int. Ed.* **2010**, *49*, 7566.

(49) Baratta, W.; Herdtweck, E.; Rigo, P. *Angew. Chem. Int. Ed.* **1999**, *38*, 1629.

(50) (a) Huang, D.; Bollinger, J. C.; Streib, W. E.; Folting, K.; Young, V., Jr.; Eisenstein, O.; Caulton, K. G. *Organometallics* **2000**, *19*, 2281. (b) Huang, D.; Huffman, J. C.; Bollinger, J. C.; Eisenstein, O. Caulton, K. G. *J. Am. Chem. Soc.* **1997**, *119*, 7398.

(51) Poverenov, E.; Efremenko, I.; Frenkel, AI.; Ben-David, Y.; Shimon, L. J. W.; Leitus, G.; Konstantinovski, L.; Martin, J. M. L.; Milstein, D. *Nature* **2008**, *455*, 1093.

(52) Kohl, S. W.; Weiner, L.; Schwartsburd, L.; Konstantinovski, L.; Shimon, L. J. W.; Ben-David, Y.; Iron, M. A.; Milstein, D. *Science* **2009,** *324*, 74.

(53) Khaskin, E.; Iron, M. A.; Shimon, L. J. W.; Zhang, J.; Milstein, D. *J. Am. Chem. Soc.* **2010**, *132*, 8542.

(54) Zhang, J.; Gandelman, M.; Shimon, L. J. W.; Rozenberg, H.; Milstein, D. *Organometallics* **2004**, *23*, 4026.

(55) Zhang, J.; Leitus, G.; Ben-David, Y.; Milstein, D. *J. Am. Chem. Soc.* **2005**, *127*, 10840.

(56) Balaraman, E.; Gnanaprakasam, B.; Shimon, L. J. W.; Milstein, D. *J. Am. Chem. Soc.* **2010**, *132*, 16756.

(57) Gnanaprakasam, B.; Zhang, J.; Milstein, D. *Angew. Chem. Int. Ed.* **2010**, *49*, 1468.

(58) Gunanathan, C.; Shimon, L. J. W.; Milstein, D. *J. Am. Chem. Soc.* **2009**, *131*, 3146.

(59) (a) Tilley, T. D. In The Silicon-Heteroatom Bond; Patai, S., Rappoport, Z. Eds.; Wiley: New York, 1991. (b) Corey, J. Y.; Braddock- Wilking, *J. Chem. Rev.* **1999**, *99*, 175.

(60) (a) Balakrishna, M. S.; Chandrasekaran, P.; George, P. P. *Coord. Chem. Rev.* **2003**, *241*, 87. (b) Mankad, N. P.; Whited, M. T.; Peters, J. C. *Angew. Chem., Int. Ed.* **2007**, *46*, 5768.

(61) (a) Auburn, M. J.; Stobart, S. R. *Inorg. Chem.* **1985**, *24*, 318. (b) Joslin, F. L.; Stobart, S. R. *J. Chem. Soc., Chem. Commun.* **1989**, 504. (c) Auburn, M. J.; Holmes-Smith, R. D.; Stobart, S. R.; Bakshi, P. K.; Cameron, T. S. *Organometallics* **1996**, *15*, 3032. (d) Gossage, R. A.; McLennan, G. D.; Stobart, S. R. *Inorg. Chem.* **1996**, *35*, 1729. (e) Brost, R. D.; Bruce, G. C.; Joslin, F. L.; Stobart, S. R. *Organometallics* **1997**, *16*, 5669. (f) Zhou, X.; Stobart, S. R. *Organometallics* **2001**, *20*, 1898.

(62) (a) Stradiotto, M.; Fujdala, K. L.; Tilley, T. D. *Chem. Commun.* **2001**, 1200. (b) Sangtrirutnugul, P.; Stradiotto, M.; Tilley, T. D. *Organometallics* **2006**, *25*, 1607. (c) Sangtrirutnugul, P.; Tilley, T. D. *Organometallics* **2007**, *26*, 5557. (d) Sangtrirutnugul, P.; Tilley, T. D. *Organometallics* **2008**, *27*, 2223.

(63) A report on the use of phosphinoalkylsilyl metal complexes as catalysts for hydroformylation of olefins appears in the patent literature: Stobart, S. R.; Grundy, S. L.; Joslin, F. L. U.S. Patent 4,950,798, 1990; Canadian Patent 1,327,365, 1994.

(64) Whited, M. T.; Rivard, E.; Peters, J. C. *Chem. Commun.* **2006**, 1613

(65) Bushnell, G. W.; Casado, M. A.; Stobart, S. R. *Organometallics* **2001**, *20*, 601.

(66) Chin, B.; Lough, A. J.; Morris, R. H.; Schweitzer, C. T.; D'Agostino, C. *Inorg. Chem.* **1994**, *33*, 6278.

(67) (a) Gusev, D. G.; Dolgushin, F. M.; Antipin, M. Y. *Organometallics* **2000**, *19*, 3429. (b) Amoroso, D.; Jabri, A.; Yap, G. P. A.; Gusev, D. G.; dos Santos, E. N.; Fogg, D. E. *Organometallics* **2004**, *23*, 4047.

(68) For reviews on late transition metal-dihydrogen complexes, see: (a) Esteruelas, M. A.; Oro, L. A. *Chem. Rev.* **1998**, *98*, 577. (b) Kubas, G. J. *Proc. Nat. Acad. Sci. U.S.A.* **2007**, *104*, 6901, and references therein.

(69) (a) Luo, X.-L.; Crabtree, R. H. *Inorg. Chem.* **1989**, *28*, 3775. (b) Cotton, F. A.; Luck, R. L. *J. Am. Chem. Soc.* **1989**, *111*, 5757. (c) Desrosiers, P. J.; Cai, L.; Lin, Z.; Richards, R.; Halpern, J. *J. Am. Chem. Soc.* **1991**, *113*, 4173.

(70) (a) Hamilton, D. G.; Crabtree, R. H. *J. Am. Chem. Soc.* **1988**, *110*, 4126, and references cited therein. (b) Heinekey, D. M.; Oldham, W. J. *Chem. Rev.* 1993, **93**, 913. (c) Jessop, P. G.; Morris, R. H. *Coord. Chem. Rev.* 1992, **121**, 155.

(71) (a) Fulton, J. R.; Holland, A. W.; Fox, D. J.; Bergman, R. G. *Acc. Chem. Res.* **2002**, *35*, 44. (b) Fulton, J. R.; Bouwkamp, M. W.; Bergman, R. G. *J. Am. Chem. Soc.* **2000**, *122*, 8799.

(72) Denney, M. C.; Pons, V.; Hebden, T. J.; Heinekey, M.; Goldberg, K. I. *J. Am. Chem. Soc.* **2006**, *128*, 12048.

(73) Mal, S. S.; Stephens, F. H.; Baker, R. T. *Chem. Commun.* **2011**, *47*, 2922.

(74) (a) Jaska, C. A.; Manners, I. *J. Am. Chem. Soc.* **2004**, *126*, 9776. (b) Stephens, S. H.; Pons, V.; Baker, R. T. *Dalton Trans*. **2007**, 2613. (c) Stephens, F. H.; Baker, R. T.; Matus, M. H.; Grant, D. J.; Dixon, D. A. *Angew. Chem. Int. Ed.* **2007**, *46*, 746. (d) Keaton, R. J.; Blacquiere, J. M.; Baker, R. T. J. Am. Chem. Soc. **2007**, *129*, 1844. (e) Paul, A.; Musgrave, C. B. *Angew. Chem. Int. Ed.* **2007**, *46*, 8153.

(75) *Comprehensive Organometalic Chemistry III, Volume 6: Compounds of Group 8*; Mingos, D. P. M., Crabtree, R. H., Bruce, M., Eds.; Elsevier Ltd.: Oxford, UK, **2007**.

(76) Walstrom, A.; Pink, M.; Caulton, K. G. *Inorg. Chem.* **2006**, *45*, 5617.

(77) A four-coordinate structure lacking agostic interactions has been proposed for $[(IMes)_2Ru(H)(CO)][BAr'_4]$ (IMes = 1,3-bis-(2,4,6-trimethylphenyl)imidazol-2-ylidene, BAr'_4 = 3,5-$(CF_3)_2C_6H_3$), although this complex has not been crystallographically characterized: Lee, J. P.; Ke, Z.; Ramírez, M. A.; Gunnoe, T. B.; Cundari, T. R.; Boyle, P. D.; Petersen, J. L. *Organometallics* **2009**, *28*, 1758.

(78) (a) Huang, D.; Streib, W. E.; Bollinger, J. C.; Caulton, K. G.; Winter, R. F.; Scheiring, T. *J. Am. Chem. Soc.* **1999**, *121*, 8087. (b) Vieille-Petit, L.; Luan, X.; Gatti, M.; Blumentritt, S.; Linden, A.; Clavier, H.; Nolan, S. P.; Dorta, R. *Chem. Commun.* **2009**, 3783.

(79) (a) MacInnis, M. C.; MacLean, D. F.; Lundgren, R. J.; McDonald, R.; Turculet, L. *Organometallics* **2007**, *26*, 6522. (b) MacLean, D. F. McDonald, R.; Ferguson, M. J.; Caddell, A. J.; Turculet, L. *Chem. Commun.* **2008**, 5146. (c) Mitton, S. J.; McDonald, R.; Turculet, L. *Organometallics* **2009**, *28*, 5122. (d) Mitton, S. J.; McDonald, R.; Turculet, L. *Angew. Chem. Int. Ed.* **2009**, *48*, 8568.

(80) Johnson, T. D.; Folting, K.; Streib, W. E.; Martin, J. D.; Huffman, J. C.; Jackson, S. A.; Eisenstein, O.; Caulton, K. G. *Inorg. Chem.* **1995**, *34*, 488.

(81) Sanford, M. S.; Henling, L. M.; Day, M. W.; Grubbs, R. H. *Angew. Chem. Int. Ed.* **2000**, *39*, 3451.

(82) The four-coordinate phosphonium alkylidene complex $[(H_2IMes)Cl_2Ru{=}C(H)PCy_3][B(C_6F_5)_4]$ also exhibits distorted trigonal pyramidal coordination geometry in the solid state: Romero, P. E.; Piers, W. E.; McDonald, R. *Angew. Chem. Int. Ed.* **2004**, *43*, 6161.

(83) (a) Koelle, U. *Chem. Rev.* **1998**, *98*, 1313. (b) Loren, S. D.; Campion, B. K.; Heyn, R. H.; Tilley, T. D.; Bursten, B. E.; Luth, K. W. *J. Am. Chem. Soc.* **1989**, *111*, 4712.

(84) Blake, R. E. Jr.; Heyn, R. H.; Tilley, T. D. *Poyhedron* **1992**, *11*, 709.

(85) The use of ^{1}H DOSY NMR to determine molecular weights in solution has recently been employed: Silvia, J. S.; Cummins, C. C. *Chemical Science* **2011**, *2*, 1474.

(86) Waldeck, A. R.; Kuchel, P. W.; Lennon, A. J.; Chapman, B. E. *Prog. Nucl. Magn. Reson. Spectrosc.* **1997**, *30*, 39.

(87) Cole-Hamilton, D. J.; Young, R. J.; Wilkinson, G. *J. Chem. Soc., Dalton Trans.* **1976**, 1995.

(88) Koelle, U.; Hörnig, A.; Englert, U. *Organometallics* **1994**, *13*, 4064.

(89) (a) Alcaraz, G.; Vendier, L.; Clot, E.; Sabo-Etienne, S. *Angew. Chem. Int. Ed.*, **2010**, *49*, 918. (b) Alcaraz, G.; Sabo-Etienne, S. *Angew. Chem. Int. Ed.*, **2010**, *49*, 7170. (c) Tang, C. Y.; Thompson, A. L.; Aldridge, S. *Angew. Chem. Int. Ed.* **2010**, *49*, 921. (d) Douglas, T. M.; Chaplin, A. B.; Weller, A. S. *J. Am. Chem. Soc.* **2008**, *130*, 14432. (e) Chaplin, A. B.; Weller, A. S. *Inorg. Chem.* **2010**, *49*, 1111. (f) Alcaraz, G.; Chaplin, A. B.; Stevens, C. J.; Clot, E.; Vendier, L.; Weller, A. S.; Sabo-Etienne, S. *Organometallics* **2010**, *29*, 5591. (g) Stevens, C. J.; Dallanegra, R.; Chaplin, A. B.; Weller, A. S.; Macgregor, S. A.; Ward, B.; McKay, D.; Alcaraz, G.; Sabo-Etienne, S. *Chem. Eur. J.* **2011**, *17*, 3011.

(90) Klooster, W. T.; Koetzle, T. F.; Siegbahn, P. E. M.; Richardson, T. B.; Crabtree, R. H. *J. Am. Chem. Soc.* **1999**, *121*, 6337.

(91) Hamilton, C.W.; Baker, R. T.; Staubitz, A.; Manners, I. *Chem. Soc. Rev.* **2009**, *38*, 279.

(92) For an example of catalytic dehydrogenation of ammonia borane by a Ru amido complex, see: Blaquiere, N.; Diallo-Garcia, S.; Gorelsky, S. I.; Black, D. A.; Fagnou, K. *J. Am. Chem. Soc.* **2008**, *130*, 14034.

(93) Parr, R. G.; Yang, W. *Density-Functional Theory of Atoms and Molecules*; Oxford University Press: New York, NY, **1989**.

(94) (a) Ahlrichs, R.; Bär, M.; Häser, M.; Horn, H.; Kölmel, C. *Chem. Phys. Lett.* **1989**, *162*, 165. (b) Treutler, O.; Ahlrichs, R. *J. Chem. Phys.* **1995**, *102*, 346. (c) Ahlrichs, R.; Furche, F.; Hättig, C.; Klopper, W.; Sierka, M.; Weigend, F. TURBOMOLE, version 6.0; University of Karlsruhe: Karlsruhe, Germany, 2009; http://www.turbomole.com.

(95) (a) Dirac, P. A. M. *Proc. Royal Soc. (London)* **1929**, *A123*, 714. (b) Slater, J. C. *Phys. Rev.* **1951**, *81*, 385. (c) Perdew, J. P.; Wang, Y. *Phys. Rev.* **1992**, *B45*, 13244. (d) Tao, J.; Perdew, J. P.; Staroverov, V. N.; Scuseria, G. E. *Phys. Rev. Lett.* **2003**, *91*, 146401. (e) Perdew, J. P.; Tao, J.; Staroverov, V. N.; Scuseria, G. E. *J. Chem. Phys.* **2004**, *120*, 6898.

(96) (a) Vahtras, O.; Almlöf, J.; Feyereisen, M. W. *Chem. Phys. Lett.* **1993**, *213*, 514. (b) Eichkorn, K.; Treutler, O.; Öhm, H.; Häser, M.; Ahlrichs, R. *Chem. Phys. Lett.* **1995**, *242*, 652.

(97) Andrae, D.; Häußermann, U.; Dolg, M.; Stoll, H.; Preuß, H. *Theor. Chim. Acta* **1990**, *77*, 123.

(98) (a) Weigend, F.; Ahlrichs, R. *Phys. Chem. Chem. Phys.* **2005**, *7*, 3297. (b) Weigend, F. *Phys. Chem. Chem. Phys.* **2006**, *8*, 1057.

(99) (a) Schäfer, A.; Huber, C.; Ahlrichs, R. *J. Chem. Phys.* **1994**, *100*, 5829. (b) Eichkorn, K.; Weigend, F.; Treutler, O.; Ahlrichs, R. *Theor. Chem. Acc.* **1997**, *97*, 119.

(100) (a) Staroverov, V. N.; Scuseria, G. E.; Tao, J.; Perdew, J. P. *J. Chem. Phys.* **2003**, *119*, 12129. (b) Zao, Y.; Truhlar, D. G. *J. Chem. Theory Comput.* **2005**, *1*, 415. (c) Furche, F.; Perdew, J. P. *J. Chem. Phys.* **2006**, *124*, 044103.

(101) Staroverov, V. N.; Scuseria, G. E.; Tao, J.; Perdew, J. P. *J. Phys. Chem.* **2004**, *121*, 11507E.

(102) Jensen, K. P. *Inorg. Chem.* **2008**, *47*, 10357.

(103) McQuarrie, D. A. *Statistical Thermodynamics*, Harper & Row: New York, NY, **1973**.

(104) Wiberg, K. B. *Tetrahedron* **1968**, *24*, 1083.

(105) Reed, A. E.; Weinstock, R. B.; Weinhold, F. *J. Chem. Phys.* **1985**, *83*, 735.

(106) Glendening, E. D.; Badenhoop, J. K.; Reed, A. E.; Carpenter, J. E.; Weinhold, F. NBO 4.M; Theoretical Chemistry Institute, University of Wisconsin, Madison, WI, **1999**.

(107) Malkin, V. G.; Malkina, O. L.; Reviakine, R.; Arbuznikov, A. V.; Kaupp, M.; Schimmelpfennig, B.; Malkin, I.; Repiský, M.; Komorovský, S.; Hrobarik, P.; Malkin, E.; Helgaker, T.; Ruud, K. ReSpect program, version 1.2, **2005**.

(108) For further details, see http://www.struked.de.

(109) *Comprehensive Organometallic Chemistry III. Volume 6: Compounds of Group 8*; Mingos, D. P. M., Crabtree, R. H., Bruce, M. Eds: Elsevier Ltd.: Oxford, UK, **2007**.

(110) Glaser, P. B.; Tilley, T. D.; *J. Am. Chem. Soc.* **2003**, 125, 13640.

(111) Campion, B. K.; Heyn, R. H.; Tilley, T. D. *Chem. Commun.* **1988**, 278.

(112) Hayes, P. G.; Waterman, R.; Glaser, P. B.; Tilley, T. D. *Organometallics* **2009**, *28*, 5082.

(113) Hesp, K. D.; Rankin, M. A.; McDonald, R.; Stradiotto, M. *Inorg. Chem.* **2008**, *47*, 7471.

(114) Borowski, A. F.; Sabo-Etienne, S.; Christ, M. L.; Donnadieu, B.; Chaudret, B. *Organometallics*, **1996**, *15*, 1427.

(115) Walstrom, A.; Pink, M.; Yang, X.; Tomaszewski, J.; Baik, M.-H.; Caulton, K. G. *J. Am. Chem. Soc.* **2005**, *127*, 5330.

(116) (a) Mazzeo, M.; Lamberti, M.; Massa, A.; Scettri, A.; Pellecchia, C.; Peters, J. C. *Organometallics* **2008**, *27*, 5741. (b) Mazzeo, M.; Lamberti, M.; D'Auria, I.; Milione, S.; Peters, J. C.; Pellecchia, C. *J. Polym. Sci.: Part A: Polym. Chem.* **2010**, *48*, 1374. (c) Aspinall, H. C.; Tillotson, M. R. *Inorg. Chem.* **1996**, *35*, 5. (d) Edwards, P. G.; Parry, J. S.; Read, P. W. *Organometallics* **1995**, *14*, 3649. (e) Danopoulos, A. A.; Edwards, P. G.; Harman, M.; Hursthouse, M. B.; Parry, J. S. *J. Chem. Soc., Dalton Trans.* **1994**, 977. (f) Edwards, P. G.; Read, P. W.; Hursthouse, M. B.; Abdul Malik, K. M. *J. Chem. Soc., Dalton Trans.* **1994**, 971. (g) Edwards, P. G.; Howard, J. A. K.; Parry, J. S.; Al-Soudani, A-R. *Chem. Commun.* **1991**, 1385.

(117) For representative examples of alternative classes of mulitdentate phosphido-based ancillary ligands, see: (a) Turculet, L.; McDonald, R. *Organometallics* **2007**, *26*, 6821. (b) Winston, M. S.; Bercaw, J. E. *Organometallics* **2010**, *29*, 6408. (c) Izod, K.; Liddle, S. T.; Clegg, W.; Harrington, R. W. *Dalton Trans.* **2006**, 3431. (d) Izod, K.; Liddle, S. T.;Clegg, W. *Chem. Commun.* **2004**, 1748. (e) Izod, K.; Liddle, S. T.;McFarlane, W.; Clegg, W. *Organometallics* **2004**, *23*, 2734, and references therein. (f) Kunz, K.; Erker, G.; Döring, S.; Fröhlich, R.; Kehr, G. *J. Am. Chem. Soc.* **2001**, *123*, 6181. (g) Altenhoff, G.; Bredeau, S.; Erker, G.; Kehr, G.; Kataeva, O.; Fröhlich, R. *Organometallics* **2002**, *21*, 4084. (h) Bredeau, S.; Altenhoff, G.; Kunz, K.; Döring, S.; Grimme, S.; Kehr, G.; Erker, G. *Organometallics* **2004**, *23*, 1836. (i) Koch, T.; Blaurock, S.; Somoza, Jr., F. B.; Voigt, A.; Kirmse, R.; Hey-Hawkins, E. *Organometallics* **2000**, *19*, 2556. (j) Chaudhury, S.; Blaurock, S.; Hey-Hawkins, E. *Eur. J. Inorg. Chem.* **2001**, 2587. (k) Koch, T.; Hey-Hawkins, E.; Galan-Fereres, M.; Eisen, M. S. *Polyhedron* **2002**, *21*, 2445. (l) Tardif, O.; Hou, Z.; Nishiura, M.; Koizumi, T.; Wakatsuki, Y. *Organometallics* **2001**, *20*, 4565. (m) Ishiyama, T.; Mizuta, T.; Miyoshi, K.; Nakazawa, H. *Organometallics* **2003**, *22*, 1096. (n) Köpf, H.; Richtering, V. *J. Organomet. Chem.* **1988**, *346*, 355.

(118) The van der Waals radius of Pd^{II} has been estimated as 1.63 Å: Bondi, A. *J. Phys. Chem.* **1964**, *68*, 441.

(119) The association of square planar complexes of d^8 metal ions in pairs or stacks is a well-known phenomenon that has been studied in both the solid state and in solution; M···M distances ranging from 2.6 – 3.5 Å have been reported in this context, and there has been extensive discussion on whether these contacts are indicative of weak bonding interactions. For selected examples see: (a) Bailey, J. A.; Hill, M. G.; Marsh, R. E.; Miskowski, V. M.; Schaefer, W. P.; Gray, H. B. *Inorg. Chem.* **1995**, *34*, 4591; (b) Navarro, J. A. R.; Romero, M. A.; Salas, J. M.; Quiros, M.; El Bahraoui, J.; Molina, J. *Inorg. Chem.* **1996**, *35*, 7829; (c) Novoa, J. J.; Aullon, G.; Alemany, P.; Alvarez, S.; *J. Am. Chem. Soc.* **1995**, *117*, 7169; (d) Pyykkö, P. *Chem. Rev.* **1997**, *97*, 597; (e) Connick, W. B.; Marsh, R. E.; Schaefer, W. P.; Gray, H. B. *Inorg. Chem.* **1997**, *36*, 913 and references therein.

(120) By use of the Gutowsky-Holm approximation: $\Delta G_c^{\ddagger} = (-RT_c)\ln[(h\pi\Delta\nu/\sqrt{2})/(k_bT_c)]$, where k_b = Boltzmann's constant, h = Planck's constant, R = the ideal gas constant, and T_c is the coalescence temperature. See: (a) Braun, S.; Kalinowski, H.-O.; Berger, S. *150 and More Basic NMR Experiments*; Wiley-VCH: Toronto, **1998**; (b) Gutowsky, H. S.; Holm, C. H. *J. Chem. Phys.* **1956**, *25*, 1228.

(121) (a) Fan, L.; Foxman, B. M.; Ozerov, O. V. *Organometallics* **2004**, *23*, 326. (b) Huang, M-H.; Liang, L-C. *Organometallics* **2004**, *23*, 2813.

(122) The use of Pd pincer complexes as a source of colloidal Pd in the Heck reaction has been described. See ref. 5d and references cited therein.

(123) Nikolai, J.; Taubmann, G.; Maas, G. *Z. Naturforsch*. **2003**, *58b*, 217.

(124) The ^{13}C NMR resonances observed for the allyl ligand in **8** are in keeping with data previously reported for (η^1-allyl)Pd^{II} complexes, including those for which crystallographic characterization data are provided. For representative examples, see: (a) Zhang, J.; Braunstein, P.; Welter, R. *Inorg. Chem.* **2004**, *43*, 4172. (b) Barloy, L.; Ramdeehul, S.; Osborn, J. A.; Carlotti, C.; Taulelle, F.; De Cian, A.; Fischer, J. *Eur. J. Inorg. Chem.* **2000**, 2523. (c) Braunstein, P.; Zhang, J.; Welter, R. *Dalton Trans.* **2003**, 507. (d) Braunstein, P.; Naud, F.; Dedieu, A.; Rohmer, M-M.; DeCian, A.; Rettig, S. J. *Organometallics* **2001**, *20*, 2966. (e) Kollmar, M.; Helmchen, G. *Organometallics* **2002**, *21*, 4771.

(125) Jones, N. D.; Meesen, P.; Smith, M. B.; Losehand, U.; Rettig, S. J.; Patrick, B. O.; James, B. R. *Can. J. Chem.* **2002**, *80*, 1600.

(126) Roddic, D. M.; Heyn, R. H.; Tilley, T. D. *Organometallics* **1989**, *8*, 324.

(127) Sluis, P. van der; Spek, A. L. *Acta Crystallogr.* **1990**, *A46*, 194–201.

(128) Spek, A. L. *Acta Crystallogr*. **1990**, *A46*, C34.

(129) Spek, A. L. *J. Appl. Cryst.* **2003**, 36, 7–13.

(130) (a) Reiher, M.; Salomon, O.; Hess, B. A. *Theor. Chem. Acc*. **2001**, *107*, 48. (b) Salomon, O.; Reiher, M.; Hess, B. A. *J. Chem. Phys*. **2002**, *117*, 4729.

(131) (a) Dirac, P. A. M. *Proc. Royal Soc. (London)* **1929**, *A123*, 714. (b) Slater, J. C. *Phys. Rev.* **1951**, *81*, 385. (c) Perdew, J. P.; Wang, Y. *Phys. Rev.* **1992**, *B45*, 13244. (d) Tao, J.; Perdew, J. P.; Staroverov, V. N.; Scuseria, G. E. *Phys. Rev. Lett.* **2003**, *91*, 146401. (e) Perdew, J. P.; Tao, J.; Staroverov, V. N.; Scuseria, G. E. *J. Chem. Phys.* **2004**, *120*, 6898.

(132) Staroverov, V. N.; Scuseria, G. E.; Tao, J.; Perdew, J. P. *J. Chem. Phys*. **2003**, *119*, 12129.

(133) Staroverov, V. N.; Scuseria, G. E.; Tao, J.; Perdew, J. P. *J. Phys. Chem.* **2004**, *121*, 11507E.

(134) Jensen, K. P. *Inorg. Chem.* **2008**, *47*, 10357.

(135) (a) Examination by a linear-transit approach gave no indication that this process is associated with a significant enthalpic barrier. (b) Free energies [kcal mol^{-1}] are given relative to {**3-4'** + $H_3B{\bullet}NH_3$}.